Development and Performance Investigation of a Solar Dryer Integrated with Latent Heat Storage

A Thesis

Submitted in Partial Fulfilment of the Requirements for the

Award of the Degree of

Doctor of Philosophy

by

Deva Kanta Rabha

(136103022)

Department of Mechanical Engineering

Indian Institute of Technology Guwahati

Guwahati - 781039

INDIA

April 2017

Department of Mechanical Engineering
Indian Institute of Technology Guwahati
Guwahati - 781039
INDIA

THESIS CERTIFICATION

This is to certify that the work contained in this thesis entitled **"Development and Performance Investigation of a Solar Dryer Integrated with Latent Heat Storage"** submitted by **Mr. Deva Kanta Rabha,** a student in the Department of Mechanical Engineering, Indian Institute of Technology Guwahati, India for the award of the degree of **Doctor of Philosophy** has been carried out under our supervision. This work has not been submitted previously elsewhere for the award of any degree or diploma.

Dr. C. Somayaji
Associate Professor
Department of Mechanical Engineering
Indian Institute of Technology Guwahati
Guwahati - 781039, Assam

Prof. P. Muthukumar
Professor
Department of Mechanical Engineering
Indian Institute of Technology Guwahati
Guwahati - 781039, Assam

ACKNOWLEDGEMENT

I wish to express my deepest gratitude to all those who have helped me in various ways during the tenure of my PhD work at IIT Guwahati. I have been supported and encouraged by many people and each one has played an indispensable role during my work. I am grateful to all of them.

First and foremost, I would like to express my deepest and most sincere gratitude to my supervisors Prof. P. Muthukumar and Dr. C. Somayaji, Department of Mechanical Engineering, Indian Institute of Technology Guwahati, for their valuable guidance, encouragement, and gracious support during my research work. Their inspiring guidance, motivation, and sincere advice have enabled me to overcome all the difficulties during my research work. I would particularly like to thank Prof. P. Muthukumar for the pain he took in correcting all my manuscripts and bringing the thesis to this present form.

I am thankful to my Doctoral Committee members, Prof. U. K. Saha, Prof. K. Mohanty, and Dr. B. Mehta for their valuable suggestions and encouragement during the period of my research work. I would like to express my sincere thanks to Prof. A. K. Dass (HOD, Mechanical Engineering Department) for providing research facilities and financial support.

I would also like thank Prof. R. Sharma (Principal, Jorhat Engineering College), Prof. P. B. Barua (HOD, Department of Mechanical Engineering, Jorhat Engineering College) and all my colleagues for their support and encouragement during my research work.

I am grateful to Higher Education (Technical) Department, Govt. of Assam for granting me three years study leave under Quality Improvement Programme.

I would like to express my sincere thanks to Mr. M. Sarma, Mr. D. Chetri, Mr. M. Baishya, and Mr. D. Khaklari, Jr. Technical Superintendent of Mechanical Engineering Department for their help and support in fabricating the experimental setup. A word of appreciation goes to Mr. N. Barua, Technical Superintendent for his enthusiastic support with various laboratory apparatus and instruments. Special thanks goes to Mr. T. Rabha for his help and support in fabricating and developing the experimental setup. I am thankful to Mr. S. Kamal, Mr. M.D.

Kevat, Mr. W. Kamai, Mr. CH. Ravi Chandra Rao, Mr. H. Niyas, Mr. B.K. Naik, Mr. R. Nitin Narmda, Mrs. D.V. N. Lakshmi, Mrs. J.P. Ekka, Mr. N.K. Kalita, and Mr. P.K. Sarkar for their help and support during my PhD.

My deepest gratitude goes to my parents and wife for their continuous love and support throughout my studies. I would especially like to thank my wife who endures all the difficulties alone during my three years stay at IIT Guwahati. Special thanks go to my mother in - law and brother for their continual support and love.

I bow my head and record my sincere gratitude to the God almighty for giving me the strength, health and the sprit to complete my research work.

Deva Kanta Rabha

ABSTRACT

Drying of food and agricultural products is indispensable for preservation and storage, easy handling, and reduction in the transportation cost. It is a moisture removal process from the hygroscopic materials. It involves the application of heat to vaporize liquid moisture from the food and agricultural products. The drying process varies from the simple open sun drying to the very complex industrial drying. Various sources of energy are used to supply the energy required for the drying process. Solar energy is the most widely used energy source in the drying process. It is used directly or indirectly to dry food and agricultural products. The open sun drying is the direct application of solar energy. In the indirect application, solar energy is used to produce hot air which is used for the drying application. It is known as the solar drying. The solar drying is an efficient drying process compared with the traditional sun drying. However, the intermittent nature and the uncertainty in the availability of the solar energy affect the reliability and the application of the solar dryer. The incorporation of the thermal energy storage or the auxiliary heater eliminates this shortcoming.

In this study, a solar dryer consisting of a solar air heater panel, a latent heat storage module, a blower, and a drying chamber has been developed. Two double - pass type solar air heaters are connected in series for the solar air heater panel. The latent heat storage module is basically a shell and tube heat exchanger. The shell side of the thermal energy storage is filled with paraffin wax as the storage material. The drying chamber is a rectangular horizontal box having six drying trays. The design calculations of the dryer comprise of the estimation of the required heat energy, air flow rate, quantity of thermal energy storage material, area of the solar air heater panel, and drying bed area. The components of the dryer were fabricated with the materials purchased from the local markets. Then the developed dryer was tested by drying some of the agricultural products available in the prevailing weather conditions of the North - Eastern part of India.

The preliminary experiments on the dryer were carried out without the thermal energy storage material. The first experiment was performed to study the kinetics of the drying process of Ghost chilli. A comparative study was also made by drying the product simultaneously in the open sun. The Ghost chilli samples were dried from its initial moisture content of 85.5% (w.b.) to the final moisture content of 10.5% (w.b.) in 123 h and 193 h in the developed solar dryer and the open sun, respectively. The moisture ratio data obtained from the drying experiment was used to perform non - linear curve fitting with eleven thin layer drying models available in the literature. The best model was chosen based on the criteria of the highest value

of the coefficient of determination, and the lowest values of the reduced chi - square and the root mean square error. Among the eleven drying models, the Page and the Modified Page models for the open sun drying and the Midilli and Kucuk model for the solar dryer drying were found to be the most suitable drying models representing the drying process of the Ghost chilli. The effective moisture diffusivity of the solar and the sun dried products was estimated by graphical method. It was found to be 3.37×10^{-6} (m^2/s) and 2.04×10^{-6} (m^2/s) for the solar drier drying and the sun drying of the Ghost chilli, respectively.

The second experiment was performed to carry out energy and exergy analyses of the drying process of the Ghost chilli and the sliced ginger. 9 kg of Ghost chilli and 13 kg of sliced ginger were dried in the dryer separately. The moisture content of the Ghost chilli was reduced to 12% (w.b.) from its initial moisture content of 85% (w.b.) in 42 h at the drying air temperature range between 42 ^oC and 61 ^oC and the air flow rate of 0.02 kg/s. The moisture content of the sliced ginger was reduced to 9% (w.b.) from its initial moisture content of 87% (w.b.) in 33 h at the drying air temperature range between 37 ^oC and 57 ^oC at the same mass flow rate. The thermal efficiency of the first solar air heater was in the range of 22.1– 40.2% and was found to be higher than that of the second solar heater (connected in series with the first one) in the range of 9.6–19.5%. The specific energy consumptions of the Ghost chilli and the ginger were found to be 18.7 kW h/kg and 8.8 kW h/kg, respectively. The overall efficiency of the dryer was found to be different for different products. It was 4% for the Ghost chilli drying and 8.5% for the sliced ginger drying. The exergy efficiency of the drying chamber was in the range of 21–98% with an average of 64% for the Ghost chilli drying, and it was in the range of 4–96% with an average of 47% for the ginger drying.

In the third experiment, the shell side of the shell and tube heat exchanger of the thermal energy storage module was filled with 34 kg of paraffin wax of the average melting temperature of 58 ^oC, and the dryer was tested by drying a local variety of red chilli. The red chilli was dried in the temperature range of 35–61 ^oC with an average of 50 ^oC. The moisture content of the chilli was reduced from 73.5% (w.b.) to 9.6% (w.b.) in 40 h. The dryer was operated daily for 10 h from 8:00 h to 18:00 h. The performance of each component of the drying system was evaluated by the energy and exergy analyses. It was found that the exergy efficiencies of the first and the second solar heaters were 0.9% and 0.8%, respectively. The energy and exergy efficiencies of the latent heat storage unit varied between 36.4% and 42.2% and 13.7% and 17%, respectively. The exergy efficiency of the drying chamber was found to be in the range of 24.3% and 98.1% with an average of 52.2%. The specific energy consumption of the red chilli and the overall efficiency of the drying system were found to be 6.8 kW h per kg of

moisture and 10.8%, respectively. The electrical energy consumption in the dryer (running the blower) was found to be 0.7 kW h per kg of moisture which was only 10.3% of the specific energy consumption. The dryer was also tested by drying green chilli. The drying of the green chilli was accomplished successfully. Eventually, economic analysis of the dryer was carried out employing annualised cost method. It was found that the cost of the product dried in the solar dryer was Rs.42.7 and that of the same product dried in the electric dryer was Rs. 81.4.

The Ghost chilli, sliced ginger, a local variety of red chilli, and green chilli were dried successfully in the developed solar dryer. Qualitatively, the colour of the agricultural products dried in the solar dryer was found to be better than that of the same products dried in the direct open sun. The energy and exergy efficiencies of the solar air heater panel decrease with increase in the number of solar air heater in series. The energy and exergy efficiencies of the drying chamber depend on the type of the product dried, loading of the drying chamber, and the drying time. The exergy efficiency and the potential of the recirculation of the exhaust air of the drying chamber increase with the progress in the drying time. The integration of the energy storage into the solar dryer reduces fluctuation in the drying air temperature during the cloudy period of the day and maintains the drying air temperature in the close range. It also extends the drying time beyond the sunshine hours of the day. Thus, the results of the study show that the developed solar dryer fulfils the intended objective of this work.

NOMENCLATURE

Notation		*Notation*	
A	dimension less coefficient	c	empirical model constant
A_{dt}	area of drying bed (m^2)	c^*	empirical constant (1/ ºC-s)
A_{SAH}	area of solar air heater (m^2)	D	distance (m)
a	empirical model constant	D_{eff}	effective moisture diffusivity (m^2/s)
a^*	empirical constant (1/s)	D_{hr}	hydraulic diameter (m)
B	dimension less coefficient	D_t	tank diameter (m)
b	empirical model constant	D_{tp}	tube pitch (m)
b^*	empirical constant ($1/s^2$)	d_{tp}	diameter of tube (m)
C	dimension less coefficient	Ex	exergy (J)
C_a	annualised cost of the dryer (Rs.)	$\dot{E}x$	exergy flow rate (J/s)
C_{ac}	annualised capital cost (Rs.)	F	frozen fraction of PCM
C_{cd}	capital cost of dryer (Rs.)	F_c	capital recovery factor
C_{dr}	cost of the dried product (Rs.)	F_o	frozen fraction of PCM solidified at the end of discharge period
C_{ele}	unit cost of electricity (Rs./kW h)	F_s	salvage fund factor
C_{f1}	specific heat of fluid at constant pressure in the 1st fluid pass (J/kg -K)	g	acceleration of gravity (m/s^2)
C_{f2}	specific heat of fluid at constant pressure in the 2nd fluid pass (J/kg-K)	g_o	drying constant (1/s)
C_{sml}	specific heat of storage material in liquid state (J/kg-K)	h	specific enthalpy (J/kg)
C_m	annual maintenance cost (Rs.)	h_{con}	convective heat transfer coefficient (W/m^2-K)
C_{re}	annual electricity cost for running the blower (Rs.)	h_{fg}	enthalpy of evaporation (J/kg)
C_{rf}	annual running fuel cost (Rs.)	h_o	drying constant (1/s)
C_{pa}	specific heat of air at constant pressure (J/kg-K)	h_r	radiative heat transfer coefficient (W/m^2-K)
C_{sm}	specific heat of storage material in solid state (J/kg-K)	h_{wi}	convective heat transfer coefficient due to wind (W/m^2-K)

i	interest rate (%)	n	number of constants
k	thermal conductivity of the fluid (W/m - K)	n_{tb}	number of tubes
k,k_o,k_1	empirical coefficients in drying models (1/s)	P	pressure (N/m^2)
L	latent heat of fusion (J/kg)	p_{bl}	power consumed by the blower (W)
L_s	slice thickness (mm)	p_t	total power input to dryer (J)
l	empirical constant	Q	heat transfer (J)
l_{SAH}	length of solar air heater (m)	$\dot{Q}$	heat transfer rate (W)
l_{tb}	length of tube (m)	Q_s	thermal energy stored (J)
M	moisture content (w.b.) (%)	Q_u	useful heat gain of SAH (W)
M_e	equilibrium moisture content (d.b.) (%)	$\dot{q}$	heat flux (W/m^2)
M_o	moisture content at $t = 0$ (d.b.) (%)	$\dot{q}_{(s,a)}$	solar radiation absorbed by the cover plate (W/m^2)
M_t	moisture content at t (d.b.) (%)	Re	Reynolds number
MR	moisture ratio	r_i	inner radius (m)
$\overline{MR}$	average moisture ratio	r_o	outer radius (m)
m	mass (kg)	R	gas constant of air (J/kg-K)
$\dot{m}$	mass flow rate (kg/s)	R_v	gas constant of water vapour (J/kg-K)
$\dot{m}_a$	mass flow rate of air (kg/s)	Rh_e	relative humidity in decimal
m_{drp}	dry mass of the product (kg)	$RMSE$	root mean square error
m_{dpa}	quantity of product dried per year (kg)	R^2	coefficient of determination
m_{dpb}	quantity of product dried per batch (kg)	SAH	solar air heater
m_v	quantity of the moisture (kg)	SEC	specific energy consumption (J/kg)
N	number of observations	T	temperature (K)
NTU	number of transfer unit	T_a	average temperature of absorber (K)
N_b	number of drying days per batch	T_b	average temperature of base plate (K)
N_y	number of drying days per year	T_{bp}	boiling point of water (K)
Nu	Nusselt number	T_c	average temperature of cover plate (K)

T_{f1i}	temperature of fluid at the inlet of the first fluid pass (K)	w_f	specific humidity of air at equilibrium condition (kg vapour/kg dry air)
T_{f1}	average temperature of fluid pass in the first pass (K)	w_i	specific humidity of drying air (kg vapour/kg dry air)
T_{f1o}	temperature of fluid at the outlet of the first fluid pass (K)	$\dot{W}$	work transfer rate (J/s)
T_{f2}	average temperature of fluid in the second fluid pass (K)	x	thickness (m)
T_{f2o}	temperature of fluid at the outlet of the second fluid pass (K)	x^2	reduced chi-square
T_{id}	drying air temperature (K)	Y	width of solar air heater (m)
T_m	melting temperature (K)	Z	height from reference plane (m)
T_{od}	dry bulb temperature of air at equilibrium condition (K)		**Greek Symbols**
T_p	average temperature of the product (K)	α_a	absorptivity of the absorber plate
T_s	apparent sun temperature (K)	α_c	absorptivity of the cover plate
T_{sky}	sky temperature (K)	ε_a	emissivity of the absorber plate
t	time (s)	ε_c	emissivity of the cover plate
t_d	drying time (h)	ε_{max}	maximum effectiveness (%)
t_{hr}	annual running hour of the dryer (h)	σ	Stefan-Boltzman constant (W/m^2-K^4)
U_b	overall bottom loss coefficient (W/m^2-K)	τ_c	transmissivity of the cover plate
U_t	overall top loss coefficient (W/m^2-K)	τ_o	non-dimension time variable
V	salvage value (Rs.)	η	efficiency (%)
V_a	annualised salvage value (Rs.)	ρ	density (kg/m^3)
V_{pf}	volume of paraffin wax (m^3)	ρ_p	bulk density of the product (kg/m^3)
V_t	tank volume (m^3)	ζ	porosity of the bed (%)
μ	viscosity (N-s/m^2)	β	dimensional parameter
V_{tb}	total volume of tube (m^3)	μ	viscosity (N-s/m^2)
v	velocity of air (m/s)		**Subscripts**
v_{wi}	wind velocity (m/s)	amb	ambient
w	specific humidity of air (kg vapour/kg dry air)	a, b	absorber to base plate

a, c	absorber to cover plate	f_1	first fluid pass
a, f_1	Absorber to first fluid pass	f_1,*c*	first fluid pass to cover plate
b, air	bottom plate to air	f_2	second fluid pass
c, air	cover plate to air	f_2, *b*	second fluid pass to base plate
c, sky	cover plate to sky	*i*	initial or inlet
ch	charging	*in*	input
cr	critical	*ins*	insulation
con	convective	*ls*	loss
d	dryer	*o*	outlet
da	drying air	*p*	product
db	dry basis	*pf*	paraffin wax
dc	drying chamber	*pr*	predicted
dest	destruction	*rd*	radiation
dich	discharging	*r*	reference
ds	drying system	*re*	received
dt	drying bed	*SAH - 1*	first solar air heater
es	energy storage	*SAH - 2*	second solar air heater
ex	experimental	*sm*	storage material
Ex	exergy	*wb*	wet basis
f	final/ fluid		

CONTENTS

Chapter - 1

Introduction

1.1 Introduction

Preservation of food and agricultural products is indispensable for food security and safety. Inappropriate methods of preservation and storage bring about losses of cereals and fruits ranging from 10% to 30% and 50% to 70%, respectively (Yaldyz and Ertekyn, 2001). Drying or dehydration is one of the oldest techniques of preservation used by humankind. The main objective of the drying is to reduce the moisture content of food and agricultural products to the safe storage level at which the products can be stored for a longer period without any deterioration. The low moisture content prevents the growth of microorganisms such as moulds, bacteria, and yeasts and reduces the chemical reactions deteriorating the quality of the products (Bahnasawy and Shenana, 2004). It also reduces the weight and volume of the products resulting in minimum packaging, storage, and transportation costs (Akpinar, 2006). Thus, the drying process prevents the spoilage of the food and agricultural products after harvest and makes them available for the consumption throughout the year.

1.2 Drying Process

Drying process involves the application of heat to vaporise moisture from the food and agricultural products and therefore, simultaneous heat and mass transfer occurs in the drying process. In addition to the heat and mass transfer, physical changes such as shrinkage, puffing, and crystallisation and biochemical changes such as colour, texture, and odour also take place during the drying process. The heat is supplied to the drying material from an external source by convection, conduction, radiation or combination of them depending on the types of the drying method. Depending on the mode of heat transfer, the drying processes are mainly classified as convective drying, conductive drying, and radiative drying. In the convective drying, hot dry air directly comes in contact with the surface of the products and removes the moisture from its surface. In the conductive drying, the moist material is brought into contact with a hot surface. In the radiation mode, the material to be dried is placed in a microwave or radio frequency electromagnetic field.

1.2.1 Convective drying

The convective drying is the most widely used drying method. In this method, the hot air is supplied either across a layer of products or parallel to one or both surfaces of the layer of the products. The heat is transferred from the hot air to the products due to the temperature gradient, and the moisture is released from the products to the air. The moisture is transferred from the drying materials by two mechanisms (Belessiotis and Delyannis, 2011).

- Transport of moisture from the inner structure of the material to the surface.
- Transfer of moisture from the surface of the material to the surrounding air.

The moisture transport within the material may take place by any or combination of the following mechanisms of the mass transfer (Mujumdar and Devahastin).

- Liquid diffusion; it takes place when the temperature of the liquid is below its boiling point.
- Vapour diffusion; it occurs when the liquid vaporizes within the material.
- Knudsen diffusion; it happens when the drying is carried out at low temperature and pressure.
- Hydrostatic pressure diffusions; it occurs when the internal vaporisation becomes higher than the transport of the moisture through the material to the surrounding.
- Combination of the above mechanisms.

In the convective drying, the moisture removal rate or the drying rate, which is defined as the mass of water vapour removed per unit time per unit mass of the dry matter, depends on the following factors (Berk, 2009).

- Internal conditions such as porosity, moisture content, size, and shape of the materials to be dried.
- External conditions: air temperature, velocity, and relative humidity.

1.2.2 Drying periods

The drying process of the hygroscopic material takes place in two stages (Midilli and Kucuk, 2003a). The first stage is known as the constant rate period. It takes place at a constant drying rate and generally occurs at the surface of the material when it is saturated with moisture. The surface of the material is maintained at the saturated condition by the rapid movement of the moisture within the material. The second stage is known as the falling rate period. It occurs when the rate of transport of moisture from the inner structure of the material becomes lower

than the moisture evaporated from the surface of the material. It starts at the critical moisture content, the moisture content corresponding to the end state of the constant rate period. There are two stages of the falling rate period. The first stage falling rate period starts when the surface of the material is not saturated with water or the constant rate period ends, and the moisture diffusion is controlled by the internal liquid movement caused by the concentration of moisture and the internal conditions. The first falling rate period ends when the moisture content of the material reaches the equilibrium moisture content corresponding to the relative humidity of the drying air. The equilibrium moisture content is the moisture content of the product at which the vapour pressure of water in the material is equal to the partial pressure of water in the surrounding air. In the second stage, the dominant mechanism of the mass transfer is the vapour diffusion (Belessiotis and Delyannis, 2011).

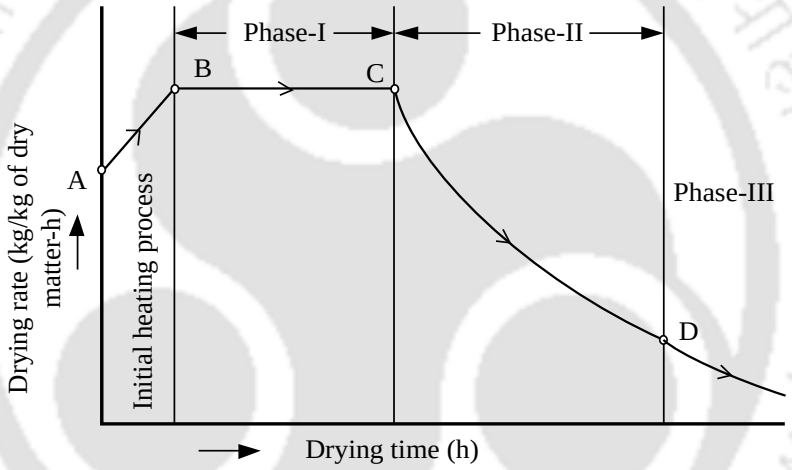

Fig. 1.1 Drying periods curve.

In Fig.1.1, the process AB represents the initial heating process of the material. The process BC represents the constant rate drying process. The point C is known as the critical point from which the falling period rate begins. The processes CD and DE denote the first and the second falling rate periods, respectively. The drying process of most agricultural products occurs in the falling rate periods.

Drying methods vary from the simple traditional open sun drying to the very sophisticated industrial drying. It is an energy - intensive operation as the latent heat of evaporation is required for the removal of moisture (Kudra, 2004). Different sources of energy such as coal, LPG, solar energy, and biomass are used to supply the energy required for the drying process. The energy requirement for most industrial dryers is met by the conventional

fossil fuels. Among the renewable energy sources, solar energy is known to be the most widely used energy source in the drying process. It has been used by humankind since time immemorial for drying foods and agricultural products. It is a clean, cheap, and environmentally friendly energy source.

1.3 Open Sun Drying

Open sun drying has been practised for drying food and agricultural products for over many centuries. In the traditional open sun drying process, the products are spread out in thin layers on the ground, concrete floor, mat or tray and are directly exposed to the wind and the sun. The products surface directly absorb the direct and diffuse radiations resulting in rising of the temperature of products. Some percentage of the converted heat of the sun radiations evaporates the moisture from the products, and the major percentage is lost by convection, conduction, and re - radiation. The moisture is removed by the surrounding atmospheric air.

The open sun drying is one of the largest applications of solar energy. It is widely practised in the rural areas of the developing countries. Small farmers of the rural areas in the developing countries (who produce around 80% of the food products) practice the open sun drying to dry food and agricultural products (Murthy, 2009). However, the open sun drying process has many limitations such as

- contamination of the products due to dust, birds drop, etc.,
- longer drying time due to slow drying rate as the product is dried at low temperature and high relative humidity,
- difficulty in controlling the drying process,
- losses of natural colours and minerals caused by the direct exposure to the sun radiation,
- losses of the products due to insects, birds, and adverse weather, and
- large drying area requirement and high labour cost.

In spite of having many disadvantages, the sun drying is widely practised in the rural areas owing to the low cost and the requirement of unskilled labour. The drawbacks of the sun drying led to the development of the solar dryers.

1.4 Solar Drying

The process of the solar drying is an efficient way of utilising solar energy in the drying process. It is a form of the convective drying. In the solar drying process, the products are dried in an

enclosed space or in a drying cabinet at an elevated temperature. The main objective of the solar drying is to supply more heat to the products than it is available under the normal sun drying conditions. In the solar dryer, the product is dried at the high temperature and low relative humidity compared to the open sun drying for the same solar radiation intensity. The high temperature increases the vapour pressure of the moisture content of the product sufficiently and also reduces the drying air relative humidity resulting in high drying rate and the moisture carrying capacity of the drying air (Weiss and Buchinger).

In the solar drying process, the external drying parameters such as drying air temperature, mass flow rate, relative humidity, and heat input can be controlled with a fan or similar type of devices and auxiliary heat sources (i.e., electricity, fossil fuels, and biomass). The deficiencies of the direct sun drying can be overcome here, and therefore, it has the following advantages:

- high drying rate,
- the products can be dried in a short period with the desired quality in a clean environment,
- the original colour and texture are preserved,
- large quantity of the products can be dried in a small space with less labour,
- drying operation can be performed during off - sunshine hours and bad weather also if a backup heating system and/or the thermal energy storages are integrated into the solar dryers, and
- the food materials and crops which are photosensitive can be dried in the solar dryer without affecting their colour, flavour, and nutritional values.

A solar drying system consists of the following components depending on the type. All the components may not be required for some of the solar dryers.

- A drying chamber with drying tray to dry the product: it may be covered with a transparent or an opaque sheet depending on the type of the dryer.
- Solar air heater: it is the main component of some of the solar dryers. It produces the hot air necessary for drying by harvesting solar energy.
- Chimney system for the natural circulation dryer and fan or blower for the forced circulation dryer to circulate air in the drying system.
- Auxiliary heating unit to supplement the heat requirement during inadequate or unavailability of the solar radiation.
- Thermal energy storage to store energy harvested from the solar radiation during the daytime and use the same during the night - time or the cloud cover.

1.4.1 Types of solar dryer

Numerous types of solar dryers have been developed for drying food and agricultural products. The solar dryers have been broadly classified into two categories depending on the movement of air, namely (Patil and Gawande, 2016).

- Passive solar dryers; and
- Active solar dryers.

The active and passive solar dryers can be further classified as (El - Sebaii and Shalaby, 2013).

- indirect - type solar dryer;
- direct - type solar dryer;
- mixed - mode - type solar dryer; and
- hybrid - type solar dryer.

1.4.1.1 Passive solar dryers

Passive solar dryers are also known as the natural circulation or natural convection solar dryers. The flow of air in the passive dryer is purely due to density difference. It uses only renewable energy sources and runs without any electricity. The passive dryers are easy to construct with the locally available materials and suitable for any remote area where the electrical grid is not available. However, it has some disadvantages. The flow rate of air is not adequate for drying larger crops mass, and the flow of air does not take place during the night - time and the bad weather. The overall drying rate is slow due to poor moisture removal rate.

1.4.1.1.1 Indirect - type passive solar dryer (IPSD)

Solar dryers are classified as the direct - type and the indirect - type depending on the exposure of the products to the solar radiation. In the IPSD, the products are not directly exposed to the solar radiation and are dried by the hot air. A simple IPSD consists of a solar air heater and a drying chamber. Ambient air is heated by the solar air heater and then flows to the drying chamber up through the bed of crops due to buoyancy forces caused by the temperature difference. The drying chamber generally consists of perforated trays or mats where the products are kept, and the hot air is supplied from the bottom of the trays. Figure 1.2 shows a typical indirect - type natural convection solar dryer developed by Pangavhane *et al.*, 2002.

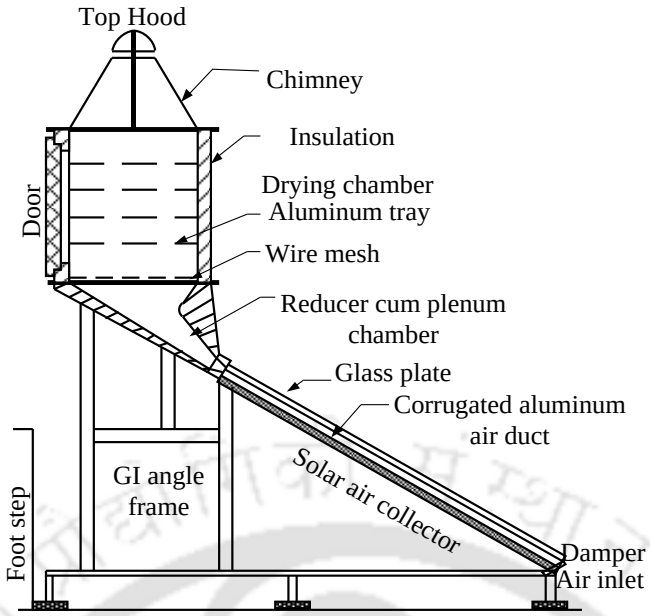

Fig. 1.2 An indirect - type natural convection solar dryer developed by Pangavhane *et al*., 2002.

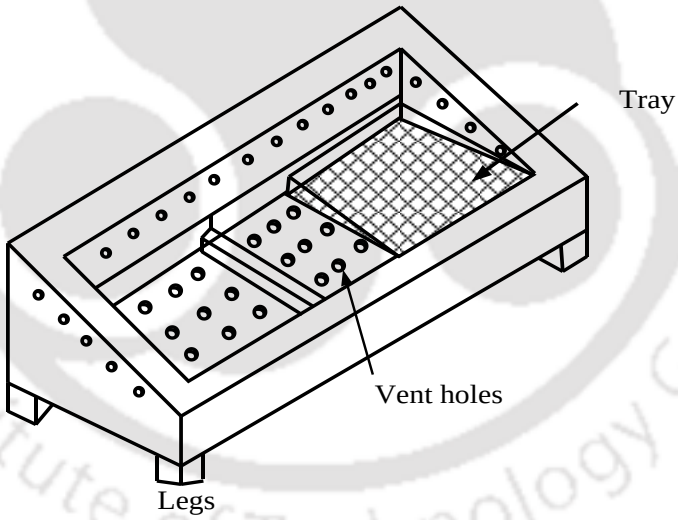

Fig. 1.3 A box - type solar dryer.

1.4.1.1.2 Direct - type passive solar dryer (DPSD)

The DPSD does not have a separate drying chamber. The product is placed in the air heating unit and absorbs the solar radiation transmitting through a transparent sheet. There are different types of the direct - type solar dryer: box/cabinet - type, tent - type, and green house - type solar dryers. The box type cabinet dryer developed by the Brace Research Institute of Canada is

shown in Fig.1.3. It consists of a wooden box, a transparent cover at the top of the box, and drying trays. The inner side of the box is painted black, and the bottom and sides of the box are insulated. The product to be dried is placed on the trays. The solar radiation transmitting through the transparent cover gets absorbed on the black surface. The temperature inside the dryer rises due to the accumulation of energy. The box is provided with vent holes for circulation of air. This type of dryer is simple and cheaper to construct but it has some limitations like overheating of the products, poor moisture removal, small capacity, and damage of colour due to exposure to the solar radiation.

1.4.1.1.3 Mixed - mode - type passive solar dryer (MMPSD)

The structural features of the MMPSD are the same as the indirect - type passive solar dryer. The drying chamber of such dryer is constructed with transparent walls. An MMPSD developed by Jain, 2005 is shown in Fig. 1.4. The solar air heater produces the hot air by trapping solar radiation, and the air flows to the drying chamber from the solar air heater due to the natural convection. The product is heated by the solar radiation transmitting through the transparent walls as well as by the hot air generated by the solar air heater. The flow rate of air and the drying rate are high in this type of dryer due to high air temperature in the drying chamber.

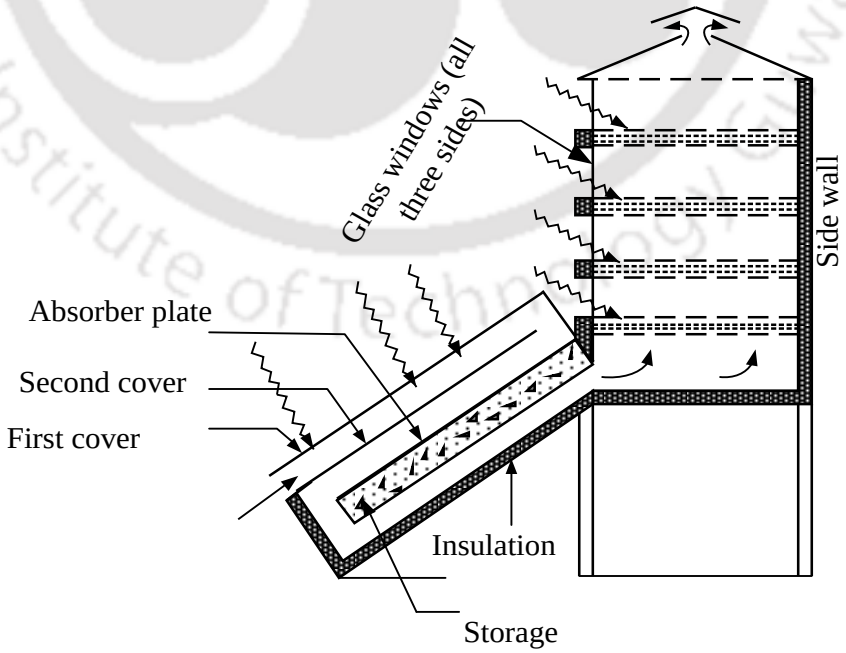

Fig. 1.4 A mixed - mode - type natural convection solar dryer (Jain, 2005a).

1.4.1.1.4 Hybrid - type passive solar dryer (HPSD)

The HPSD is integrated with either a thermal energy storage unit or an auxiliary heating device. The thermal energy storage stores the excess heat harvested during the daytime in the form of sensible or latent heat. The heat retained in the storage is used during off - sunshine hours or cloudy periods. Some of the common storage materials used in the solar dryers are rock, pebbles, paraffin wax, water, etc.

Solar energy is intermittent in nature and time dependent. The drying operation is interrupted during the cloudy period and rainy days. Therefore, an auxiliary heating system is incorporated into the dryer to continue drying operation during the adverse weather and the night - time also. The auxiliary heating system may be wood stoves, electric heaters, and liquid or gas fuel burners. Figure 1.5 shows a hybrid - type passive solar dryer developed by Madhlopa and Ngwalo, 2007. The dryer consists of a solar air heater with a thermal energy storage, a biomass backup heater, a drying chamber, and a chimney.

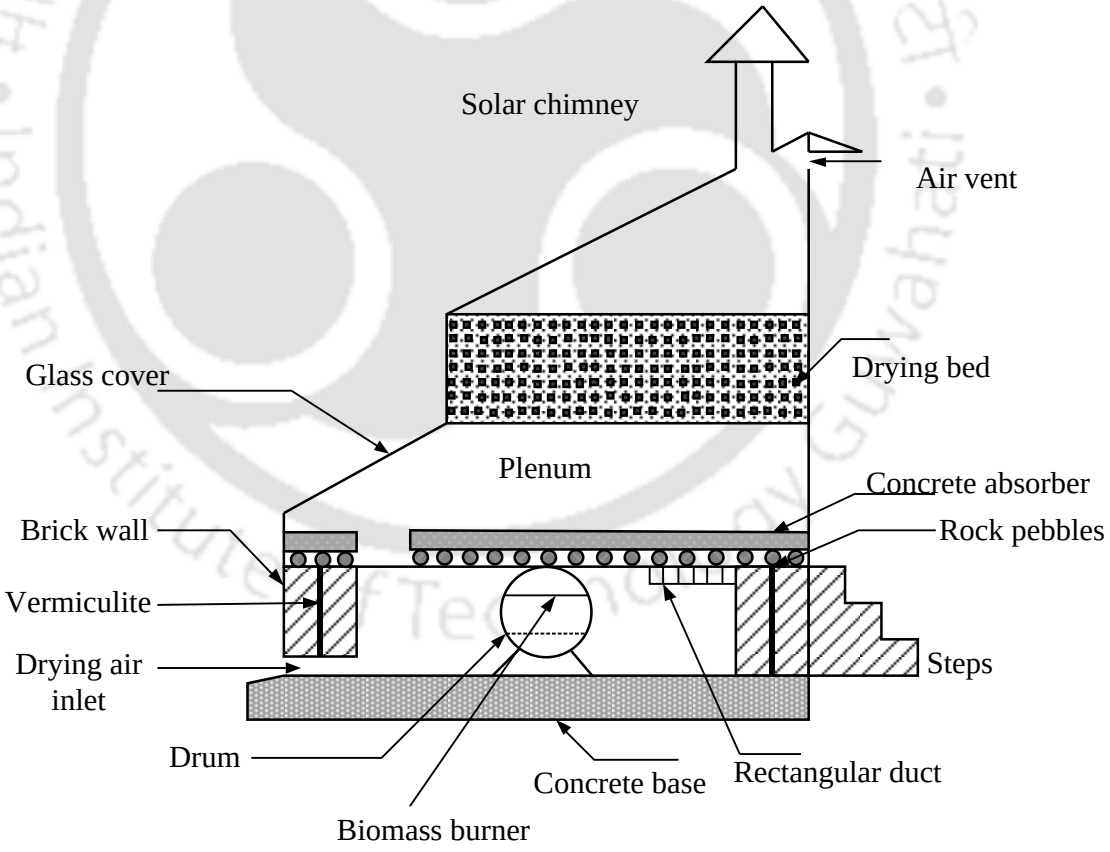

Fig. 1.5 A hybrid - type natural convection solar dryer (Madhlopa and Ngwalo, 2007).

1.4.1.2 Active solar dryers

Active solar dryers are also known as the forced circulation or forced convection solar dryers. In the active solar dryers, an external device like a fan or similar type of device supplies the hot air required for the drying operation. The electrical power required for running the fan or blower is supplied from either the grid or a solar photovoltaic module. The active dryer has some advantages over the passive dryer. It reduces the drying time by enhancing the rate of heat transfer. In this type of dryer, the flow rate of air and the temperature can be controlled.

1.4.1.2.1 Indirect - type active solar dryer (IASD)

The IASD consists of mainly a solar air heater, a drying unit, and a fan for circulation of air and air ducts. The fan of the dryer helps in proper controlling of the air flow rate which is an important parameter affecting the drying rate. The indirect - type active solar dryer with an electrical heater developed by Reyes *et al.*, 2013 for drying chilli is shown in Fig. 1.6. A centrifugal fan is provided to supply air through the air heater to the drying chamber.

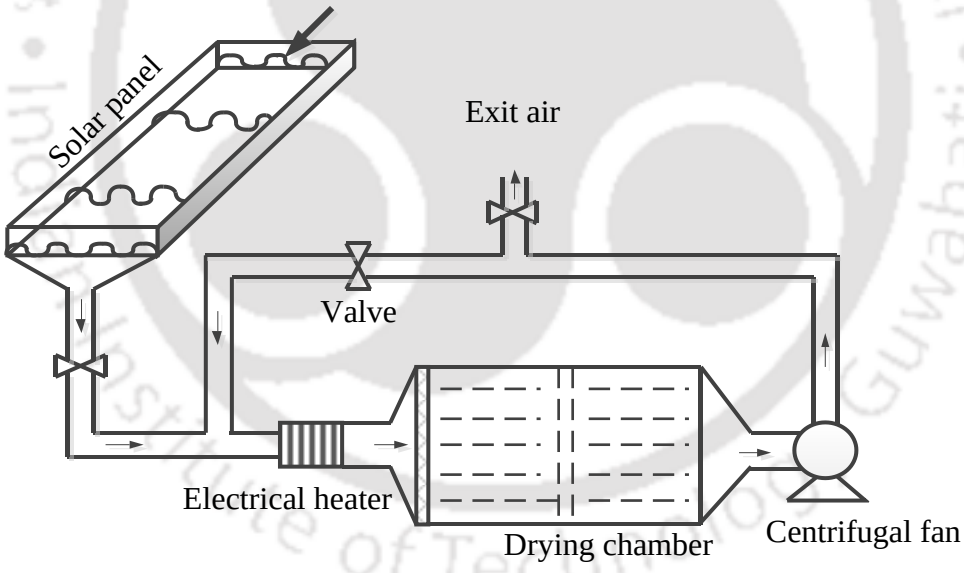

Fig. 1.6 An indirect - type active solar dryer (Reyes *et al.*, 2013).

1.4.1.2.2 Direct - type active solar dryer (DASD)

The constructional feature of the DASD is the same as the direct - type-passive solar dryer. In this type of dryer, an exhaust fan is provided to expedite the removal of saturated moist air from the drying chamber - cum - the air heater. The exhaust fan runs on electricity supplied by the grid or the solar photovoltaic module. Figure. 1.7 shows a greenhouse type DASD

developed by Janjai *et al.*, 2011 for drying banana. In this dryer, the fans run on the electricity produced by the photovoltaic panel.

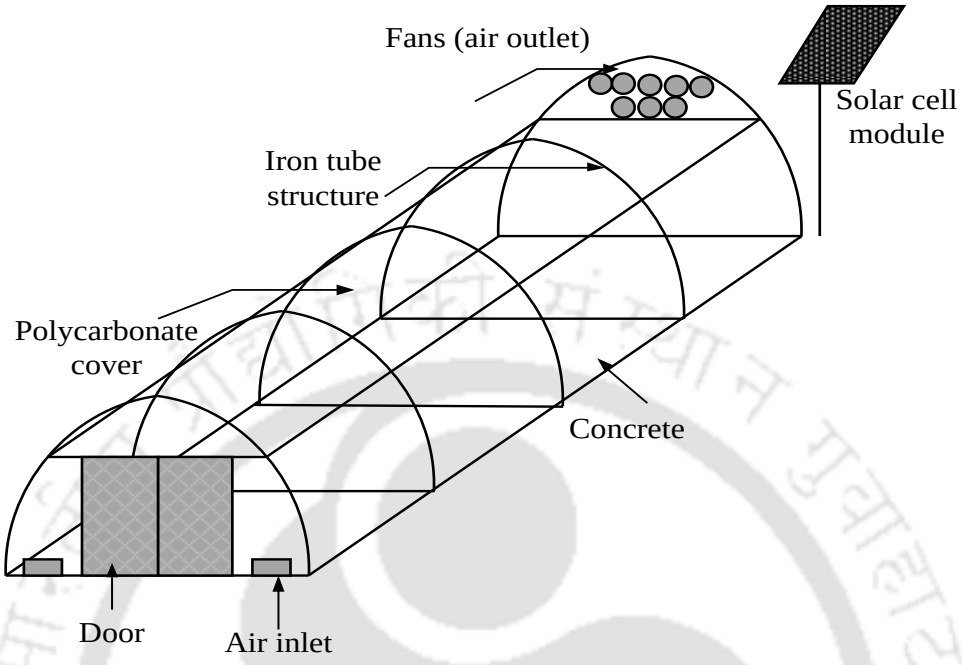

Fig. 1.7 A direct - type active solar dryer (Janjai *et al.*, 2011).

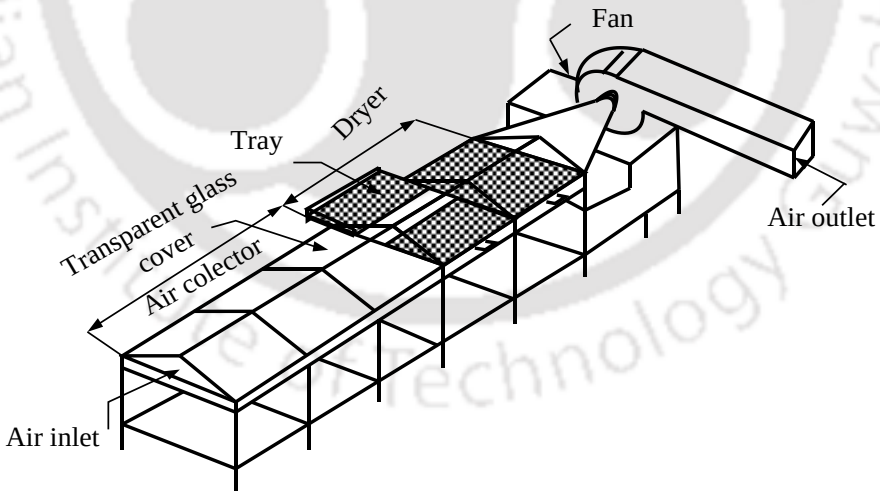

Fig. 1.8 A mixed - mode - type active solar dryer (Usub *et al.*, 2010).

1.4.1.2.3 Mixed - mode - type active solar dryer (MMASD)

The MMASD generally consists of a solar air heater, a blower or fan, and a drying chamber with transparent walls. An MMASD developed and tested by Usub *et al.*, 2010 is shown in

Fig. 1.8. The working principle of the active mixed - mode - type dryer is the same as the passive mixed - mode - type. The solar radiation incident on the air heater surface and the product surface in the drying chamber produce the necessary heat required for the drying operation. However, in the active mixed - mode - type solar dryer, an external device is used to circulate the drying air.

1.4.1.2.4 Hybrid - type active solar dryer (HASD)

The HASD is integrated with auxiliary heating systems such as electric heater, LPG or HSD burner, and biomass backup heater with the provision of operating the dryer in single mode or in combination. It is also provided with the thermal energy storage. The incorporation of the auxiliary heater into the solar dryer makes the drying system more reliable. The auxiliary heater supplies the energy required for producing the hot air during off - sunshine hours and the cloudy weather or to maintain the drying air temperature at a fixed value. Therefore, the HASD can be operated irrespective of the weather conditions, and the drying operation can be extended beyond the off - sunshine hours. Sometimes the hybrid dryer is integrated with both the thermal energy storage and the auxiliary heating unit. The high capital cost and complicated structure are the main drawbacks of this drying system. Figure 1.9 shows the hybrid solar dryer developed by Ryes *et al*., 2014. This drying system has both the thermal energy storage and the auxiliary heating unit.

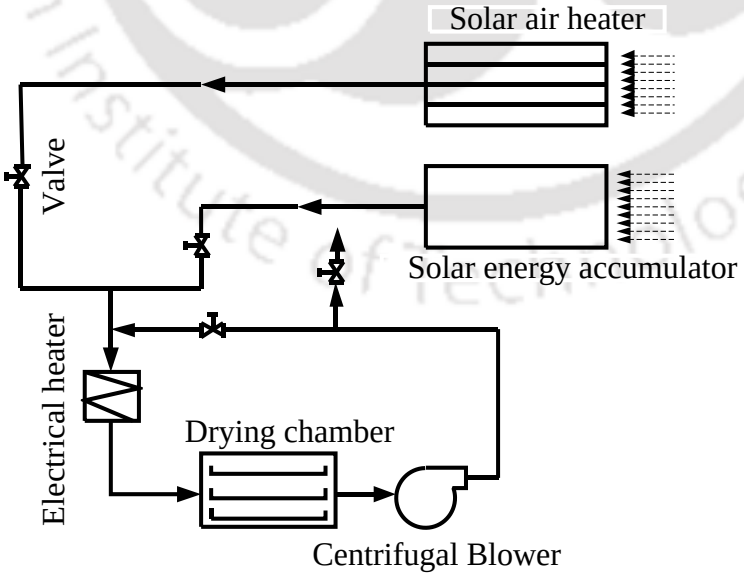

. **Fig. 1.9** A hybrid-type active solar dryer developed by Reyes *et al.*, 2014.

1.5 Thermal Energy Storage and Auxiliary Heating System

The intermittent nature and uncertainty in the availability are the main shortcomings of solar energy. The daily and seasonal fluctuations in the solar radiation, rainy days, and night period affect the drying operation in the solar dryer and thus its reliability. In the solar drying process also, sometimes products spoil due to unavailability of the solar radiation for several consecutive days and get affected by microbial organisms during the drying process itself (Sarsavadia, 2007). The quality of some products degrades owing to the longer drying period. Besides, the high temperature during the peak - sunshine hours causes hardening, shrinkage, and burning of the surface of the products in the solar dryer. The hybridization of the solar dryer, where the conventional energy sources like electrical heater, biogas burner, LPG, etc. or thermal energy storages are integrated into the dryer unit, eliminates these problems.

In the hybrid solar dryer, the drying operation can be extended beyond the sunshine hours with the help of an auxiliary heat source or the energy storage, and products could be saved from the possible damaged caused by the infestation of the microbial organisms during the bad weather (Amer *et al.*, 2010). The surplus solar energy of the peak hours can be stored in a thermal energy storage and can be used during inadequate solar radiation period or off-sunshine hours. The product can also be saved from the possible effects of overheating during the peak sunshine hours. Constant drying rate is maintained during the low-intensity solar radiation period by extracting the heat from the thermal energy storage and smoothing the drying air temperature. It eliminates the need for the auxiliary heat source for a short duration during the fluctuation in the solar radiation. However, a large size heat storage and a solar collector panel are needed for meeting the energy requirement for several consecutive cloudy days which adds large capital cost to the dryer. The hybrid solar dryers have recently received much attention because of their operational flexibility in all weather conditions. Numerous experimental and simulated models of the hybrid solar dryer were developed for drying different agricultural products.

1.5.1 Sensible heat storage (SHS) and latent heat storage (LHS)

Thermal energy storages may be latent heat storage (LHS) or sensible heat storage (SHS) or chemical energy storage (Singh *et al.*, 2010). These are temporary storages of high or low-temperature energy. The commonly used thermal energy storages in the solar dryer are the SHS and the LHS. In the SHS, the temperature of the solid or liquid materials such as gravel, pebbles, brick, sand, water, and oil is raised to store the thermal energy. The heat storage

capacity of the SHS depends on the heat capacity and the change in the temperature of the storage material. The amount of the sensible heat stored in a mass of material can be expressed by the following equation.

$$Q_s = m_{sm} C_{sm} (T_f - T_i) \tag{1.1}$$

where m_{sm} is the mass of the storage material, C_{sm} is the specific heat of solid material, T_i is the initial temperature, and T_f is the final temperature.

The solar dryer with integrated SHS is relatively less expensive and suitable for the rural areas as the storage materials are easily available. It can be constructed on- site very easily as the SHS does not require any storage vessel or heat exchanger. The main deficiency of the SHS system is in its inability to supply the drying air at a constant temperature. It also needs a large storage volume.

In the latent heat storage system (LHS), the thermal energy is stored due to the transition of the phase of the materials from solid to liquid or liquid to vapour or vice versa. The phase change from liquid to vapour and vice versa is not used because of the large volume of the vapour phase. The amount of heat stored in a latent heat storage material while melting the storage material completely and raising the temperature from T_i to T_f can be expressed as follows.

$$Q_s = m_{sm} \left[C_{sm} (T_m - T_i) + L_{sm} + C_{sml} (T_f - T_m) \right] \tag{1.2}$$

where T_m denotes the melting temperature, L_{sm} is the latent heat of fusion of the storage material, C_{sm} is the specific heat of the material in the solid state, and C_{lsm} is the specific heat of the material in the liquid state.

Many organic and inorganic phase change materials (PCM) are used as the LHS materials. The LHS has many advantages over the SHS. The main advantage is the high energy storage capacity per unit mass compared with the sensible heat storage materials. It can supply hot air at nearly constant temperature (Dincer and Rosen, 2011).

1.6 Solar Air Heater (SAH) or Collector

The solar air heater is one kind of heat exchanger that generates hot air by trapping solar radiation. It is one of the major components of the solar dryer. A conventional solar air heater generally consists of a transparent cover, an absorber plate, a base plate, and a collector box

with insulation. The schematic diagram of a conventional solar heater is shown in Fig.1.10. The cover plate of the SAH is made of the material which is transparent to the incoming solar radiation and opaque to the long wave radiation. Window glass or plastics sheet of thickness 4 to 5 mm is suitable for the cover plate. The absorber plate is a thin metal sheet, 1 mm in thickness, painted black and is placed in a certain space beneath the cover plate. A metal sheet is provided as the base plate beneath the absorber plate and above the insulation. The bottom and sides of the box are insulated to reduce the heat losses.

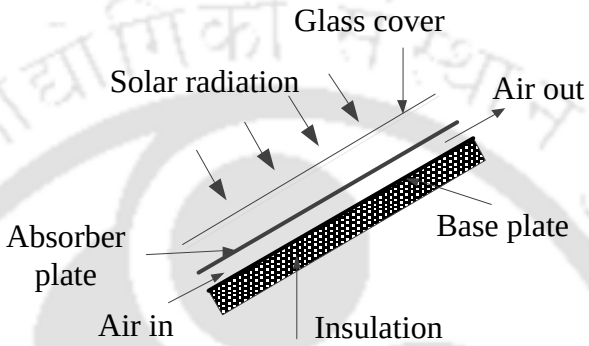

Fig. 1.10 Schematic diagram of a conventional flat plate solar air heater.

The working principle of the solar air heater is simple. The solar radiation transmitting through the transparent cover falls on the surface of the absorber plate and gets absorbed because of which the temperature of the plate rises. Some part of the converted heat of the absorber plate is transferred to the air flowing over it, and the remaining part is lost to the surrounding from the top surface by the convection and the re - radiation and by conduction through the back and edges. The air is circulated in the air heater due to buoyancy effect or fan or blower. The performance of the solar air heater depends on the rate of heat transfer from the absorber plate to the air. To improve the heat transfer rate as well as the thermal performance of the solar air heaters, different types of solar air heaters have been developed. They are classified based on the heater cover plate, absorber surface, and air flow path as follows (Garg and Prakash, 2006; Oztop *et al*., 2013; Saxena *et al*., 2015).

- *Bare plate, single cover, and double cover solar air heaters*: The bare plate solar air heater does not have the cover plate. The absorber plate is directly exposed to the solar radiation. In the double cover solar air heaters, two cover plates are used mainly to reduce - radiation losses.

- *Single - pass and double - pass:* In the single - pass system, the air flows in the duct either formed by the absorber and base plates or by the absorber and cover plates. In the two - pass or double - pass air heater, the air is first passed between the two cover plates and then passed under the absorber plate.
- *Finned - plate solar air heater:* It is the modified version of the simple flat plate solar air heater where fins are added to the absorber plate to increase the heat transfer rate.
- *Corrugated - plate solar air heater:* The corrugated absorber plate either in the rounded or V - shaped is used to increase the heat transfer area.
- *Matrix - type solar air heater:* In this type of solar air heater, matrix materials like loosely packed material is placed in the air path to increase the heat transfer rate by increasing the surface area and the turbulence.
- *Overlapped - type solar heater:* In this type of the solar air heater, transparent glass plates are arranged in series. The glass plate consists of two part; a clear part and a black part. The clear part of one plate overlaps the black part of the other plate.
- *Transpiration solar air heater:* This type of solar air heater does not contain the absorber plate. Closely packed matrix material functions as the absorber plate.

1.7 Background and Primary Objective of This Study

North - Eastern region (NER) of India, which comprises of seven sisters states (Assam, Arunachal Pradesh, Meghalaya, Mizoram, Manipur, Nagaland, Tripura) plus the Himalayan state Sikkim has a mainly subtropical climate of hot, humid summers, severe monsoons, and mild winters and has low annual average global solar radiation (4.5 to 5.6 kW h/m^2-day).

The climatic conditions and the soil of the NER are suitable for the cultivation of varieties of agricultural products such as tea, rubber, ginger, turmeric, chilli, cardamom, cashew nut, and black pepper. It accounts for 72% of the ginger, 85% of the large cardamom, and 51% of the tea productions of India (Rhaman *et al.,* 2009; Mande *et al.,* 1999; Baruah, 2006). These agricultural products have high demand in the global market. All these agricultural products contribute immensely to the economy of the NER of India. Generally, most of these products are dried in the open sun or exposing them to smoke produced by burning of wood logs in the open fire furnace. Because of the uncontrolled heating and the direct exposure to the smoke and the sun, the quality of the dried products degrades. The climatic condition of the NER is characterized by the frequent rain fall, high humidity, low annual average solar radiation, and long rainy days. The solar radiation fluctuates during the

daytime due to the appearance of clouds in the sky, especially during summer. However, the daily average solar radiation in a good sunshine day is very high. Therefore, the drying of the products has to be completed within the period of the availability of the solar radiation which is possible only by drying the products in the solar dryer instead of drying in the direct sun. Since solar radiation fluctuates frequently due to cloud cover, a solar dryer integrated with either a thermal energy storage unit or an auxiliary heat source may be the most suitable solar dryer for the NER region. Therefore, the primary objective of this study is to develop a solar dryer integrated with a latent heat storage module and to test the dryer in the sub - tropical climate of the NER region by drying some of the important agricultural product grown in this region.

1.8 Structure of the Thesis

The thesis has been organised in eight chapters. The present chapter covers the introduction and the background and primary objective of this study. The remaining chapters are arranged as follows.

Chapter - 2: A brief review of the literature related to the hybrid solar dryers, a study of thin layer kinetics of the solar and open sun drying of food and agricultural products, and energy and exergy analyses of the solar drying process, and the objectives of this study are elaborated in this chapter.

Chapter - 3: This chapter presents the basic design calculations for estimating the air flow and energy requirements for the drying system. Thermal modelling of a double - pass solar air heater and the effects of different parameters on its efficiency are also presented in this chapter. This chapter also describes the sizing of the air heater panel and the drying chamber for the developed dryer.

Chapter - 4: The details of the developed dryer and the fabrication of the different components of the dryer are discussed in this chapter. The instrumentation for conducting the performance test of the drying system is also explained in this chapter.

Chapter - 5: This chapter deals with the experimental investigation of the thin layer drying kinetics of the Ghost chilli. Detailed discussion on the thin layer drying kinetics analysis and the identification of the best model for describing the drying process of the Ghost chilli are presented.

Chapter - 6: Experimental studies on the drying characteristics of Ghost chilli and sliced ginger without heat storage material are presented in this chapter. Energy and exergy analyses of the drying process of these products are carried out and the results are discussed.

Chapter - 7: Experimental investigation on the solar dryer with the thermal energy storage for drying a local variety of red chilli and the energy and exergy analyses of all the components of the drying system are presented in this chapter. The economic analysis is also presented in this chapter.

Chapter - 8: Conclusions, the scope for improvement of the developed solar dryer, and future works are presented in this chapter followed by reference and appendices.

Chapter - 2

Literature Review

2.1 Review on Hybrid - Type Solar Dryers (HSD)

Numerous experimental studies and numerical simulations on the hybrid solar dryers were reported in the literature. In this part of this chapter, the previously published works on the hybrid solar dryers are reviewed focusing on the types of the energy storage material and the auxiliary heating system employed in the solar dryers.

2.1.1 HSD with thermal energy storage (TES)

A large number of solar dryers integrated with the thermal energy storage are reported in the literature. Mainly sensible heat storage and the latent heat storage are used in the solar dryers. The commonly used sensible heat storage materials are stone, pebble, brick, concrete, rock, and water. The most widely used latent heat storage material in the solar dryer is the paraffin wax of different melting temperatures. The charging of the storage material in the solar dryer is done either directly or indirectly. In the direct charging process, the storage material is directly exposed to the solar radiation by employing it in the solar air heater. In this case, the solar heater works as the thermal energy storage - cum - air heater. While in the indirect charging process, the hot fluid (air, water, and other heat transfer fluids) produced by the solar air heater or water heater is supplied to the energy storage.

2.1.1.1 HSD with sensible heat storage (SHS)

The solar dryer with integrated SHS is relatively less expensive and suitable for the rural areas as the energy storage materials are easily available. It can be constructed on- site very easily and does not require any storage medium and heat exchanger. The main shortcomings of the SHS system are that it cannot supply the drying air at constant temperature and requires a large storage volume. Nevertheless, many investigators developed experimental and theoretical models of the solar dryers with the sensible heat storage system.

Garg *et al*. (1985) presented an experimental study of a solar air heater connected in series with an integrated rock (size 3 - 5 cm in diameter) storage - cum - solar air heater developed for the drying purpose. In this system, the air supplied by a centrifugal blower was first heated by the solar air heater. It was further heated up while passing through the solar air heater - cum - energy storage. The performance of the system was evaluated for a single and double glazing, rock bed of different thicknesses, and for different mass flow rates of air. They reported that the solar air heater exit temperature was high at the low mass flow rate of air and the solar radiation intensity affected the optimum thickness of the rock bed storage. The thermal losses from the storage reduced with increase in the number of glazing.

Ayensu and Asiedu - Bondzie (1986) designed and developed a natural convection solar dryer integrated with a mass of granite rocks (3 cm in diameter) as the energy storage material to investigate the drying characteristics of cassava leaves, cassava chips, pepper, and fish. The design parameters of the dryer were the mass flow rate of air, the height of the chimney, solar air heater area, and thickness of the drying bed. The dryer was fabricated with the locally available materials. It was capable of reducing the moisture content of the cassava leaves from 70% (w.b.) to 14% (w.b.) in 60 h which was only 50% of the time required for drying in the direct sun. The efficiency of the solar air heater was 22%, and the rock bed energy storage was able to store 75.4 MJ/m^3 of thermal energy. The dryer was cheap and suitable for the rural areas.

Tiwari *et al.* (1994) presented a mathematical model of an indirect - type forced convection solar dryer coupled with a sensible heat storage and a solar air heater with a reflector. In this dryer, the energy storage material was located at the bottom of the drying chamber. Energy balance equations were developed for different components (solar air heater, energy storage, drying chamber, and product) of the dryer and solved analytically to optimise the design parameters. Analytical expressions for the solar air heater outlet temperature, the temperature of the storage material, and the crop were derived. They reported that the additional solar energy provided by the reflector reduced the drying time and the optimum drying air temperature could be obtained by adjusting the storage capacity.

Chuahan *et al.* (1996) developed a mathematical model of a batch - type deep bed coriander dryer integrated with a double - pass single glazing solar air heater and another double - pass single glazing solar air heater coupled with a mass of rock bed storage (rock diameter 4 cm) unit based on the mass and energy balance equations. The temperature of the air, grain, and rock beds, the instantaneous moisture content of the grain, and relative humidity of the air were estimated by solving the model in the finite difference method. The performance

of the dryer was evaluated for two operating modes. In the mode - 1, the coriander was dried in the daytime by the hot air produced in the air heater only without using the heat from the storage. In the second mode, the coriander was dried both in the sunshine and off - sunshine hours. The hot air produced by the air heater dried the product during the sunshine hours while in the off - sunshine hours, the hot air was supplied by the thermal storage charged by a separate air heater. They reported that the grain and air temperatures decreased with increasing depth of the grain bed. The temperature difference between the grain and the air decreased with advancing in drying time. The relative humidity of air increased with increase in the grain bed depth. The moisture content of the coriander was reduced from 28% (d.b.) to 11.4% (d.b.) in 27 cumulative sunshine hours operating the dryer in the mode - 1 while, it took 31 cumulative hours operating the dryer in the mode - 2.

El - Sebaii *et al.* (2002) developed and tested an indirect - type natural convection solar dryer with a solar air heater - cum - energy storage. The energy storage material (sand) was placed under the absorber plate of the air heater. The dryer was tested with and without the storage material by drying fruits (seedless grapes, figs, and apples) and vegetables (peas, tomatoes, and onion) in the temperature range of 45.5–55.5 °C. The products were dried with and without pre - treatment. The large size products were cut into small pieces before drying. They reported that the pre - treatment did not accelerate the drying rate of the large size products which were cut into small pieces. However, the pre - treatment affected the drying rate of the small size products. As it reduces the resistance of the outside membrane of the product to the moisture transfer. The author recommended that the large size product should be cut into small pieces and the small size products should be treated with chemicals before drying to enhance the drying rate.

Jain and Jain (2004) developed a transient analytical model of a deep bed grain (paddy) solar dryer to optimise the design parameters. The dryer had an inclined double cover multi - pass solar air heater with an in-built granite - grits bed thermal energy storage unit. The energy storage material was located under the absorber plate. The air was first passed in the space formed by the two glass covers of the air heater and then passed over the absorber plate. Eventually, the air left the heater flowing below the storage material. Energy balance equations were derived for each component and air stream of the air heater. Similarly, mass and energy balance equations were derived for the grain bed of the dryer. The model was solved for the climatic condition of Delhi (latitude 28°35 N, longitude 77°17 E) during October. The effect of the change in tilt angle, length and breadth of the air heater, and the mass flow rate on the temperature of the grain bed were studied. They reported that the grain temperature increased

with increase in the tilt angle of the solar air heater up to 30° which was the latitude angle of the place. The grain bed temperature increased with increase in the length of the heater from 2 m to 4 m. There was no change in the temperature beyond the length of 6 m. The grain bed temperature decreased with increase in the mass flow rate of air from 0.014 kg/s to 0.042 kg/s. Afterwards, there was a small change in the grain temperature. The drying rate and the efficiency increased with increase in the mass of the grain.

Jain (2005a) presented a mathematical model of a multi - tray mixed - mode - type solar dryer coupled with a multi - pass solar air heater with in-built granite grits sensible heat storage unit. The structure of the air heater of this dryer was the same as the air heater of the study of Jain and Jain, 2004. The model was also solved for the same climatic conditions. The performance of the dryer was evaluated assuming paddy as the model product. The effect of the tilt angle, length and breadth of the solar air heater, and the mass flow rate of air on the temperature of the crop were studied. The thin layer drying equation was used to determine the drying rate and the hourly reduction in the moisture content in different trays. The drying rate of the product at different trays was different, and the efficiency of the dryer increased with increase in the mass of the crop. The author reported that the optimum tilt angle, the length of the heater, and the mass flow rate were 30°, 4 m, and 0.028 kg/s, respectively.

Jain (2005b) developed a thermal model of a greenhouse - type solar dryer consisting of a roof - type greenhouse and a drying chamber integrated with a pebbles packed - bed sensible heat storage unit. In this dryer, the greenhouse worked as the solar air heater. The floor of the green house and a wall located between the green house and the drying chamber absorbed the solar radiation and the air inside the green house was heated up. The hot air was drawn from the green house by the blowers located on the wall and was supplied through the storage materials located just below the drying trays. The model was solved for the climatic conditions of Delhi during the month of May, and onion as model the drying product. The investigator studied the effect on the drying air temperature of the change in the length and breadth of the greenhouse and the mass flow rate. The investigator reported that a greenhouse of the size of 6 m × 4 m, a mass flow rate of 0.278 kg/s, and 0.25 m packed bed thickness were the optimum parameters for drying 2280 kg of onion in 24 h.

Aguilar - Castro *et al.* (2012) developed a mixed - mode type solar dryer with a sensible heat storage unit for drying plaster molds. The dryer consisted of a solar water heater, a water storage tank, a heat exchanger, and transparent walls drying chamber. In this system, the hot water produced by the heater was circulated through a heat exchanger and stored in the storage tank. The hot air required for the drying application was produced by supplying the air around

the heat exchanger tubes. Usually, the product was dried by the solar radiation transmitting through the walls of the drying chamber but in the case of inadequate solar radiation, the storage supplied the supplementary energy requirement. The drying time of the molds was reduced drastically while they were dried in the dryer. It took only 4 days in the dryer while in the direct sun drying, it took 2 - 3 weeks. The energy consumption was also lower than in the conventional dryer. They reported that solar energy was not utilised properly in the dryer leading to rise in the inner temperature of the drying chamber and plaster calcination. To avoid this, a cooling system was used resulting in additional energy consumption in the dryer.

Nabnean *et al*. (2016) designed a solar dryer integrated with a sensible heat storage unit for drying osmotically dehydrated cherry tomatoes. The dryer consisted of a solar water heater panel, a water - cum - thermal energy storage tank, a heat exchanger, two pumps, a blower, and a drying cabinet. In this drying system, the solar water heater produced hot water which was stored temporarily in the storage tank and then hot water from the storage was circulated by a pump through a heat exchanger coil located inside the drying cabinet. The blower supplied ambient air across the heat exchanger tubes to raise its temperature. It was eventually supplied to the drying chamber. Some percentage of the exhaust air of the drying chamber was recirculated. One hundred kg of cherry tomatoes was dried the dryer in the temperature varying between 30 °C and 65 °C. The moisture content of the product was reduced from 59–62% (w.b.) to the desired moisture content of 15% (w.b.) in 4 days. The authors evaluated the performance of the solar water heater and quality of the dried product and also carried out economic analysis. They reported that the colour of the product dried in the dryer was bright reddish brown while the natural sun dried product colour was light yellow brown. The thermal efficiency of the heater was in the range of 21–69% and the payback of the dryer was 1.37 years. The solar dried product dried faster than that of the natural sun dried product.

2.1.1.2 HSD with sensible heat storage and auxiliary heater

The sensible heat storages used in the solar dryers are the diurnal type and cannot supply energy requirement during inadequate sunshine for a longer period and a long bad weather. Therefore, a backup energy source is required in conjunction with solar energy to continue the drying operation during adverse weather and to maintain the desired temperature of the drying air. Amer *et al.* (2010) developed a solar dryer consisting of a solar air heater, a heat exchanger - cum - energy storage, an auxiliary heater, a fan, a water pump, and a drying chamber. The solar air heater, the heat exchanger, and the drying chamber were fabricated as a single unit. The heat exchanger was placed between the glaze and the absorber of the air heater, and the drying

chamber was located below the absorber plate. During the daytime, both the hot air and water were produced in the solar heater. The hot water was stored in the storage tank and was utilized in the night - time for producing the hot air required for the drying operation. The drying system had the provision of the recirculation of the exhaust air of the drying chamber and was tested by drying ripe banana. The average temperature of the air at the solar heater outlet was 54.3 °C, and the average hot water temperature at the end of the day in the storage was 40 °C. At the night - time, the water temperature was raised from 40 °C to 70 °C by an electric heater located inside the storage, and then it was circulated through the heat exchanger by the pump. The hot water produced drying air at a temperature of 50 °C during the night - time. The efficiencies of the drying system were 37.4% and 31.7% in the solar and hybrid modes, respectively.

Madhlopa and Ngwalo (2007) designed and constructed a passive solar dryer with a biomass backup heater. The biomass backup heater, an SHS, and a solar air heater were constructed as an integrated system. The solar air heater was placed at the top of the integrated system. The absorber plate of the heater was a thin concrete layer, below which a layer of the granite rocks of diameter 0.025 m was placed as the energy storage medium. The biomass backup heater was located below the layer of the storage material. The dryer was tested in three modes; solar, biomass, and solar - biomass modes by drying pineapples. They reported that the drying rate in the solar mode was slower than the other modes. But the pickup efficiency was high in this mode. The pickup efficiencies of the dryer were 20%, 15%, and 17% in the solar, biomass, and solar - biomass modes, respectively. The dryer could be operated satisfactorily irrespective of the weather condition although it had some problems like uneven drying and reverse thermo - syphoning through the chimney of the dryer during the night period. Therefore, the authors suggested that the hot flue gas of the biomass backup heater should be circulated around the solar chimney.

Leon and Kumar (2008) developed a hybrid solar - biomass dryer and tested it drying red chilli. The dryer consisted of an unglazed transpired solar air heater, a biomass gasifier stove, a heat exchanger, an energy storage unit of pebble bed, a mixing chamber, and two blowers. In the daytime, the ambient air was heated to 103.3 °C by the flue gas of the biomass gasifier stove and then passed through the pebble bed to store the thermal energy at an average temperature of 87 °C. The biomass stove was stopped when the energy storage was fully charged. The heat retained in the storage was retrieved during the night - time or inadequate solar radiation period for producing the drying air or to maintain the drying air temperature to the desired level during the shortfall in the daytime. The energy storage could supply the hot

air at the temperature of 60 ± 3 °C for about 18 h. During the daytime, the unglazed transpired solar air heater supplied the necessary hot air required for the drying operation. About 65% of the sun drying time was saved by drying the chilli in this dryer. The overall thermal efficiency of the drying system was 11.06%. The authors also evaluated the sensory quality (colour, texture, and aroma) of the dried product and found that the overall quality of the chilli dried in the solar - biomass dryer was better than that of the cabinet dryer and the open sun dried products. The dryer could be used for drying chilli in all weather conditions.

Hossain *et al.* (2008) tested a hybrid solar dryer composed of a solar air - cum - water heater with a reflector, a water storage tank with an electrical heater, and a drying chamber. A heat exchanger was placed between the absorber and the glaze of the solar heater. A pump circulated water from the water storage tank through the heat exchanger. During the daytime, both the hot air and water were produced in the solar heater. The energy stored in the hot water of the storage tank was used for producing the hot air required for continuing the drying operation during the night - time, and the deficit energy was supplied by the supplementary electric heater located in the storage. The dryer was operated in different modes by drying halves of tomatoes. The quality of the dried tomato was evaluated based on the colour and the content of Ascorbic acid, Lycopene, and total Flavonoids. They reported that the colour of the pre - treated tomato sample was better than that of the non - treated one. The pre - treatment also controlled the microbial growth partially. When the tomato was dried below 45 °C, the microbial infestation was observed. Therefore, they recommended drying tomatoes at or above 45 °C without pre - treatment. The pre - treatment of the tomato with 8 g/L of Sodium Meta - Bisulphite prevented the microbial growth completely at the low-temperature drying. The average efficiency of the drying system varied between 17% and 29%.

Fargali *et al.* (2008) developed a mathematical model of a hybrid solar drying system based on the energy balance principle. The drying system consisted of a flat plate solar water heater, a storage tank, a biogas fuel burner, and a PV system with battery, a heat exchanger, a control system, and a drying chamber. In this system, the hot water produced by the solar water heater was stored in the storage tank and the biogas burner maintained the water temperature to the desired value. The ambient air supplied by a fan was heated by the heat exchanger located at the entrance of the drying chamber through which the hot water was circulated. The electrical energy requirements for all the equipment was supplied by the PV module. However, the authors did not consider the PV array and the battery systems in the modelling.

Mohajer *et al.* (2013) tested a dual purpose drying and water heating system. The system consisted of a dual purpose solar heater, a drying chamber, an electrical heater attached

to the drying chamber, and a water storage tank. The system could produce hot air and water simultaneously and therefore, could be used for drying as well as for producing hot water. The electric heater located in the drying chamber enabled the dryer to operate in all weathers. They tested the dryer with and without operating the electric heater by drying parsley, dill, and coriander. When the dryer was tested without activating the electric heater, it produced the hot air and water at the maximum temperature of 44.3 °C at a flow rate of 0.021 kg/s and 60.3 °C at a flow rate of 0.001 kg/s, respectively. This system has the scope of domestic applications for drying and producing hot water.

Cipliene *et al.* (2015) developed a hybrid solar dryer for drying motherwort (Leonurus cardiaca L.). The drying system consisted of a solar air heater array of area 12 m^2, a solar flat plate water heater array of area 8 m^2, two drying chambers, a storage tank, a pump, a fan, a heat exchanger, and a mixing chamber. The motherwort was dried in the temperature varying between 30 °C and 45 °C. In this drying system, the solar air heater produced the hot air necessary for the drying operation during the daytime which was mixed with the ambient air in the mixing chamber to maintain the drying air temperature in the above temperature range. The energy required during the low solar radiation or off - sunshine hours was supplied by the hot water stored in the storage tank. The working fluid of the solar heater was glycol. The water in the storage tank was heated by the hot glycol of the heater. The product was dried in three stages. In the first stage, the raw product was dried with the ambient air in one of the drying chambers for 24 h. Then it was shifted to the other drying chamber where it was dried with the preheated air at an average temperature of 34.5±6.1 °C. Around 99.93 MJ of energy accumulated in the heat storage during the daytime which was sufficient to produce the drying air at a temperature of 30 °C for 11 h.

Ayyappan *et al.* (2016) developed a greenhouse dryer and tested the dryer with different sensible heat storage materials (rock, sand, and concrete) by drying copra. The heat storage materials maintained a high temperature inside the dryer above the ambient during the night - time. The difference between the ambient and dryer inside temperatures during the night - time was in the range of 2–2.5 °C, 3–4 °C and 5–6 °C with concrete, sand, and rock, respectively as the storage material. The drying time required to reduce the moisture content of the copra from 52% (w.b.) to 7% (w.b.) were 78 h, 66 h, and 53 h when the dryer was operated with the concrete, sand, and rock as the thermal energy storage material, respectively. It took 152 h in the direct sun. The overall thermal efficiencies of the dryer with the concrete, sand, and rock as the thermal energy storage materials were 9.5%, 11%, and 11.7%, respectively.

2.1.1.3 HSD with latent heat storage (LHS)

Recently, the solar dryers integrated with the LHS have received attention due to many advantages associated with it such as high energy storage capacity, dissipation of energy at nearly constant temperature, and low volume and mass. Devahastin and Pitaksuriyarat (2005) studied experimentally the viability of using a latent heat storage unit in the solar dryer. The experimental setup consisted of a compressor to supply air, an electric heater to produce hot air, and a latent heat storage unit. The latent heat storage unit was a vertical cylindrical vessel of acrylic. A U - shape copper tube attached with disc type fins was placed inside the vessel. The space between the tube and the vessel was filled with the paraffin wax of the melting temperature in the range of 35–54 °C. Air at a temperature of 70–90 °C was circulated through the tube during the charging process. The effect of the air velocity (1 m/s and 2 m/s) and the temperature on the charging and discharging characteristics of the LHS was studied. They reported that the charging time of the storage decreased with increase in the air temperature and the velocity. The air velocity did not affect the discharge time. The incorporation of the LHS saved 40% and 34% energy at the air velocity of 1 m/s and 2 m/s, respectively.

Shalaby and Bek (2014) designed and tested an indirect - type forced convection solar dryer composed of two solar air heaters, a drying chamber integrated with an LHS unit, and a blower. Two vertical cylindrical containers filled with paraffin wax of the melting temperature of 49 ^{o}C and thirty - two copper tubes embedded uniformly in the wax were used as the energy storage. The storage was placed at the bottom of the drying compartment. They tested the dryer with and without the storage by drying two medicinal plants; O. Basilicum and T. Neriifolia. The average temperature of the air at the inlet of the drying chamber with and without the PCM in the energy storage was 45 ^{o}C and 51 ^{o}C, respectively at the constant air flow rate of 0.089 kg/s. The accumulated heat released from the storage maintained the drying air temperature higher than the ambient temperature by 2.5–7.5 ^{o}C for 5 h after the sunset. In the initial first 4 h of operation of the dryer, the temperature of the air at the inlet of the drying chamber with the storage was less than without the storage. Afterwards, the drying air temperature was higher than without the PCM in the storage.

Shringi *et al.* (2014) developed a hybrid solar dryer consisting of a simultaneous charging and discharging PCM - based energy storage unit, an evacuated tube heat - pipe solar heater, and a drying chamber. The heat storage was charged by supplying a working fluid of the mixture of 60% of propylene glycol and 40% water heated in the heater of the temperature varying between 54 ^{o}C and 118 ^{o}C. The heat retained in the storage was recovered from the

storage by circulating air through a heat exchanger coil embedded in the PCM and the air temperature was raised to the values between 39 °C and 69 °C. Garlic cloves were dried in the dryer to study its drying kinetics and to evaluate the performance of the dryer in terms of the energy utilisation ratio and the exergy efficiency. They observed that the Midilli model was the most suitable model to describe the drying process of the garlic clove, and only falling rate drying period was visible in the drying process. The exergy efficiency was in the range of 5–55% in the first 3 h of the drying period without recirculation of the exhaust air. Thereafter, the exhaust air was recirculated in the dryer, and the exergy efficiency increased to between 67% and 88%.

Jain and Tewari (2015) developed a passive solar dryer integrated with a PCM based energy storage unit and tested the dryer by drying mint. The dryer consisted of a solar air heater, an energy storage system, a reflector, an in-built natural draft system, and a drying chamber. Forty - eight cylindrical tubes of length 0.75 m and 0.05 m in diameter filled with 48 kg of paraffin wax were positioned below the drying trays in the zigzag arrangement as the energy storage unit. For the natural draft system, the top of the drying chamber was fitted with a black absorber plate, and a toughened glass was placed above the absorber plate. A packed bed of PCM was placed below the absorber plate. In this drying system, the energy storage maintained the drying air temperature around 6 °C higher than the ambient temperature for 5–6 h after the sunset. The dryer was tested by drying pre - treated mint leaves, and it took 24 h to reduce the moisture content of 12 kg of mint leaves from 4.8 kg of water/kg of dry matter to 0.11 kg of water/kg of dry matter. They also carried out economic analysis and reported that the payback period of the dryer was 1.5 years.

Agrawal and Sarviya (2016) studied the heat transfer characteristics of the charging and discharging processes of a shell and tube latent heat storage unit designed for the purpose of applying in the solar dryer. They also investigated the effectiveness of the application of the heat storage unit in the drying process of sliced potato. The LHS unit was basically a shell and tube heat exchanger consisting of two concentric cylinders of the diameter of 0.127 m (shell diameter) and 0.025 m (tube diameter). The space between the shell and tube was filled with the paraffin wax of the melting temperature ranging from 41 °C to 55 °C. The hot air produced by an electric heater was supplied through the tube during the charging period, and the air at a temperature of 30 °C was supplied during the discharging period. The charging process was studied at different air temperatures (80, 85 and 90 °C) and at a fixed air flow rate. The discharging process was studied at different mass flow rates of air (0.0015, 0.0022 and 0.003 kg/s). They reported that the melting time of the wax decreased with increase in the heat

transfer fluid temperature. The charging time decreased by 9% and 16% with increase in the air temperature from 80 °C to 85 °C and from 85 °C to 90 °C, respectively. The discharging time decreased with increase in the mas flow rate of air. Higher discharge temperature was observed for the low mass flow rates of air. The air temperature was raised to between 35 °C and 47 °C for about 10 h at the mass flow rate of 0.003 kg/s during the discharging period. Sliced potato was dried in the dryer at different air flow rates. They reported that the drying rate of the potato was high at the low air velocity due to more energy recovery from the storage.

2.1.1.4 HSD with auxiliary energy source and LHS

Many researchers have developed solar dryers with both backup auxiliary heating unit and latent heat storage unit to provide flexibility in the operation of the dryers irrespective of the weather conditions. One advantage of having both the storage and the auxiliary heat source in a solar dryer is that during a short cloudy period, the energy requirement for the drying operation can be used from the storage without activating the auxiliary heat source. Cakmak and Yildiz (2011) developed a solar dryer attached to two different types of the solar air heater and dried seeded grape to study its kinetics of drying. One of the solar air heaters was integrated with a Calcium Chloride Hexahydrate - based latent heat storage unit which stored heat during the daytime, and the same was utilised to produce the hot air for drying after the sunset. The other solar air heater without the energy storage supplied the hot air to the drying chamber during the daytime. The accumulated heat of the storage helped in continuing the drying operation till 22:00 h. The seeded grape was treated with a potassium solution and dried in the dryer at different air velocities (0.5–1.5 m/s) and under the open sun. The moisture content of the grapes was reduced to 9% (d.b.) from the initial moisture content of 300% (d.b.) in 56 h and 200 h in the solar dryer and the open sun drying, respectively. The authors reported that the grape dried in a short period at the high velocity, and the drying rate was fast when the dryer was operated with the heater - cum - energy storage. The Midilli model suitably represented the kinetics of the drying process of the seeded grapes. They also determined the effective diffusivity which was in the range of $5.4 \times 10^{-10} - 1.35 \times 10^{-9}$ m^2/s.

Esakkimuthu *et al.* (2013) studied the feasibility of using an HS - 58 paraffin wax - based LHS unit in a solar dryer for storing surplus energy during the peak hours of sunshine. The energy storage was essentially a cylindrical shell. Large numbers of spherical balls filled with the wax were kept inside the shell, and the air was supplied through the shell. The charging and discharging characteristics of the storage unit were studied at different mass flow rates (0.05, 0.083, and 0.111 kg/s). During the charging period, the temperature of the air coming

out of a solar air heater was raised to 70 °C by an electric heater before supplying to the heat storage. The electric heater contributed 40% of the total energy. They reported that the ambient air at the mass flow rate of 0.055 kg/s was able to recover the maximum amount of heat from the storage, and the heat transfer was uniform at this flow rate during the charging and discharging processes.

Reyes *et al.* (2014) dried mushroom in a hybrid solar dryer consisting of a solar air heater, a PCM - based energy accumulator, an electric heater, and a blower. During the daytime, the ambient air was first heated in the solar air heater, and then the temperature was raised to 60 °C by the electric heater. The solar energy accumulator was basically a solar air heater. One hundred finned attached copper tubes and filled with 14 kg of paraffin wax of the melting temperature in the range of 58–60 °C were positioned above the absorber plate of the heater. The tubes were exposed to the sun rays transmitting through the cover plate of the heater. The heat available in the accumulator was sufficient to produce hot air at the temperature of 20 ^{o}C above the ambient for 2 h, and the necessary heat required for maintaining the air temperature at 60 °C was supplied by the electric heater. The incorporation of the accumulator saved 40–70% electrical energy. The dryer was tested by drying mushroom. They evaluated colour, shrinkage, and texture of the dried product and the performance of the drying system. The thermal efficiency of the solar air heater and the accumulator were in the range of 22–67% and 10–21%, respectively.

2.1.2 Solar dryer with auxiliary heat source

A large number of solar dryers with backup heating systems were developed to avoid discontinuation of the drying operation during the adverse weather and the night - time or to maintain drying air temperature at the desired value during insufficient solar radiation period. Sarsavadia (2007) developed an indirect - type forced convection solar dryer integrated with an electric backup heater for drying onion in the temperature range of 55–75 °C. The dryer had the provision of recirculating some percentage of the exhaust air. The recirculation of 90% of the exhaust air saved up to 70.7% of the total energy consumption for drying onion. The investigator observed that the percentage of the energy contributed by the solar air heater and the electric heater increased with increase in the mass flow rate, and decreased with increase in the drying air temperature. The author suggested that a dryer having an exhaust air recirculation provision should be operated with the maximum permissible temperature and the low air flow rate. The specific energy consumption for drying onion was in the range of 12.04–38.77 MJ/kg.

Bena and Fuller (2002) developed a direct - type natural convection solar dryer integrated with a biomass burner. The drying cabinet and the biomass - burner were developed as a single unit. It was mainly a brick chamber. The drying cabinet of the dryer covered with a transparent plastic sheet was placed on the top of the brick chamber that housed the biomass burner. The performance of the dryer was investigated by drying sliced pineapple. In the daytime, the pineapple was dried directly by the solar radiation, and during the night - time or inadequate solar radiation, the drying operation was continued by operating the biomass burner. They reported that the drying rate was not uniform in the dryer. In the daytime, the product of the top tray dried faster than the product of the bottom trays, and it was opposite at the night - time. The overall thermal efficiency of the dryer in the solar - biomass mode was 8.6%. In the solar mode, the thermal efficiency of the dryer was 22% while it was 6% in the biomass mode. The energy consumption in the biomass mode was four times higher than in the solar mode. The authors recommended increasing the number of the cover plates of the drying chamber, enlarging the flue gas diameter pipe of the biomass burner, and increasing the flue gas path inside the dryer to improve the overall performance of the dryer.

Prasad *et al.* (2006) developed and investigated the performance of a direct - type natural convection solar dryer integrated with a biomass backup heater by drying turmeric. The constructional feature of this dryer was almost the same as the dryer developed by Bena and Fuller (2002). The turmeric was dried in the dryer during the daytime by the solar radiation. The drying operation was continued during the night - time using the biomass backup heater. The turmeric treated in the boiling water dried faster than the untreated and the open sun dried products. The drying time of the turmeric varied between 36 h and 42 h in the solar dryer while in the natural sun drying, the product was dried in 266 h. The untreated turmeric contained more volatile oil than the treated and the sun dried products. The overall efficiency of the dryer was 28.6%. The authors concluded that turmeric should be dried without pre - treatment for better quality product. One disadvantage of this dryer was the low velocity of the drying air during the daytime which was in the range of 0.2–0.25 m/s.

Boughali *et al.* (2009) developed and tested an indirect - type natural convection solar dryer consisting of a single - pass solar air heater, an electric resistance heater with a temperature controller, and a drying chamber by drying sliced tomato. The drying system had a vertical cross flow drying chamber. The outlet of the air heater was connected to the top of the drying chamber having an electric heater. A fan located at the bottom of the drying chamber drew air through the air heater and across the electric heater coil in the downwards direction. The auxiliary heater was set to activate when the air heater outlet temperature became lower

than 50 °C. The experiment was carried out at different mass fluxes (0.04–0.08 kg/m^2-s). They reported that the air heater efficiency increased with increase in the mass flux of air until it reached the value of 0.056 kg/m^2-s. The energy consumption in the auxiliary heater increased with increase in the mass flow rate of air and decreasing solar heater outlet temperature. The drying time of the tomato decreased with increasing drying air temperature and velocity from 50 °C to 75 °C and from 1 m/s to 2 m/s, respectively. They observed that the tomato dried at the air temperature of 65 °C and the air velocity of 1.5 m/s had better colour and shape. The payback period of the dryer was 1.27 years. They conclude that when an auxiliary heater is used in combination with the solar air heater, the dryer should be operated at the minimum mass flow rate to reduce the auxiliary heater energy consumption.

Smitabhindu *et al.* (2008) developed a mathematical model of a solar dryer used for drying banana for optimising the size and the operating parameters of the dryer. It consisted of a solar air heater array, an LPG burner, a drying chamber, and a blower. In this drying system, the solar air heater produced the hot air necessary for the drying operation. In the case of the inadequate temperature of the drying air, the LPG burner supplied the supplementary heat and raised the temperature. Some portion of the exhaust air of the dryer could be recycled. The mathematical model was validated with the experimental results. They also developed an economic model to evaluate the annual drying cost. The objective of the optimisation was to reduce the drying cost per unit dried product. They reported that the optimum solar air heater area and the recycle factor for drying 250 kg of banana in the dryer were 26 m^2 and 90%, respectively.

Lokeswaran and Eswaramoorthy (2013) tested a natural convection semi - cylindrical shape solar greenhouse dryer having an area of 40 m^2 by drying coconut. It was integrated with a biomass backup heater. In this dryer, solar energy was the main source of energy, and the biomass burner was used during unavailability of solar energy. The performance of the dryer was investigated in the solar - biomass, greenhouse, and the biomass heater modes. They reported that the performance of the dryer in the solar - biomass mode was better than in the other modes**.** The coconut dried from the moisture content of 53.4% (w.b.) to 9.2% (w.b.) in 26 h, 30 h, 44 h, and 88 h in the biomass mode, solar - biomass mode, green house mode, and the direct sun, respectively. The biomass required in the solar - biomass mode was 50% less than in the biomass mode. The fluctuation in the temperature was the main shortcoming of this drying system because of the biomass heater. Therefore, the incorporation of a temperature control system could eliminate this problem.

Reyes *et al.* (2013) dried mushroom in a solar dryer consisting of a solar heater, an electric heater, and a centrifugal fan with the objective to quantify the quality parameters of the mushroom. The electric heater was used to raise the temperature of the air coming out of the air heater to a predetermined value of 50 °C or 60 °C. The operation of the dryer in the hybrid mode saved around 3.5–12.5% energy. They observed that the drying rate was not affected by the slice thickness during the first 90 min of the drying period. The drying rate increased with increase in the drying air temperature. The recirculation of the exhaust air reduced the drying time which was unexpected as the high humidity in the drying air reduces the moisture holding capacity. The authors reasoned that the high humidity reduced the collapse of the superficial cellular structures of the mushroom resulting in the removal of more moisture. They also carried out colour quality analysis and observed that the mushroom turned dark during drying. The overall thermal efficiency of the drying system was in the range of 3.5–11.5%.

Lopez - Vidana *et al.* (2013) tested a hybrid solar dryer consisting of a V - corrugated absorber plate solar air heater, an LPG burner, a drying chamber, and radial fans by drying tomato. The performance of the dryer was evaluated operating the dryers in three different modes; LPG heating mode (LPGH), LPG - solar heating mode (LPGSH), and solar heating mode (SH). In the LPGH mode, the energy requirement for producing the drying air in the temperature range between 55 °C and 60 °C was supplied by the LPG burner. In the hybrid mode, the air was first heated by the air heater, and the supplementary energy requirement for raising the drying air temperature to between 55 °C and 65 °C was provided by activating the LPG burner. The dryer was tested by drying blanched tomatoes. The investigators evaluated the performance of the air heater and found that the efficiency of the solar air heater increased with increase in the mass flow rate of air. The thermal efficiency of the heater varied from 11.4% to 38.2% with the change of mass flow rate from 0.038 kg/s to 0.434 kg/s. The efficiency of the dryer changed with progressing of the drying time. When the dryer was operated in the LPGH mode, the efficiency was high during the initial period (86%), and it reduced to 7% at the end of the drying period. The efficiency of the dryer in the solar and hybrid modes varied between 4% and 24% and between 8% and 71%, respectively. It was reported that around 20% fuel was saved by operating the dryer in the hybrid mode.

Sekyere *et al.* (2016) designed and developed a laboratory scale natural convection mixed - mode - type solar dryer. The dryer consisted of a solar simulator, an air heater with a black painted concrete absorber plate, a thin layer of pebbles, an electric resistance heater, and a transparent drying chamber. The pebble bed was placed just below the concrete layer. The electric heater was attached to the pebbles bed. The dryer was tested by drying treated

pineapples in four modes. In the mode - 1, solar energy was used during the daytime, and the backup heater was used in the night - time. In the mode - 2, the dryer was operated only with the electric resistance heater both in the daytime and the night - time. In the mode - 3, both solar energy and the electric heater were used in the daytime and in the mode - 4, only solar energy was used. The product dried in less time in the solar - backup heater hybrid mode. It took longer drying time in the solar mode.

2.1.3 Solar assisted heat pump dryer

Another class of the solar dryer which has received the attention of the researchers recently is the heat pump assisted solar dryer. Generally, a heat pump assisted solar drying system comprises of a vapour compression cycle (compressor, condenser, expansion valve, and evaporator or dehumidifier) unit along with the solar heater and the supplementary components. In the heat pump assisted solar dryer, both the sensible and latent heats can be recovered by condensing the moisture from the saturated air coming out of the drying chamber in the dehumidifier or the evaporator and then reheating the dehumidified air in the condenser. The heat pump assisted solar dryers are suitable for the low-temperature drying applications (Patel and Kaur, 2012) and have many advantages like high energy efficiency, improved drying at the low temperature due to low humidity, better quality dried product, etc. (Daghigh *et al.*, 2010, Fatouh *et al.*, 2006). In the solar assisted heat pump dryer, solar energy is utilised for either heating the dehumidified air in solar air heater or heating the working fluid of the heat pump. In the latter case, the hot air requirement for drying is generated by circulating the air through the condenser coil. Few solar assisted heat pump dryers were proposed with different configurations for drying agricultural products.

Chen *et al*. (2005) developed and tested a closed - loop solar dryer consisting of a 75 W photovoltaic module with two (DC 12V 100A) batteries and AC/DC converter, a transparent drying chamber, an electrical heater, a blower, and a refrigeration system. The PV module supplied the power requirements for all the equipment. The evaporator dehumidified the moist air coming out of the drying chamber, and the blower supplied the dehumidified air through the electric heater to raise the temperature to a pre - set value. The product was also exposed to the sun rays transmitted through the transparent walls of the drying chamber. The dryer was tested by drying lemon slices gradually increasing the temperature from 36 °C to 52 °C. The quality of the dried lemon was compared with the lemon dried in a conventional hot air dryer at a constant temperature of 60 ^{o}C and in the outdoor sun. They reported that the sensory quality of the lemon sliced dried in the dryer was better than the product dried in the other two modes.

Mortezapour *et al.* (2012) investigated the performance of a solar dryer integrated with a hybrid solar heater, a heat pump system, and an auxiliary heater by drying saffron. The hybrid solar heater which produced both the thermal and electrical energies was essentially a photovoltaic module. The hot and humid air coming out of the drying chamber was dehumidified and cooled in the evaporator. Then the air was circulated over both the surfaces of the PV panel and removed heat as well as cooled the surface. The hot air leaving the PV panel was further heated while passing through the condenser, and its desired temperature was maintained by an auxiliary heater located just before the drying chamber. The authors investigated the performance the dryer with and without operating the heat pump unit at different mass flow rates of air (0.008, 0.012 and 0.016 kg/s) and the drying air temperatures (40, 50 and 60 ^{o}C). The thermal and electrical efficiencies of the hybrid solar heater increased with increasing the mass flow rate of air. The maximum thermal and electrical efficiencies of the panel were 10.8% and 28%, respectively. The cold air circulation over the surface of the PV panel improved its efficiency. They reported that the drying time and the energy consumption decreased with increase in the mass flow rate of air and the drying air temperature. The application of the heat pump reduced energy consumption by 33%.

Sevik (2013a) designed and tested a solar dryer comprising a heat pump, a double - pass solar air heater, a PV panel, a drying chamber, and an automatic controller by drying sliced carrot. In this system, the ambient air supplied by a fan was heated in the solar air heater and then it was passed through the condenser coil of the heat pump unit. The air temperature was maintained between 49 °C and 51 °C close to the optimum drying air temperature of the carrot. The PV module provided the electrical energy requirement for the unit. The author determined only the thermal efficiency of the air heater which was around 71%. The overall performance of the dryer was not evaluated.

Sevik *et al.* (2013b) developed a heat pump assisted solar drying system for drying mushroom. The drying system consisted of a heat pump system, three solar air heaters connected in series, a water storage tank, a dehumidifier, a blower and two pumps, a control system, and a drying chamber. The evaporator of the heat pump was located in the water - cum - heat storage tank. The system could be operated in three modes. In the mode - 1, when the heater array produced the hot air at the required temperature for the drying operation, the heat pump was not operated, and the surplus energy was stored in the energy storage. In the mode - 2, the dehumidifier and the heat pump units were activated when the water temperature in the storage tank dropped below a specified value. The cold water was circulated through the dehumidifier coil and was heated up. In the mode - 3, the heat pump was activated when the

solar radiation was not sufficient. Mushrooms were dried in the air temperature range of 45–55 °C in the solar mode, heat pump mode, and the hybrid mode. The investigators reported that the drying time was different for different modes for the same drying air temperature and the energy utilisation ratio (It is defined as the ratio of the energy utilised during a drying process to the useful energy gained from the solar air heater.) was high at the beginning of the drying operation. The COP of the heat pump and the energy utilisation ratio of the dryer were in the range of 2.1–3.1, and 0.42–0.62, respectively.

Mohanraj (2014) developed a solar heat pump dryer for drying copra. It consisted of a heat pump system and a drying chamber. The components of the heat pump systems were a solar collector, an evaporator, condenser, liquid receiver, an evaporator with a fan and a control valve. During the daytime, the working fluid (glycol) of the heat pump was circulated through the collector to absorb solar energy. Then it was compressed by the compressor and passed through the condenser coil. A blower drew ambient air across the condenser coil where the temperature of the air was raised to 41–48 ^{o}C and then supplied to the drying chamber. During the off - sunshine hours, the working fluid was circulated through the evaporator coil located in the atmosphere, and the necessary heat for producing the hot drying air was taken from the ambient. The copra was dried in 40 h from the initial moisture content of 52% (w.b.) to the final moisture content of 9.2% (w.b.) in the above temperature range. The performance of the system was evaluated in terms of the COP and the specific moisture extraction rate (SMER). The COP of the hybrid system varied between 2.3 and 2.7. The maximum COP was recorded during the peak hour due to absorption of more solar energy. The SMER was 0.79 kg/kW h.

2.1.4 Overall observations

The previous research works on the hybrid solar dryer have been reviewed. The hybrid solar dryers are categorised according to the type of the thermal energy storage materials and the auxiliary heating systems employed in the dryer. It is observed that the sensible heat storage materials used in the solar dryer are rock, pebble, sand, and water. Mainly small size heat storage materials of the size ranging from 2.5 cm to 5 cm in diameter or length were used in the solar dyer (Table 2.1). The only fluid used as the heat storage liquid in the solar dryer was water. The application of water as the sensible heat storage fluid in the solar dryer has received attention recently because of its easy availability, high specific heat, and low cost. While water is used as the heat storage fluid, the solar water collector is used instead of the solar air heater.

Table - 2.1

Different sensible and latent heat storage materials used in the solar dryers.

Materials	**Size (diameter) /melting temperature**	**Reference**
Rock	3–5 cm	Garg *et al.* (1985)
Granite rock	3 cm	Ayensu and Asiedu - Bondzie (1986)
Rock	4 cm	Chauhan *et al.* (1996)
Clay, granite, sand	–	El - Sebaii *et al.* 2002
Granite grit	–	Jain and Jain (2004); Jain (2005a)
Pebbles	–	Jain (2005b)
Granite rock	2.5 cm	Madhlopa and Ngwalo (2007)
Paraffin wax	35–54 °C	Devahastin and Pitaksuriyarat (2005)
Paraffin wax	49 °C	Shalaby and Bek (2014)
Paraffin wax	41–55 °C	Agrawal and Sarviya (2016)
Calcium chloride Hexahydrate	-	Cakmak and Yildiz (2011)
Paraffin wax	58 °C	Esakkimuthu *et al.* (2013)
Paraffin wax	56–58 °C	Reyes *et al.* (2014)

The commonly used latent heat storage material in the solar dryer is the paraffin wax of different grades (having different melting temperatures). The melting temperature ranges from 35 °C to 58 °C (Table 2.1). The PCM of the LHS is charged directly by either the solar radiation or the hot working fluids (water, air, glycol, etc.). In the case of the direct charging, the PCM is filled in tubes or small containers which are placed above the absorber plate of the collector and exposed to the solar radiation. In the case of the indirect charging, the temperature of air or the other working fluids is raised by the solar heater, and then it is circulated through the tubes embedded in the PCM to charge it. Sometimes, the solar heater is used as a preheater. In this case, the hot fluid temperature is maintained at the pre - set value by an auxiliary heater before it passes through the storage during the charging period. In most solar dryers, the electric heater was used as the auxiliary heat source because of its easy installation and control. The application of biomass as the heat source in the solar dryer is limited. The main disadvantage of the biomass backup heater is the uneven heating and fluctuation in the air temperature.

Most hybrid dryers are complex systems having large numbers of components. It may involve large capital investment. However, a few economic studies were reported in the

literature. The commonly used working fluids in the solar dryers are air and water. The hot air produced by the air heaters or auxiliary heaters is used for removing the moisture from the product. Water is used as either heat storage fluid or an energy carrier from the solar heater to the storage. Few investigators used working fluid like glycol in the solar collector as an energy carrier to the storage materials. The performance of the natural convection hybrid solar dryer is affected by the inadequate mass flow rate of air. When the natural convection solar dryers are integrated with the biomass back - up heaters, the reverse thermo - syphoning is a major problem during the low-intensity solar radiation and the night - time. The heat pump assisted solar dryer is suitable for the low temperature drying applications and drying heat sensitive materials. Very limited studies on the heat pump assisted solar drying are reported in the literature.

2.2 Review on Drying Kinetics Studies of the Thin Layer Solar and Open Sun Drying Processes of Food and Agricultural Products

A large number of studies were reported on the thin layer drying kinetics analysis of food and agricultural products dried in the solar dryer and under the direct sun. Different types of food and agricultural products such as vegetables, spices, fruits, herbs and medicinal plants, and fishes were dried in different types of solar dryers and under the open sun.

2.2.1 Drying of vegetables and spices

Yaldyz and Ertekyn (2001) studied drying kinetics of some vegetables namely pumpkin, green pepper, stuffed pepper, green bean, and onion. The products were dried at different drying air velocities (0.5 m/s, 1m/s, and 1.5 m/s) in an indirect - type solar dryer consisting of a solar air heater with corrugated absorber plate and a drying chamber with an exhaust fan. The vegetables dried between 30.29 h and 90.43 h in the solar dryer and between 48.59 h and 121.8 h in the natural sun drying. All the products dried in the falling rate period. The investigators reported that the drying rate of the pumpkin was higher at the low air velocity (0.5 m/s) at the first 15 h of the drying period, and then it increased with increasing air velocity. The drying time of the green pepper (35.9–40.7 h) increased with increasing drying air velocity, and it was lowest at the air velocity of 0.5 m/s. The drying time of the stuffed pepper increased with increasing air velocity. It was 71.8 h at the air velocity of 0.5 m/s and 89.6 h at the velocity of 1.5 m/s. The drying rate was high at the air velocity of 0.5 m/s till 53 h. Thereafter, there was no improvement in the drying rate with the change in the air velocity. The green been dried in 67.8

h and 75.6 h at the drying air velocity of 0.5 m/s and 1.5 m/s, respectively. The drying rate was high at the velocity of 0.5 m/s during the first 15 h of the drying period, and afterwards, it increased at the high air velocity. However, the onion dried at the faster rate at the high velocity. The drying time was less at the high velocity, and it was 82.7 h at the velocity of 1.5 m/s and 90.43 h at the velocity of 0.5 m/s. The Diffusion model described the drying behaviour of the green pepper and the pumpkin, the Two - term model for the onion and the stuffed pepper, and the Page model for the green bean.

Borah *et al*. (2015) dried whole and sliced turmeric rhizomes in a solar conduction dryer to study its drying kinetics and to evaluate the performance of the dryer. They reported that turmeric rhizomes dried in the falling rate period. Only four thin layer drying models were tested to identify the best drying model, and the Page model was found to be suitably described the drying behaviour of the turmeric rhizomes. The drying rate of the sliced turmeric was faster than the whole turmeric in the first 6 h of the initial drying period. This was due to the free moisture content on the surface of the sliced turmeric resulting in the removal of more moisture. They also determined the effective moisture diffusivity which was 1.852×10^{-10} m^2/s and 1.456×10^{-10} m^2/s for the sliced and whole turmeric, respectively. The average thermal efficiency of the dryer was 55%.

Sacilik *et al*. (2006) dried organic tomatoes in a direct - type passive solar tunnel dryer to study its thin layer drying kinetics. The tomato was also dried in the direct sun to compare its drying time and the colour quality with product dried in the solar dryer. They evaluated the colour quality of the dried product in a Hunter lab colour difference meter and found that the colour quality of the product dried in the dryer was better than that of the sun drying one. The drying rate was high in the solar dryer, and 26.9% of the drying time was saved by drying the tomato in the solar dryer. The drying process occurred in the falling rate period, and the approximation of diffusion model was considered as the best model. The coefficients and the constants of the best model were expressed in terms of the temperature and the relative humidity of the drying air.

Akpinar and Bicer (2008) studied thin layer drying kinetics of long green peppers dried in the open sun and in a forced convection solar dryer. When the pepper was dried in the dryer in the air temperature range from 43.9 °C to 64.8 °C, the moisture content was reduced to 10% (d.b.) from its initial moisture content of 400% (d.b.) in 104 h. It took 152 h in the direct sun drying. To find out the most suitable drying model, thirteen thin layer drying models were tested. The authors reported that the Logarithmic model and the Midilli and Kucuk model were

the two most suitable drying models for describing the thin layer drying kinetics of the green pepper dried in the solar dryer and the open sun, respectively.

Tunde - Akintunde (2011) investigated the thin layer drying characteristics of treated and untreated solar and sun-dried chilli peppers. It was dried in a direct - type solar dryer in a mean drying air temperature of 45 °C. The chilli samples were blanched in water and steam and socked in an osmotic solution before drying. The drying time of the solar dried sample was in the range of 35 - 50 h while it varied between 45 h and 75 h in the direct sun. The pre-treated chilli samples dried at the faster rate compared with the untreated ones. Thus, pre - treatment reduces the resistance to the internal movement of moisture. The drying process occurred in the falling rate period, and the Page model yielded the best results for both the drying processes.

Lopez *et al.* (2014) carried out drying kinetics modelling of chickpea dried in a natural convection solar dryer consisting of a porous absorber plate solar air heater and a drying chamber. The moisture content of the chickpea was reduced to 0.02 kg water/kg (d.b.) from its initial moisture content of 0.52 kg water/kg dry mass (d.b.) in 40 h during April and 32 h during May. The high mass flow rate of air (0.0276 kg/s) occurred in the dryer during May compared to April (0.0228 kg/s.). Seven thin layers drying models were tested to identify the best model to describe the drying behaviour of the chickpea. Out of the seven models, the exponential model satisfactorily described the drying behaviour of the chickpea.

2.2.2 Drying of fruits

Akpinar (2008) investigated the drying kinetics of white mulberry dried in a forced convection solar dryer and the open sun with natural convection. The moisture content of the mulberry was reduced to 0.17 g water/g dry matter from the average initial moisture content of 4.55 g water/g dry matter in 104 h and 152 h in the solar dryer drying and the open sun drying, respectively. The drying process of the white mulberry took place in the falling rate period, and the Logarithmic and the Verma *et al*. models satisfactorily described the thin layer drying behaviour of the white mulberry. The investigator also determined the diffusivity coefficient which was 3.56×10^{-9} m^2/s and 2.4×10^{-9} m^2/s for the solar drying and the open sun drying, respectively.

Togrul and Pehlivan (2002) developed a mathematical model of the thin layer solar drying process of apricots dried in a forced convection solar dryer attached to a conical concentric solar air heater. The moisture content of the SO_2 pre - treated apricots was reduced to 18% (w.b.) from its initial moisture content of 77.8% (w.b.) in 68–78 h in the solar dryer while it took 112 h in the direct sun drying. The drying experiments were carried out at different

mass flow rates of drying air (50, 60 and 70 kg/h). The maximum drying air temperature (80 °C) was recorded at the air heater outlet at the mass flow rate of 50 kg/h. The drying process of the apricots took place in the falling rate period, and the Logarithmic model adequately described the drying process of the product. The investigators also obtained the relationship of the constants and the coefficient of the best model with the drying air temperature, velocity, and the relative humidity.

Yaldyz *et al.* (2001) studied the thin layer drying kinetics of pre - treated sultana grape and the effect of air velocity and the temperature on the drying kinetics. The drying experiments were carried out in the same dryer used by Yaldyz and Ertekyn (2001). The grapes were pre-treated in a mixture of potassium carbonate, olive oil, and water. The product was dried at different velocities of air (0.5, 1.0 and 1.5 m/s). The drying rate was high at the air velocity of 1 m/s compared to other velocities during the first 34 h of the drying period. Afterwards, the drying rate increased at the air velocity of 1.5 m/s. The experimental results showed that the drying process of the sultana grapes occurred in the falling rate period, and the two - term model satisfactorily described the drying behaviour of this product. The coefficients and the constants of the best model were expressed as the function of the drying air velocity.

Midilli and Kucuk (2003a) presented the mathematical modelling of the thin layer drying process of the shelled and unshelled pistachios. The pistachios were dried in a forced convection solar dryer at the drying air temperature ranging from 40 ºC to 60 °C in a fixed air velocity of 1.23 m/s and also in the direct sun. Eight thin layer drying models were applied to determine the best model for representing the drying kinetics of the pistachios. They reported that the Logarithmic model adequately represented the drying behaviour of the shelled and unshelled pistachios in the forced convection solar drying. For the natural sun drying, the Two - term model satisfactorily described the drying behaviour of both the shelled and unshelled pistachios. The investigators also expressed the constant and the coefficients of the suitable models in terms of the drying air temperature.

Lahsasni *et al.* (2004) studied thin layer drying characteristics of prickly pear peel dried in an indirect - type forced convection solar dryer integrated with an auxiliary heater. The effect of the drying air temperature and the mass flow rate on the drying rate of the product were investigated. The drying air temperature and the mass flow rate varied between 50 ^{o}C and 60 ^{o}C and 0.0277 m^3/s and 0.0833 m^3/s, respectively. The drying rate increased with increase in the drying air temperature and the mass flow rate, and the drying process of the prickly pear peel occurred in the falling period. The effect of the drying air temperature on the drying rate

was more than the mass flow rate. The Midilli - Kucuk model satisfactorily described the drying process of this product.

El - Beltagy *et al.* (2007) dried pre - treated strawberries of different shapes (whole, half, quarter and 3 mm discs) in an indirect - type active solar dryer to study its drying behaviour. They reported that the drying process of the strawberry comprised both the constant and falling rate periods. The drying time decreased with the change in the shape from whole, half, quarter to 3 mm discs. The chemical composition of the strawberry was not affected by the pre - treatment. The Newton or exponential model suitably described the drying process of the product.

Koua *et al.* (2009) investigated and modelled the thin layer drying behaviour of plantain banana, mango, and cassava dried in a direct - type natural convection solar dryer. The drying processes of all these products comprised of a short constant rate period followed by a long falling period. The Henderson and Pabis model adequately represented the drying behaviour of all the products. They also determined the effective diffusivity and observed that its value decreased with increase in the initial moisture content of the products. The effective diffusivities of the plantain banana, mango, and cassava varied from 1.44×10^{-9} to 1.30×10^{-9} m^2/s, 1.29×10^{-9} to 1.18×10^{-9} m^2/s, and1.23×10^{-9} to 1.59×10^{-9} m^2/s, respectively.

Dissa *et al.* (2011) determined the solar drying characteristic of two varieties of mangoes (Amelie and Brooks) dried in a direct - type passive solar dryer. They also estimated the effective diffusivity and the efficiency of the drying system and studied the effect of the tray position on the drying rate. The effective diffusivity did not change much with the varieties of mango but it decreased with advancing of the drying days. The tray positions significantly affected the drying rate and the effective diffusivity. Higher drying rate of the product was observed in the top tray which was exposed to the solar radiation. The thermal efficiency of the dryer decreased with progressing of the drying days. The Amelie variety dried more rapidly than the Brooks. The drying processes of these varieties of the mangoes comprised of a short constant rate period followed by a long falling rate period. The Two - term and the Approximations of the diffusion models accurately predicted the drying characteristics of the products.

Doymaz (2005) studied the open sun drying kinetics of figs. The figs were dried in the ambient temperature range from 35 ºC to 47 °C, and the moister content of the product was reduced to 25% (w.b.) from its initial moisture content of 74% (w.b.) in 80 h. The drying process of the figs occurred in the falling rate period. The Verma et al. model adequately

described the drying process of the figs, and the effective moisture diffusivity of this fruit was 2.47×10^{-10} m^2/s.

Togrul and Pehlivan (2004) studied the drying kinetics of apricot, grapes, figs, peaches, and plums dried in the direct sun in the ambient temperature range from 27 °C to 43 °C. The apricot was treated with SO_2 and $NaHSO_3$, and the remaining products were dried without pre-treatment. The pre - treated apricot dried faster than the other fruits, and the peach dried faster than the grape, fig, and plum. The drying processes of all the fruits took place in the falling rate period. The diffusion model was the best model to describe the drying processes of the SO_2 treated apricot and figs. The modified Henderson and Pabis model adequately described the drying processes of the apricot without pre - treatment, grapes, and plums, and the Verma et al. was the best model for the peaches.

2.2.3 Drying of herbs and medicinal plants

Akpinar (2006) investigated the thin layer direct sun drying behaviour of mint, parsley, and basil. The author reported that the drying processes of these aromatic plants took place in the falling rate period. Twelve thin layer drying models were tested to find out the best model. The modified Page model was the most suitable model for describing the thin layer drying behaviour of the mint and the basil leaves. For the parsley leaves, the Verma model was the best model. Effective moisture diffusivities for all the leaves were determined, and the values were found to be 7.04×10^{-12} m^2/s, 4.53×10^{-12} m^2/s, and 6.44×10^{-12} m^2/s for the mint, parsley, and the basil leaves, respectively.

El - Sebaii and Shalaby (2013) designed and fabricated an active solar dryer consisting of a double cover V - corrugated solar air heater, a blower, and a cross flow drying chamber. Mint and thymus leave were dried in the dryer at an average drying air temperature of 53.5 °C and a mass flow rate of 0.0223 kg/s to determine the best thin layer models representing the drying process of the products. The thymus and mint leave dried in 34 h and 5 h, respectively. They observed that the drying processes of both the products took place in the constant rate and falling rate periods. Generally, herbs and medicinal plants dry in the falling rate period. Therefore, the author suggested for further study at different mass flow rates of air and the drying air temperatures to verify its abnormal behaviour. The best model for describing the drying behaviour of the mint and thymus leaves were the Midilli and Kucuk model and the Page and modified Page model, respectively.

Mohamed *et al.* (2005) identified the best thin layer drying model for Citrus aurantium leaves. The experiments were performed in an indirect - type forced convection solar dryer.

The leaves were dried in the temperature range of 50–60 °C and the flow rate of air between 0.0277 m^3/s and 0.0833 m^3/s. The authors reported that only falling rate period was visible in the drying process of the Citrus aurantium leaves. The drying rate increased with increasing drying air temperature, and the highest value of the drying rate occurred at the drying air temperature of 60 °C and the mass flow rate of 0.0566 kg/s. The best model for describing the drying process of the Citrus aurantium leaves was the Midilli and Kucuk model. The coefficients and constants of this model were expressed in term of the drying air temperature.

Nourhene *et al.* (2008) studied the drying kinetics of four varieties of olive leaves (Chemlali, Chemchali, Zarrazi and Chetoui)) dried in a forced convection solar dryer. The leaves were dried at a constant mass flow rate of air (0.0556 m^3/s) but at different temperatures of drying air (40–60 °C). The drying air temperature affected the drying rate of the leaves. The drying rate increased with increase in the drying air temperature. They determined the appropriate model, the effective moisture diffusivity, and the activation energy of the drying processes of the leaves and observed that the drying processes of all the varieties of olive leaves took place in the falling rate period. The Page model was the most appropriate model to describe the drying process. The moisture diffusivity and the activation energy were in the range of 2.95×10^{-10}– 3.6×10^{-9} m^2/s and 51.52–83.6 kJ/mol, respectively.

Mohamed *et al.* (2008) investigated the effect on the thin layer drying kinetics of the Gelidium sesquipedale of the drying air temperature and the mass flow rate. The product was dried in a forced convection solar dryer at different drying air temperatures (40–60 °C) and flow rates (0.028–0.083 m^3/s). The results showed that the drying air temperature significantly affected the drying rate of the product. The drying time decreased with increasing drying air temperature. The effective moisture diffusivity increased with increase in the drying air temperature and the mass flow rate of air. The best model to describe the drying process of the Gelidium sesquipedale was the Two-term model, and the product dried in the falling rate period. The coefficients and the constants of the best model were expressed as a function of the drying air temperature.

Kane *et al.* (2008) studied the drying characteristics of Mexican tea leaves dried in an indirect - type forced convection solar dryer. The tea leaves were dried in the temperature range from 45 °C to 60 °C and the mass flow rates of air varying between 0.0227 m^3/s and 0.0556 m^3/s. They reported that the drying air temperature and the flow rate affected the drying rate of the tea leaves, and the drying rate increased with increase in the drying air temperature and the mass flow rate. The Mexican tea leaves dried in the falling rate period, and the Wang and Singh model was the best model for describing the drying process of this product. The investigators

also determined the effective diffusion coefficient and the activation energy at different drying air temperatures and the mass flow rates. The effective diffusion coefficient increased with increase in the drying air temperature and the mass flow rate. The authors reported from the visual inspection of the colour of the dried tea leaves that the optimum drying air temperature and the mass flow rate at which the colour and the texture were preserved, were 50 °C and 0.0227 m^3/s, respectively.

The authors Lahsasni *et al.*, 2004; Mohamed *et al.*, 2005; Nourhene *et al*., 2008; Mohamed *et al*., 2008; and Kane *et al*., 2008 used the same indirect - type forced convection solar dryer for drying different herbs and medicinal plants.

Varun and Sharma (2014) investigated the drying behaviour of fenugreek leaves dried in an indirect - type natural convection solar dryer and in the direct sun. The leaves were dried in the temperature range between 49.45 °C and 77 °C in the solar dryer. The product dried in the dryer in 50% less time in comparison with the sun drying. The drying process of the fenugreek leaves occurred in the falling rate period, and the Wang and Singh model was the best descriptive model for both the solar and the sun drying processes.

Sallam *et al.* (2015) studied the drying behaviour of whole mint plant dried in two separate solar dryers with different modes of air flow. Two identical direct and indirect solar dryers operating in both natural convection and forced convection modes were used to perform the study. The authors reported that the drying time of the mint plant in the direct type dryer was less than in the indirect one in the natural convection mode because of high temperature. The drying rate in the forced convection mode was higher than in the natural convection, and it was same for both the direct and indirect dryers. They attributed this cause to the same drying air temperature for both the dryers. The whole mint dried in the falling rate period. The Diffusion approach and the Verma et al. model were the two best models to describe the drying behaviour of the natural convection drying in both the dryers and the Verma et al. model was the best model for the forced convection. The effective diffusivity was also evaluated, and it was more in the forced convection mode.

Gulcimen *et al*. (2016) dried sweet basil in a forced convection solar dryer consisting of a solar air heater and a drying chamber. They studied the kinetics of the drying process of sweet basil and also the performance of the air heater by attaching fins with the absorber plate at different angles (30–60°) and mass flow rates (0.012–0.033 kg/s). It was reported that the highest efficiency of the air heater was obtained at an angle of 30°. The efficiency increased with increasing mass flow rate, and the maximum efficiency was 63% at the mass flow rate of 0.033 kg/s. The sweet basil was dried at different mass flow rates, and the drying time

decreased with increasing mass flow rate. The drying time varied from 425 min to 600 min with increasing mass flow rate from 0.012 kg/s to 0.033 kg/s. The Page model satisfactory described the drying process of the sweet basil. They also proposed a new model for the drying process of the sweet basil.

2.2.4 Drying of fish and other products

Chavan *et al.* (2008) presented mathematical modelling of the thin layer drying behaviour of the Indian mackerel dried in a hybrid solar - biomass dryer and in the direct sun. The natural convection solar dryer consisted of a solar air heater, a biomass heater, and a drying chamber. The biomass air heater was used during the night - time to produce the hot air required for continuing the drying operation after the sunset. The investigators also studied the sensory attributes of the dried fish including taste, texture, odour, appearance, and overall acceptability to evaluate the optimum drying conditions. They reported that the overall acceptability of the dried product increased with increase in the drying air temperature from 45 ^{o}C to 50 ^{o}C. The solar drying process took less time in comparison with the sun drying. The fish dried in 24 h in the solar dryer while it took 44 h in the sun drying. The drying process of the Indian mackerel occurred in the falling rate period. The Midilli and the Two - term models were the most suitable models to predict the drying process in the solar dryer drying and the open sun drying, respectively. In addition to the mathematical modelling, they also investigated the performance of the dryer and found that the overall thermal efficiency of the dryer was 6.3%. The efficiency was low due to the partial loading of the dryer.

Jain and Pathare (2007) studied the drying kinetics of the open sun drying of fish (prawn and chelwa fish) and observed that the drying processes of these fishes took place in the falling rate period, and the Logarithmic model best described the drying processes of both the fishes. The investigators also determined the effective moisture diffusivities which were 11.11×10^{-10} m^2/s and 8.708×10^{-11} m^2 /s for prawn and chelwa fish, respectively.

Usub *et al.* (2010) designed and developed a mixed - mode - type solar tunnel dryer consisting of a flat plate air heater with a thermal energy storage, a tunnel dryer unit, and blower and studied the drying behaviour of silkworm pupae. The product was dried at different air flow rates (0.21–0.53 kg/s) and temperatures (33–45 ^{o}C). The colour, lipid, and fatty acid contents of the solar dried sample were compared with the sun dried one. The colour of the sample dried in the solar dryer was better than that of the sun dried one, and the optimum mass flow rate for better quality colour for the solar drying process was 0.32 kg/s. The fatty acid and

lipid contents did not change much in the solar dried product as compared with the sun dried one. Both the constant rate and the falling rate periods were observed in the drying process of the silkworm pupae, and the constant rate drying period was quite long. They stated that the Midilli - Kucuk model precisely represented the drying behaviour of the silkworm pupae, and the coefficients and constants of this model were expressed as a function of the drying air temperature, relative humidity, and the mass flow rate.

2.2.5 Overall observations

Numerous studies on the modelling of the thin layer drying processes of food and agricultural products in the solar dryer and under the open sun were reported. The distribution of the works performed on different products is shown in Fig. 2.1. The highest studied product is fruits (35.5%) followed by herbs and medicinal plants (29.03%) and vegetables and spices (25.8%). The study on the other products like fish, meat, etc. is limited. There is no information about the thin layer solar drying study of the meat.

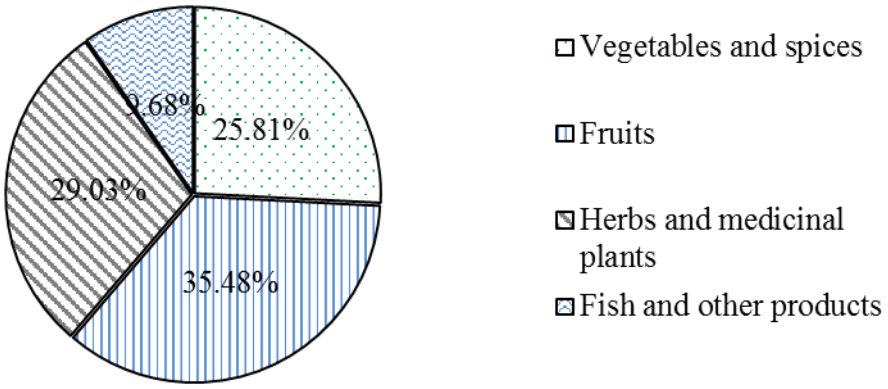

Fig. 2.1 Distribution of the studies on the thin layer solar and sun drying processes of food and agricultural products.

In most experiments, the products were dried at the drying air temperatures range from 35 ^{o}C to 60 ^{o}C. The maximum temperature of the drying air reported was 80 ^{o}C, and Togrul and Pehlivan (2002) dried apricot using concentric solar air heater at this temperature. The drying process of vegetables and herbs occurred in the falling rate period apart from the mint and thymus leaves. El - Sebaii and Shalaby (2013) found that the mint and thymus leaves dried both in the falling rate and constant rate periods. The authors were doubtful about their findings as the drying behaviour of these two products were unusual and, therefore, suggested further study to verify whether the two leaves dry in the constant rate period or not. Both the constant

rate and falling rate periods were observed in the drying process of mango, strawberry, cassava, and banana. The drying process of the studied remaining fruits took place in the falling rate period only. The drying process of fishes also occurred in the falling rate period. Therefore, the diffusion process controls the drying process of the many products. In addition to the study of identifying the appropriate model, a few investigators also estimated the effective moisture diffusivity coefficient of some of the products, and it was varied between 10.26×10^{11} m^2/s and 3.6×10^{-9} m^2/s. Experimental uncertainty analysis was performed by a few authors (Akpinar 2008; Shringi *et al*., 2014; Akpinar and Bicer, 2008) which is only 9.67% of the cited works, although it should be considered in the modelling and the analysis of the thin layer drying process (Kucuk *et al*., 2014). The study on the effects of the drying air temperature, mass flow rate, and relative humidity on the drying kinetics are limited.

It is observed from this review that dryers should be operated at the optimum operating conditions to obtain high-quality product and to reduce energy consumption. The too low temperature in the beginning of the drying operation causes the growth of microorganisms before drying is complete. Too high temperature and low humidity bring about surface hardening of the products which prevents the moisture diffusion (Boughali *et al*., 2009). The pre - treated product dried in a shorter period in comparison with the non - treated one, and it also prevents the growth of microorganism during the drying period. Therefore, products should be treated before drying. The large size products should be cut into small size to enhance the drying rate as well as to reduce the drying time. Solar drying is faster than the open sun drying. All the types of solar dryers were used to study the drying characteristics of the vegetables, fruits, herbs and medicinal plants, and other products. The drying air velocity affects the drying rate of different stages of the drying period, and therefore, a dryer should be operated at the optimum drying air velocity to reduce the electrical energy consumption in the forced convection solar dryer.

2.3 Energy and Exergy Analyses of the Solar Drying Process

Effective use of energy resources in a thermal system can be ascertained by the energy and exergy analyses based on the first law and the second law of thermodynamics, respectively. Nowadays, the exergy analysis along with the energy analysis has become a powerful tool in the optimisation of the complex thermodynamic systems. The energy analysis deals with only the quantity of energy and makes only energy balance of a system. It cannot make any difference of the heat available at different temperatures or other energy sources (Nag, 2001). The quantity of heat available at different temperatures may be the same but the quality is not.

The heat available at the high temperature has the high quality in comparison with the heat available at the low temperature.

The exergy analysis or the second law analysis deals with the quality of energy, irreversibility, and the entropy generation. It can measure the quality of energy and quantifies the wasted work potential. The exergy analysis provides more realistic views of a thermodynamic process. It determines the causes and magnitude of irreversibility in any thermodynamics process (Saidur *et al*., 2010) and identifies the locations, causes, and sources of deviations of the actual process from the ideal one (Rosen and Dincer, 2003). Thus, the energy analysis identifies the quantity of the wastage energy in a drying system while the exergy analysis determines the quality of that energy and gives information about the potential for the utilization of the wastage energy. Therefore, the energy and exergy analyses are widely used by the researchers for the thermodynamic analysis of the thermal systems.

Drying is an energy intensive operation as the latent heat of evaporation is required for evaporating the moisture from the materials to be dried (Aghbashlo, 2013; Kudra, 2004). Therefore, the drying system should be operated energy efficiently to reduce energy cost as well as to reduce environmental impact. These factors place the emphasis on the better design of the new dryer, improvement in the design of the existing dryers, good operational practice, and the utilisation of the renewable energy sources as much as in the drying process. Many investigators applied energy and exergy analyses in the performance evaluation of the solar drying systems or the solar drying process of different agricultural products. Large numbers of studies have been performed on the exergy analysis of the solar drying process of different agricultural products.

2.3.1 Review on energy and exergy analyses of the solar drying process

Many studies were reported in the literature on the energy and exergy analyses of the solar drying process of agricultural products. The studies undertaken by many investigators have been reviewed in this part of the chapter. Midilli and Kucuk (2003b) performed energy and exergy analyses of the drying process of the shelled and unshelled pistachios dried in an indirect - type forced convection solar dryer integrated with an auxiliary heater. The shelled and the unshelled pistachios were placed in two separate shelves and were dried in a cross flow drying chamber with the drying air temperature varied between 34 ºC and 82 ºC. They reported that the unshelled pistachios consumed more energy than the shelled pistachios. The energy utilisation (EUR) was also high in the case of the unshelled pistachios (0–34.8%) compared with the shelled pistachios (0–24.9%). The author reasoned that the EUR of the unshelled

pistachios was high due to the structure and more moisture content of the product. The exergy inflow to the drying chamber increased with increase in the solar radiation intensity. The exergy loss was more and the EUR was high in the case of the unshelled pistachio drying. The exergy efficiency of the shelled pistachios and the unshelled pistachios varied between 27.84% and 100% and 10.86% and 100%, respectively.

Celma and Cuadros (2009) developed a laboratory scale solar dryer consisting of a solar air heater, a drying chamber, and an optional operating fan. The dryer was operated in the natural convection mode to obtain the data for the energy and exergy analyses of the drying process of the olive mill wastewater. The authors reported that the EUR was high on the 2nd day of the drying process (0–30.08%) compared with the 1st day (0–22.06%). The exergy inflow to the drying chamber varied with the change in solar radiation intensity. The exergy losses increased linearly with increase in the EUR. Most of the exergy loss occurred during the 2nd day of the drying process of the product. The exergy loss varied between 53.24% and 100% in the first day and 34.4% and 100% in the second day. The exergy efficiency showed decaying behaviour with increased in the inlet temperature of the drying chamber.

Ozgener and Ozgener (2009) performed energy and exergy analyses of a passive solar greenhouse dryer. The investigators conducted the experiment in the temperature range from 40 ºC to 49.9 ºC and velocity range from 0.1 m/s to 0.3 m/s. It was reported that the greenhouse temperature and the solar radiation affected the drying rate of the product. The average exergy efficiency of the drying process was in the range of 63–73%. The exergy efficiency was affected by the greenhouse inside temperature, relative humidity, and the solar radiation intensity. The exergy efficiency decreased with increase in the mass flow rate as it consumed more energy.

Akpinar (2010) investigated the thin layer drying kinetics of mint leaves and also performed energy and exergy analyses of the drying process of the product. The mint leaves were dried in the temperature range 51.5 ºC and 66.3 ºC in a forced convection indirect - type solar dryer consisting of a solar air heater and a drying cabinet. The author reported that the EUR varied between 7.8% and 46.3%. It decreased with increase in the drying time. The exergy efficiency was in the range of 34.7–87.7%. The exergy efficiency increased with increase in drying time. When the exergy efficiency increased, the EUR decreased.

Akbulut and Durmus (2010) performed energy and exergy analyses of the thin layer drying process of mulberry dried in a forced convection indirect - type solar dryer. The investigators reported that the EUR ratio decreased with increase in the drying time. It was less on the 2nd day (27.1–45.4%) compared with the first day (15.9–89.3%) for the mass flow rate

of 0.002 kg/s. They also reported that the EUR decreased with increase in the mass flow rate of air. The average value of EUR varied between 55.2% and 20.15% when the mass flow rate of air was varied between 0.014 kg/s and 0.036 kg/s, respectively. The exergy loss increased with increase in the mass flow rate of air. The exergy efficiency ranged from 21.3% to 93.3 %.

Chowdhury *et al.* (2011) dried Jackfruit leather in a solar tunnel dryer and performed energy and exergy analyses on the experimental data. The drying system consisted of a solar air heater, a transparent drying unit, and fans with photovoltaic module. The investigators dried 50 kg of jackfruit leather and found that the overall efficiency of the dryer varied between 39.2% and 48.1%. They also estimated the energy and the exergy efficiencies of the solar air heater which were in the range of 27.5–42.5% and 32–69%, respectively. It was reported that the exergy inflow of the solar air heater increased with increase in the solar radiation. The average exergy efficiency of the dryer was 41.4%.

Sami *et al.* (2011) developed a mathematical model of an indirect - type forced convection solar dryer based on the energy and exergy analyses assuming chilli as the model product. The authors investigated the energy and exergy performances of the solar air heater and the drying chamber. It was reported that the difference between the exergy inflow and outflow of the drying chamber decreased with increase in the drying days. Less amount of exergy was destroyed in the 2^{nd} day in comparison with the 1^{st} day. The exergy inflow of the drying chamber was more during the first few hours (till 12:00 h of every day) and then showed a decreasing behaviour. The exergy efficiency of the drying chamber in the 2^{nd} day was more compared with the 1^{st} day. They also studied the effect of some parameters on the exergy inflow and exergy efficiency of the solar air heater. The exergy inflow of the solar air heater increased with increase in the length of the heater but it decreased with increase in mass flow rate of air.

Boulemtafes - Boukadoum and Benzaoui (2011) performed energy and exergy analyses of the solar drying process of mint in an indirect - type natural convection solar dryer. The investigators reported that there was a linear relationship between the exergy loss and the EUR. The highest exergy loss occurred in the 2^{nd} day of the drying operation.

Lamnatou *et al.* (2012) carried out energy and exergy analyses of a solar dryer integrated with an evacuated tube solar air heater. Investigators dried apples, carrot, and apricots in the dryer and identified the suitable drying model for each product. They also evaluated the EUR at different velocities ranging from 0.3 m/s to 0.9 m/s and found that the EUR increased with increase in the mass of the product samples. They stated that the low EUR indicated partial loading of the dryer. The experiment was carried out without loading the dryer fully. It was loaded with only 220–440 g of the products. The EUR of the carrot drying process

was 20% (sample mass 220 g) and 60% (sample mass 440 g) and the corresponding pick - up efficiencies were only 2% and 5%. The exergy loss increased with increase in the EUR. The apples were dried at different velocities (0.3, 06 and 0.9 m/s). The EURs of the apple drying process were 21%, 44%, and 24% at the air velocity of 0.3, 0.6, and 0.9 m/s, respectively. The pick - up efficiency was high at the low air velocity than the high velocity of air. The lowest exergy loss took place at the low air velocity.

Fudholi *et al.* (2014a) investigated the performance of a forced convection indirect - type solar dryer by drying 40 kg of red chilli. The dryer consisted of a panel of finned absorber double pass solar air heater, a blower, an auxiliary heater, and a cross flow drying chamber. The red chilli was dried in 33 h (5 d) from the initial moisture content of 80% (w.b.) to the final moisture content of 10% (w.b.) in the drying air varied between 28 ºC and 55 ºC. The efficiency of the solar heater varied between 11% and 74% at the mass flow rate of 0.07 kg/s. The overall thermal efficiency of the drying system, pick - up efficiency (Pick-up efficiency determines the efficiency of moisture removal of the drying air from the product. It defined as the ratio of the moisture picked up by the air in the drying chamber to the theoretical capacity of the air to absorb moisture.), and the specific energy consumption were 12.7%, 44.9%, and 5.3 kW h/kg, respectively. They reported that the exergy efficiency varied between 43% and 97%.

Fudholi *et al.* (2014b) carried out energy and exergy analyses of the drying process of the red seaweed and also carried out kinetics analysis of the drying process of the product. The investigators dried 40 kg of red seaweed from the initial moisture content of 94.6% (w.b.) to the final moisture content of 10% (w.b.) in 15 h in the drying air temperature range from 35–60 °C. They reported that the efficiency of the solar air heater varied from 26% to 80% with an average of 35%. The thermal efficiency of the drying system and the pick - up efficiency were 27% and 95%, respectively. The specific energy consumption was 2.62 kW h/kg, and the exergy was in the range of 1−93%.

Fudholi *et al.* (2015) carried out performance analysis of a forced convection indirect type solar dryer by drying palm oil fronds. The investigators loaded the dryer with 100 kg of the palm oil fronds and estimated the efficiency of the solar air heater, system drying efficiency, pick - up efficiency, specific moisture extraction ratio, exergy losses, and exergy efficiency. The auxiliary heater was not used during the drying operation. The efficiency of the air heater varied from 9% to 48% with an average of 31%. They reported that the efficiency of the solar air heater increased with decrease in the intensity of the solar radiation. The overall drying efficiency, the pick - up efficiency, and the average exergy efficiency were 19%, 67%, and 47%, respectively.

Fudholi *et al.* (2016) dried salted Jewfish in a hybrid solar dryer consisting of a diesel burner, fans, photovoltaic plate, and a solar air heater. 51 kg of fish was dried in the dryer at an average drying air temperature of 50 ºC and a mass flow rate of 0.0778 kg/s. The authors studied the drying kinetics of the fish and also performed energy and exergy analyses of its drying process. Specific energy consumption (2.92 kg/kW h) and average exergy efficiency (31 %) were evaluated. The investigators did not mention whether the diesel burner was used during the drying experiment or not.

Mokhtarian *et al.* (2016) carried out exergy analysis of the drying process of pistachio in a solar dryer with and without exhaust air recirculation. The drying system consisted of porous absorber plate solar air heater, fan, and a drying chamber. There were two solar air heaters in the drying system. One was used to produce the hot air required for drying the product, and the other one was used to heat the exhaust of the dryer before recirculating in the drying chamber. The product was dried by three methods. In the method - 1, the exhaust air of the drying chamber was recirculated when the outlet air relative humidity dropped to $\leq 15\%$. In the method - II and III, the product was dried by the air heated in the air heater without recirculation and in the sun, respectively. They reported that the drying time of the pistachio was reduced with the recirculation of the exhaust air. The average pickup efficiency (40%) and average exergy efficiency (50%) were also high with the recirculation. It was 1.8 times more than without the recirculation. The energy utilisation ratio was also high in the case of the method - 1. Eventually, they concluded that the solar dryer with the recirculation was more effective in comparison with the drying system without recirculation and the sun drying process.

2.3.2 Overall observations

Energy and exergy analyses are becoming a very important tool in the thermodynamics analysis of the drying system. It has been used by many researchers to investigate the performance of the solar dryers. The common drying system performance parameters used by the researchers are specific energy consumption, energy utilisation ratio, the energy efficiency of the drying system, pickup efficiency, and exergy efficiency. The EUR and the exergy efficiency are the two most widely used performance parameters in the drying system (Table 2.2).

These parameters show opposite trends with the progressing of the drying time. Lower EUR indicates lower utilisation of the supplied energy. The exergy efficiency increases with decrease in the EUR. The EUR decreases with the progress of the drying time while the exergy efficiency increases with increase in the drying time.

Table 2.2

Energy and exergy analyses of the solar drying process undertaken by different researchers.

Type of dryer	Product	Efficiency (%)	EUR	Pick-up efficiency (%)	SPEC kWh/kg	Exergy Efficiency %	Ref.
FC - IDT - with auxiliary heater	Shelled Pistachio	-	0–24	-	-	27.8–100	Midilli and Kucuk (2003b)
	Unshelled pistachios	-	0–34.8	-	-	10.9–100	
NC - IDT	Olive mill wastewater	-	0–30.1	-	-	34.4–100	Celma and Cuadros (2009)
NC - GHD	NA	-	-	-	-	63–73	Ozgener and Ozgener (2009)
FC - IDT	Mint leaves	-	7.8–46.3	-	-	34.7–87.7	Akpinar (2010)
FC - IDT	Mulberry		20.2–55.2			21.3–93.3	Akbulut and Durmus (2010)
FC - IDT	Jackfruit leather	42.47		-	-	41.4 (avg.)	Chowdhury *et al.* (2011)
FC - IDT	Apples	-	21–44	-	-	-	Lamnatou *et al.* (2012)
	Carrot		20–60	2–5	-	-	
FC - IDT - with auxiliary heater	Red chilli	12.7	-	44.9	5.26	43–97	Fudholi *et al.* (2014a)
FC - IDT - with auxiliary heater	Red seaweed	27.1	-	97	2.62	1–93	Fudholi *et al.* (2014b)
FC - IDT with latent heat storage	Coriander	-	-	-	-	67–88	Shringi *et al.* (2014)
FC - IDT - with auxiliary heater	Palm oil fronds	19	-	67	-	10–70	Fudholi *et al.* (2015)
FC - IDT	Salted Jewish fish	23–41	-	-	-	17–44	Fudholi *et al.* (2016)

NC - IDT = Natural convection - indirect type; NC - GHD = Natural convection - green house dryer; FC - IDT = Forced convection - indirect type

With the elapse of the drying time, the moisture content of the dried product decreases, hence more energy is available in the exhaust of the drying chamber resulting in higher exergy efficiency.

The loading of the drying chamber, the inlet temperature, and the mass flow rate of the drying air also affect the EUR and the exergy efficiency. Partial loading of the dryer causes low EUR. The exergy loss increases with increase in air velocity. Therefore, the meticulous planning of the recirculation of the exhaust air in the drying chamber and the optimum loading and the mass flow rate can maximise the utilisation of input energy.

The structure and the moisture contents of the products greatly affect the energy consumption in the drying process. The product with shell consumes more energy than the product without the shell. In addition, the solar air heater plays an important role in the overall efficiency of the drying system. To maximise the utilisation of the available solar energy in the solar dryer, it is necessary to use high-efficiency solar air heater.

2.4 Research Gaps and Objective

A comprehensive review of the development of the hybrid solar dryer, the kinetics analysis of the thin layer solar and sun drying processes of the food and agricultural products, and the energy and exergy analyses of the solar drying process has been carried out. The recent studies on the hybrid solar dryer have focussed on the application of the latent heat storage as the thermal energy storage in the solar dryer. The heat pump assisted solar drying is another growing area of study on the solar drying. The incorporation of the energy storages, auxiliary heaters, and the heat pump into the solar dryer provide operational flexibility of the solar dryer irrespective of the weather conditions.

Large numbers of studies on the thin layer solar and sun drying processes of the food agricultural products and the mathematical modelling were reported in the literature. The highest study product is the fruit (35.5%) followed by the herb (29%) and the vegetable (25.8%). The remaining percentage is the fish and other products. No study was reported on the thin layer drying process of the meet. The food and agricultural products can be dried in the solar dryer in the temperature range between 35 °C and 60 °C. A high quality dried product can be obtained by drying the food and agricultural products in the solar dryer in contrast to the open sun drying. Although a great deal of efforts has been made to develop the solar dryers for drying food and agricultural products, the following areas still demand the attention of the researchers.

- The paraffin wax was the widely applied latent heat storage material in the solar dryer. The application of the other phase change materials in the solar dryer need to be investigated.
- Most works reported on the solar dryer were experimental in nature. The future direction of study in the solar dryer lies in the development of the mathematical model of the existing dryers, optimization of operating parameters, and the economic study.
- The application of the software packages such as COMSOL multi - physics, ANSYS, and FLUENT in the simulation of the hybrid solar dryers are very limited.
- The thin layer kinetics studies of the solar dried products like fish, meat, and some other products are still unexplored. Limited information is available about the modelling of the thin layer drying process of the products dried in the solar dryers with the energy storage and the heat pump assisted solar dryers.
- The main disadvantage of the natural convection solar dryer is the low air velocity and the reverse thermo - syphoning during the night - time when it is operated with the biomass heater. Therefore, further investigation is required to improve this drawback.
- It is observed from the literature review of the exergy analysis of the solar drying system that many investigators presented exergy analysis of the drying processes of the agricultural products dried mainly in the indirect - type forced convection solar dryer. Complete exergy analysis of the solar drying system integrated with the auxiliary heat sources and the thermal energy storage are not reported in the literature.
- The exergy analysis of the heat pump assisted solar dryer and the mixed - mode type solar dryer was also not reported in the literature.
- Most works focused only on the exergy analysis of the drying process. The detailed exergy analysis of the system including the components needs to be carried out.

In addition to these general research gaps, it has been observed that

- The thin layer kinetics and energy and exergy analyses of the dying process of Ghost chilli are not reported in the literature.
- The studies on the exergy analysis of the solar drying system focused only on the exergy analysis of the drying chamber and the drying process of a specific product,
- The drying of chilli in a solar dryer integrated with a latent heat storage unit is not reported in the literature.
- The detailed energy and exergy analyses of the solar dryer integrated with latent heat storage have not been performed by the researchers.

Therefore, the main objective of this study is to develop a forced convection solar dryer integrated with a paraffin wax based latent heat storage module to dry some of the valuable agricultural products available in the subtropical climate of the North - Eastern region of India. The following are the sub - objectives of the present study;

- **Kinetics studies of the solar and sun drying processes of the Ghost chilli:** In this study, the kinetics of the drying process of the Ghost chilli will be studied by drying it in the solar dryer and the open sun. The best drying models representing the drying process of the Ghost chilli in the solar dryer and the sun drying will be identified applying non - linear curve fitting.

- **Energy and exergy analyses of the drying processes of the Ghost chilli and the sliced ginger:** In this part of this study, Ghost chilli and sliced ginger will be dried in the solar dryer without energy storage. Then, energy and exergy analyses of the drying process of the two products will be performed with the experimental data.

- **Performance investigation of the complete drying system with thermal energy storage:** The solar dryer with thermal energy storage will be tested by drying red and green chilli. The energy and exergy efficiencies of each component of the solar dryer will be evaluated by energy and exergy analyses.

- **Economics analysis:** In the economic analysis, the cost of drying per kg of dried product in the solar dryer will be compared with the electric dryer by annualized cost method.

Chapter - 3

Design of the Solar Dryer with Thermal Energy Storage

3.1 Developed Solar Dryer

The major components of the solar dryer developed in this study are solar air heater, a paraffin wax - based latent heat storage module, a drying chamber, and a blower. It is a forced convection - type hybrid solar dryer. The mass and energy flow diagram of the dryer is shown in Fig. 3.1. Two forms of energy are used to run this drying system; they are solar energy and electrical energy. Solar energy is the main source of energy. The electrical energy is used to run the blower which circulates air through the different components of the drying system. The solar air heater produces the hot air required for drying the agricultural product by harvesting solar energy. The hot air is then passed through the thermal energy storage where some part of the heat is transferred to the storage material from the air during the charging period, and the remaining heat is used in the drying chamber. During the discharging period or the low and off - sunshine periods, the accumulated heat is released from the storage material to the air flowing through the thermal energy storage. The air is then supplied to the drying chamber by the blower where heat is transferred from the air to the agricultural product, and the moisture is transferred from the product to the air. Eventually, the air leaves the drying system in a moist condition.

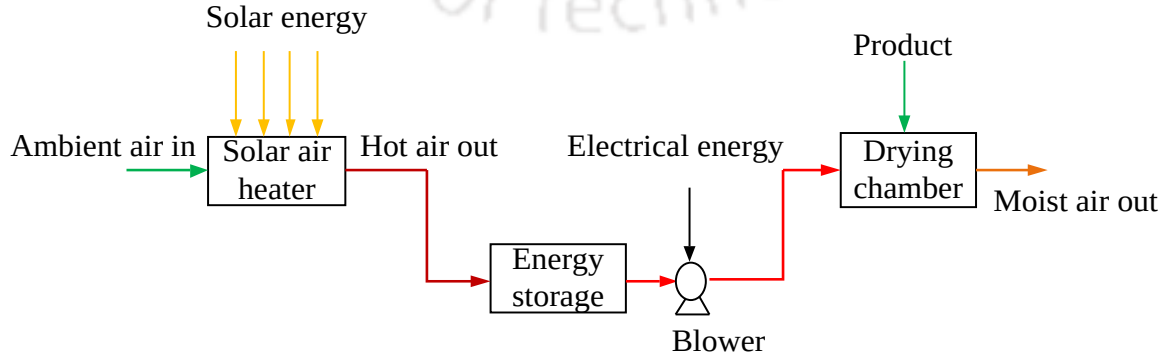

Fig. 3.1 Mass and energy flow diagram of the developed solar dryer.

The drying process in the solar dryer is basically a convective drying. The energy requirement for removing the moisture from the materials is supplied by the hot air. Therefore, the basic design calculations include the estimation of the energy and air flow requirements of the drying system. The components of the drying system are then sized based on the energy and air flow requirements.

3.2 Estimation of Energy and Air Flow Requirements

The quantity of the energy and air flow requirements depends on the quantity of the moisture to be removed from the agricultural product under the specified conditions. These parameters can be determined by the energy balance equation as well as from the principle of the Psychrometry. The quantity of the moisture (m_v) to be removed during drying is given by Eq. (3.1) (Ayensu and Asiedu - Bondzie, 1986).

$$m_v = \frac{m_p\left(M_i - M_f\right)}{\left(100 - M_f\right)} \tag{3.1}$$

where (m_p) is the mass of the product, M_i is the initial moisture content on wet basis (w.b.), and M_f is the final moisture content (w.b.), both in percentage.

The moisture content of any product on wet basis and dry basis in percentage can be obtained by Eqs. (3.2) and (3.3), respectively (Keey,1992).

$$M_{wb} = \frac{m_{ip} - m_{drp}}{m_{ip}} \times 100 \tag{3.2}$$

$$M_{db} = \frac{m_{ip} - m_{drp}}{m_{drp}} \times 100 \tag{3.3}$$

where m_{ip} is the initial mass of the product, and m_{drp} is the dry mass of the product.

The relation between the wet basis and dry basis moisture contents is expressed as follows

$$M_{wb} = \frac{M_{db}}{100 + M_{db}} \tag{3.4}$$

The quantity of the energy required to evaporate m_v kg of moisture can be determined by

$$Q_v = m_v h_{fg} \tag{3.5}$$

The latent heat of evaporation of water (h_{fg}) can be determined employing Eq. (3.6) and it is to be increased by a factor of 10 – 20% because of the bound moisture (Forson *et al.*, 2007).

$$h_{fg} = R_v T_{cr} T_{bp} \ln\left(\frac{P_{cr}}{10^5}\right) \frac{\left(T_{cr} - T_p\right)^{0.38}}{\left(T_{cr} - T_{bp}\right)^{1.38}} \tag{3.6}$$

where is the R_v gas constant for water vapour, T_{cr} and P_{cr} are the critical temperature and pressure of water at the atmospheric condition, respectively and T_{bp} is the boiling point of water at the atmospheric condition.

The average temperature of the product (T_p) can be determined as (Forson *et al.*, 2007).

$$T_p = 0.25\left(3T_{id} + T_{amb}\right) \tag{3.7}$$

where T_{id} is the drying air temperature, and T_{amb} is the ambient temperature.

The quantity of air required for the drying operation can be determined from the psychrometric chart as well as from the energy balance equation if the equilibrium moisture content is known for a given drying air condition (Sharma *et al.*, 1986). If the ambient air is heated from a state (A) to a state (B) as shown in Fig. 3.2, the dry bulb temperature of the air increases, and the relative humidity of air decreases. When the drying air at the temperature of T_{id} and the relative humidity of Rh_{id} passes through the drying materials, the relative and specific humidities of the air increase until the equilibrium state (C) is reached. The moisture content of the product at that state is known as the equilibrium moisture content. If w_i is the specific humidity of air at the beginning of the drying process, and w_f is the specific humidity air corresponding to the equilibrium condition. The total mass of drying air (m_{da}) is calculated with Eq. (3.8).

$$m_{da} = \frac{m_v}{w_f - w_i} \tag{3.8}$$

If T_{od} is the dry bulb temperature of the air corresponding to the equilibrium state C, then the total amount of drying air (m_{da}) required for evaporating of m_v kg of moisture can be determined from the energy balance equation Eq. (3.9).

$$Q_v = m_{da} C_{pa} \left(T_{id} - T_{od} \right) \tag{3.9}$$

where C_{pa} is the specific heat of humid air, and it is expressed as follows. Eq. 3.9 allows to calculate (Q_v) required, once m_{da} is known.

$$C_{pa} = 1.005 + 1.88w \tag{3.10}$$

where w denotes the specific humidity of air.

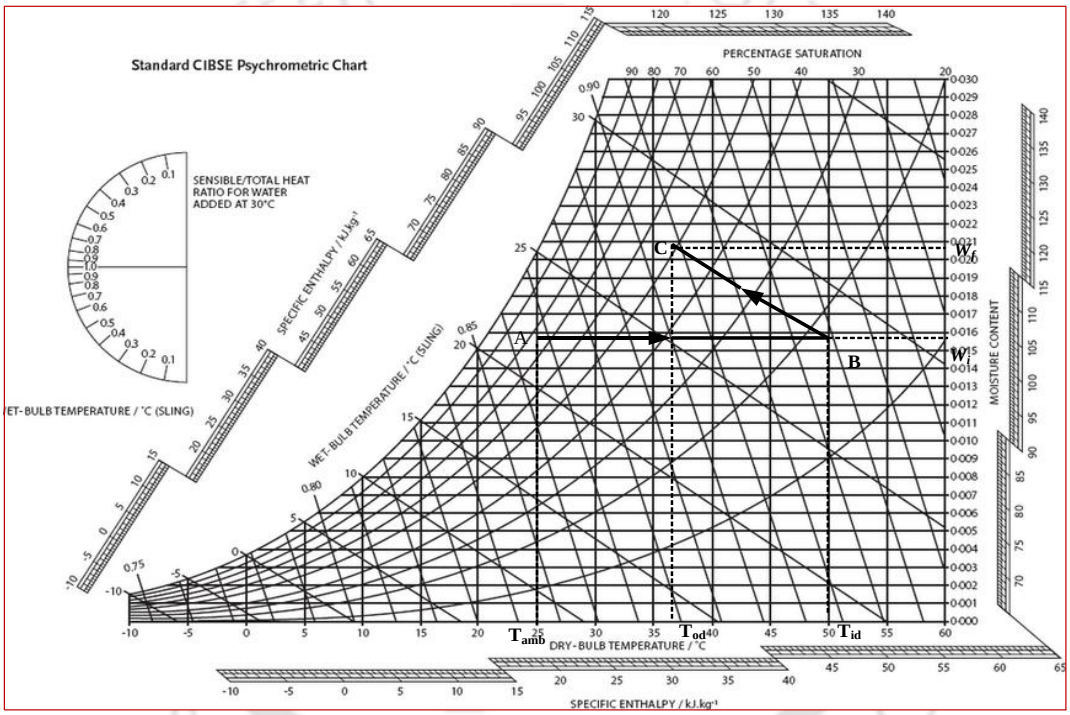

AB = Sensible heating process; BC = Adiabatic drying process

Fig. 3.2 Sensible heating and theoretical drying processes in the psychrometric chart.

3.2.1 Drying of chilli

The hybrid dryer is expected to be used for drying some of the high-value agricultural products of the North - Eastern region of India. The initial design of the dryer is made for drying chilli. The primary information necessary for estimating the energy and air flow requirements are the total mass of the product, the initial and final moisture contents of the product, and the total drying time. The initial moisture content of chilli varies between 87.5% (w.b.) and 88.9% (w.b.). The final moisture content or safe storage moisture content varies from 4.8% (w.b) to 9

% (w.b.) (Hossain and Bala, 2002). The drying time depends on the drying air temperature, mass flow rate, velocity, and the relative humidity. The size, shape, and the inner structure of the product also affect the drying time. However, these factors are not considered during sizing of the components of the drying system. The components are sized completely based on the simple energy and air flow requirements.

The following assumptions are made for estimating the energy and air flow requirements.

- The average initial moisture content of the chilli is 88% (w.b.).
- The desired final moisture content is 9% (w.b.).
- The outlet air temperature of the solar air heater varies throughout the day due to variation in the solar radiation. However, an average value of the drying air temperature is assumed which is equal to 50 °C.
- The average ambient temperature and the relative humidity of the place where the dryer is to be located are assumed to be 25 °C and 75%, respectively.

When the ambient air at 25 °C and 75% relative humidity is heated to 50 °C, the relative humidity is reduced to 17% at the constant specific humidity of 0.01509 kg of water vapour per kg of dry air (from psychrometric chart) as shown in Fig. 3.2. The specific heat of the humid air is 1.03 kJ/kg-K. The amount of the moisture to be removed from 10 kg of chilli while reducing the initial moisture content of 88% (w.b.) to the final moisture content of 9% (w.b.) is 8.7 kg. The average temperature of the product is 43.8 °C. Substituting the value of $T_{cr} =$ 647.5 K, $P_{cr} = 221.2$ bar, $T_{bw} = 373$ K, and $R_w = 461$ J/kg-K in Eq. (3.6) and increasing by a factor of 1.15, the latent heat of evaporation is found to be 2.7 MJ/kg which is almost equal to the typical value 2.72 MJ (Ayensu and Asiedu - Bondzie, 1986). The amount of the heat required for the evaporation of 8.7 kg of water is 23.6 MJ.

The equilibrium relative humidity of the red chilli on the dry basis can be suitably predicted with the modified Oswin desorption isotherm model (Kaleemullah and Kailappan, 2004). The modified Oswin model is expressed as follows.

$$Rh_e = \frac{1}{\left[\left\{(A + BT_{id})/M_e\right\}^C + 1\right]} \tag{3.11}$$

where A, B, and C are the dimensionless coefficients, Rh_e is the relative humidity in decimal, M_e is the equilibrium moisture content (d.b.), and T_{id} is the drying air temperature in °C.

$A = 19.299$

$B = -0.19449$

$C = 1.517$

If the equilibrium moisture content is 10% (d.b.), and the drying air temperature is 50 ºC, then the relative humidity of the drying air at the equilibrium condition is found to be 51.6%. The specific humidity and the dry bulb temperature corresponding to the relative humidity of 51.6% are 0.0205 kg of vapour/kg of dry air and 37 ºC, respectively. Substituting the value $w_i = 0.01509$ of water vapour per kg of dry air and $w_f = 0.0205$ of water vapour per kg of dry air in Eq. (3.8), the total mass of air required to remove 8.7 kg of moisture from the chilli is found to be 1608 kg.

Table 3.1

Summary of the basic design calculations.

Parameters	**Value**
Type of product	Chilli
Initial moisture content	88% (w.b.)
Desired final moisture content	9% (w.b.)
Initial mass of the product	10 kg
Expected drying time	42 h
Average drying air temperature	50 ºC
Ambient air temperature and relative humidity	25 ºC and 75%
Mass of water to be removed	8.7 kg
Total energy requirement	23.6 MJ
Total mass flow of air	1763 kg
Mass flow rate of air	0.012 kg/s

The total mass of air can also be determined from the energy balance equation as given below.

$$m_v h_{fg} = m_{da} C_{pa} \left(T_{id} - T_{od} \right) \tag{3.12}$$

Applying Eq. (3.12) for $T_{od} = 37$ ºC and $T_{id} = 50$ ºC the total mass of air is found to be 1763 kg which is almost similar to the total mass of the air estimated using the psychrometric chart.

The drying time of the chilli dried in different types of solar dryer varied from 32 h to 55 h (Leon and Kumar, 2008; Banout *et al*, 2011; Akintunde, 2011; Fudholi *et al*. 2014a). The size of the other components of the drying system depends on the mass flow rate of air. The air flow rate also affects the energy requirement. The energy requirement increases with increase in the air flow rate and decreases with increase in the drying air temperature (Sarsavadia, 2007). The higher is the mass flow rate, the larger is the size of the component. Therefore, assuming an average value of the drying time of 42 h and the total mass flow of the air of 1763 kg, the mass flow rate of air is found to be 42 kg/h. The summary of the basic design calculations is given in Table. 3.1.

3.3 Solar Air Heater

Solar energy is the main source of energy in the developed dryer. The energy requirement of the dryer is supplied solely from solar energy apart from the electrical energy used for running the blower. The energy requirements for drying and storing in the heat storage have to be supplied by the solar air heater during the sunshine hours of the day. Therefore, proper selection of the size of the solar air heater is crucial to get the required quantity of the heat energy. The size of the solar air heater for a given application depends on the solar radiation intensity, efficiency, and the energy requirement. The efficiency of the solar air heater is affected by many parameters such as mass flow rate of air, the length of the heater, and inlet air temperature. Therefore, to get the accurate size of the air heater, the parametric study of the air heater is carried out at the required conditions of the drying system.

3.3.1 Thermal Analysis of the Solar Air Heater

The solar air heater chosen for this drying system is two - pass or double pass - type. In this type of the solar air heater, the air is first passed between the cover and absorber plates and then passed under the absorber plate as shown in Fig. 3.3. The efficiency of this type of air heater is 10 to 15% higher than that of the conventional air heater (Sukhatme and Nayak, 2010). It does not incur any additional cost. Thermal analysis of the solar air heater is carried out to predict the outlet temperature and the efficiency of the air heater. The following assumptions are made for the thermal analysis of the solar air heater.

- The flow is steady.
- The temperature of the wall of the duct is assumed to be uniform but not same for each wall.

- The fluid temperature is assumed to be uniform throughout the cross section.
- Side losses are neglected.

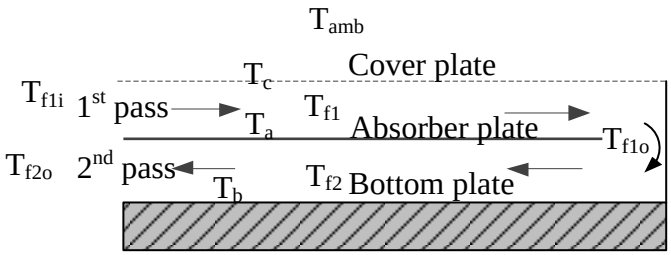

Fig. 3.3 Schematic diagram of the double pass solar air heater.

Here, T_{amb} = ambient temperature,

T_c = average temperature of the cover plate,

T_{f1i} = temperate of fluid (air) at the inlet of the first fluid pass,

T_{f1} = average temperature of the first fluid pass,

T_{f1o} = temperature of fluid at the outlet of the first fluid pass,

T_a = average temperature of the absorber plate,

T_{f2} = average temperature of fluid in the second fluid pass,

T_b = average temperature of the bottom plate, and

T_{f2o} = temperature of fluid at the outlet of the second fluid pass

The steady state heat flux balances on various components of the air heater are discussed below.

(a) Cover plate

The steady state heat flux balance of the cover plate is shown in Fig. 3.4.

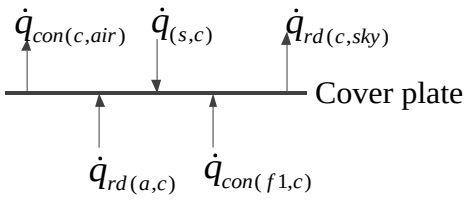

Fig. 3.4 The steady state heat flux balance of the cover plate.

The steady state heat flux balance equation for the cover plate can be written as

$$\dot{q}_{(s,c)} + \dot{q}_{rd(a,c)} + \dot{q}_{con(f1,c)} = \dot{q}_{con(c,air)} + \dot{q}_{rd(c,sky)} \tag{3.13}$$

The solar radiation absorbed by the cover plate is

$$\dot{q}_{(s,c)} = \alpha_c I \tag{3.14}$$

where I is the solar radiation intensity, and α_c is the absorptivity of the cover plate.
The radiative heat transfer between the absorber and cover plates is

$$\dot{q}_{rd(a,c)} = h_{rd(a,c)} \left(T_a - T_c\right) \tag{3.15}$$

where $h_{rd(a,c)}$denotes the convective heat transfer coefficient between the air and the cover plate. The radiation heat transfer coefficient is given by

$$h_{rd(a,c)} = \frac{\sigma}{\frac{1}{\varepsilon_a} + \frac{1}{\varepsilon_c}} \left(T_a^3 + T_c^3\right)\left(T_a + T_c\right) \tag{3.16}$$

where α_a represents the absorptivity of the absorber plate, ε_a and ε_c are the emissivities of the absorber and cover plates, respectively, and σ represents the Stefan-Boltzmann constant.
The heat loss at the top of the air heater due to convection and radiation is given by

$$\dot{q}_{con(c,air)} + \dot{q}_{rd(c,sky)} = U_t \left(T_c - T_{amb}\right) \tag{3.17}$$

The convective heat transfer between the fluid in the first fluid pass and the top cover is

$$\dot{q}_{con(f1,c)} = h_{con(f1,c)} \left(T_{f1} - T_c\right) \tag{3.18}$$

The convective heat transfer coefficient is

$$h_{con(f1,c)} = \frac{Nuk_f}{D_{hr}} \tag{3.19}$$

where Nu is the Nusselt number, k_f is the thermal conductivity of the fluid, and D_{hr} is the hydraulic diameter of the fluid pass.
The Nusselt number is computed from the following relation (Sukhatme and Nayak, 2010).

$$Nu = 0.158\,\mathrm{Re}^{0.8} \tag{3.20}$$

where Re denotes the Reynolds number.

The hydraulic diameters of the rectangular duct formed by the cover and absorber plates and the absorber and the base plates are obtained by Eqs. (3.21) and (3.22), respectively.

$$D_{hr(c,a)} = \frac{4D_{(c,a)}Y}{2(D_{(c,a)} + Y)} \tag{3.21}$$

$$D_{hr(a,b)} = \frac{4D_{(a,b)}Y}{2(D_{(a,b)} + Y)} \tag{3.22}$$

where $D_{(c,a)}$ is the distance between the cover and absorber plates, $D_{(a,b)}$ is the distance between the absorber and base plates, and Y is the width of the rectangular duct.

The overall top loss coefficient is computed according to

$$U_t = h_{wi} + h_{r(c,sky)} \tag{3.23}$$

The convective heat transfer coefficient due to wind is computed as (McAdams, 1954)

$$h_{wi} = 5.7 + 3.8v_{wi} \tag{3.24}$$

where v_{wi} is the velocity of the wind.

The radiation heat transfer coefficient between the cover plate and the sky is (Duffie and Beckman, 2006).

$$h_{rd(c,sky)} = \varepsilon_c \sigma \frac{(T_c^2 + T_{sky}^2)(T_c^2 - T_{sky}^2)}{(T_c - T_{amb})} \tag{3.25}$$

The sky temperature is given by the empirical relation (Garg and Prakash, 2006).

$$T_{sky} = T_{amb} - 6 \tag{3.26}$$

Substituting Eqs. (3.14), (3.15), (3.17) and (3.18) into Eq. (3.13) results in

$$\alpha_c I + h_{rd(a,c)}\left(T_a - T_c\right) + h_{con(f1,c)}\left(T_{f1} - T_c\right) = U_t\left(T_c - T_{amb}\right) \tag{3.27}$$

(b) First pass of fluid

Figure 3.5 shows the steady state heat flux balance of the first fluid pass. The steady state heat flux balance is given by the following equation.

$$\dot{q}_{f1} + \dot{q}_{con(f1,c)} = \dot{q}_{con(a,f1)} \tag{3.28}$$

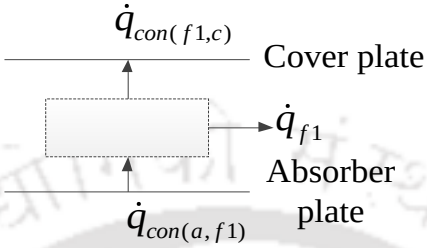

Fig. 3.5 The steady state heat flux balance of the first pass of fluid.

The net heat transfer to the fluid in the first pass (Ong, 1995)

$$\dot{q}_{f1} = \frac{2\dot{m}_{f1}C_{f1}\left(T_{f1} - T_{f1i}\right)}{Yl_{SAH}} \tag{3.29}$$

$$N_1 = \frac{2\dot{m}_{f1}C_{f1}}{Yl_{SAH}} \tag{3.30}$$

where $\dot{m}_{f1}$ is the mass flow rate of fluid in the first fluid pass, C_{f1} is the specific heat of fluid at constant pressure, and l is the length of the heater.

The convective heat transfer between the absorber plate and the first fluid pass is

$$\dot{q}_{con(a,f1)} = h_{con(a,f1)}\left(T_a - T_{f1}\right) \tag{3.31}$$

The convective heat transfer between the fluid in the first pass and the cover plate and between the fluid in the first pass and the absorber plate is assumed to be equal.

$$h_{con(f1,c)} = h_{con(a,f1)} \tag{3.32}$$

Inserting Eqs. (3.18), (3.29–3.31) into Eq. (3.28), the following relation yields

$$N_1\left(T_{f1} - T_{f1i}\right) + h_{con(f1,c)}\left(T_{f1} - T_c\right) = h_{con(a,f1)}\left(T_a - T_{f1}\right) \tag{3.33}$$

(c) Absorber plate

Figure 3.6 exhibits the steady state heat flux balance of the absorber plate. The steady state heat flux balance equation for the absorber plate is given by Eq. (3.34)

$$\dot{q}_{(s,a)} = \dot{q}_{con(a,f1)} + \dot{q}_{rd(a,c)} + \dot{q}_{con(a,f2)} + \dot{q}_{rd(a,b)} \tag{3.34}$$

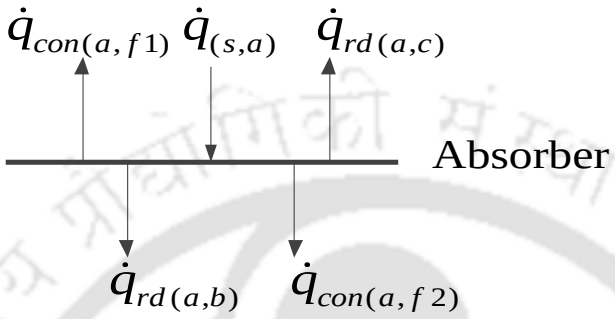

Fig. 3.6 The steady state heat flux balance of the absorber plate.

The incident solar radiation absorbed by the absorber plate is given as follows

$$\dot{q}_{(s,a)} = \alpha_a \tau_c I \tag{3.35}$$

where α_c is the absorptivity of the absorber plate, and τ_c is the transmissivity of the cover plate. The convective heat transfer between the absorber plate and the second pass of fluid is

$$\dot{q}_{con(a,f2)} = h_{con(a,f2)}\left(T_a - T_{f2}\right) \tag{3.36}$$

The radiation heat transfer between the absorber plate and the bottom plate is

$$\dot{q}_{rd(a,b)} = h_{rd(a,b)}\left(T_a - T_b\right) \tag{3.37}$$

The radiation heat transfer coefficient between the absorber plate and the bottom plate is

$$h_{rd(a,b)} = \frac{\sigma}{\frac{1}{\varepsilon_a} + \frac{1}{\varepsilon_b}}\left(T_a^3 + T_b^3\right)\left(T_a + T_b\right) \tag{3.38}$$

Substituting Eqs. (3.15), (3.31), (3.35–3.38) into Eq. (3.34) results in

$$\alpha_a \tau_c I = h_{con(a,f1)}\left(T_a - T_{f1}\right) + h_{rd(a,c)}\left(T_a - T_c\right) + h_{con(a,f2)}\left(T_a - T_{f2}\right) + h_{rd(a,b)}\left(T_a - T_b\right) \tag{3.39}$$

(d) Second pass of fluid

The steady state heat flux balance equation for the second fluid pass is shown in Fig. 3.7. The steady state heat flux balance equation for the second fluid pass is written as follows

$$\dot{q}_{f2} + \dot{q}_{con(f2,b)} = \dot{q}_{con(a,f2)} \tag{3.40}$$

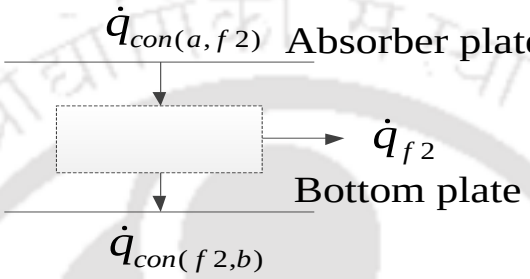

Fig. 3.7 The steady state heat flux balance of the second pass of fluid.

The net heat transfer to the 2nd fluid pass

$$\dot{q}_{f2} = \frac{2\dot{m}_{f2} C_{f2}\left(T_{f2} - T_{f1o}\right)}{Yl_{SAH}} \tag{3.41}$$

$$N_2 = \frac{2\dot{m}_{f2} C_{f2}}{Yl_{SAH}} \tag{3.42}$$

where $\dot{m}_{f2}$ is the mass flow rate of fluid in the second fluid pass, and C_{f2} is the specific heat of the fluid.

The convective heat transfer between the second pass of fluid and the absorber plate is

$$\dot{q}_{con(f2,b)} = h_{con(f2,b)}\left(T_{f2} - T_b\right) \tag{3.43}$$

Putting Eqs. (3.36), (3.41)–(3.43) into Eq. (3.40)

$$N_2\left(T_{f2} - T_{f1}\right) + h_{con(f2,b)}\left(T_{f2} - T_b\right) = h_{con(a,f2)}\left(T_a - T_{f2}\right) \tag{3.44}$$

(e) Bottom plate

Figure 3.8 shows the steady state heat flux balance of the bottom plate of the heater. The steady state heat flux equation is given by Eq. (3.45).

$$\dot{q}_{rd(a,b)} + \dot{q}_{con(f2,b)} = \dot{q}_{con(b,air)} + \dot{q}_{rd(b,sky)} \tag{3.45}$$

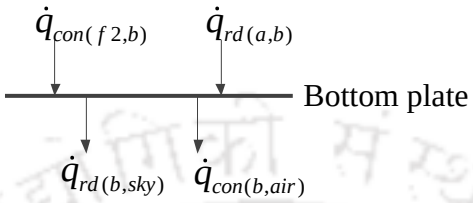

Fig. 3.8 The steady state heat flux balance of the bottom plate.

Heat loss at the bottom of the air heater is

$$\dot{q}_{con(b,air)} + \dot{q}_{rd(b,sky)} = U_b \left(T_b - T_{amb}\right) \tag{3.46}$$

Overall bottom loss coefficient is given by (Karim *et al.*, 2014).

$$U_b = \frac{1}{\frac{x_{ins}}{k_{ins}} + \frac{1}{h_{wi}}} \tag{3.47}$$

where x_{ins} is the thickness of insulation, and k_{ins} is the thermal conductivity of the insulation. Substituting Eqs. (3.37), (3.43) and (3.46) into Eq. (3.45).

$$h_{rd(a,b)}\left(T_a - T_b\right) + h_{con(f2,b)}\left(T_{f2} - T_b\right) = U_b\left(T_b - T_{amb}\right) \tag{3.48}$$

Rearranging Eqs. (3.27), (3.33), (3.39), (3.44) and (3.48)

$$\left[h_{con(f1,c)} + h_{rd(a,c)} + U_t\right]T_c - h_{con(f1,c)}T_{f1} - h_{rd(a,c)}T_a = \alpha_c I + U_t T_{amb} \tag{3.49}$$

$$h_{con(f1,c)}T_c - \left[h_{con(f1,c)} + h_{con(a,f1)} + N_1\right]T_{f1} + h_{con(a,f1)}T_a = -N_1 T_{f1i} \tag{3.50}$$

$$h_{rd(a,c)}T_c + h_{con(a,f1)}T_{f1} - \left[h_{con(a,f1)} + h_{rd(a,c)} + h_{con(a,f2)} + h_{rd(a,b)}\right]T_a + h_{con(a,f2)}T_{f2} + h_{rd(a,b)}T_b = -\alpha_a \tau_{rc} I \tag{3.51}$$

$$2N_2T_{f1}+h_{con(a,f2)}T_a-\left[h_{con(a,f2)}+h_{con(f2,b)}+N_2\right]T_{f2}+h_{con(f2,b)}T_b=N_2T_{f1i} \tag{3.52}$$

$$h_{rd(a,b)}T_a+h_{con(f2,b)}T_{f2}-\left[h_{con(f2,b)}+h_{rd(a,b)}+U_b\right]T_b=-U_bT_{amb} \tag{3.53}$$

Mean temperature of fluid in the first pass and the second pass are expressed as

$$T_{f1}=\frac{T_{f1i}+T_{f1o}}{2} \tag{3.54}$$

$$T_{f2}=\frac{T_{f1o}+T_{f2o}}{2} \tag{3.55}$$

The outlet temperature of the double pass air heater is given by (Karim *et al.*, 2014).

$$T_{f2o}=T_{f1i}+\frac{\left(Q_{f1}+Q_{f2}\right)Yl_{SAH}}{\dot{m}_fC_f} \tag{3.56}$$

The thermal efficiency of the air heater is given by

$$\eta_{SAH}=\frac{\dot{m}_fC_f\left(T_{f2o}-T_{f1i}\right)}{IA_{SAH}} \tag{3.57}$$

$$\dot{m}_f=\dot{m}_{f1}=\dot{m}_{f2} \tag{3.58}$$

$$C_f=C_{f1}=C_{f2} \tag{3.59}$$

A computer programme was prepared to the solve Eqs. (3.49–3.53) in the MATLAB to predict the temperature of the air streams, efficiency, and the outlet temperature of the air heater. The results are obtained for the solar radiation and the ambient temperature on 14th March 2015 (latitude 26.18º, Guwahati, India) measured with an Apogee make pyranometer model SP - 110, and the properties of materials mentioned in Table 3.2 are used in the calculation.

Figure 3.9 shows the hourly variation in the solar intensity and the ambient temperature between 7:00 h and 16:00 h. The maximum intensity of the solar radiation (910 W/m^2) was observed between 11:00 h and 12:00 h. The maximum ambient temperature (31 ^{o}C) was

recorded at 14:00 h around two and half hour later from the time of the maximum solar radiation intensity. The average solar radiation in the period 7:00 h to 16:00 h was 632 W/m^2.

Table 3.2

Dimensions and properties of the solar air heater air components.

Particulars	**Dimension/properties**
Absorber material	Galvanised sheet (thickness 0.85 mm)
Back insulation	Polyurethane foam (thickness of 25 mm)
Glazing	Plastic sheet of thickness 5 mm
Space between the absorber and cover plates	0.075 m
Space between the absorber and base plates	0.04 m
Absorptivity of the absorber plate	0.95
Absorptivity of the cover plate	0.06
Emissivity of the absorber plate	0.92
Emissivity of the cover plate	0.90
Emissivity of the bottom plate	0.25
Transmissivity of the cover plate	0.85
Thermal conductivity of the insulation	0.026 W/m-K

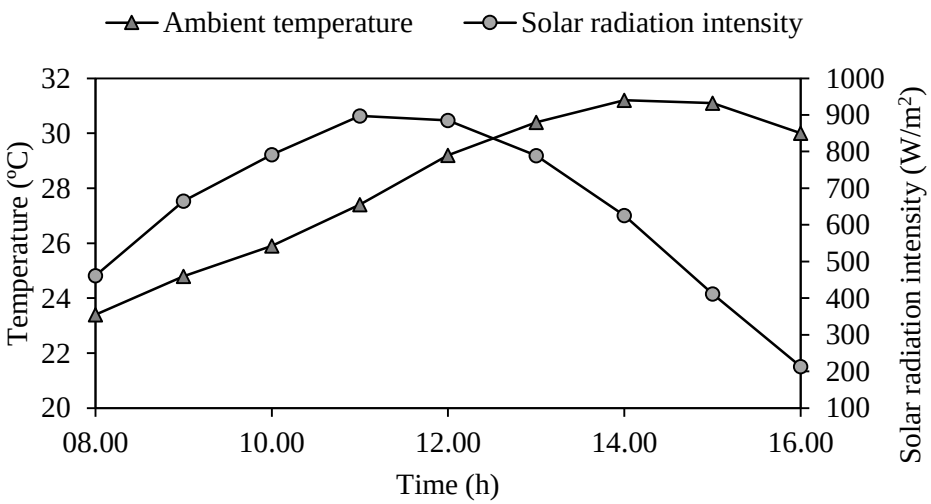

Fig. 3.9 Variation in the solar radiation and the ambient temperature.

3.3.2 Comparison with literature

To validate the simulation model, the numerical results are compared with the simulation results reported by Choudhury *et al.*, 1995 for the intensity of the solar radiation $I = 700$ W/m^2, ambient temperature $T_{amb} = 300$ K, $W = 1$m, $l = 2$ m $D_{(c,a)} = D_{(a,b)} = 0.03$ m. The comparison is shown in Fig. 3.10. The simulation model produces almost the same outlet air temperature at different mass flow rates and both the predictions match very closely.

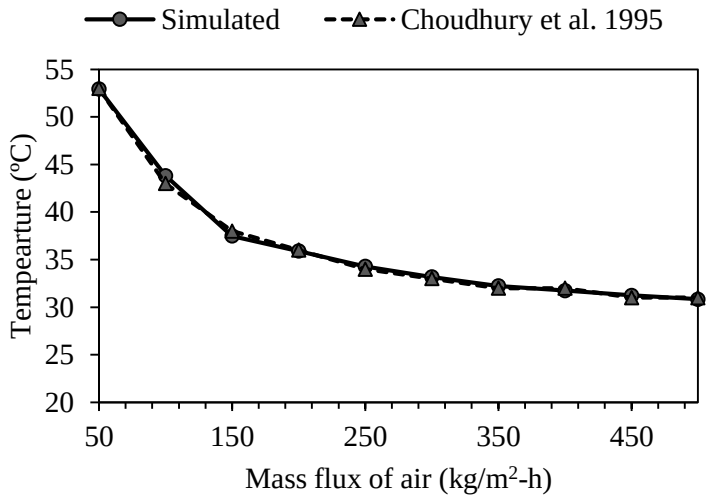

Fig. 3.10 Validation of the numerical model.

The simulation results are also compared with the experimental results as shown in Fig.3.11. It is observed that the trends of the experimental and the simulated results are almost the same. A deviation of 10% is found between the actual and the theoretical outlet air temperatures.

3.3.3 Parametric study of the solar air heater

Parametric study of the solar air heater is carried out to investigate the effect of the mass flow rate of air and the length of the heater on the outlet temperature and the thermal efficiency of the heater. So that the accurate value of the thermal efficiency and the length of the heater can be chosen for determining the total area of the heater for this application. The variation in the outlet air temperature and the efficiency against the length of the heater for a fixed mass flow rate (0.012 kg/s) of air and the solar radiation intensity (632 W/m^2) is plotted in Fig.3.12. It is observed that the efficiency decreases with increase in the length. The outlet air temperature increases linearly with increase in the length up to 2 m.

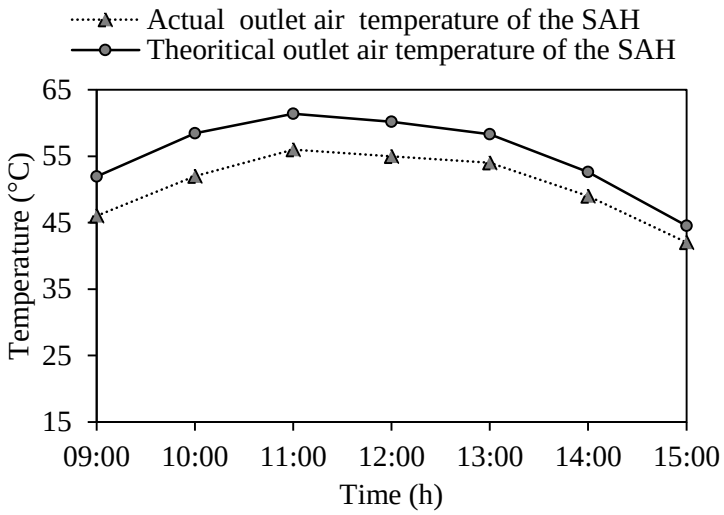

Fig. 3.11 Actual and theoretical outlet air temperatures of the solar air heater.

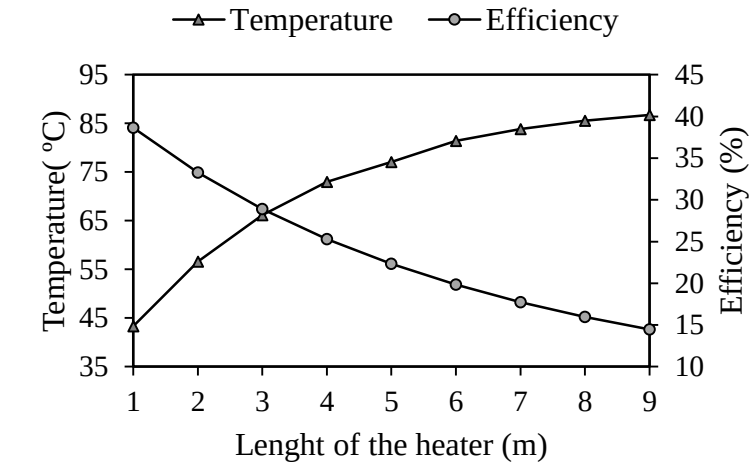

Fig. 3.12 Effect of the solar air heater length on the air outlet temperature and efficiency.

Figure 3.13 exhibits the variations in the outlet temperature for different lengths of the heater. The maximum outlet temperature increases from 50 °C to 99 °C with increase in the length from 1 m to 5 m at the mass flow rate of 0.012 kg/s and the solar radiation intensity of 632 W/m^2. It is observed from Fig. 3.14 that the efficiency of the solar air heater increases linearly with increase in the mass flow rate up to 0.096 kg/s. The efficiency does not improve with increase in the mass flow rate beyond the mass flow rate of 0.5 kg/s.

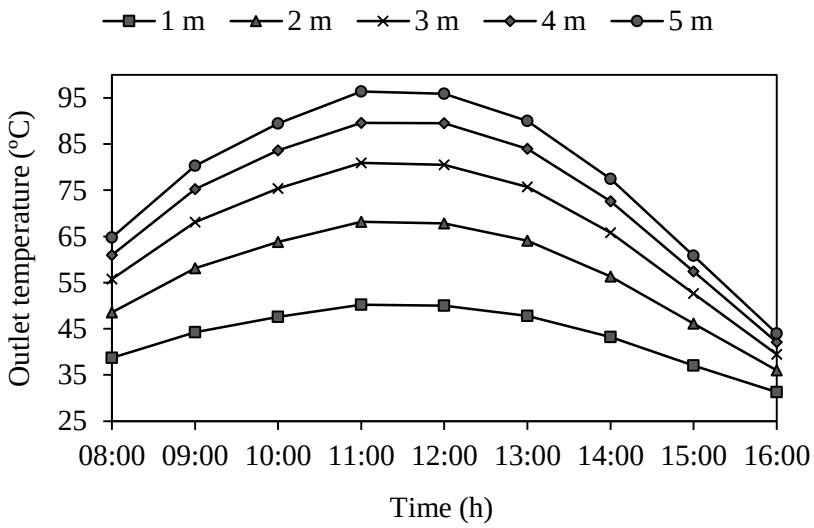

Fig. 3.13 Outlet temperatures of the heater vs lengths.

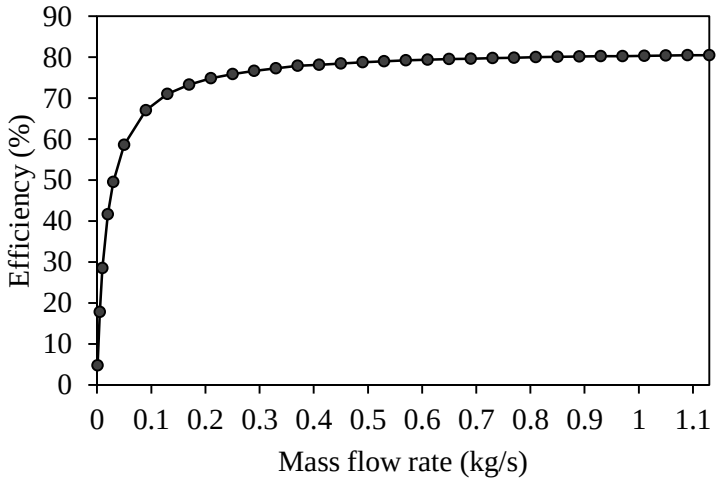

Fig. 3.14 Effect of the mass flow rate on the efficiency of the heater.

3.4 Sizing of the Energy Storage

A shell and tube type latent heat storage unit is chosen as the thermal energy storage for the developed drying system to reduce the fluctuation in the drying air temperature as well as continuing the drying process for a few hours after the sunset. The desired average drying air temperature for the solar dryer is 50 ºC. The minimum melting temperature of the PCM should be 5 to 10 ºC higher than the desired temperature of the fluid (Lane, 1983). Assuming a temperature difference of 10 ºC is desired between the air and the melting temperature of the PCM, then the melting temperature of the PCM should be around 60 ºC, and the charging temperature of the fluid should be around 70 ºC. Therefore, paraffin wax of the average melting

temperature in the range of 58–60 ºC is selected as the energy storage material since it is non-toxic and easily available in the local market.

The storage unit is basically a shell and tube heat exchanger. The paraffin wax is stored in the shell side, and the air flows inside the tubes. During the charging process of the energy storage, the heat is transferred from the hot air through the wall of the tubes to the paraffin wax. The heat transfer process is reversed during the discharging process. The thermal storage has been designed based on the method proposed by Shymasundar et al. (1992) which is useful for the preliminary design of the shell and tube latent heat storage. The thermal storage is expected to supply air at the average temperature of 50 ºC for 2 off - sunshine hours of the day. The amount of the paraffin wax required for supplying the air at that temperature is 38 kg. The design calculation of the storage is elaborated in Appendix (A).

3.5 Sizing of the Solar Air Heater

The total area of the solar air heater required for producing the hot air at a given temperature can be determined if the following information is known.

- the total amount of heat required to be supplied,
- duration of the sunshine hours,
- efficiency of the solar heater for a given mass flow rate, and
- the average solar radiation intensity on the surface of the solar air heater.

If t is the total sunshine hours per day, Q_{uSAH} is the total quantity of the useful heat gained from the solar air heater, and I is the average solar radiation intensity, and then the total area of the solar air heater can be estimated by the following equation (Benil, 2013; Omojaro and Aldabbagh, 2010).

$$\eta_{SAH} = \frac{Q_{uSAH}}{\left(I\alpha_a\tau_c\right)tA_{SAH}} \tag{3.60}$$

The amount of heat required for the dryer is the sum of the heat needed for producing the hot air at 50 ºC during the sunshine hours and the heat required for melting the paraffin wax of the storage. The total amount of heat needed during t sunshine hour per day is estimated by the equation given below

$$Q_{uSAH} = \left[\dot{m}_a C_{pa} t\left(T_{id} - T_{amb}\right) + m_{pf} C_{pf}\left(T_m - T_{amb}\right) + L_{pf}\right] \tag{3.61}$$

where $\dot{m}_a$ denotes the mass flow rate of the drying air, T_{id} is the average drying air temperature, m_{pf} is the mass of PCM, and L_{pf} is the latent heat of fusion of the wax. The first part of the right-hand side of the equation denotes the amount of the heat necessary to produce the hot air during *t* sunshine hour of the day. The second part represents the amount of heat stored in the storage unit to supply the hot air during the off - sunshine hours.

Table 3.3

Summary of the sizing of the solar air heater.

Particulars	**Value**
Expected sunshine hour per day (h)	7
Mass flow rate of air (kg/s)	0.012
Average drying air temperature (ºC)	50
Amount of heat required for supplying air at 50 ºC for 7 h (MJ)	8.6
Amount of heat required for melting 38 kg of paraffin wax (MJ)	9.5
Total amount of heat required per day (MJ)	18
Average solar radiation intensity (W/m^2)	632
Average efficiency of the solar air heater (%)	31.5
Total area of the air heater (m^2)	4.4

The following assumptions are made in the estimation of the total energy requirement.

- The average drying air temperature is 50 ºC although it changes with the change in the solar radiation intensity throughout the day.
- The expected daily sunshine hours is 7 h.
- The paraffin wax melts completely during the charging process.
- It is observed that the efficiency of the two - pass solar air heater of the length of 2 to 3 m is in the range of 28–35% at the mass flow rate of 0.012 kg/s. Therefore, an average value of 31.5% is assumed as the SAH efficiency.
- The average melting temperature of the paraffin wax is 58 ºC.
- Average solar radiation intensity is 632 W/m^2 in a good sunshine day.

Applying Eq. (3.61), for $\dot{m}_a = 0.012$ kg/s $t = 7$ h, $T_{id} = 50$ ºC, $T_{amb} = 25$ ºC, $m_{pf} = 38$ kg $T_m = 58$ ºC $L_{pf} = 189$ kJ/kg, $C_{pf} = 2.384$ kJ/kg-K, the amount of heat estimated to be supplied by the solar air heater in a good sunshine day is 18 MJ.

Applying Eq. (3.60), and taking the average solar radiation intensity I = 632 W/m^2, and $\eta_{SAH} = 31.5\%$, the area of the solar air heater required for supplying 18 MJ of heat is 4.4 m^2. The summary of the sizing of the solar air heater is given in Table 3.3.

It is to be noted that the total of energy required (during the entire drying period) for removing the moisture present in 10 kg of product is estimated as 23.6 MJ which is the energy required to remove 8.7 kg of moisture from the product. However, the collector has been sized for supplying energy for heating the ambient air from 25 ºC to 50 ºC for 7 h and also to supply the energy required for the complete melting of 38 kg of paraffin wax during 7 h sunshine hour operation of the dryer. Therefore, the air-heaters have been sized to supply 18 MJ heat on each day, considering a minimum drying period of 42 h (7 h per day). The total energy supplied for the whole drying period is 108 MJ (required useful heat gain of the solar air heater) which is the energy supplied to the storage and the drying chamber. The total energy input to the drying system (considering 31.5% thermal efficiency of the solar air heater) is 342.85 MJ.

3.6 Sizing of the Drying Chamber

Numerous types of the dryer are available for the food industry. They may be classified on the basis of

- operation: batch and continuous types,
- heating method: convection (air and steam), conduction (contact), and radiation (infrared and microwave),
- physical state of the drying materials: solid, liquid, and paste,
- movement of the material: static and moving fluidized, and
- pressure of operation: atmosphere and vacuum pressure.

The commonly used dryer in the solar drying system is the batch - type static convective dryer. The cabinet and the tunnel dryers are the examples of such type of dryers. They are inexpensive and easy to construct with the locally available materials. It consists of a closed compartment and drying trays. The drying trays containing the materials to be dried are placed inside the compartment. The hot air is then supplied by a blower or fan to remove the moisture from the product.

The type of dryer chosen for this drying system is a semi - continuous type tunnel dryer. It is basically a horizontal rectangular shape drying chamber. The drying trays can be put into the drying chamber at one end and can be removed from the other end. The hot air flows parallel to the layers of the product.

The design calculations in sizing of the drying chamber include the estimation of the number of drying trays and overall size of the drying chamber. The number of trays can be obtained by knowing the total area of the drying bed and the size of the drying trays. The basic information required for the calculations are

- mass of the product to be dried,
- bulk density of the product,
- bed porosity, and
- thickness of the drying bed.

The area of the drying bed can be estimated if the bulk density and the thickness of the product to be dried and the porosity are known. The following equation is employed to find out the drying bed area neglecting the loading void fraction.

$$A_{dt} = \frac{m_p}{x_{dt}\rho_p\zeta} \tag{3.62}$$

where m_p is the mass of the product, x_{dt} is the drying bed thickness, ρ_p is the bulk density of the product, and ζ is the porosity of the bed.

The mass of chilli to be dried, $m_p = 10$ kg, $\rho_p = 308.8$ kg/m^3 (Hossain and Bala, 1999), $x_{dt} = 20$ mm and $\zeta = 50\%$, then the total area of the drying bed is 3.23 m^2.

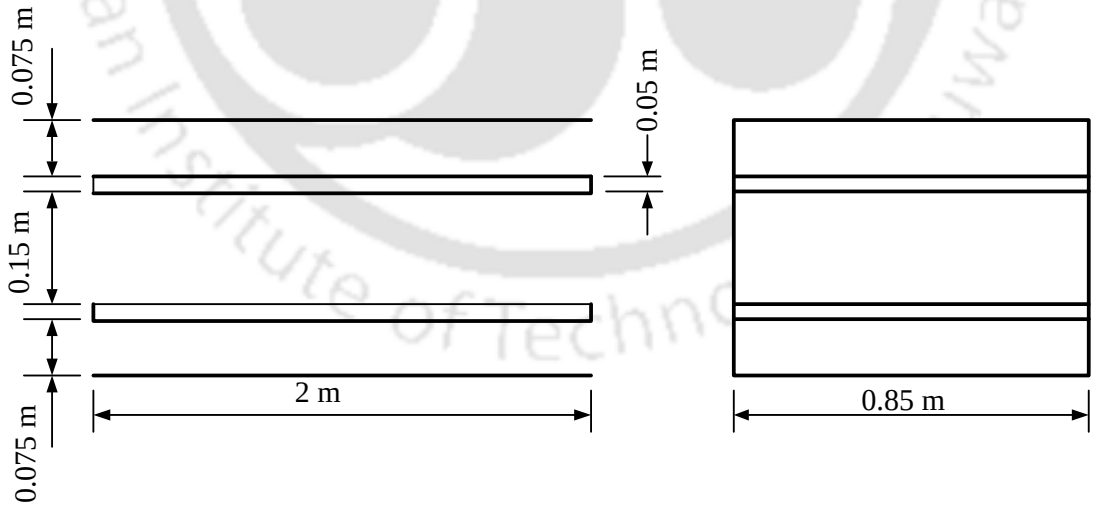

Fig. 3.15 Dimensions of the drying chamber (not in scale).

The length of the tray is 0.6 m and the width is 0.8 m, the number of trays required is approximately 6. The trays are arranged in two stages, each stage consists of 3 nos. of trays.

Total height required for each stage = (no of gaps × distance between two successive trays) + (no of trays × height of each tray).

The number of gaps = 1, the distance between two successive trays = 0.15 m, the height of each tray = 0.05 m then the total height of the tray loading section is 0.25 m as shown in Fig. 3.15.

Height of the drying chamber = (total height of the tray loading portion + height above the top tray + height of bottom tray from the walls of the dryer).

The distance of the bottom and top trays from the dryer inner surface is the same and is equal to 75 mm, then the height of the drying chamber is 0.4 m. Therefore, the size of the drying tunnel is taken as (2 m × 0.85 m × 0.4 m). The summary of the sizing of the drying chamber is given in Table 3.4.

Table 3.4

Summary of the drying chamber sizing.

Particulars	**Value**
Mass of the agricultural product to be dried (kg)	10
Total area of the drying bed (m^2)	3.2
Size of the drying trays	0.8 m × 0.6 m × 0.05 m
Distance between two stages (m)	0.15
Distance between the tray and wall of the drying chamber (mm)	75
Overall size of the drying chamber	1.8 m × 0. 85 m ×0.4 m

3.7 Summary

The mass flow of air and the energy requirements depend on the quantity and the moisture content of the product to be dried. For drying 10 kg of chilli from the initial moisture content of 88% (w.b.) to the final moisture content of 9% (w.b.) in 42 h, 23.6 MJ of energy is required. This amount of energy is expected to be supplied by 1763 kg of air at an average temperature of 50 ºC. Thermal analysis of a double - pass solar air heater is carried out to select the efficiency and the size of the solar air heater for the expected operating conditions of the dryer.

The size of the solar air heater panel (4.4 m^2) is estimated from the energy requirement for the drying purpose as well as for the storage. The amount of the thermal storage material (38 kg of paraffin wax) is calculated from the amount heat to be supplied for a given period at a given mass flow rate. The size of the drying chamber is calculated from the amount of the product and the bed thickness of the product to be dried. The area of the drying bed is 3.23 m^2.

Chapter - 4

Fabrication and Detailed Instrumentation of the Solar Dryer

4.1 Working Principle of the Solar Dryer

The developed solar dryer consists of a solar air heater panel, a shell and tube paraffin wax-based latent heat storage module, a tunnel dryer, and a blower. The schematic diagram of the dryer is shown in Fig. 4.1 (a) and its pictorial view is depicted in Fig. 4.1 (b). Solar energy is the main source of energy of the drying system. It is harvested by employing a solar air heater panel. In this drying system, two double - pass solar air heaters are connected in series to get the desired drying air temperature. Air at the ambient temperature is first passed through the first solar air heater (SAH - 1) where it is heated up by trapping the solar energy incident on its surface. The air exiting from the SAH - 1 is passed through the second solar air heater (SAH - 2) where it is heated up further. Then, it comes out of the SAH - 2 and passes through the tubes of the shell and tube based energy storage module located between the air heater panel and the drying chamber. The energy storage has nine tubes which are enclosed by a shell. The space between the tubes and the shell can be filled with the heat storage material. During the charging period, when the temperature of the air coming out of the air heater is higher than the temperature of the storage material, the heat is transferred from the air to the storage material. During the discharging period, when the temperature of the air coming out of the solar air heater is lower than the temperature of the storage material, the accumulated thermal energy is released from the storage material resulting in increase in the temperature of the air. The blower located between the thermal energy storage and the drying chamber draws air through the air heaters and the tubes of the storage and eventually, supplies it to the drying chamber.

Six trays are arranged in two stages in the drying chamber. Each stage has three trays. The trays can be loaded from one end of the drying chamber and unloaded through another door provided near the other end. The hot air flows over and under the products layer on the drying trays and escapes to the atmosphere after removing the moisture from the surface of the products.

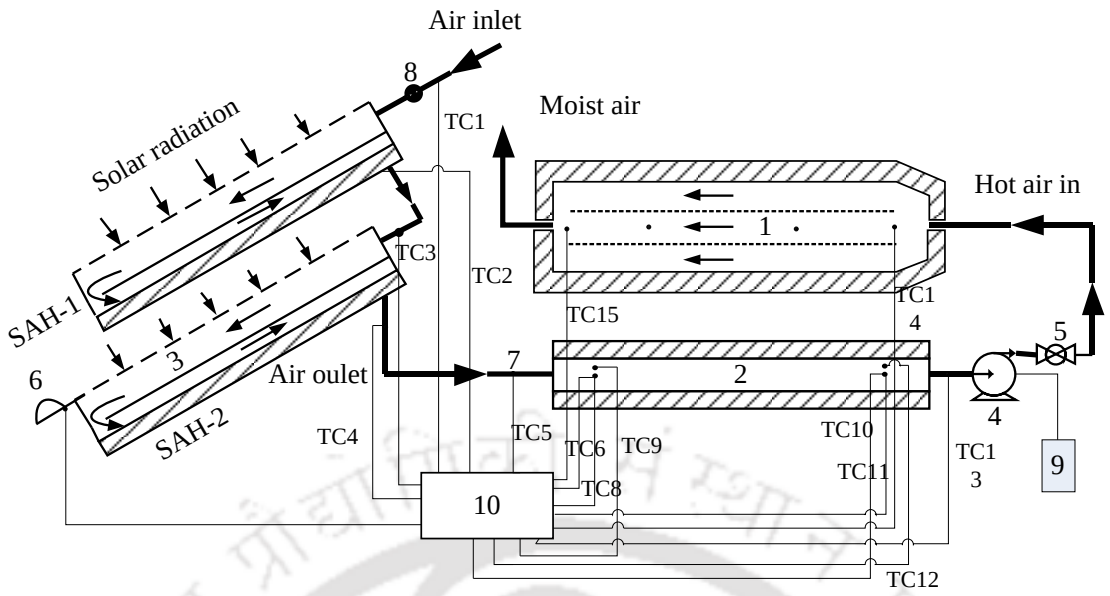

(a)

1. Drying chamber; 2. Shell and tube heat exchanger for the thermal energy storage; 3. Solar air heater (SAH); 4. Air blower; 5. Ball valve; 6. Pyranometer; 7. Thermocouple (TC); 8. Flow meter; 9. Energy meter; 10. Data acquisition system

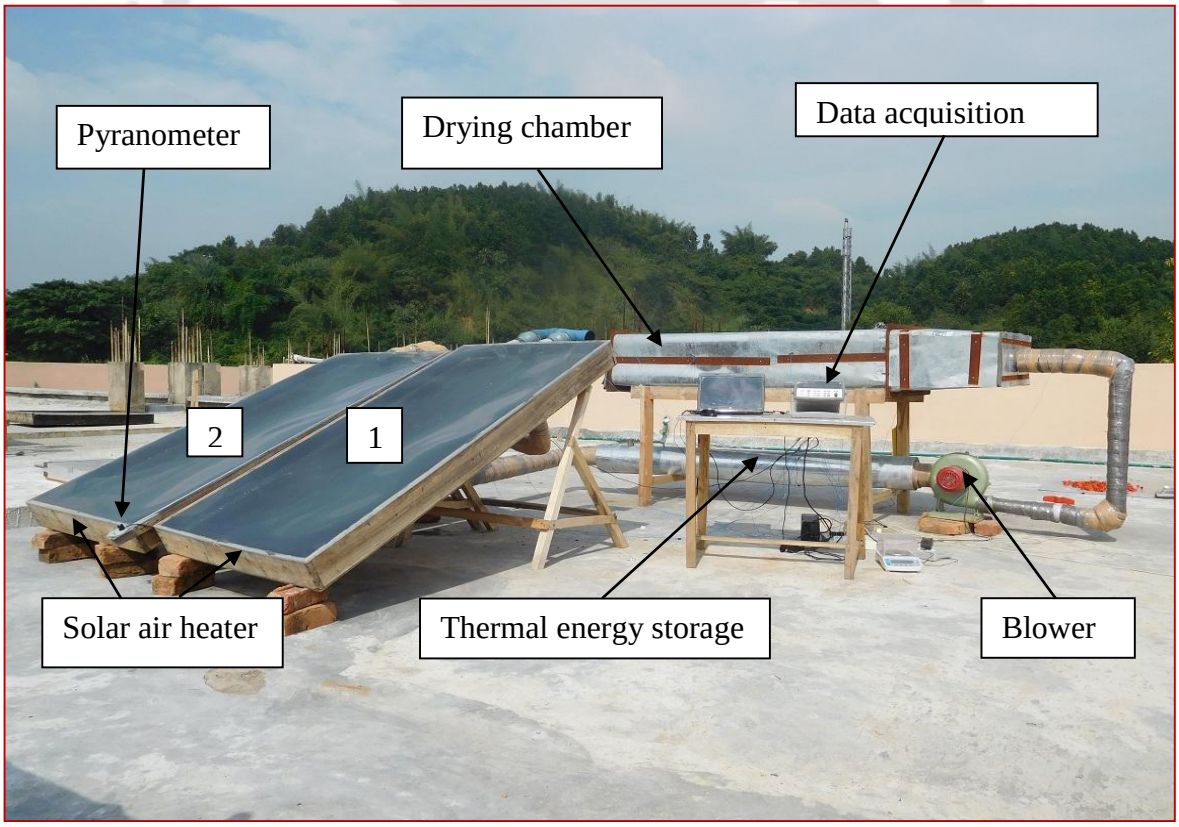

(b)

Fig. 4.1 (a) Schematic layout diagram of the solar dryer. (b) Pictorial view of the solar dryer.

4.2 Fabrication of the Components

The materials used for the construction of the components of the dryer were purchased from the local markets. The components were fabricated in the Institute's workshop and assembled and commissioned on a roof top of the institute's building.

4.2.1 Fabrication of the solar air heater

The solar air heater chosen for the drying system is two - pass or double pass type. The basic components of this type of air heater are absorber plate, cover plate or glaze, base plate, and wooden box. Initially, a rectangular wooden box of size 2.04 m × 1.04 m were constructed from 20 mm thick Goomer teak. A plywood sheet of size 2.04 m × 1.04 m and thickness of 6 mm was fitted into the box and then polyurethane foam insulation of thickness 25 mm was placed above the plywood. To reduce the re - radiation loss, a base plate of aluminium of thickness 0.2 mm was fitted above the insulation. A 0.85 mm galvanised iron sheet painted black was used as the absorber plate and fitted at a gap of 40 mm from the base plate. The glaze or the cover plate was a plastic sheet of thickness 4 mm and size 2.04 m × 1.04 m and fitted on the other side (the top) of the box. To circulate air inside the air heater, two circular inlets of 63.5 mm in diameter and one exit 101mm in diameter were provided at one end and bottom of the box, respectively. The air first flows through the passage formed by the absorber and cover plates and then passes under the absorber plate. Three rectangular ducts of size 0.2 m × 0.05 m were provided on the absorber plate opposite to the inlet for circulating the air from the upper channel to the lower channel. The CAD view of the heater is shown in Fig. 4.2. The front view, side view, and top view are shown in Fig. 4.3. Two heaters were oriented towards the South at the local latitude of 26.18^{o}, Guwahati, Assam and connected in series.

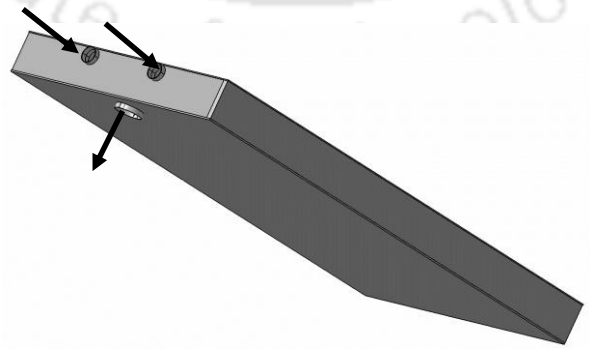

Fig. 4.2 CAD view of the solar air heater.

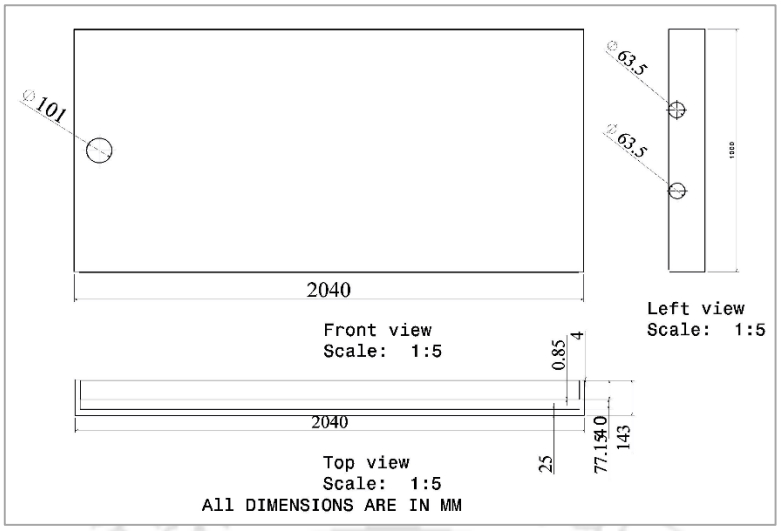

Fig. 4.3 Front view, top view, and side view of the solar air heater.

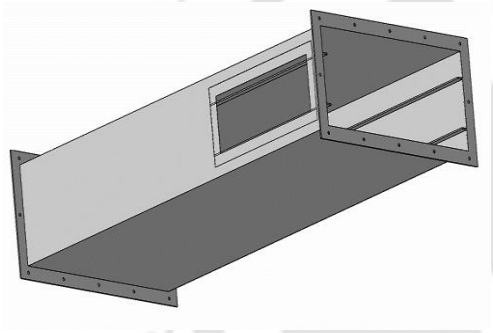

Fig. 4.4 CAD view of the drying chamber.

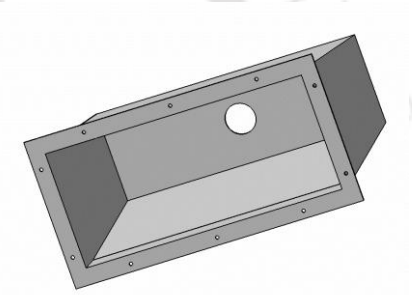

Fig. 4.5 CAD view of the plenum chamber.

4.2.2 Fabrication of the drying chamber

The drying chamber is basically a rectangular box of size 2 m × 0.85 m × 0.4 m as shown in Fig. 4.6. The CAD view of the drying chamber is shown in Fig. 4.4. Mild steel sheets of thickness 1.2 m were welded to fabricate the drying chamber. The walls of the drying chamber were insulated with polyurethane foam of thickness 25 mm and then covered with thin GI sheet. Two lines of L - shaped mild steel plate of size 25 mm × 30 mm were welded to the vertical walls of the box to support the drying trays. One end of the box is used as the door for putting the drying trays into the drying chamber. A plenum chamber (Fig. 4.5) of size 0.6 m × 0.85 m × 0.3 m is bolted to the other end of the box for distributing the air uniformly. Another door is provided on a vertical side wall of the box near the plenum chamber for unloading the trays. Six trays of size 0.8 m × 0.6 m × 0.025 m can be arranged in the drying chamber in two stages, each with 3 trays. The gap between the two stages is 0.15 m. The trays are made of wooden

frame and aluminium mesh. It can be glided horizontally from the air outlet of the drying chamber or tray loading door to the unloading door in the direction opposite to the air flow.

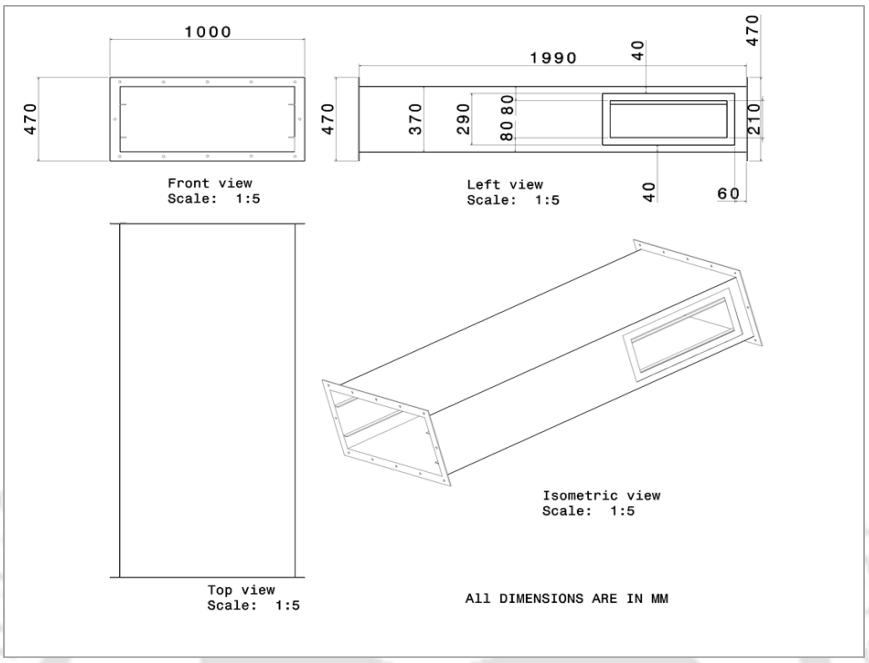

Fig. 4.6 Front view, top view, side view and isometric view of the drying chamber.

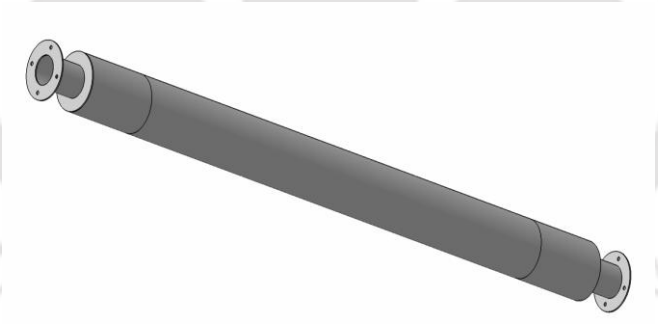

Fig. 4.7 CAD view of the shell and tube energy storage.

4.2.3 Fabrication of the shell and tube energy storage

The energy storage module is basically a shell and tube heat exchanger. It consists of 9 stainless steel tubes of 25.4 mm in diameter and 2 m in length, and the tubes are enclosed by a shell of diameter 0.18 m. The arrangement of the tubes is shown in Fig. 4.8 and the CAD view is depicted in Fig.4.7. One tube is placed along the axis of the shell, and the remaining eight tubes are arranged in a pitch circle of diameter 0.11 m at an equal distance. The shell was made of mild steel sheet of the thickness of 2.5 mm in a rolling machine. Two flanges or headers of the

equal size with 9 holes of 26 mm in diameter were welded to the both ends of the shell, and the tubes were then inserted through the holes and welded to the flanges. Another two short shells of 0.3 m in length and 0.18 m in diameter were welded to the both ends of the main shell to distribute the air. The shell side is insulated with polyurethane foam of thickness 25 mm to reduce wall heat losses.

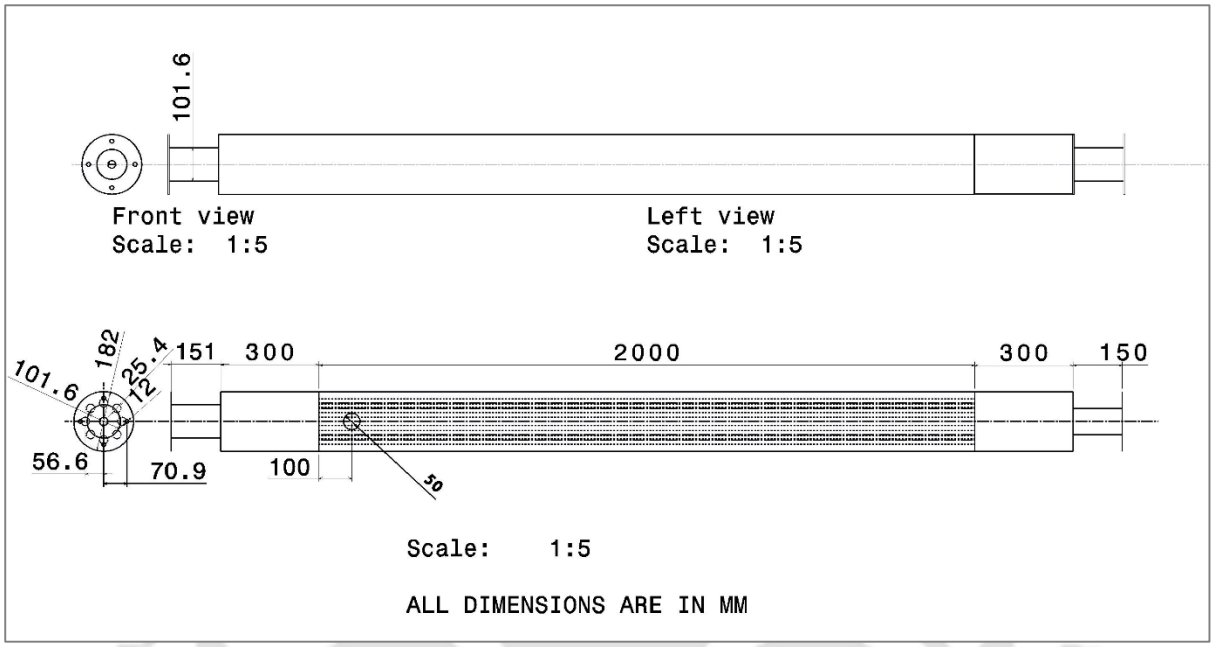

Fig. 4.8 Front view, left view, and sectional view of the energy storage.

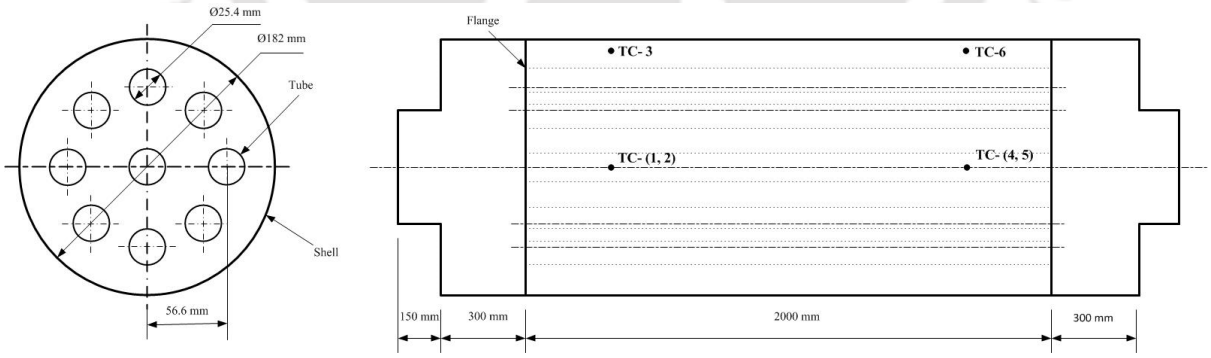

Fig. 4.9 Positions of the thermocouples in the energy storage (Not in scale).

Six thermocouples (TC) are provided in the storage to measure the temperature of storage material at different locations. The thermocouples TC - 1, TC - 2, and TC - 3 are located near the inlet of the storage unit, and the thermocouples TC - 4, TC - 5 and TC - 6 are located near the outlet of the storage as illustrated in Fig. 4.9.

4.2.4 Blower

A blower of the capacity of 0.417 kW (0.56 HP) was placed between the thermal energy storage and the drying chamber to circulate the air in the drying system.

The detailed of the materials used in the fabrication and the specification of the main components of the dryer are given in the table below.

Table 4.1

Materials and specification of the different components.

Main components	Components	Materials	Specification
Solar air heater	Absorber	Galvanised (GI) sheet	Size (1 m × 2 m) , thickness (0.85 mm)
	Glaze	Plastic sheet	Size (1.04 m × 2.04 m), thickness (4 mm)
	Base plate	Aluminium	Size (1 m × 2 m), thickness (0.2 mm)
	Insulation	Polyurethane foam	Thickness (25 mm)
	Box	Wood and plywood	Thickness (20 mm) and (6 mm)
Drying chamber	Wall	Mild steel sheet	thickness (1.2 mm)
	Tray	Wood and GI mesh	Size (0.8 m × 0.6 m)
	Insulation	Polyurethane foam	Thickness (25 mm)
Shell and tube energy storage unit	Shell	Mild steel	Thickness (2.5 mm), diameter (0.18 m), length (2 m)
	Pipe	Stainless steel	Diameter (25.4 mm), length (2 m)
	Insulation	Polyurethane foam	Thickness (25 mm)
Blower			0.56 HP (0.417 kW)

4. 3 Measuring Equipment

The dryer was installed on a roof top of the institute's building. The instruments necessary for the measurement of the operating parameters were connected to the drying system. The following equipment were used in the drying system for the measurement of the solar radiation, temperature, humidity, mass flow rate, mass loss of the product, and the velocity.

(i) Pyranometer: One of the important measuring equipment is the pyranometer. It is used for the measurement of the solar radiation intensity incident on the surface of the air heater panel. The pyranometer was mounted on the solar air heater. A pyranometer of the Make: Apogee; Model: SP - 101; Calibration factor: 5 W/m^2 per mV; Non - linearity: <1 % (up to 1750 W/m^2) was used to measure the solar radiation intensity (Fig. 4.10).

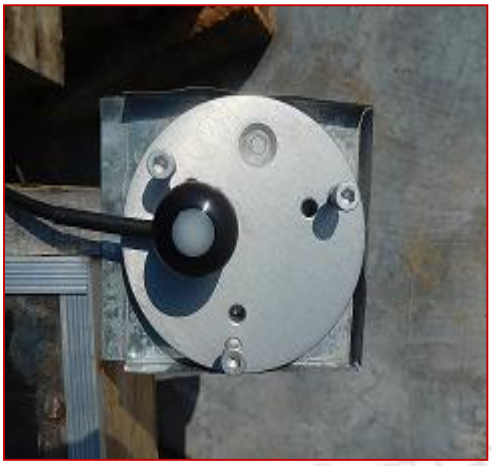

Fig. 4.10 Pyranometer.

Fig. 4.11 T - type thermocouple.

(ii) Thermocouples: T - type thermocouples (Fig. 4.11) with accuracy ± 0.2 ºC were used to measure the temperature at different locations of the drying system. The thermocouple wires were calibrated in constant temperature bath before installing in the drying system.

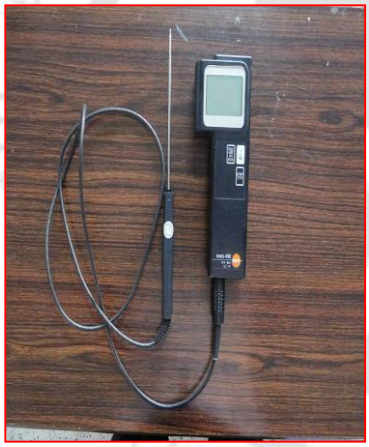

Fig. 4.12 Hot wire anemometer.

Fig. 4.13 Electronic weighing balance.

(iii) Hot wire anemometer: The velocity of air inside the drying chamber was measured with a hot wire anemometer (Make: TESTO; Reading accuracy ± 0.01 m/s; Measuring range 0 - 25 m/s) (Fig. 4.12).

(iv) Electronic weighing balance: The loss of mass of the agricultural product was measured with a digital weighing balance (Make: K. Roy: Model: DJ 602A, Reading accuracy: 0.01 g, Measuring range: 0–600 g) (Fig. 4.13).

(v) Power meter: The power consumed by the blower was measured with a power meter (Make: MECO meters Pvt. Ltd; Model: PG09/PG09H, accuracy ± 1 W) (Fig. 4.14).

Fig. 4.14 Power meter.

Fig. 4.15 U - tube differential manometer.

(vi) Orifice meter: An orifice meter was designed and fabricated for the measurement of the flow rate of air. It was placed at the inlet of the first air heater. The pressure drop across the orifice plate of the meter was measured with a U - tube differential manometer (Make: Bombay Instrument Ltd. Measuring range 150–0–150) (Fig.4.15). The specification of the orifice meter is given in Table 4.2 and the schematic of orifice meter is shown in Fig. 4.16.

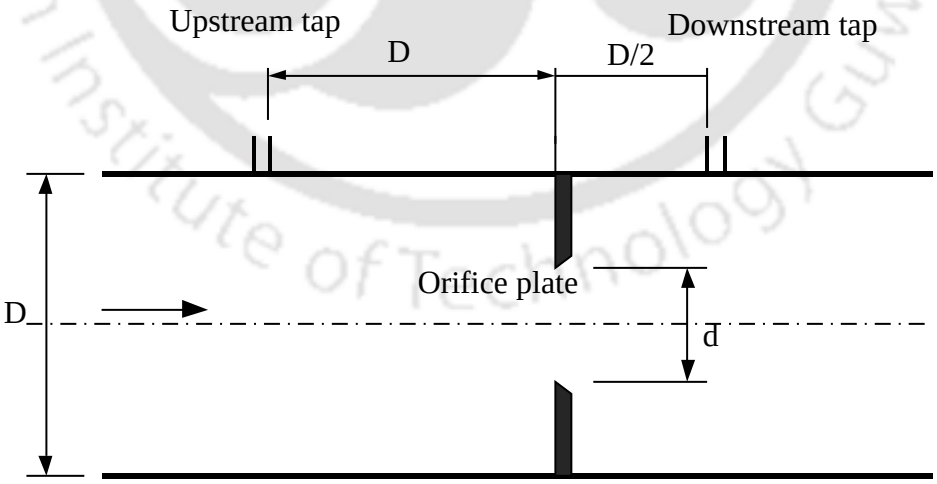

Fig. 4.16 Schematic of the orifice meter.

Table 4.2

Specifications of the orifice meter.

Diameter of pipe (D)	101 mm
Diameter of the orifice(d)	60.6 mm
$\frac{d}{D} = \beta$	0.6
Position of the upstream tapping	D
Position of the downstream tapping	D/2
Coefficient of discharge	0.63

4.4 Summary

The various components of the developed dryer were fabricated from the locally available materials such as wood, mild steel, polyurethane foam, plastic, and plywood. Two double pass solar air heaters of the gross size of 2.04 m × 1.04 m, a shell and tube heat exchanger of the shell diameter of 0.18 m, and 2.6 m in length with 9 tubes of diameter 25.4 mm, and a rectangular drying chamber of the size of 2 m × 0.85 m × 0.4 m were assembled together to develop the dryer.

Chapter - 5

Thin Layer Drying Kinetics Analysis of Ghost Chilli

5.1 Thin Layer Drying Kinetics

Drying is a complex process involving unsteady simultaneous heat and mass transfer. It is a least understood process in the microscopic level because of the deficiencies in the mathematical description (Erbay and Icier, 2009). Drying kinetics of materials may be described by their transport properties and those of the drying medium. The various transport properties which control the drying kinetics of food and agricultural materials are thermal and moisture diffusivities, thermal conductivity, and heat and mass transfer coefficients at the interface (Togrul and Pehlivan, 2002).

The drying processes of food and agricultural products are modelled from the distributed models and the lumped parameter models. The distributed models take into account both the internal and external heat and mass transfers and depend on the Luikov equations (Erbay and Icier, 2009). These models can determine the moisture and the temperature gradients in the product. In the lumped parameter model, the product temperature is assumed to be uniform. Most lumped parameter model equations are derived from the distributed model with simplified assumptions (Jayas *et al,* 1991).

The thin layer drying [drying of a single layer of particles or slices (Akpinar, 2006)], equations provide a proper understanding of the drying kinetics of food and agricultural products. They are categorised as theoretical, semi - theoretical, and empirical equations (Midilli and Kucuk, 2003a). The theoretical equations take into account the internal resistance to moisture transfer and are derived from the Fick's second law of diffusion. The semi - theoretical and empirical equations consider only the external resistance to moisture transfer between the product and the drying air. The semi - theoretical models are derived from Fick's second law of diffusion and the modification of its simplified form. The empirical models are derived from the experimental data and the dimensional analysis. The moisture ratio is directly correlated with the drying - time in the empirical models (Babalis *et al.*, 2006).

Table 5.1

Commonly used semi - empirical and empirical thin layer drying Models.

Model	Model Equation	Ref.
Semi-empirical models		
(a) Models derived from Newton's law of cooling		
Lewis (Newton)	$MR = \exp(-kt)$	Lewis (1921)
Page	$MR = \exp(-kt^n)$	Yaldy and Erteky (2001)
Modified Page - 1	$MR = \exp(-kt)^n$	Overhults *et al.* (1973)
Modified Page - 2	$MR = \exp-(kt)^n$	White *et al.*, (1981)
Modified Page - 2	$MR = \exp-k\left(\frac{t}{l^2}\right)^n$	Diamante and Munro (1993)
(b)Models derived from Fick's second law of diffusion		
Henderson and Pabis (Single term)	$MR = a\exp(-kt)$	Henderson (1974)
Logarithmic	$MR = a\exp(-kt)+c$	Chandra and Singh (1995)
Midilli-Kucuk	$MR = a\exp(-kt^n)+b^*t$	Midilli *et al.*(2002)
Demir et al.	$MR = a\exp[(-kt)]^n+b$	Demir *et al.* (2007)
Two-term	$MR = a\exp(-k_1t)$ $+b\exp(-k_2t)$	Henderson and Pabis (1961)
Two-term exponential	$MR = a\exp(-kt)$ $+(1-a)\exp(-kat)$	Sharaf - Eldeen *et al.* (1980)
Modified two-term exponential (Verma et al.)	$MR = a\exp(-kt)+$ $(1-a)\exp(-g_ot)$	Verma *et al.* (1985)
Diffusion approach model or approximation of diffusion	$MR = a\exp(-kt)+$ $(1-a)\exp(-kbt)$	Akpinar *et al.* (2003)
Modified Henderson and Pabis model (Three term exponential)	$MR = a\exp(-kt)+b\exp(-g_ot)$ $+c\exp(-h_ot)$	Karathanos (1999)
Empirical models		
Thompson	$t = a\ln(MR)+b[\ln(MR)]^2$	Thompson *et al.* (1968)
Wang and Singh	$MR = 1+b^*t+a^*t^2$	Wang and Singh (1978)
Kalemullah	$MR = \exp(-c^*T)+b^*t^{(pT+n)}$	Kaleemullah (2002)

The thin layer drying equations are easy to use in the modelling of the solar dryers due to less complexity and the requirement of less data, unlike the distributed model. The drying constant of the thin layer drying equation combines all the transport properties and describes the drying phenomenon in a unified way. The detailed review of the thin layer drying equations were undertaken by Erbay and Icier, 2009 and Kucuk *et al.*, 2014. The commonly used thin layers drying equations are listed in Table 5.1.

Development of an appropriate model of a particular product is significant for designing a new drying system or improving an existing dryer and identifying the optimum operating parameters for precise prediction of the simultaneous heat and mass transfer phenomenon in the drying process (Kucuk *et al.*, 2014). Drying systems need to be designed properly to meet the desired operating parameters of a particular product and to get the satisfactory performance in view of the energy requirements and quality of the product (Chavan *et al.*, 2008). The drying air velocity, temperature, relative humidity, and size of the material affect the kinetics of the drying process and model parameters (Rajkumar *et al.*, 2007). Full-scale experimental investigation of the dryer of different configurations under diverse conditions is a costly affair and time-consuming. Therefore, modelling of the drying process of a specific product under the given drying conditions and the simulation model of the dryer are necessary for predicting the performance of dryer.

A thin layer model of the drying process of a particular product can be developed by the experimental method. In the thin layer drying experiment, air at the constant flow rate, temperature, and relative humidity is supplied through a thin layer of food or agricultural product. The mass of the product is measured at a regular interval of time until the equilibrium moisture content is reached. Then the moisture content of the product is calculated at a regular interval of time. The moisture content at any given time on wet basis can be evaluated by applying Eq. (5.1) (Ekechukwu, 1999). Then MR vs time curve is plotted. The MR at constant relative humidity is obtained by Eq. (5.2). However, when the relative humidity of the drying air fluctuates, the MR is obtained by the Eq. (5.3) (El - Sebaii and Shalaby, 2013).

$$M_t = 1 - \left[\frac{(1 - M_i) m_{ip}}{m_{tp}} \right] \tag{5.1}$$

$$MR = \frac{(M_t - M_e)}{(M_i - M_e)} \tag{5.2}$$

$$MR = \frac{M_t}{M_i} \tag{5.3}$$

where M_t is the moisture content at a given time (w.b.), m_{ip} is the initial mass of the product, m_{tp} is the mass of product at a given time, M_i is the initial moisture content (w.b.), and M_e is the equilibrium moisture content (w.b.).

The regression analysis is carried out with different thin layer drying models to find out the models constants and the coefficients. The goodness of fit is judged by calculating statistical parameters such as coefficient of determination (R^2), reduced chi - square (x^2), root mean square error (*RMSE*), and mean relative deviation modulus. The widely used statistical parameters are R^2,x^2 and *RMSE*. The best model is chosen based on the criteria of the highest value of R^2 and the lowest values of x^2 and *RMSE*. The values of the R^2, x^2 and *RMSE* are calculated applying Eqs. (5.4)–(5.6) (Goyal *et al*., 2007; Shi *et al*., 2013; Sharma *et al*., 2005, Koukouch *et al*., 2015; Aghbashlo *et al*., 2009).

$$R^2 = 1 - \frac{\sum_{i=1}^{N}(MR_{pr,i} - MR_{ex,i})^2}{\sum_{i=1}^{N}(\overline{MR_{pr}} - MR_{ex,i})^2} \tag{5.4}$$

$$x^2 = \frac{\sum_{i=1}^{N}(MR_{ex,i} - MR_{pr,i})^2}{N - n} \tag{5.5}$$

$$RMSE = \sqrt{\frac{1}{N}\sum_{i=1}^{N}\left(MR_{ex,i} - MR_{pr,i}\right)^2} \tag{5.6}$$

Effective moisture diffusivity is an important factor which combines various diffusion process in solids such as the molecular diffusion, capillary flow, Knudsen flow, hydrodynamic flow and surface diffusion. It indicates the flow of moisture in the material. The effective moisture diffusivity can be calculated from Eq. (5.7) by the method of slopes (Vega *et al.*, 2007).

$$MR = \frac{8}{\pi^2}\exp\left[\frac{-D_{eff}\pi^2 t}{4L_s^{\,2}}\right] \tag{5.7}$$

Where D_{eff} is the effective moisture diffusivity, L_s is the length of the product thickness and t is the drying time. In the method of slop, a curve is plotted between ln (MR) and t. The slope

of the curve gives the rate constant k which is equal to $\left(\frac{\pi^2 D_{eff}}{4L_s^{\,2}}\right)$.

Experimental investigation and mathematical modelling of the thin layer drying kinetics of different types of pepper were carried out in a variety of solar dryers. Condri *et al*. (2001), Hossain and Bala (2007), Janjai *et al*. (2008), Leon and Kumar (2008), Akpinar and Bicer (2008), Banout *et al*. (2011), Akintunde (2011), Kaewkiew *et al*. (2012) dried sweet pepper and garlic (forced convection - type greenhouse tunnel dryer), blanched and un - blanched red hot and green chilli (mixed - mode - type solar tunnel dryer), chilli and Rosella flower (roof integrated solar dryer), chilli (hybrid solar dryer with energy storage and biomass heater), long green pepper (forced convection solar dryer and under the open sun), red chilli (double pass - type solar dryer), pre - treated and untreated chilli pepper (solar dryer and the open sun), chilli (large size parabolic shape greenhouse dryer), red chilli (solar dryer integrated with double pass - type solar air heater with finned absorber and auxiliary heater), and red pepper and grape (mixed - mode - type greenhouse solar dryer), respectively.

It is observed that the kinetics study of the drying process of the Ghost chilli dried in a solar dryer or any type of dryer and under the open sun is not reported in the literature. Therefore, the developed dryer without any storage is initially tested by drying Ghost chilli to study its thin layer drying kinetics and to identify a suitable thin layer drying model describing the drying process of this chilli.

5.2 Ghost Chilli (Capsicum Chinense Jacq.)

The North - Eastern Region of India produces wide varieties of chilli such as Ghost chilli and bird's eye chilli (Dubey *et al*., 2015). The Ghost chilli (Capsicum Chinense Jacq.) (Fig. 5.1) also locally known as the Bhut Jolokia or Naga Jolokia, is one of the hottest chillies in the world and has a very high heat level of 855,000 Scoville heat units (SHU). It was rated as the world's hottest chilli in the Guinness Books of World Records in 2007 (Mathur *et al.*, 2000). The size of the Ghost chilli varies from 60 mm to 85 mm in length and 20 mm to 30 mm in width with different colours such as red, yellow, and orange. The fruit size is conical with smooth or rough surface and its weight varies from 6.9 g to 8.97 g.

The Ghost chilli is used either raw or dry as spice or pickles, and generally, it is dried in the open sun or smoke dried for preservation. It is also used for developing chilli grenade by Defence Research and Development Organisation (DRDO) of India (en.wikipedia.org). The skin of this chilli is very thin, and the fully ripe Ghost chilli is easily perishable. Therefore, it

has to be consumed within a few days of harvest. The climatic condition of the NER is characterized by frequent rain fall, high humidity, low annual average solar radiation, and long rainy days. The harvesting time of the Ghost chilli coincides with the rainy season of the NER from May to October. Drying process has to be speeded up to avoid spoilage of the chilli. Therefore, this product should be dried in the solar dryer instead of drying in the open sun. In view of the above, identification of a suitable drying model is necessary for designing and developing a suitable solar dryer.

Fig. 5.1 Photos of Ghost chilli with plant.

5.3 Experimental Procedure

Freshly harvested fully ripe Ghost chilli was purchased from the local market and checked to discard the spoiled ones. Nine kg of the chilli were weighed and placed on the drying trays of the drying chamber. A sample of 200 g was taken in a small tray to measure the moisture removal rate and placed in the first stage of the trays. Another sample of 200 g was placed outside in the open sun. The drying experiment was carried out every day for 8 h starting from 8:00 h to 16:00 h. After the experiment (at the end of the day), the samples were kept in the airtight containers. During the experiment, the temperature of air at different locations of the drying system, relative humidity of the ambient air and the hot air at the inlet and outlet of the drying chamber, mass flow rate and velocity of the air at the inlet of the drying chamber, and the intensity of solar radiation were measured. The loss of the mass of the chilli sample was measured at 1 h interval using the digital balance. The relative humidity of the drying air was

estimated from the psychrometric chart using the wet bulb and dry bulb temperatures. The velocity of air near the first stage of the drying trays was measured using the hot wire velocity meter. The orifice meter was used to measure the mass flow rate of air. The thermocouples and the pyranometer were connected to a data acquisition system to record the temperature of the air at different locations and the solar radiation intensity, respectively at a regular interval of time (10 sec). The initial and final moisture contents were determined by the oven method also known as the gravimetric method. In this method, the sample of the product is placed in a hot air oven under standard drying conditions 105 ± 2 ºC until a steady mass is obtained. The final mass is known as the bone-dry mass (Keey, 2001).

5.4 Drying Analysis

The moisture content of the chilli at different times during the drying period was calculated by employing Eq. (5.1). The relative humidity of the drying air fluctuated continuously during the experiment due to change in the drying air temperature and the solar radiation intensity. Therefore, the MR was estimated employing Eq. (5.3). The MR obtained from the experimental results was plotted with time, and the non - linear curve fitting was performed in the Microsoft Excel with the selected models. Eleven thin layer drying models given in Table 5.1 were tested to identify the most suitable drying model. The coefficient of determination, reduced chi - square, root mean square error and model constants were determined by employing Eqs. (5.4)–(5.6). The best model was chosen based on the criteria of the highest value of R^2 and the lowest values of x^2 and RMSE.

5.5 Results and Discussions

The drying experiment was carried out consecutively for five days from 29th September 2015 to 3rd October 2015. During the experiment, the ambient air temperature and the relative humidity were found to vary from 29 ºC to 37 ºC and 57.4% to 85.5%, respectively. The average velocity of air near the first stage of the drying trays measured with the anemometer was found to be 1.7 m/s, and the corresponding mass flow rate was found to be 0.02 kg/s. The drying air temperature was in the range of 44–66 ºC with an average of 57 ºC. The variation in the solar radiation intensity and the ambient temperature recorded for five consecutive days during the experiment is shown in Fig. 5.2. The intensity of the solar radiation varied between 166 W/m^2 and 1011 W/m^2 with an average of 641 W/m^2. The solar radiation was found to be fluctuating in the third and the fourth days of the experiment due to the sudden appearance of

clouds in the sky. The maximum solar radiation intensity was recorded at around 11:30 h of the day.

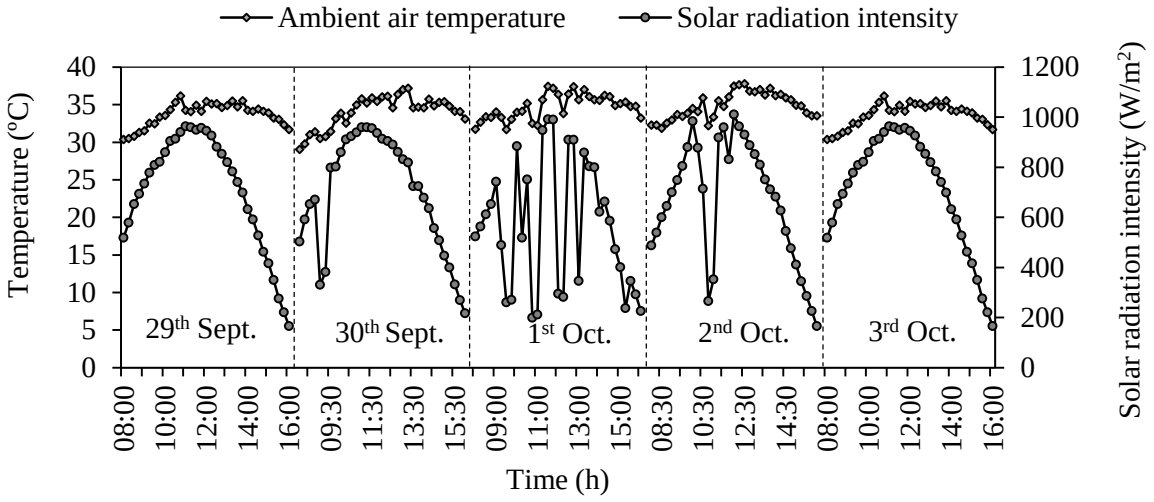

Fig. 5.2 Variation in the solar radiation and the ambient temperature for five consecutive days.

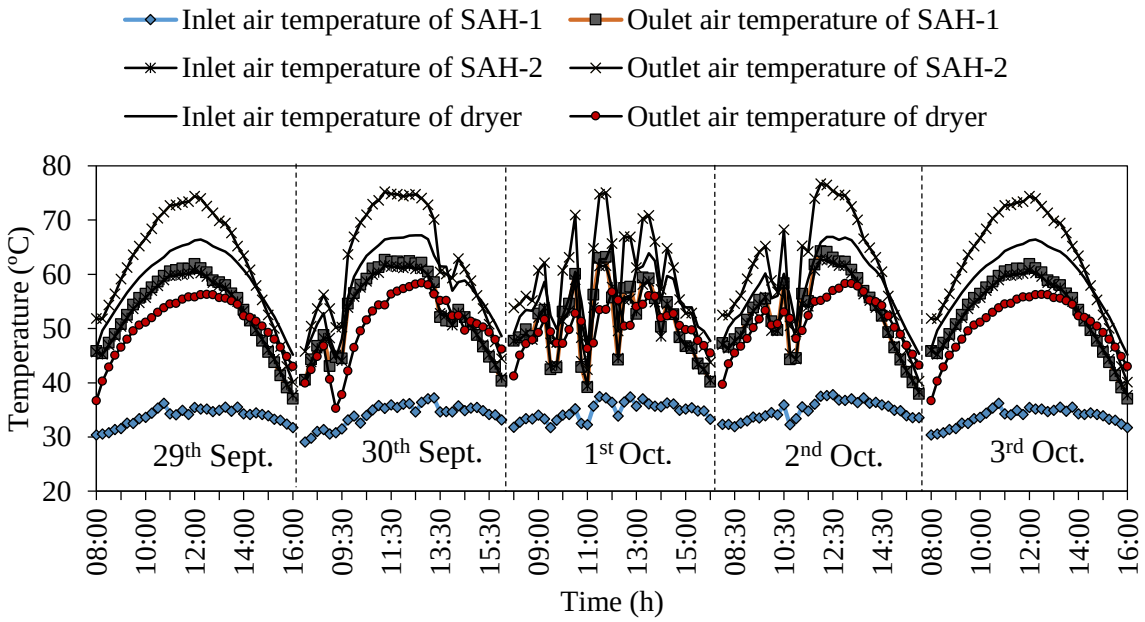

Fig. 5.3 Variation in the air temperature at different locations of the drying system.

The variation in the air temperature with time at different locations of the dryer is shown in Fig. 5.3. The maximum temperature of the air coming out of the solar air heater was found to be 75 °C during the peak sunshine hour. It was observed that the temperature of the air at the inlet of the drying chamber was not same as the temperature of the air coming out of the air heater. This was due to the heat losses in the connecting ducts between the air heater and

the drying chamber. Between 14:30 h and 16:00 h, the temperature of the air at the inlet of the drying chamber was found to be slightly higher than the temperature of the air coming out of the air heater. This was mainly due to the accumulation of the sensible heat in the shell and tube material of the heat exchanger. When the temperature of the air leaving from the air heater became low due to the low solar radiation intensity, the sensible heat of the shell and tube material was utilized for heating the air.

The variation in the relative humidity of the air entering and leaving the drying chamber and the ambient air with time is shown in Fig. 5.4. The relative humidity was recorded low between 11:00 h and 14:00 h when the intensity of the solar radiation and the ambient temperature were high.

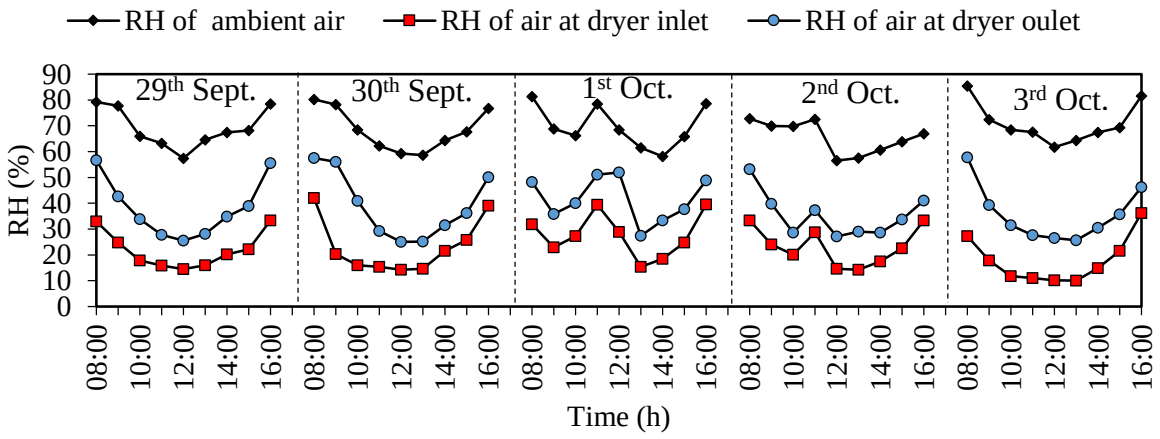

Fig. 5.4 Variation in the relative humidity (RH) of the ambient air and the air at the inlet and outlet of the drying chamber.

The change in the moisture content of the chilli sample with the drying time is shown in Fig. 5.5. The interruption in the curve represents the night periods of the drying operation from 16:00 h to the next day 8:00 h. The moisture content of the chilli sample was reduced to 0.12 g of water /g of dry matter (d.b.) from its initial moisture content of 5.9 g of water /g of dry matter (d.b.) in 123 h in the solar dryer, while it was achieved in 193 h in the open sun drying including the night period. The open sun drying took more time to reach the final moisture content due to the slow drying rate. It is observed from the moisture content vs. time curve that the drying process of the Ghost chilli occurs only in the falling rate period, and the constant rate period is completely absent in the drying period. Therefore, diffusion is a predominant phenomenon in the drying process of the Ghost chilli.

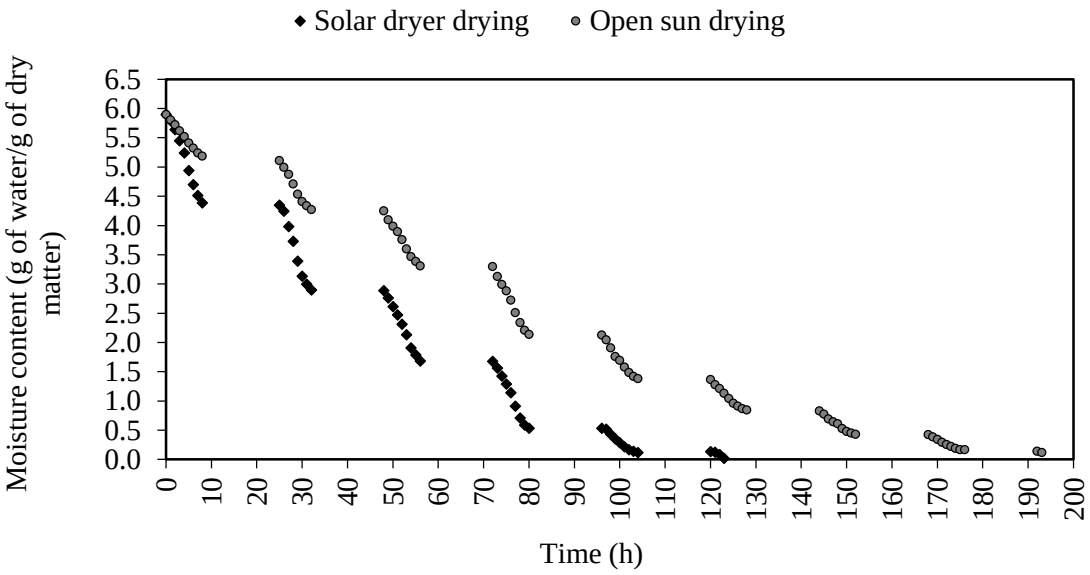

Fig. 5.5 Moisture content variation with drying time.

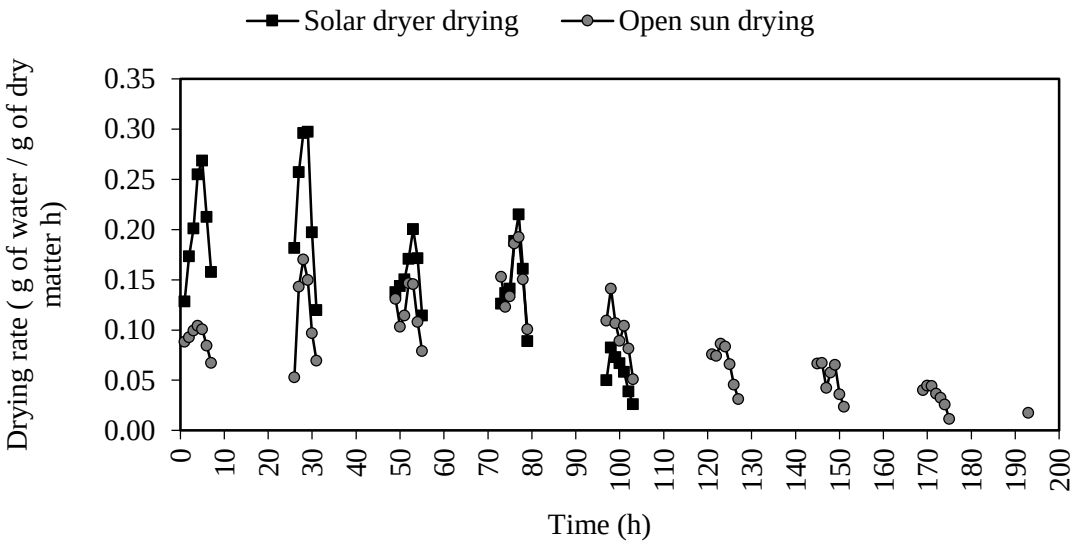

Fig. 5.6 Drying rate vs drying time.

The change in the drying rate with the drying time is shown in Fig. 5.6. It is observed that the drying rate of the Ghost chilli dried in the solar dryer is faster than that of the open sun drying, and it decreases continuously with the progress of the drying time. The drying rate was found to be fluctuating both in the solar drying and the open sun drying, which was mainly caused by the variation in the solar radiation and the corresponding changes in the air temperature. During summer, the solar radiation changes frequently in the NER of India due to the clouds in the sky. The maximum drying rate was visible during the peak sunshine hour of the day when the solar radiation intensity and the drying air temperature were maximum.

The drying rate of the chilli dried in the solar dryer was faster than that of the open sun drying till the first 55 h of the drying period, and afterwards, the drying rate became low due to the low moisture content in the chilli compared to the sun dried one.

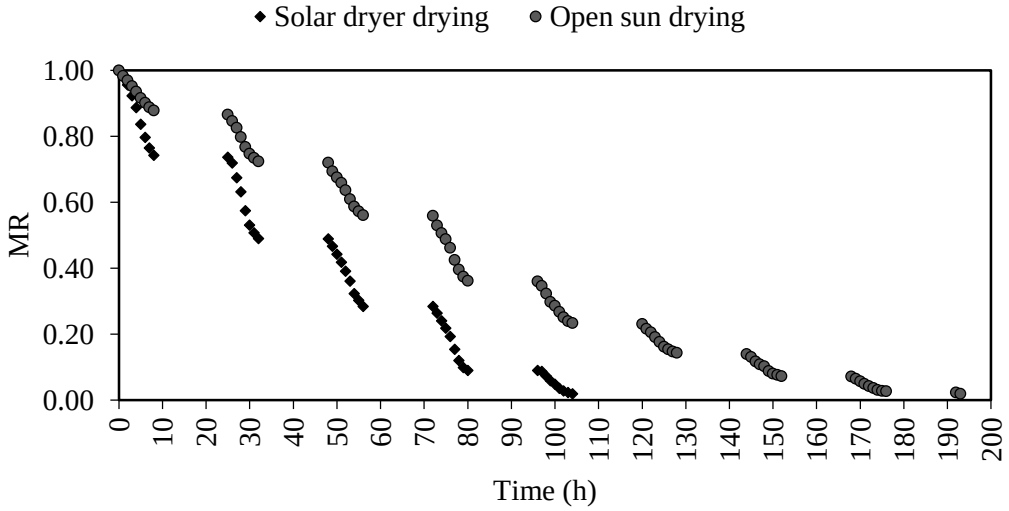

Fig. 5.7 MR vs drying time.

The experimental MR data plotted with the drying time is shown in Fig. 5.7. The MR vs the drying time curve is required for performing the non - linear regression analysis for identifying the best drying model. The thin layer drying models, given in Table. 5.1 were fitted into the experimental MR vs drying time curve by the non - linear regression analysis. The results of the regression analysis are given in Tables 5.2 and 5.3 for the open sun drying and the solar dryer drying, respectively. The fitness of the model's equations was evaluated based on values of the coefficient of determination (R^2), reduced chi - square (x^2), and the root mean square error (*RMSE*). The model having the highest value of R^2, and the lowest values of x^2 and *RMSE* was selected as the best model to represent the drying process of the Ghost chilli. It was found from the regression analysis of the MR data of the open sun drying of the Ghost chilli that the Page and the Modified Page models yielded the highest value of R^2 and the lowest values of x^2 and *RMSE*, and the values were same for both the models except the model constants. The values were $R^2 = 0.9971$, $x^2 = 0.00029$, and $RMSE = 0.01665$. For the thin layer solar drying process, the Midilli and Kucuk model gives the highest value of R^2 and the lowest value of x^2 and RMSE. They were $R^2 = 0.99696$, $x^2 = 0.0003$, and $RMSE = 0.01687$. The values of the coefficients and constants of the best models are highlighted with bold colour. Therefore, the Page and the modified Page models were considered as the most appropriate models for representing the thin layer open sun drying process of the Ghost chilli while for the solar drying the most appropriate model was the Midilli and Kucuk model.

Therefore, the best models for the sun drying process of the Ghost chilli are expressed as follows.

The Page model can be expressed as $MR = \exp\left\{-0.00396(t)^{1.56823}\right\}$ (5.8)

The modified Page model is given by $MR = \exp\left\{-(0.02941t)^{1.56823}\right\}$ (5.9)

Similarly, for the solar drying the best model (Midilli and Kucuk model) is given by

$$MR = 1.00206\exp(-0.02046t^{1.20216}) - 0.00360t \quad (5.10)$$

Table 5. 2

Fitting statistics of the various thin layer models of the open sun drying of Ghost chilli.

Model name	**Coefficients and constants**	R^2	x^2	*RMSE*
Newton	k = 0.03004	0.94103	0.00589	0.07628
Page	**k = 0.00396; n = 1.56825**	**0.99719**	**0.00029**	**0.01665**
Modified page model	**k = 0.02941; n = 1.56823**	**0.99719**	**0.00029**	**0.01665**
Henderson and Pabis	k = 0.04811; a = 1.089246	0.96295	0.00382	0.06050
Modified Henderson and Pabis	a =7.69866; k = 0.06131, b = –2.41837; g_o = 0.07194 c = –4.33077; h_o = 0.07104	0.99488	0.00055	0.02248
Logarithmic	a = 1.55082; k = 0.01657 c = –0.49346	0.99266	0.00076	0.02691
Two - term	a = 0.97379; k_0 = 0.03427 b = 0.16444; k_1 = 0.03428	0.96295	0.00387	0.06050
Two - term exponential	a =2.02287; k = 0.04805	0.99171	0.00084	0.02861
Wang and Singh	a^* = –0.02121; b^* = 0.00010	0.99147	0.00087	0.02901
Diffusion	a = 3.1089; b = 0.40796, k = 0.00960	0.98965	0.00106	0.03195
Midilli and Kucuk	a = 1.13081; b = –0.00933 k = 0.08239; n = 0.47526	0.98031	0.00206	0.04407

It is observed from the drying kinetics of the Ghost chilli and the studies of the other researchers on the drying kinetics of different chillies (Table 5.4) that mainly the Page,

Logarithmic, and the Midilli and Kucuk models are the most suitable models that represent the thin layer kinetics of the drying process of different chilli peppers dried in different types of dryers under various drying conditions.

Table 5.3

Fitting statistics of the various thin layer models of the forced convection solar drying of Ghost chilli.

Model name	**Coefficients and constants**	R^2	x^2	*RMSE*
Newton	k = 0.04962	0.98327	0.00453	0.06653
Page	k = 0.01300; n = 1.43655	0.99171	0.00081	0.02788
Modified Page model	k = 0.04865; n = 1.43656	0.99171	0.00081	0.02788
Henderson and Pabis	a = 1.10964; k = 0.05528	0.96795	0.00315	0.05483
Modified Henderson and Pabis	a = 1.85137; k = 0.07488, b = –0.20292; g_o = 0.20702 c = – 0.67557; h_o = 0.14471	0.98770	0.00134	0.03396
Logarithmic	a = 1.51688; k = 0.033169 c = – 0.53589	0.99642	0.00036	0.01833
Two - term	a = 1.0669; k_0 = 0.05528 b = 0.04207; k = 0.05528	0.96795	0.00331	0.05483
Two - term exponential	a = 1.93272; k = 0.07583	0.98799	0.00118	0.03355
Wang and Singh	a^* = – 0.03505; b^* = 0.00027	0.99629	0.00036	0.01864
Diffusion	a = – 0.51790; k = – 0.00278 b = 8.28112	0.99530	0.00259	0.04840
Midilli and Kucuk	**a = 1.00206; k = 0.02046, n = 1.20216; b = –0.00360**	**0.99696**	**0.00031**	**0.01687**

Table 5.4

Studies performed on the thin layer drying process of different peppers.

Type of pepper	Dryer	Drying conditions	Drying models/function	Ref.
Green sweet pepper	Forced convection solar dryer and open sun drying	$T = 43.9 - 64.8$ ºC v = not available	Logarithmic (solar drying) and Midilli and Kucuk (sun drying)	Akpinar and Bicer (2008)
Red chilli pepper	Direct cabinet type solar dryer and open sun drying	Mean , $T = 45$ ºC v = not available	Page	Akintunde (2011)
Red pepper	Cabinet dryer	$T = 50 - 60$ ºC	Page	Doymaz and Pala (2002)
Green chilli Balujuri	Overflow-underflow/through flow drying chamber	$T = 40 - 60$ ºC $v = 0.1 - 1$m	Page	Hossain and Bala (2002)
Sweet pepper	Cabinet dryer	$T = 40 - 70$ ºC $v = 1.5$ m/s	Logarithmic	Vengaiah and Pandey (2007)
Red bell pepper	Convective dryer	$T = 50 - 80$ ºC $v = 2.5$ m/s	Modified Page	Vega *et al.* (2007)
Green bell pepper	Ventilated oven	$T = 30 - 70$ ºC	Page and Newton	Faustino *et al.* (2007)
Bird's eye chilli	Fluidized bed dryer	$T = 50 - 70$ ºC $v = 0.85 - 1.09$ m/s	Second degree polynomial function	Tasirin *et al.* (2007)
Green pepper	Microwave oven	T and v not available	Midilli and Kucuk model	Darvishi *et al.* (2014)

The comparison of the experimental MR and the respective predicted MR by the established models are shown in Figs. 5.8 and 5.9 (a) and (b). The comparison of the experimental MR and the predicted MR by the most suitable drying model (Midilli and Kucuk Model) for the solar dryer drying of Ghost chilli is shown in Fig. 5.8. Figure 5.9 (a) and (b)

exhibits the comparison of the experimental MR and the predicted MR by the Modified Page model and the Page model, respectively for the open sun drying of the Ghost chilli. The predicted MR data follow a straight line for both the solar dryer drying and the open sun drying which validates the suitability of the established models.

The effective moisture diffusivity was estimated by the graphical method. The moisture diffusivity was found to be 3.37×10^{-6} (m^2/s) and 2.04×10^{-6} (m^2/s) for the solar drier drying and the sun drying, respectively.

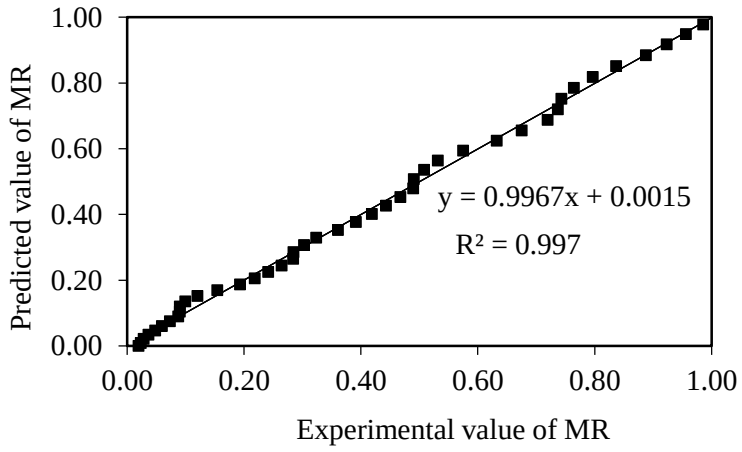

Fig. 5.8 Comparison of the experimental and the predicted MR by the Midilli and Kucuk model for the solar dryer drying.

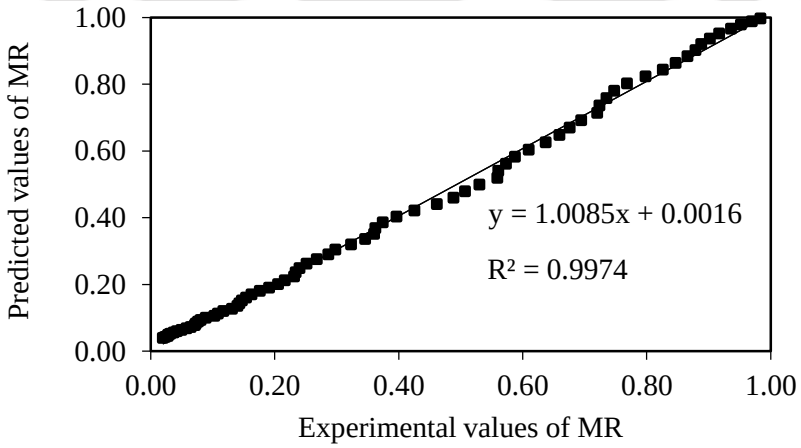

Fig. 5.9(a) Comparison of the experimental and the predicted MR by the Modified Page model for the open sun drying.

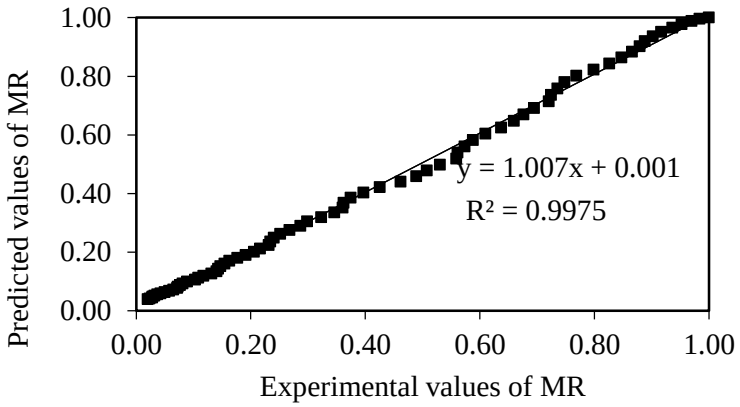

Fig. 5.9(b) Comparison of the experimental and the predicted MR by the Page model for the open sun drying.

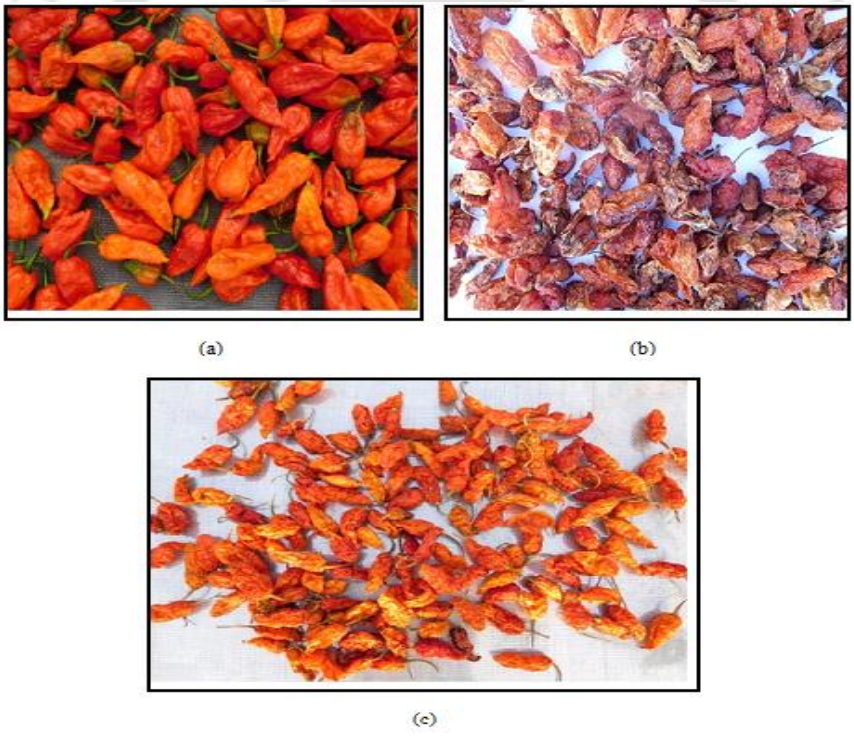

Fig. 5.10(a) Frsehly harvested ripe Ghost chilli pods (b) The open sun-dried Ghost chilli pods (c) The solar dryer dried Ghost chilli pods.

Figure 5.10 (a) exhibits the photograph of the freshly harvested Ghost chilli, and Figs. 5.10 (b) and (c) show the photographs of the same Ghost chilli after the open sun drying and the solar dryer drying. It has been observed quantitatively that the colour texture and quality of the solar dried Ghost chilli are better than in the open sun dried one. Further, the drying was

more uniform in the solar dryer. The original colour of the freshly harvested Ghost chilli was preserved in the solar drying sample. The colour of the solar dryer drying sample was bright reddish and yellowish while the open sun drying sample was pale and dark red.

5.6 Summary

Ghost chilli was dried in the newly developed solar dryer and under the open sun to study its drying kinetics. The chilli pods were dried in the solar dryer at the drying air temperature varying between 44 ºC to 66 ºC with an average of 57 ºC. The chilli dried from the initial moisture content of 85.5% (w.b.) to the final moisture content of 10.5% (w.b.) in 123 h (including the night period) in the solar dryer and 193 h in the open. The drying rate was faster in the solar dryer than in the open sun drying. The drying process of the Ghost chilli occurred only in the falling rate period. Eleven thin layers drying models were compared with the experimental MR data to identify the most suitable drying model. The results showed that the Midilli and Kucuk model was the most suitable thin layer drying model to describe the drying process of the Ghost chilli dried in the solar dryer, and the Page and the Modified Page model were the two most suitable models for the open sun drying process of the Ghost chilli. The effective moisture diffusivity of the solar dried and the open sun dried product was 3.37×10^{-6} (m^2/s) and 2.04×10^{-6} (m^2/s), respectively.

Chapter - 6

Energy and Exergy analyses of the Drying Process of Ghost Chilli and Sliced Ginger

6. 1 Introduction

The operating cost of dryers increases day by day owing to continuous depletion of fossil fuels resources and high prices of energy. In view of this, the available energy sources have to be used efficiently and judiciously to reduce the energy consumption as well as the environmental impact without compromising the quality of the dried products. Energy and exergy analyses play a vital rule in optimising drying conditions and improving the performance of drying systems. The energy analysis based on the first law of thermodynamics has some limitations. It estimates the quantity of energy required for a given system but it does not provide any information about the quality of the energy (Akpinar and Koçyigit, 2010; Park *et al*., 2014). The exergy analysis provides more realistic views of a thermodynamic process. It determines the causes and magnitude of irreversibility in any thermodynamics process (Saidur *et al*., 2012) and identifies the locations, causes, and sources of deviations of the actual process from the ideal one (Rosen and Dincer, 2003). The energy and exergy efficiencies of the drying system can be improved by selecting optimum drying conditions and identifying the causes of inefficiency and accordingly, taking corrective measures. It also helps in planning the operational procedures of the dryer so that maximum amount of moisture can be removed by supplying the minimum amount of energy.

Numerous studies on the energy and exergy analyses of the solar drying process of agricultural products dried in different types of solar dryer have been reported in the literature. Midilli and Kucuk (2003), Celma and Cuadros (2009), Akbulut and Durmus (2010), Akpinar (2010), Boukadoum and Benzaoui (2011), Chowdhury *et al*. (2011), Fudholi *et al*. (2014a), Fudholi *et al*. (2014b), Fudholi *et al*. (2015) presented the energy and exergy analyses of the drying process of shelled and unshelled pistachios (indirect - type forced convection solar dryer), olive mill waste water (indirect - type natural convection solar dryer), mulberry (indirect - type forced convection solar dryer), mint leaves (forced convection solar dryer), mint leaves (natural convection cabinet dryer), jackfruit leather (mixed - mode-type solar tunnel dryer),

dried red chilli, red seaweed, and oil fronds (indirect - type forced convection solar dryer), respectively. The detailed review is given in section 2.3 in chapter – 2.

It has been found that the energy and exergy analyses of the solar drying processes of the Ghost chilli and the sliced ginger dried in a forced convection solar dryer have not been reported in the literature. Therefore, the main objective here is to perform the energy and exergy analyses of the drying processes of the Ghost chilli and the sliced ginger in this newly developed solar dryer.

6.2 Experimental Procedure

The drying experiments were performed during October (Ghost chilli) and November (sliced ginger) 2015 every day starting from 9:00 h to 15:00 h. Every day, the surfaces of the air heaters were cleaned to remove dust and dirt, and the drying system was run for half an hour before loading it with the agricultural products. Nine kg of freshly harvested ripe Ghost chilli and 13 kg of sliced ginger were dried during the experiment. The experiment was performed separately for each product. The ginger was washed and cleaned in the tap water one day before the experiment. Then it was peeled and sliced into 4 mm to 10 mm thickness manually before it was loaded into the drying chamber. To measure the moisture removal rate, a sample of 200 g of the uniform size of each product was placed in a small tray. The losses of the mass of the samples were measured with the digital balance at 1 h interval. The position of the drying trays was changed at 2 h interval to dry the products uniformly. The agricultural products were kept inside the dryer during the night period by closing the tray loading and unloading doors. The velocity of air near the drying trays was measured with the hot wire velocity meter. An orifice meter installed at the inlet of the SAH - 1 measured the flow rate of air. The power consumption of the blower was measured with the digital energy meter. The T - type thermocouples and the pyranometer were connected to the data acquisition system to record the temperature at different locations of the drying system and the solar radiation intensity, respectively at a regular interval of time (15 sec). The initial and the final moisture contents of the products were determined by the oven method or Gravimetric methods.

6.3 Energy Analysis

The energy analysis of the drying system was performed on the basis of the general mass and energy conservation equations. The data obtained from the experiments were used to perform the energy and exergy analyses. The basic data requirements are the temperature of the air

streams at different locations, the mass flow rate of air, the energy inflows and outflows of the drying system, and the mass of moisture removed from the product. The energy inflows of the drying system are the solar and electrical energy. The energy outflows of the drying system are heat losses from the solar air heaters, heat losses at different sections of the connecting ducts, heat losses from the walls of the drying chamber, and heat loss in the exhaust of the drying chamber. During the energy analysis, the flow in the drying system was assumed to be steady. The general mass and energy conservation equations for the steady flow open system can be expressed as follows (Cengel and Boles, 2010).

$$\sum \dot{m}_i = \sum \dot{m}_o \tag{6.1}$$

$$\dot{Q} - \dot{W} = \sum \dot{m}_o \left(h_o + \frac{v_o^2}{2} + Z_o g\right) - \sum \dot{m}_i \left(h_i + \frac{v_i^2}{2} + Z_i g\right) \tag{6.2}$$

where $\dot{m}_i, \dot{m}_o$ = mass flow rate of air at the inlet and outlet, respectively

h_i, h_o = enthalpy of air at the inlet and outlet, respectively

v_i, v_o = velocity of air at the inlet and outlet, respectively

Z_i, Z_o = height of the inlet and outlet from reference plane, respectively

$\dot{Q}$ = heat transfer rate

$\dot{W}$ = work transfer rate

g = acceleration due to gravity

In the drying chamber, the effects of the kinetic and potential energy were neglected for the following reasons.

- The dryer was horizontal,
- The inlet and outlet of the solar air heaters were located at the same height from the ground, and
- The change in velocity between the inlet and the exit was negligible.

Therefore, the mass and energy conservation equations for the SAH can be expressed by Eqs. (6.3)–(6.5).

$$\dot{Q}_{in} - \dot{Q}_{ls} = \dot{m}_a (h_o - h_i) \tag{6.3}$$

The heat input ($\dot{Q}_{in}$) to the solar air heater is given by Eq. (6.4)

$$\dot{Q}_{in} = \alpha_a \tau_c I A_{SAH} \tag{6.4}$$

$$\dot{m}_i = \dot{m}_o = \dot{m}_a \tag{6.5}$$

where $\dot{Q}_{ls}$ is the heat loss in the solar air heater, $\dot{m}_a$ is the mass flow rate of air, h_i and h_o are the specific enthalpies at the inlet and outlet of the solar air heater, respectively.

The right hand term of Eq. (6.3) is known as the useful heat gained by the SAH, and it can be obtained by measuring the inlet and outlet temperatures of the air heaters and the mass flow rate of air. The useful heat gained of the SAH – 1 can be evaluated by Eq. (6.6) (Midilli and Kucuk, 2003; Celma and Cuadros, 2009).

$$\dot{Q}_{uSAH-1} = \dot{m}_a C_{pa} (T_{oSAH-1} - T_{iSAH-1}) \tag{6.6}$$

where T_{iSAH-1} and T_{oSAH-1} are the inlet and outlet air temperatures of the first solar air heater, respectively, and C_{pa} is the specific heat of air.

The instantaneous first law efficiency of the SAH is defined here as the ratio of the useful heat gained to the solar radiation incident on the absorber surface of the heater. Although, it is generally defined as the ratio of the useful heat gained to the solar radiation incident on the air heater plane (Benli, 2013; Bahrehmand and Ameri, 2015, Omojaro and Aldabbagh, 2010). Therefore, it is expressed by Eq. (6.7) for the SAH - 1.

$$\eta_{SAH-1} = \frac{\dot{m}_a C_{pa} (T_{oSAH-1} - T_{iSAH-1})}{\alpha_a \tau_c I A_{SAH-1}} \tag{6.7}$$

The heat losses from the SAH - 1 can be calculated by Eq. (6.8).

$$\dot{Q}_{lsSAH-1} = \alpha_a \tau_c I A_{SAH-1} - \dot{Q}_{uSAH-1} \tag{6.8}$$

Similarly, the useful heat gain, the instantaneous thermal efficiency, and the heat losses of the SAH - 2 can be expressed by Eqs. (6.9), (6.10) and (6.11), respectively.

$$\dot{Q}_{uSAH-2} = \dot{m}_a C_{pa} (T_{oSAH-2} - T_{iSAH-2}) \tag{6.9}$$

$$\eta_{SAH-2} = \frac{\dot{m}_a C_{pa} (T_{oSAH-2} - T_{iSAH-2})}{\alpha_a \tau_c I A_{SAH-2}} \tag{6.10}$$

$$\dot{Q}_{lsSAH-2} = \alpha_a \tau_c I A_{SAH-2} - \dot{Q}_{uSAH-2} \tag{6.11}$$

where A_{SAH-1} and A_{SAH-2} are the areas of the SAH - 1 and SAH - 2, respectively, T_{iSAH-2} and T_{oSAH-2} are the inlet and outlet air temperatures of the SAH - 2, respectively.

The size of the two air heaters were the same, and the inlet temperature of the SAH - 1 was assumed to be equal to the ambient temperature and therefore,

$$A_{SAH-1} = A_{SAH-2} = A_{SAH} \tag{6.12}$$

$$\text{And } T_{iSAH-1} = T_{amb} \tag{6.13}$$

The overall efficiency of the SAHs was determined by Eq. (6.14).

$$\eta_{SAH} = \frac{\dot{m}_a C_{pa}(T_{oSAH-2} - T_{iSAH-1})}{(A_{SAH-1} + A_{SAH-2}) I \alpha_a \tau_c} \tag{6.14}$$

The specific energy consumption (SEC) is defined as the ratio of the total energy input to the drying system to the total moisture removal from the product. It was computed by Eq. (6.15) reported by Fudholi *et al.*, 2014a.

$$SEC = \frac{p_t}{m_v} \tag{6.15}$$

The total energy input (p_t) is the sum of the solar energy incident on the surface of the solar air heaters and the electrical energy consumed by the blower. It was calculated by the following equation.

$$p_t = \left[(A_{SAH-1} + A_{SAH-2}) I + p_{bl}\right] t_d \tag{6.16}$$

where p_{bl} is the power consumed by the blower.

The total mass of the moisture (m_v) evaporated from the products during the drying period (t_d) was calculated as follows (Ayensu and Asiedu-bondzie, 1986).

$$m_v = \frac{m_p (M_i - M_f)}{100 - M_f} \tag{6.17}$$

Where, M_i and M_f are the initial and the final moisture contents of the product, respectively.

The thermal efficiency which is defined as the ratio of the actual temperature drop to the maximum possible temperature drop of the drying air in the drying chamber was evaluated by the following equation (Kudra, 2004; Saravacos and Maroulis, 2011).

$$\eta_{dc} = \frac{T_{id} - T_{od}}{T_{id} - T_{amb}} \tag{6.18}$$

where T_{id} and T_{od} are the inlet and outlet air temperatures of the drying chamber, respectively and T_{amb} is the ambient temperature.

The overall thermal efficiency of the drying system is defined as the ratio of the energy required to evaporate the moisture from the product to the total energy input into the drying system. It is expressed as follows.

$$\eta_{ds} = \frac{m_v h_{fg}}{p_t} \tag{6.19}$$

6.4 Exergy Analysis of the Drying Chamber

The exergy losses associated with the drying chamber are the exergy loss with the air leaving the drying chamber, the exergy losses from the walls of the dryer due to heat losses, and the exergy loss (exergy investment) in drying of the product (Dincer and Rosen, 2007). The exergy inflow and outflow of a drying chamber are shown in Fig. 6.1. The newly developed dryer is a batch type, and therefore, the exergy outflow of the product is neglected during the exergy analysis of the drying chamber although some amount of exergy outflow may occur along with the product when the drying operation is stopped.

The exergy analysis was performed based on the general form of the flow exergy equation for the steady flow system. The following assumptions were made for the exergy analysis.

- The flow was assumed to be steady,
- The effects of the kinetic and the potential energy were neglected, and
- The effect of the moisture content on the heat capacity of the air is neglected

Therefore, the general form of the exergy equation can be expressed as follows (Nag, 2010).

$$\dot{E}x = \dot{m}_a \left[C_{pa}(T - T_r) - T_r \left\{ C_{pa} \ln\left(\frac{T}{T_r}\right) - R \ln\left(\frac{P}{P_r}\right) \right\} \right] \tag{6.20}$$

where T and P are the temperature and the pressure of air at a given time, respectively, T_r and P_r are the reference temperature and pressure, respectively.

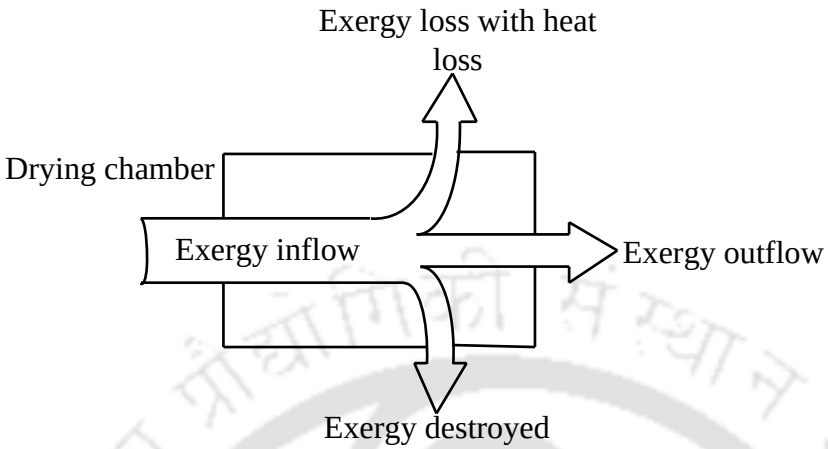

Fig. 6.1 Exergy flow diagram of the drying chamber.

The change in the pressure between the inlet and the exit of the drying chamber is negligible, and the Eq. (6.20) can be written as (Corzo *et al*., 2008; Aviara *et al*., 2014; Amjad *et al*., 2016).

$$\dot{E}x = \dot{m}_a C_{pa}\left[(T - T_r) - T_r \ln\left(\frac{T}{T_r}\right)\right] \tag{6.21}$$

Therefore, the exergy inflow and outflow of the drying chamber can be expressed by Eqs. (6.22) and (6.23), respectively.

$$\dot{E}x_{id} = \dot{m}_a C_{pa}\left[(T_{id} - T_r) - T_r \ln\left(\frac{T_{id}}{T_r}\right)\right] \tag{6.22}$$

$$\dot{E}x_{od} = \dot{m}_a C_{pa}\left[(T_{od} - T_r) - T_r \ln\left(\frac{T_{od}}{T_r}\right)\right] \tag{6.23}$$

The exergy loss in drying of the product is obtained by

$$\dot{E}x_{ls} = \dot{E}x_{id} - \dot{E}x_{od} \tag{6.24}$$

The exergy efficiency of the drying chamber is defined as the ratio of the exergy outflow to the exergy inflow of the drying chamber. It is expressed by Eq. (6.25) (Celma and Cuadros, 2009; Aghbashlo *et al*., 2013).

$$\eta_{Ex,dc} = \frac{\dot{E}x_{od}}{\dot{E}x_{id}} \tag{6.25}$$

6. 5 Results and Discussion

The experimental results and analysis of the drying processes of the two products are elaborated in the following sections.

6.5.1 Drying of Ghost chilli

The drying experiments of the Ghost chilli were performed for seven consecutive days (25th – 31st October 2015), starting from 9:00 h to 15:00 h. The variations in the solar radiation and the ambient temperature for the seven consecutive days during the experiments are shown in Fig. 6.2. The interruptions of the curves indicate the night period. The solar radiation intensity during the test period varied from 353 W/m^2 to 971W/m^2 with an average of 785 W/m^2. The maximum solar radiation intensity was recorded between 10:30 h and 11:30 h. The ambient air temperature was in the range of 27–32 ^{o}C with an average of 30 °C.

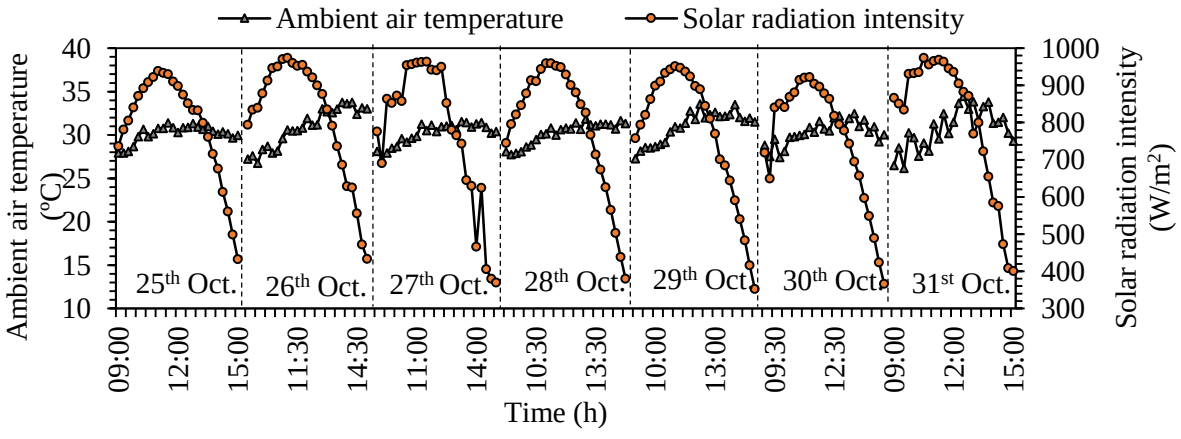

Fig. 6.2 Variation in the solar radiation intensity and the ambient temperature for seven consecutive days.

The moisture content of the chilli sample was reduced to 3% (w.b.) from its initial moisture content of 85.5% (w.b.) in 36 h in the drying air temperature range from 42 ^{o}C to 61

°C (Figs. 6.3 and 6.4). However, the whole mass of chilli dried in slightly higher drying time which was 42 h. The sample dried in less time because the sample - tray was placed near the plenum chamber of the dryer in the first stage of the drying trays throughout the experiment for which it was exposed to the drying air at relatively higher temperature. However, the positions of the main drying trays were changed at a regular interval of time (2 h) during the experiment, and thereby the chilli pods in the drying trays were exposed to different drying air temperatures.

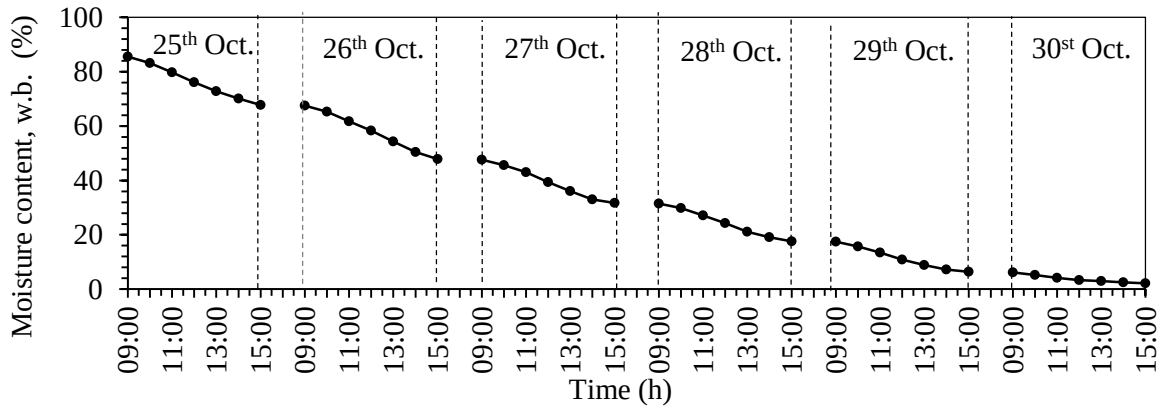

Fig. 6.3 Variation in the moisture content of the Ghost chilli sample with drying time.

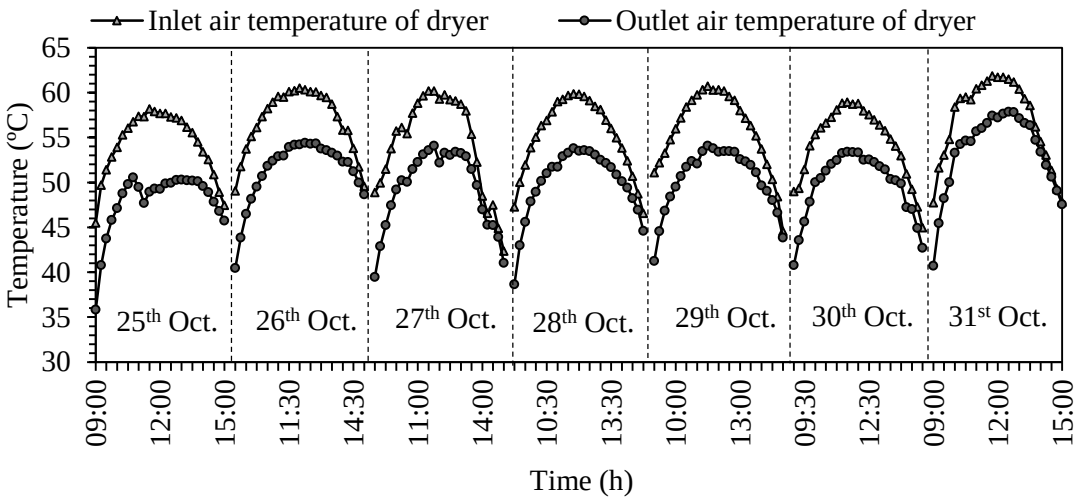

Fig. 6.4 Inlet and outlet air temperatures variation of the drying chamber with time.

Figure 6.5 exhibits the inlet and outlet temperatures variations of the SAH for seven consecutive days. The outlet temperature of the SAH - 1 and the SAH - 2 varied from 37 °C to

60 °C and 43° C to 69 °C, respectively at the constant air mass flow rate of 0.02 kg/s. The variation in the thermal efficiencies of the solar heaters (from 9:00 h to 15:00 h) for seven consecutive days is shown in Fig. 6.6.

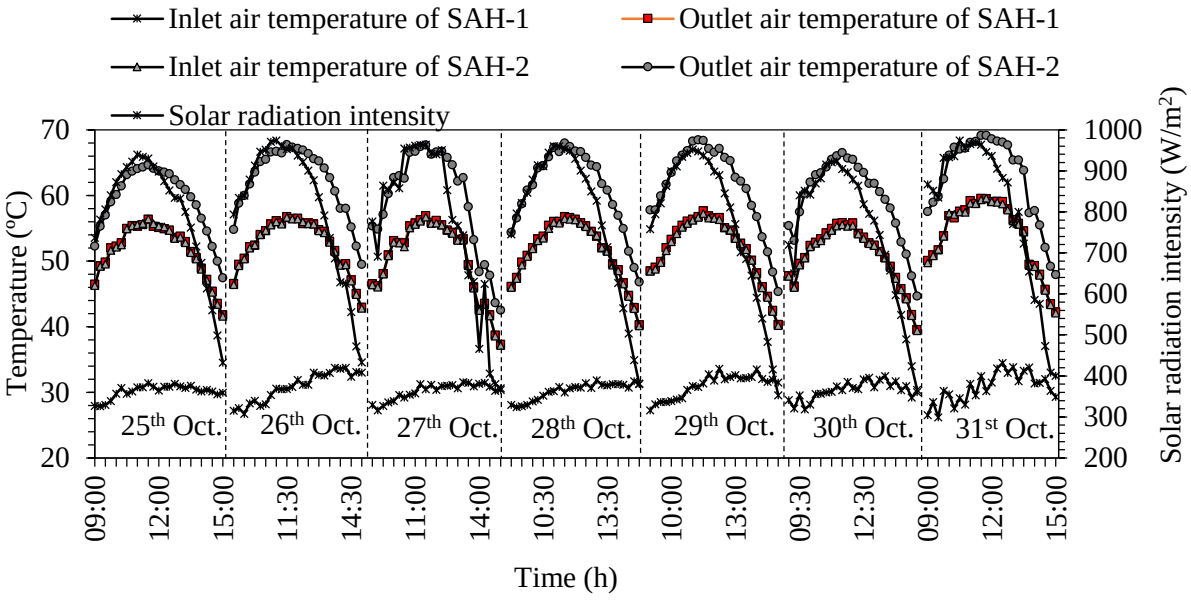

Fig. 6.5 Change in the air temperature with time at different locations of the SAHs.

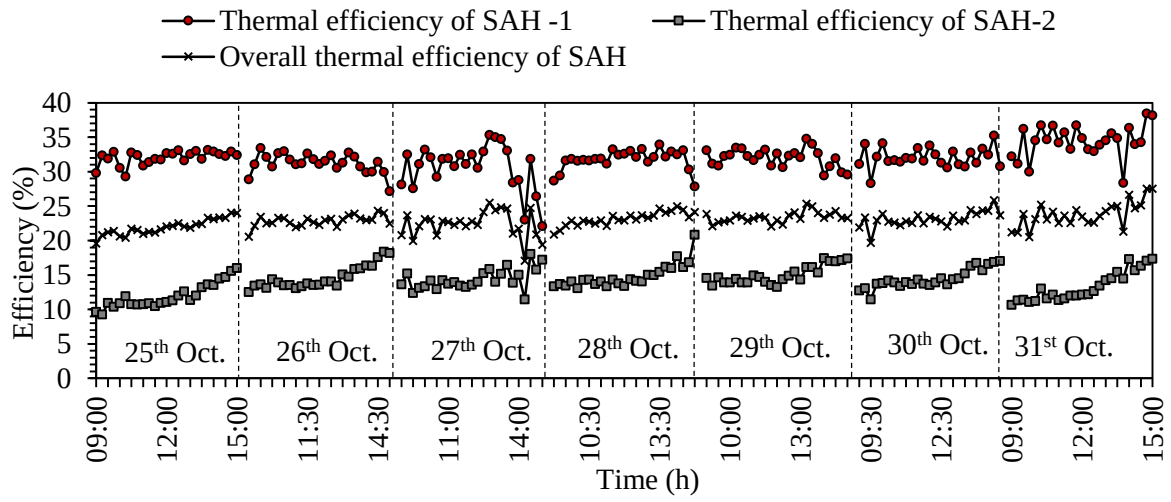

Fig. 6.6 Variation in the thermal efficiency of SAHs for seven consecutive days.

The thermal efficiencies of the air heaters were calculated employing equation Eq. (6.7) for $\alpha = 0.95$ and $\tau = 0.85$ (Similar values were reported by Duffie and Beckman, 2006 and Sangpradit, 2014). The thermal efficiency of the SAH - 1 and the SAH - 2 were found to be in the range of 22.1–38.4% with an average of 32.1% and 9.6–18.4% with an average of 14.1%, respectively. The average overall efficiency of the air heaters array was 22.9%. The efficiency

of the SAH - 2 was found to be lower compared with the first one because of the high inlet air temperature of the heater. The outlet temperature of the SAH - 1 which ranged between 37 °C and 60 °C was the inlet temperature of the SAH - 2. The high inlet air temperature causes a high temperature of the absorber plate of the solar air heaters. As a result, the heat losses from the absorber plate of the heater increases because of the re - radiation and the convection (Sukhatme and Nayak, 2010). Hence the high inlet air temperature was the cause of the low efficiency of the SAH - 2. The efficiency of the solar heaters was found to be high at the low solar radiation. A similar pattern of the result was reported by Fudholi *et al*., 2015.

The average power consumed by the blower and the solar radiation incident on the surface of the air heaters were found to be 250 W and 785 W/m^2, respectively. The total area of the solar heater panel was 4 m^2. Applying Eq. (6.19) for $t_d = 42$ h, $h_{fg} = 2.72$ MJ/kg, $I = 785$ W/m^2 and $p_{bl} = 250$ W, the overall thermal efficiency of the drying system was found to be low, viz. 4%, because of which the specific energy consumption was found to be high, viz. 18.7 kW h/kg. This may be due to the low loading capacity of the dryer. As shown in Fig.6.4, the maximum drop in air temperature between the inlet and the outlet of the drying chamber was 8 °C during the peak sunshine hours, when the inlet and outlet temperatures of the drying chamber were 61 °C and 53 °C, respectively. This shows that a major part of the energy available in the drying air was not utilised and wasted in the exhaust. The overall thermal efficiency is expected to improve with increasing the loading capacity of the dryer. The drying chamber has sufficient space to accommodate six more trays with which the loading capacity of the dryer may be increased to around 20 kg. Therefore, a further experiment is required to find out the optimum loading capacity of the dryer.

The exergy inflow and outflow, the exergy loss, and the exergy efficiency variation with time are shown in Fig. 6.7. The exergy inflow and outflow of the dryer varied from 4.4 W to 30 W and 2 W to 22 W, respectively, and the exergy loss was in the range of 1–12 W. The exergy efficiency of the dryer varied between 21% and 98% with an average of 64%. It is observed that the exergy efficiency is low at the beginning of the drying process of the next day after the interruption during the night period. It increases rapidly in the first hour and then remains almost steady for about 3 h. It again starts increasing in the last 2 h. Fudholi *et al*. (2015) reported the similar pattern of the exergy efficiency curve for the solar dryer.

At the beginning of the drying operation on each day after the interruption during the night period, more heat is consumed to raise the temperature of the chilli pods and the wall material of the drying chamber from the ambient conditions, resulting in less exergy outflow of the drying chamber. When the temperature of the chilli pods and the wall material reach a

steady state, the exergy efficiency remains almost steady. In the latter part of the day from 13:00 h to 15:00 h, the inlet temperature of the drying chamber decreases with decreasing solar radiation intensity, resulting in low exergy inflow of the drying chamber. However, the exhaust air temperature does not decrease at the same rate as the temperature of the air entering the drying chamber (Fig.6.4). This is due to the accumulated heat released from the drying chamber walls material into the air causing the addition of exergy. Hence, more exergy is available with the air stream at the outlet of the drying chamber compared to the inlet leading to the high exergy efficiency in the latter part of each day.

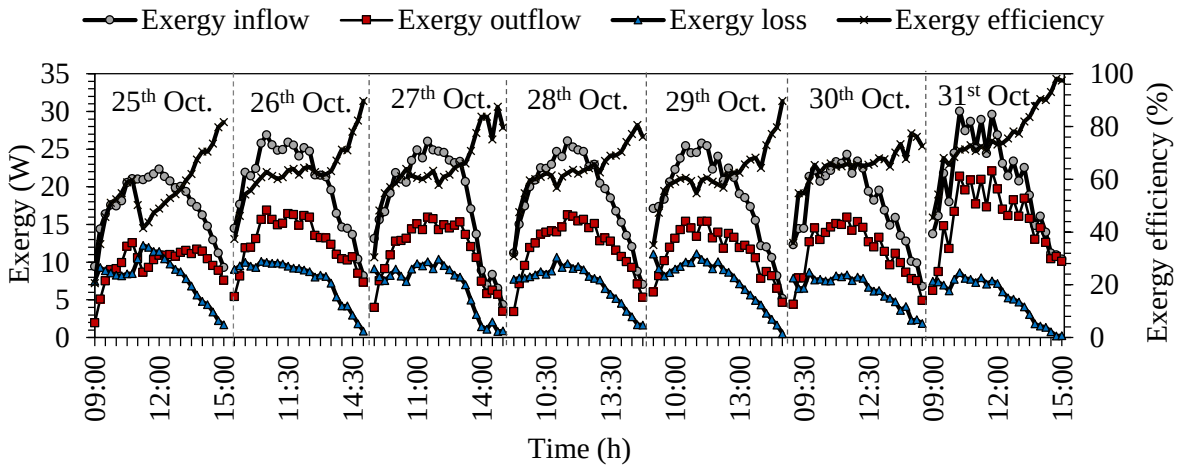

Fig. 6.7 Variation in the exergy inflow and outflow, exergy loss, and the exergy efficiency of the drying chamber for seven consecutive days.

Figure 6.8 exhibits the exergy and thermal efficiencies variation in the drying chamber. The exergetic efficiency curve has an opposite trend to the thermal efficiency curve. When the thermal efficiency increases, the exergy efficiency decreases. The higher energy consumption in the dryer leads to the higher thermal efficiency and the lower exergy efficiency. Thus, the low exergy efficiency indicates more energy requirement for drying the product. The energy utilisation ratio of a dryer is defined as the ratio of the actual enthalpy drop of air across the drying chamber to the maximum possible enthalpy drop of the drying air. If the enthalpy of the saturated vapour is neglected than the energy utilisation ratio becomes equal to the thermal efficiency. Akpinar (2010) reported the similar trend of the exergy efficiency curve and the energy utilisation ratio.

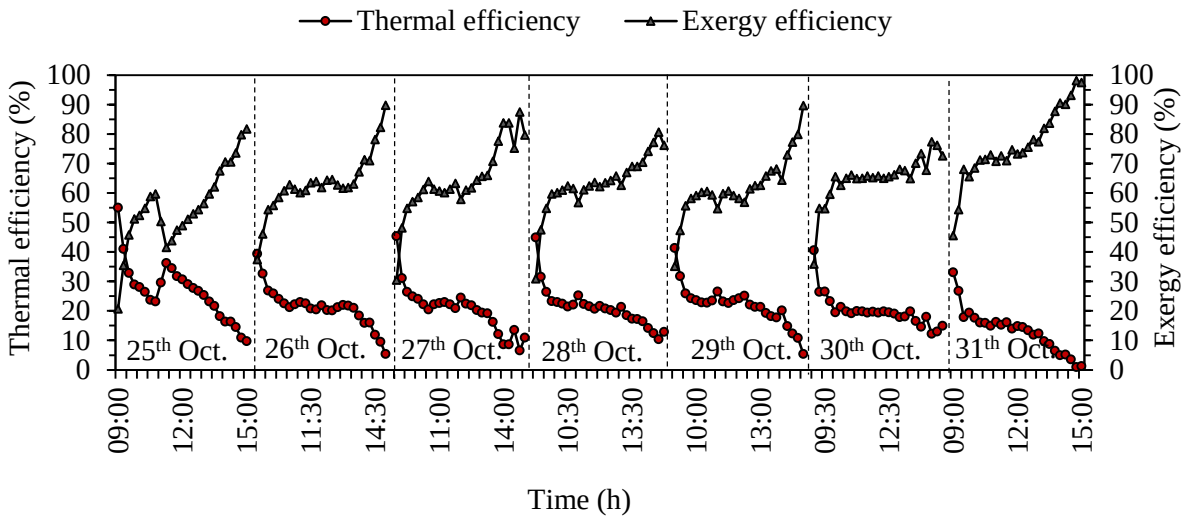

Fig. 6.8 Change in the exergetic and thermal efficiencies with the drying time.

It should be noted that the exergy efficiency has approached to around 100% towards the last days of the drying processes. This was due to the less moisture content in the products during the last stage of the drying process. The exergy investment during drying of the product was very less. The temperature drop of the drying air between the inlet and outlet of the drying chamber decreases with decrease in the moisture content of the products. As a result, the exergy inflow and outflow of the drying chamber become almost the same. This leads to very high exergy efficiency (98%). Fudholi *et al*. (2014b), Celma and Cuadros (2009), Midilli and Kucuk (2003), Fudholi *et al*. (2014a), Akbulut and Durmus (2010), and Akpinar (2010) reported similar results for exergy efficiency for drying red seaweed (47–97%) olive mill waste water (34.4–100%) pistachio (15.6–100%), red chilli (1–93%) mulberry (21.3–93.3%), and mint (34.7–87.7%) in the solar dryer, respectively.

6.5.2 Drying of sliced ginger

The drying experiment with the ginger was carried out by drying 13 kg of the sliced ginger consecutively for 5 days (9^{th} to 13^{th} November 2015) starting from 9:00 h to 15:00 h every day. The sliced ginger sample was dried in 30 h from its initial moisture content of 86.3% (w.b.) to the final moisture content of 3.5% (w.b.) (Fig.6.9). However, the moisture content of the whole mass of the sliced ginger was reduced to 10% (w.b.) in 33 h. The change in the air inlet and outlet temperatures of the SAHs and the solar radiation intensity are shown in Fig. 6.10. The outlet temperature of the SAH panel varied between 36 ºC and 65 ºC with an average

of 55 ºC. The solar radiation intensity was in the range of 207–944 W/m^2 with an average of 695 W/m^2. The solar radiation fluctuated throughout the experiment on the second day.

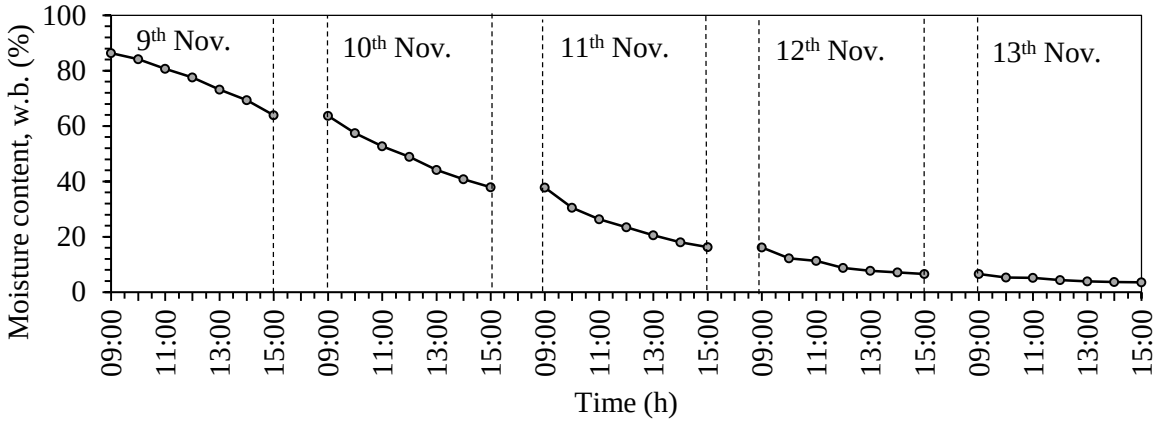

Fig. 6.9 Variation in the moisture content of the ginger with the drying time.

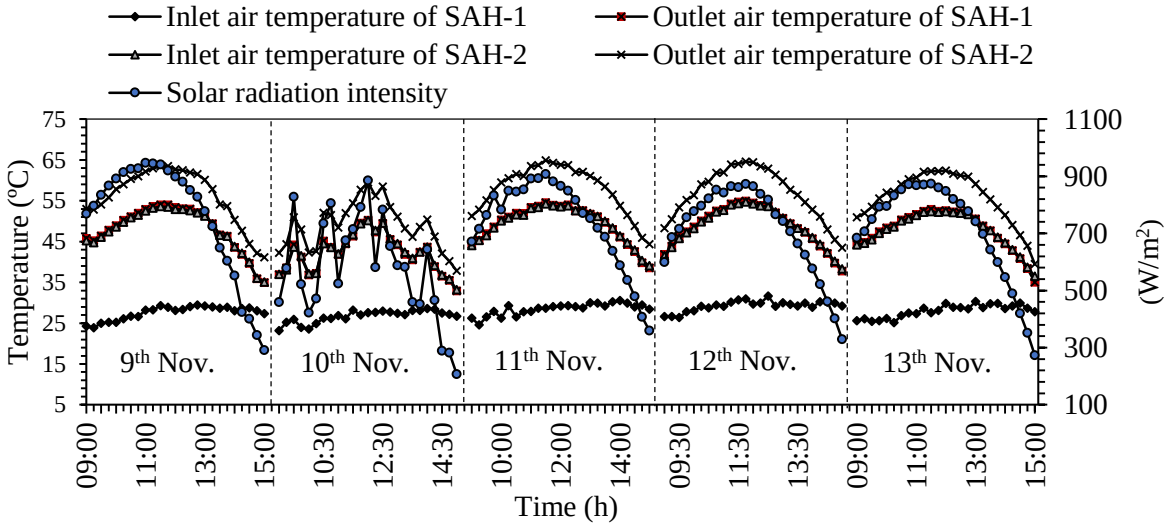

Fig. 6.10 Change in the air temperature with time at different locations of the SAHs.

The thermal efficiencies of the solar air heaters (Fig.6.11) were found to be slightly higher than in the previous experiment which was due to the lower ambient temperature. The average ambient temperature recorded during October was 30 °C while it was 28 °C during November 2015. In the second day, the efficiency fluctuated continuously due to the fluctuation in the solar radiation intensity. The average overall efficiency of the solar air heaters array was found to be 23.3%.

Figure 6.12 shows the variation in the ambient temperature, the solar radiation intensity and the inlet and outlet temperatures of the drying chamber for the five consecutive days. The

ambient temperature varied from 24 °C to 31 °C with an average of 28 °C. The solar radiation intensity and the drying air temperature were in the range of 207–944 W/m^2 with an average of 695 W/m^2 and 37–57 °C with an average of 50 °C, respectively.

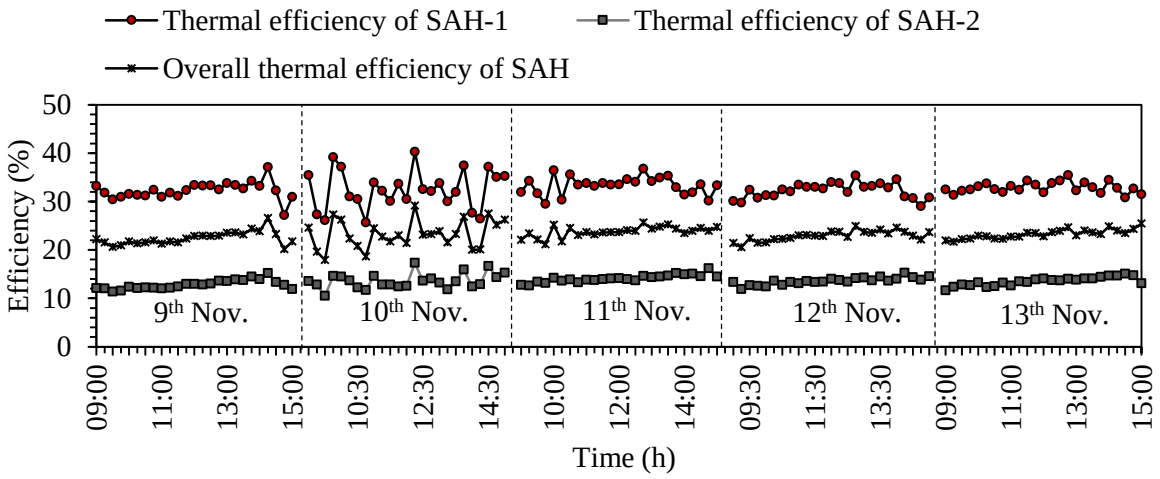

Fig. 6.11 Variation in the thermal efficiency of SAHs for five consecutive days during ginger drying.

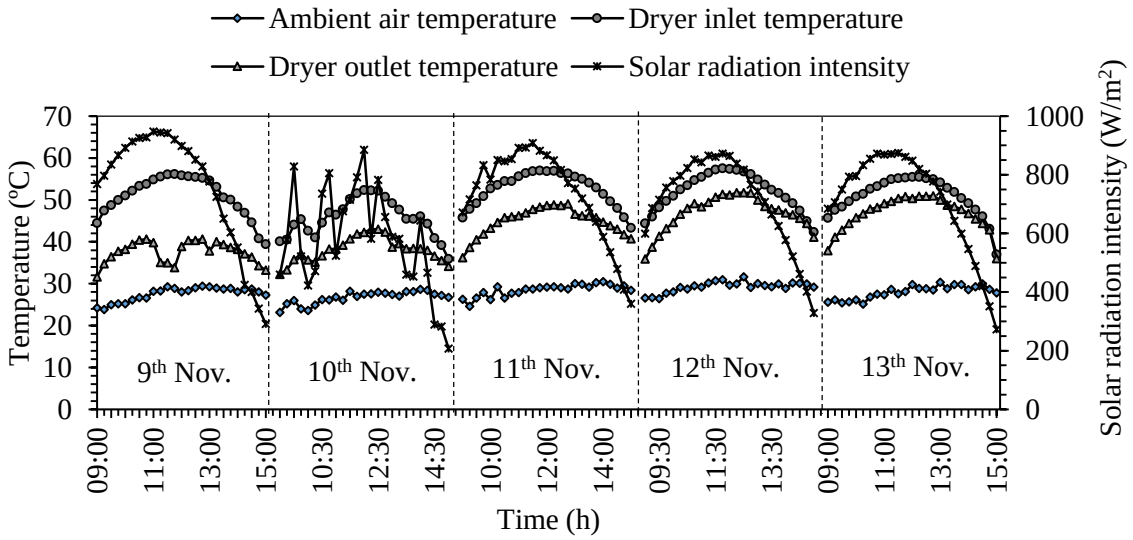

Fig. 6.12 Variations in the ambient temperature, solar radiation intensity, and the inlet and outlet temperatures of the drying chamber during ginger drying.

The exergy inflow and outflow, the exergy losses, and the exergetic efficiency of the drying chamber are shown in Fig. 6.13. The exergy inflow and outflow of the drying chamber were found to be varied from 2.6 W to 23.6 W and 1.1 W to 15.7 W, respectively. The maximum exergy inflow of the drying chamber coincided with the peak sunshine hour. The

exergetic efficiency was found to be in the range of 4–94% with an average of 47%, and it increased gradually with advancing in drying time.

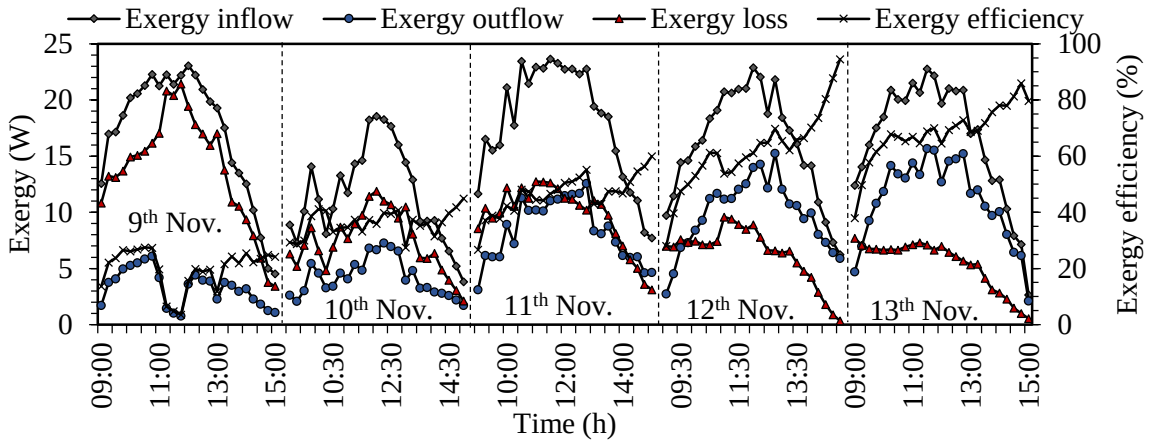

Fig. 6.13 Exergy inflow and outflow, exergy loss and the exergetic efficiency change with the drying time.

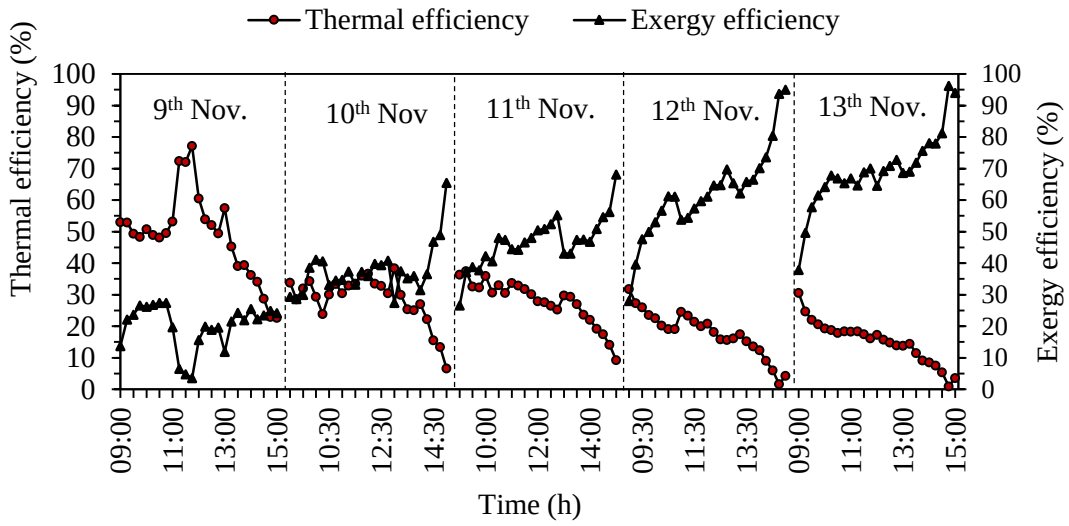

Fig. 6.14 Change in the thermal and the exergetic efficiencies of the drying process of the ginger for five consecutive days.

Figure 6.14 exhibits the thermal and exergetic efficiencies variation in the drying chamber from 9:00 h to 15:00 h for five consecutive days (9th - 13th November 2015). The thermal efficiency varied from 1% to 77%. The pattern of the thermal efficiency curve of the drying process of the sliced ginger is slightly different from the Ghost chilli one. In the case of the Ghost chilli, the thermal and exergetic efficiency curves on each day for the seven consecutive drying days are almost similar in trend for the whole drying period. However, in

the case of the ginger drying process, the exergetic efficiency increases gradually from the first to the third day, and afterwards the curves are similar in the pattern for the last two days. Thus, the sliced ginger drying process exhibited higher energy efficiency and the lower exergetic efficiency during the first few days of its drying. This may be due to moisture saturated surface of the sliced ginger during the initial period for which more heat is consumed during the initial period. With the elapse of the drying time, the free moisture diminishes from the surface and the moisture starts diffusing from the inner structure of the product to the surface.

The specific energy consumption and the overall thermal efficiency were estimated by applying Eqs. (6.15) and (6.19) for $t_d = 33$ h, $I = 695$ W/m^2 and p_{bl}=250 W and found to be 8.8 kW h/kg and 8.5%, respectively.

Table 6.1

Summary of the performance of the solar dryer while drying Ghost chilli and sliced ginger.

Particulars	Ghost Chilli	Sliced Ginger
Initial mass (kg)	9	13
Initial moisture content, w.b. (%)	85.5	86.3
Final moisture content, w.b. (%)	9.7	10
Total drying time (h)	42	33
Thermal efficiency of the SAH - 1 (%)	22.1–38.4	26.1–40.2
Thermal efficiency of the SAH - 2 (%)	9.6–18.4	10.5–19.5
Overall thermal efficiency of the air heaters (%)	23	23.3
Specific energy consumption of the product (kW h/kg)	18.7	8.8
Overall thermal efficiency of the drying system (%)	4	8.5
Exergy inflow of drying chamber (W)	4.4–30	2.6–23.6
Exergy outflow of drying chamber (W)	2–22	1–15.7
Exergy efficiency of the drying chamber (%)	21–98	4–94
Average exergy efficiency (%)	64	47

The results show that the overall thermal efficiency of the drying system is comparatively low, and the specific energy consumption is relatively high for both the products. It may be attributed to the longer drying period, the short drying operation per day, and the low loading capacity of the dryer. The dryer was operated daily for six hours because of which more drying days was required for completing the drying process. When the drying

operation was restarted after the interruption, low exergy efficiency and high exergy losses were observed in the first few hours, which indicated that more heat energy was eaten up by the products and the wall material of the drying chamber.

High exhaust air temperature of the drying chamber was recorded during the peak sunshine hours and therefore, meticulous planning for recirculation of the exhaust air, operation of the dryer with the thermal storage to extend the drying time beyond the sunshine hours, and increasing the loading capacity may slightly improve the overall performance of the drying system. It may be also worthwhile to modify the dryer to operate in the mixed mode - type (replacing the top cover of the drying chamber with a transparent cover plate) and to investigate the drying characteristics. The summary of the performance of the solar dryer is presented in Table 6.1.

6.6 Summary

Ghost chilli and sliced ginger were dried successfully in the newly developed forced convection solar dryer, and energy and exergy analyses of the drying processes of the two products were performed. The inlet air temperature significantly affects the thermal efficiency of the solar air heater. The high inlet air temperature leads to the low thermal efficiency of the solar air heater. The thermal efficiency of the SAH-1 and SAH-2 was in the range of 22.1-38.4% and 9.6-18.4%, respectively when ghost chilli was dried and it was 26.1-40.2% and 10.5-19.5% for the ginger drying. The energy and exergetic efficiencies may change during successive drying and also from product to product. The sliced ginger drying process exhibited higher overall thermal efficiency (8.5%) and lower exergetic efficiency (Avg. 47%) during the initial stage of the drying period. The exergetic efficiency increases with progressing in the drying time. The overall exergetic efficiency of the drying process of Ghost chilli (21–98% with an average of 64%) was higher than that of the sliced ginger (4–94% with an average of 47%). The specific energy consumption depends on the type of the product dried, drying time, and the loading of the dryer. The specific energy consumption of Ghost chilli (18.7 kW h/kg of moisture) was higher than that of the sliced ginger (8.8 kW h/kg of moisture). The high exergy and low thermal efficiencies of the drying chamber manifest considerable energy losses with the exhaust air.

Chapter - 7

Performance Tests on the Solar Dryer with the Latent Heat Storage

7.1 Introduction

Recently, the solar dryer with latent heat storage has received much attention due to many advantages associated with it over the sensible heat storage system. Numerous solar dryers of different structures and working principles integrated with different configurations of latent heat storage systems were developed by many researchers (Devahastin and Pitaksuriyarat, 2005; Cakmak and Yildiz, 2011; Esakkimuthu *et al*., 2013; Shalaby and Bek, 2014; Shringi *et al*., 2014; Jain and Tewari, 2015; Reyes *et al*., 2014; Agrawal and Sarviya, 2016). The details of their studies have been elaborated in the literature review. It is observed from the literature that most previously published works on the solar dryer with integrated LHS unit were carried out to study the feasibility of the using of LHS in the solar dryer. Few studies were performed to study the effects of the air velocity and the temperature on the charging and discharging characteristics of the latent heat storage unit of the dryer and the drying kinetics of the agriculture products dried. Further, the studies on the exergy analysis of the solar drying system focused only on the exergy analysis of the drying chamber and the drying process of a specific product. Complete energy and exergy analyses of each component of the drying system integrated with a latent heat storage unit has not been reported in the literature. In addition, drying of red chilli in a solar dryer integrated with a latent heat storage unit have not been reported in the literature. Therefore, the latent heat storage of the developed dryer was filled with paraffin wax and tested by drying red chilli. The performance of each component of the drying system was evaluated by the energy and exergy analyses. The details of the experimental procedures, energy and exergy analyses of the drying system, and experimental results are discussed in the following sections of this chapter.

7.2 Experimental Procedure

The shell side of the heat exchanger was filled with 34 kg of paraffin of average melting temperature of 58 ºC produced by Indian Oil Corporation, Digboi refinery, Assam, India. Then

the dryer was tested by drying an agricultural product available during the month of April in this subtropical North - Eastern region of India. The product is red chilli. Ripe chilli of a local variety was collected from a local market and was kept in a cold and dry place for 24 h for getting complete ripe. Then the trays of the drying chamber were loaded with 20 kg of the chilli. The loading density of the dryer was 6.9 kg/m^2. It is to be noted that the dryer was initially designed for drying 10 kg of chilli in 6 nos. of drying trays. When the dryer was tested with 9 kg of ghost chilli, the overall thermal efficiency of the drying system was found to be only 4%. Therefore, to improve the thermal efficiency further, three more drying trays were incorporated in the solar dryer. With total of 9 drying trays, 20 kg of red chilli was loaded.

To measure the moisture removal rate, a sample of 100 g was taken in a small sample - tray. The sample - tray was placed near the plenum chamber (in the first stage of the main - trays). Another sample of 100 g was dried simultaneously outside in the direct sun in a perforated tray. The mass of the both samples was measured at 1 h interval. The positions of the main trays were changed from the tray loading door to unloading door at a regular interval of time (2 h). Every day, the drying experiment was started from 8:00 h and stopped at 18:00 h. The samples were kept in airtight containers after completion of the experiment on each day. The initial and final moisture contents of the chilli were determined by the oven method. The temperatures of the air at different locations of the drying system, solar radiation intensity, power consumed by the blower, mass flow rate of the drying air and other parameters were measured by following the similar procedures as the earlier experiments.

7.3 Energy Analysis

The energy analysis of the components of the drying system was carried out based on the general mass and energy conservation equations assuming the flow to be steady during the energy analysis. The steady flow general mass and energy conservation equations are expressed as follows (Cengel and Boles, 2010).

$$\sum \dot{m}_i = \sum \dot{m}_o \tag{7.1}$$

$$\dot{Q} - \dot{W} = \sum \dot{m}_o \left(h_o + \frac{v_o^{\,2}}{2} + Z_o g\right) - \sum \dot{m}_i \left(h_i + \frac{v_i^{\,2}}{2} + Z_i g\right) \tag{7.2}$$

In the drying system, the effects of the kinetic and potential energy are neglected for the following reasons.

- The dryer is horizontal,
- The inlet and outlet of the solar air heaters are located at the same height from the ground,
- The change in the air velocity between the inlet and the exit is negligible, and
- The energy storage is horizontal.

7.3.1 Energy analysis of the energy storage

The instantaneous heat input to the storage during the charging process is expressed by Eq. (7.3).

$$\dot{Q}_{ch} = \dot{m}_a C_{pa} (T_{i,es} - T_{o,es}) \tag{7.3}$$

where $T_{i,es}$ and $T_{o,es}$ are the inlet and outlet temperatures of the energy storage, respectively. Then net heat input or transferred to the storage material during the charging period is given by Eq. (7.4).

$$Q_{ch} = \int_0^t \dot{Q}_{ch} dt \tag{7.4}$$

Similarly, the instantaneous heat and net heat recovered from the storage during the discharging period are given by Eqs. (7.5) and (7.6).

$$\dot{Q}_{dich} = \dot{m}_a C_{pa} (T_{o,es} - T_{i,es}) \tag{7.5}$$

$$Q_{dich} = \int_0^t \dot{Q}_{dich} dt \tag{7.6}$$

The overall energy efficiency of the storage or the percentage of the energy recovered is defined as the ratio of the net heat recovered to the net heat input. It is expressed by the following equation (Dincer and Rosen, 2011).

$$\eta_{es} = \frac{Q_{dich}}{Q_{ch}} \tag{7.7}$$

The energy analysis of the solar air heaters and the drying chamber have been discussed in the section 6.3 of the previous chapter.

7.4 Exergy Analysis

Exergy analysis was performed for each component of the drying system. The following assumptions were made during the exergy analysis.

- The flow was assumed to be steady,
- The effects of the kinetic and potential energy were neglected,
- The exergy loss in the product was negligible.
- The change in the pressure between the inlet and out was neglected

Therefore, the steady flow exergy equation is expressed as follows (Nag, 2010).

$$\dot{E}x = \dot{m}_a \left[C_{pa}(T - T_r) - T_r \left\{ C_{pa} \ln\left(\frac{T}{T_r}\right) - R \ln\left(\frac{P}{P_r}\right) \right\} \right] \tag{7.8}$$

7.4.1 Exergy analysis of the SAH

The exergy received by the working fluid (air) of the SAH - 1 and the SAH - 2 are given by Eqs. (7.9) and (7.10), respectively.

$$\dot{E}x_{re,SAH-1} = \dot{m}_a C_{pa} \left[\left(T_{o,SAH-1} - T_{i,SAH-1}\right) - T_r \ln\left(\frac{T_{o,SAH-1}}{T_{i,SAH-1}}\right) \right] \tag{7.9}$$

$$\dot{E}x_{re,SAH-2} = \dot{m}_a C_{pa} \left[\left(T_{o,SAH-2} - T_{i,SAH-2}\right) - T_r \ln\left(\frac{T_{o,SAH-2}}{T_{i,SAH-2}}\right) \right] \tag{7.10}$$

The exergy input to the SAH is expressed by Eq. (7.11) (Yadav *et al*., 2014).

$$\dot{E}x_{in,SAH} = \left[1 - \frac{T_r}{T_s}\right] \dot{Q}_{in} \tag{7.11}$$

The apparent sun temperature (T_s) is assumed to be 4500 K (Jafarkazemi and Ahmadifard, 2013). The exergy efficiency of the solar air heater is expressed as follows (Akpinar and Koçyigit, 2010; Park *et al*., 2014).

$$\eta_{Ex,SAH} = 1 - \frac{\dot{E}x_{dest}}{\dot{E}x_{in,SAH}} \tag{7.12}$$

$$\text{Or } \eta_{Ex,SAH} = \frac{\dot{E}x_{re,air}}{\dot{E}x_{in,SAH}} \tag{7.13}$$

The exergy destruction in the solar heater is given by Eq. (7.14) (Esen, 2008; Bayrak *et al*., 2013).

$$\dot{E}x_{dest} = \left(1 - \frac{T_r}{T_s}\right)\dot{Q}_{in} - \dot{m}_a C_{pa}\left[\left(T_{o,SAH} - T_{i,SAH}\right) - T_r \ln\left(\frac{T_{o.SAH}}{T_{i,SAH}}\right)\right] \tag{7.14}$$

7.4.2 Exergy analysis of the energy storage

The instantaneous exergy input to the energy storage during the charging process is given by Eq. (7.15) (Dincer and Rosen, 2011).

$$\dot{E}x_{ch} = \dot{m}_a C_{pa}\left[\left(T_{i,es} - T_{o,es}\right) - T_r \ln\left(\frac{T_{i,es}}{T_{o,es}}\right)\right] \tag{7.15}$$

The instantaneous exergy recovered from the storage during the discharging process is given by Eq. (7.16).

$$\dot{E}x_{dich} = \dot{m}_a C_{pa}\left[\left(T_{o,es} - T_{i,es}\right) - T_r \ln\left(\frac{T_{o,es}}{T_{i,es}}\right)\right] \tag{7.16}$$

The net exergy input and exergy recovered during the charging and discharging periods are calculated by employing Eqs. (7.17) and (7.18), respectively.

$$Ex_{ch} = \int_0^t \dot{E}x_{ch}\,dt \tag{7.17}$$

$$Ex_{dich} = \int_0^t \dot{E}x_{dich}\,dt \tag{7.18}$$

The exergy efficiency of the energy storage or the percentage of exergy recovered is defined as the ratio of the net exergy recovered from the energy storage during the discharging period to the net exergy input to the storage during the charging period. It is expressed as follows (Koca *et al*., 2008).

$$\eta_{Ex,es} = \frac{Ex_{dich}}{Ex_{ch}} \tag{7.19}$$

The exergy analysis of the drying chamber has been already elaborated in section 6.4 of the previous chapter.

7.5 Results and Discussions

The drying experiment was conducted during the period of 24th to 27th April 2016. The experiment was performed every day for 10 h from 8:00 h to 18:00 h. The changes in the ambient air temperature, the inlet and outlet air temperature of the solar air heaters, and the solar radiation intensity during the experiment are shown in Fig. 7.1. The ambient temperature varied between 24 ºC and 34 ºC and the highest ambient temperature was recorded 2–3 h after the peak sunshine hours of the day. The maximum solar radiation intensity was recorded between 10:49 h and 11:33 h and was in the range of 878–936 W/m^2. The maximum outlet air temperature of the SAH panel was 70 ºC, and it was observed on the first day of the experiment. A slight fluctuation in the solar radiation was noticed on the last day of the experiment due to cloud cover.

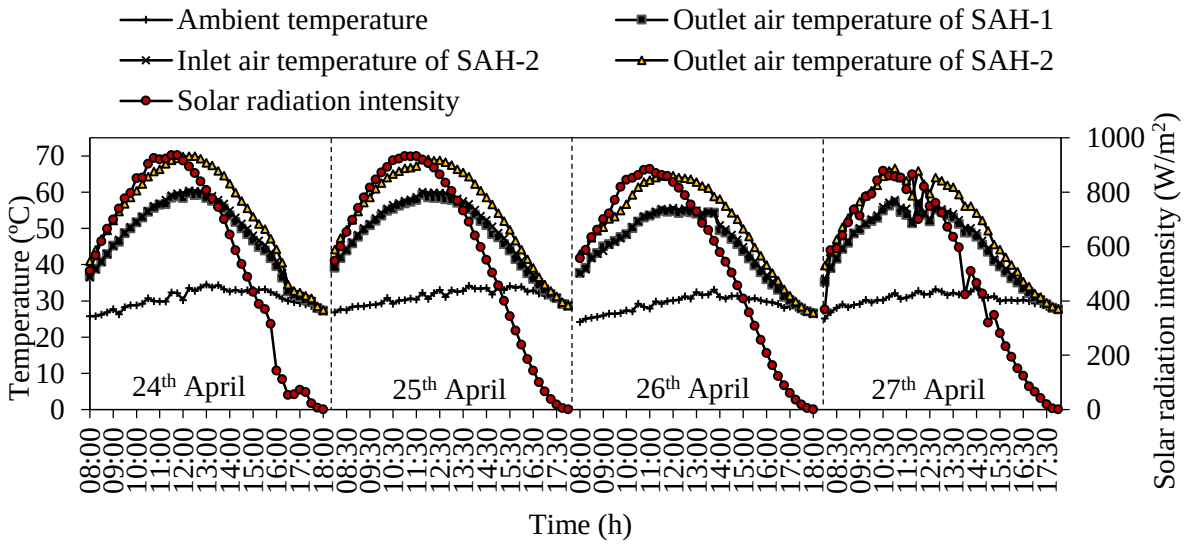

Fig. 7.1 Change in the ambient temperature, solar radiation intensity, and the inlet and outlet air temperatures of the SAHs with time.

The variation in the energy and exergy efficiencies of the solar air heaters for four consecutive days are shown in Fig. 7.2. The average energy and exergy efficiencies of the SAH

- 1 were found to be higher than the SAH - 2. The average energy efficiency of the SAH - 1 and the SAH - 2 were found to be 32.5% and 14.1% at a mass flow rate of 0.019 kg/s, respectively. The average exergy efficiency of the SAH - 1 and the SAH - 2 were found to be 0.9% and 0.8%, respectively. Alta *et al*. (2010) reported almost similar value (0.83%) of exergy efficiency of a solar air heater with a finned absorber plate. The exergy efficiencies of the solar air heaters were found to be low. The exergy efficiency of the solar air heater increased with increase in the solar radiation intensity. The highest exergy efficiency coincided with the peak sunshine hours of the day.

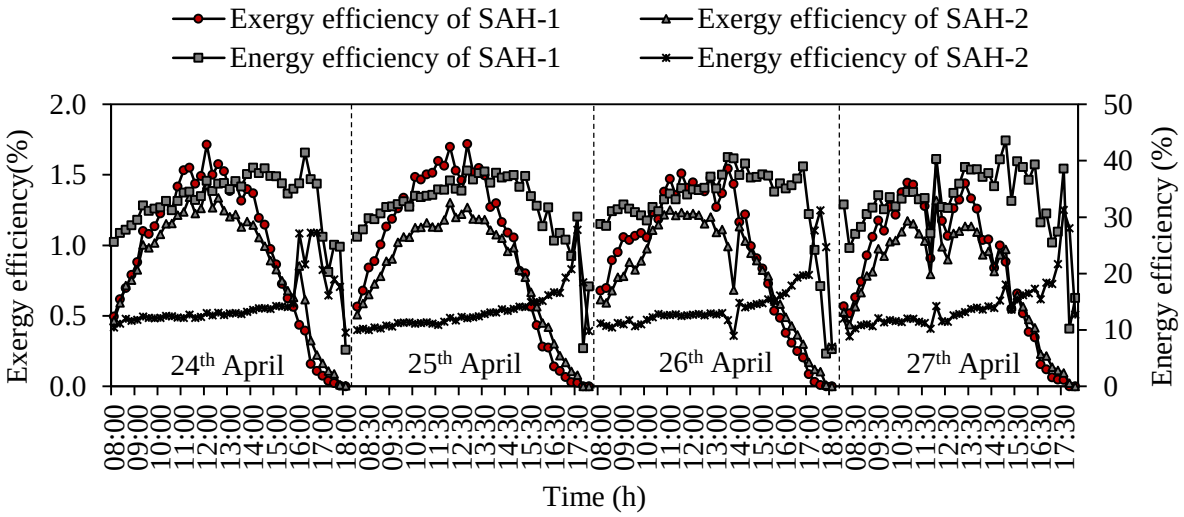

Fig. 7.2 Change in the energy and exergy efficiencies of the SAHs with time.

The variation in the inlet and outlet temperatures and the heat input and heat recovered during the charging and discharging processes of the energy storage are shown in Fig. 7.3. The highest drop in temperature of the air between the inlet and outlet of the storage during the charging process of the paraffin wax was found to be 10 ºC while the rise in temperature of the air during the discharging process was 9 ºC. The discharging of heat from the storage began from 14:15 - 14:45 h when the air temperature coming out the SAH became lower than the wax temperature. The point of intersection of the inlet and outlet air temperatures curves of the storage denotes the ending of the charging period and the beginning of the discharging period.

It was observed that the inlet air temperature of the storage varied with the change in the solar radiation intensity, i.e. increased with time, and reached the maximum value between 11:55 h and 2:19 h. After that, it started decreasing and became almost equal to the ambient temperature at around 16:15 h due to very low solar radiation intensity. However, the outlet air temperature of the storage remained higher than the ambient temperature by 6–8 ºC after

16:15 h until the experiment was stopped at 18:00 h. The charging and the discharging processes of the storage occurred depending on the air temperature coming out of the SAH and the wax temperature. In most bright sunshine days, the charging process took place during the period 8:00 h to 14:30 h

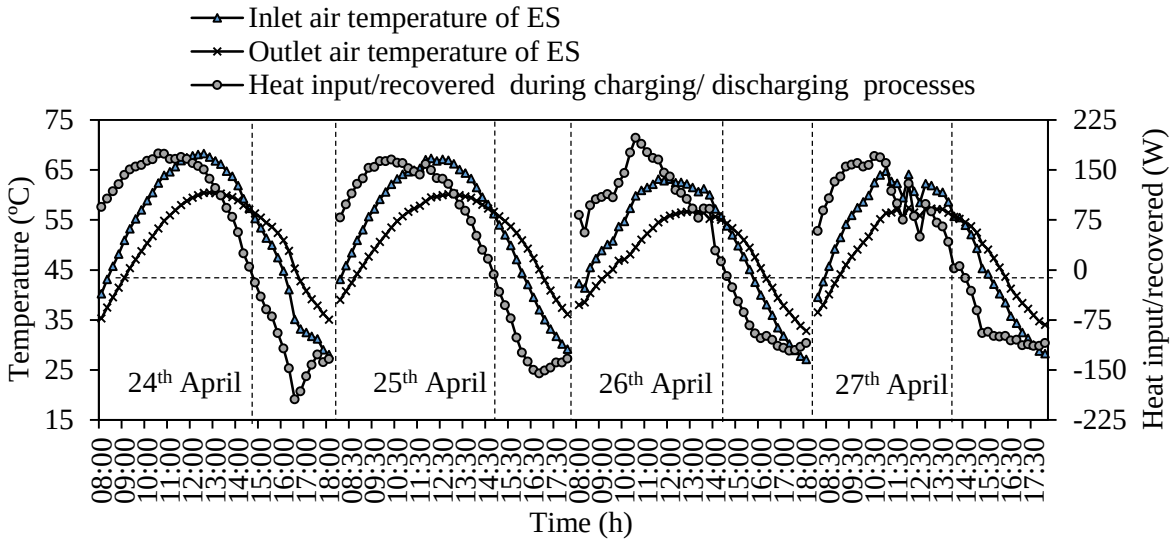

Fig. 7.3 Variation in the inlet and outlet air temperatures and the heat input and recovered during the charging and discharging processes of the ES.

The inlet air temperature of the storage was in the range of 28–68 ºC with an average of 52 ºC while, the outlet temperature was in the range of 34–60 ºC with an average of 50 ºC. In the 4th day of the experiment, the solar radiation intensity fluctuated during the period 10:30 h to 12:30 h due to the cloud cover. The effect of fluctuation in the solar radiation was reflected in the outlet air temperature of the solar air heater as well as in the inlet air temperature of the storage. However, the heat storage diminished the fluctuation in the air temperature and supplied air to the drying chamber at nearly constant temperature. The average instantaneous heat input and heat recovered during the charging and discharging processes of the energy storage varied from 105 W to 130 W and 89 W to 116 W, respectively. In Fig. 7.3, the positive heat and negative heat on the secondary Y - axis indicate the heat input to the storage and recovered from the storage, respectively.

Figure 7.4 exhibits the change in the exergy input and exergy recovered during the charging and discharging processes of the thermal energy storage with time. The exergy input to the thermal storage increased with increase in the inlet air temperature or the solar radiation intensity. The average instantaneous exergy input and exergy recovered were found to be in the range of 7.9–10.5 W and 2.9–3.9 W, respectively. As expected, it was observed that the

exergy input increased with increasing heat input. Similarly, the exergy recovered increased with increasing heat recovered.

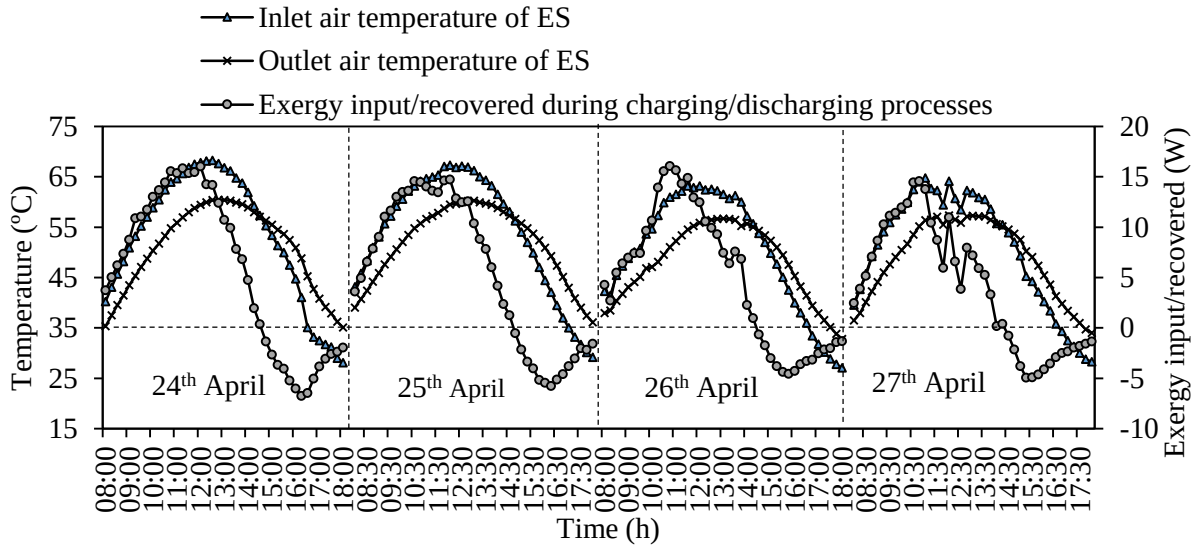

Fig. 7.4 Exergy input and exergy recovered during the charging and discharging processes of the ES.

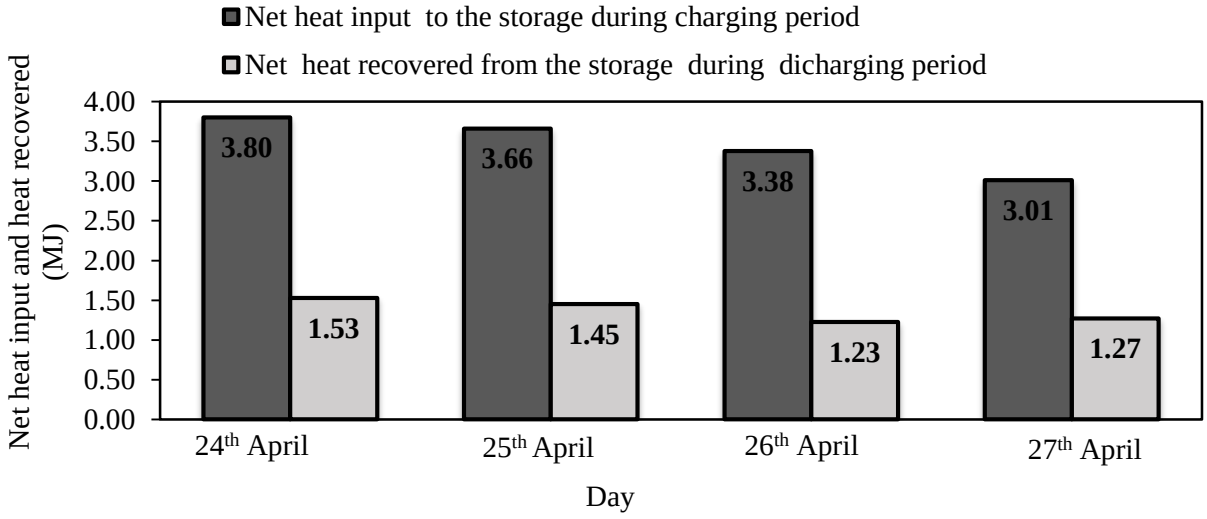

Fig. 7.5 Net heat input and heat recovered during the charging and discharging periods of the ES.

The net heat input and heat recovered during the charging and discharging periods of the storage are shown in Fig. 7.5. The net heat input and heat recovered were found to be varying between 3.1 MJ and 3.8 MJ and 1.2 MJ and 1.5 M, respectively. The average energy efficiency or the percentage of the energy recovered was found to be in the range of 36.4−42.2%. The effectiveness of the energy storage which is defined as the ratio of actual

total energy stored to the maximum total energy that can be stored (Dincer and Rosen, 2011) was found to be in the range of 31.1–41.6%. The thermal energy was not retrieved from the storage after 18:00 h as the air coming out of the storage at the temperature below 36 °C was not much effective for drying the chilli. Hence, the drying operation was stopped at that time. The unrecovered heat caused the high temperature of the wax at the end of the experiment. It was in the range of 35−43 °C. Figure 7.6 exhibits the net exergy input and exergy recovered during the charging and discharging periods. The net exergy input and exergy recovered were found to be in the range of 0.2–0.3 MJ and 0.04–0.05 MJ, respectively. The overall exergy efficiency ranged from 13.7% to 17%.

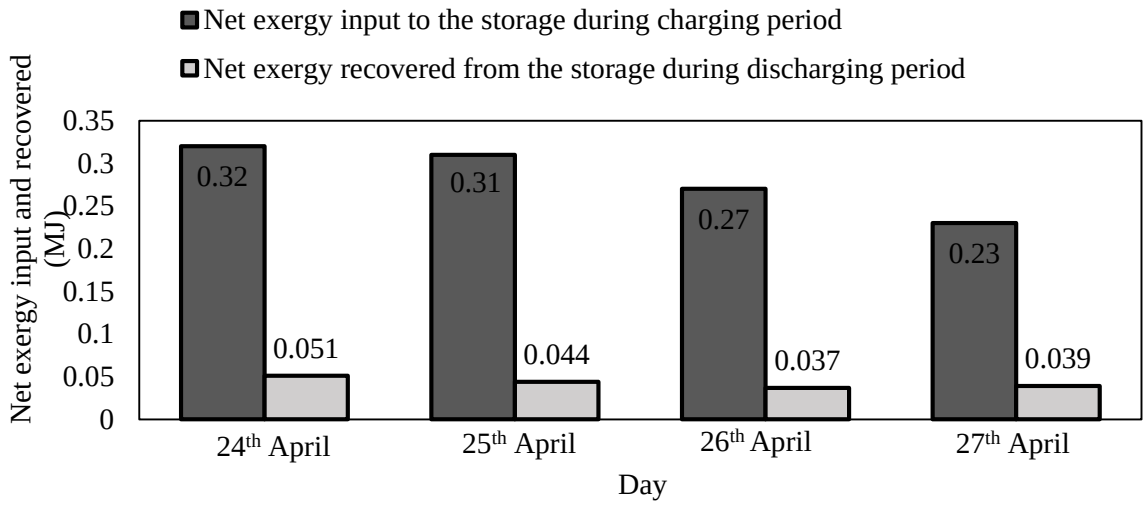

Fig. 7.6 Net exergy input and exergy recovered during the charging and discharging periods.

The variation in the wax temperature at different locations in the storage during the charging and discharging processes are shown in Fig. 7.7 and a magnified view of the temperature of the wax for one day is shown in Fig. 7.8. The locations at which the wax temperature was measured, are illustrated in Fig.4.9 of chapter - 4. As usual, it was observed that the temperature of the wax near the inlet increased and decreased first during the charging and discharging processes, respectively. The wax temperature increased with increasing inlet air temperature and reached the highest temperature of 60 ºC at around 13:00 h, later than the peak sunshine hours.

The energy analysis does not give any information about the melting and the freezing of the wax. The freezing and the melting of the PCM can be known from the measurement of the temperature of the PCM and the temperature of the charging fluid at the inlet and outlet of the storage. When the temperature of the PCM at different locations after reaching the melting

point does not change during the charging process and also the temperature of charging fluid does not change while passing through the storage, then one can assume that the PCM has melted completely.

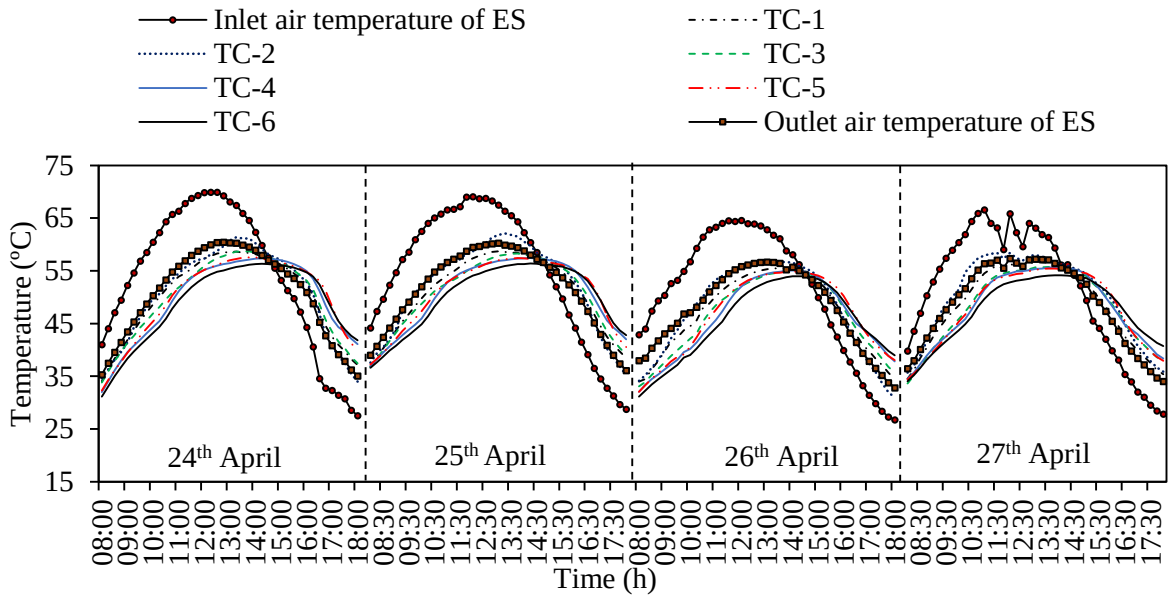

Fig. 7.7 Variation in the paraffin wax temperature at different locations during the charging and discharging processes.

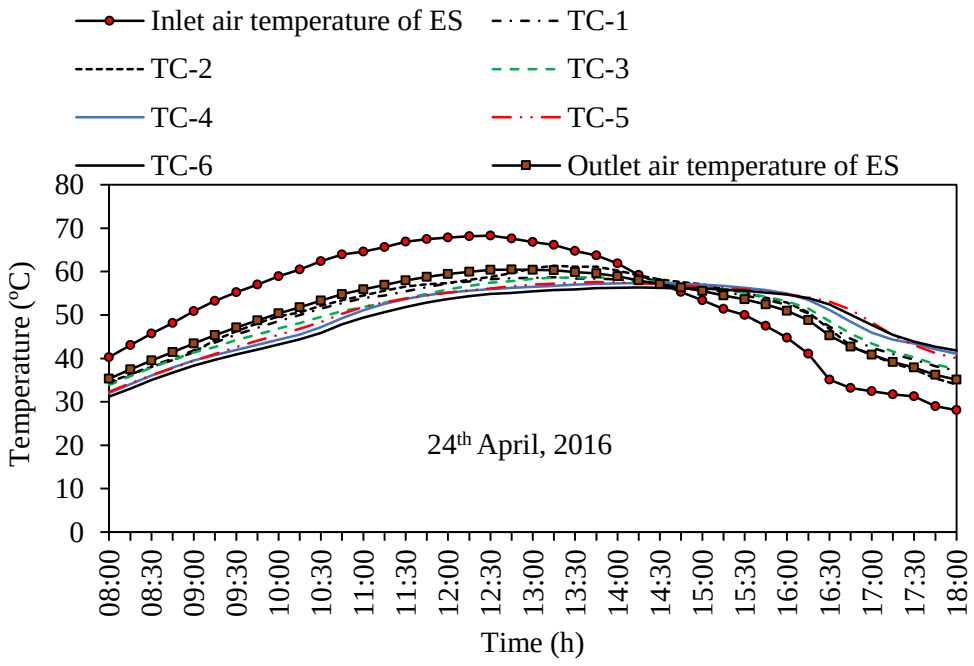

Fig. 7.8. A magnified view of the wax temperature for one day (24th April 2016).

Figure 7.9 exhibits the variation in the inlet and outlet temperatures and the exergy efficiency of the drying chamber. The inlet air temperature of the drying chamber was in the range of 35–61 ºC with an average of 50 ºC. The exergy efficiency increased with advancing drying days. The highest exergy efficiency was observed in the last two days of the drying periods. This was due to the low moisture content in the chilli towards the end of the drying process. The exergy efficiency also increased with the progress of the drying time of the day, and it increased steeply in the later part of the day. The exergy efficiency of the drying chamber was in the range of 24.3–98% with an average of 52.2%. Fudholi *et al.* (2014a), Celma and Cuadros (2009), Midilli and Kucuk (2003), Fudholi *et al*. (2014b), Akbulut and Durmus (2010), Akpinar (2010) reported similar results for drying red sea weed (47–97%), olive mill waste water (34.4–100%), pistachio (15.6–100%), red chilli (1–93%), mulberry (21.3–93.3%), and mint (34.7–87.7%) , respectively in the solar dryer.

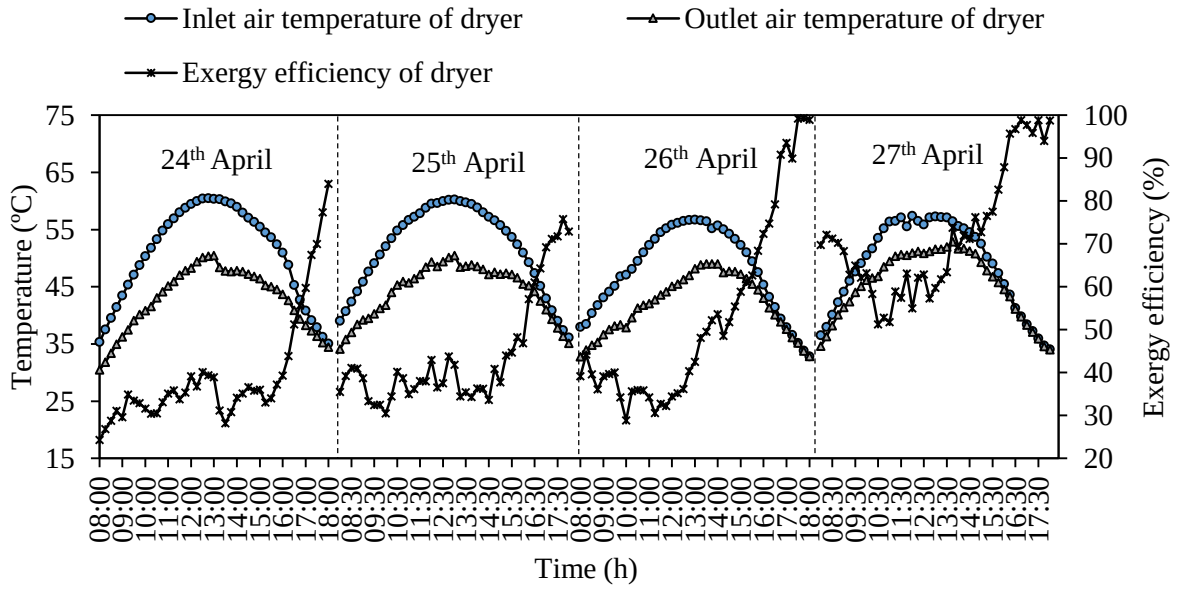

Fig. 7.9 Change in the inlet and outlet air temperatures of the drying chamber for four consecutive days.

Figure 7.10 shows the change in the moisture content of the solar and open sun dried chilli samples. The moisture content of the samples was reduced from the initial value of 73.5% (w.b.) to the final value of 9.6% (w.b.) in 35 h and 78 h in the solar dryer drying and the open sun drying, respectively. The sun drying sample took 122.8% longer drying time in comparison with the sample dried in the newly developed dryer. The product dried in the solar dryer was free from dust and hygienic. Figure 7.11 (a) exhibits the photograph of the ripe chilli pepper

taken before drying and Fig. 7.11 (b) and (c) shows the photographs of the chilli pepper taken after drying in the solar dryer and the open sun, respectively.

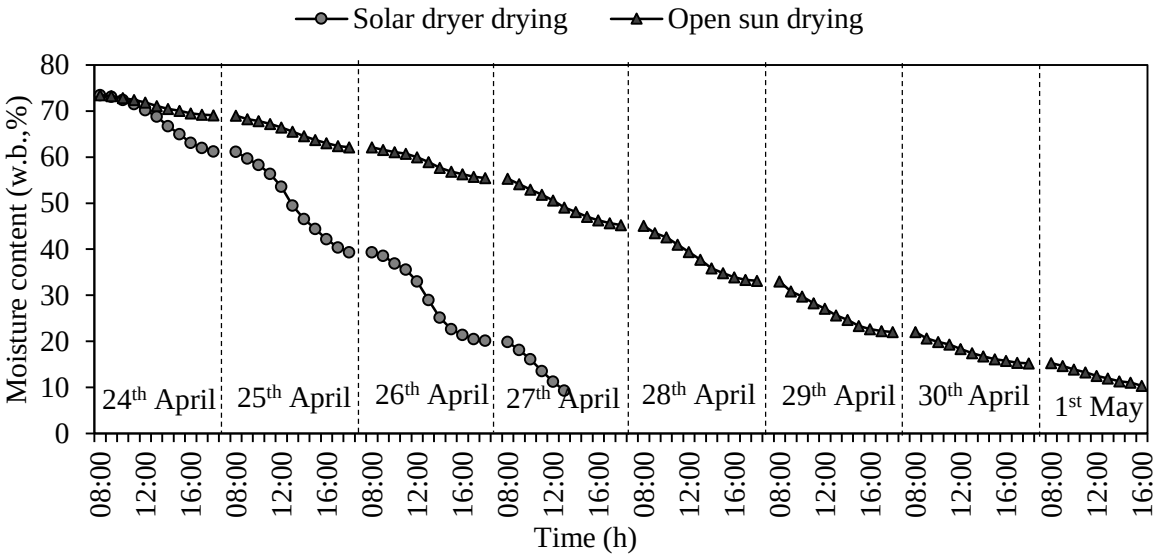

Fig. 7.10 Change in the moisture content of the solar and sun dried samples.

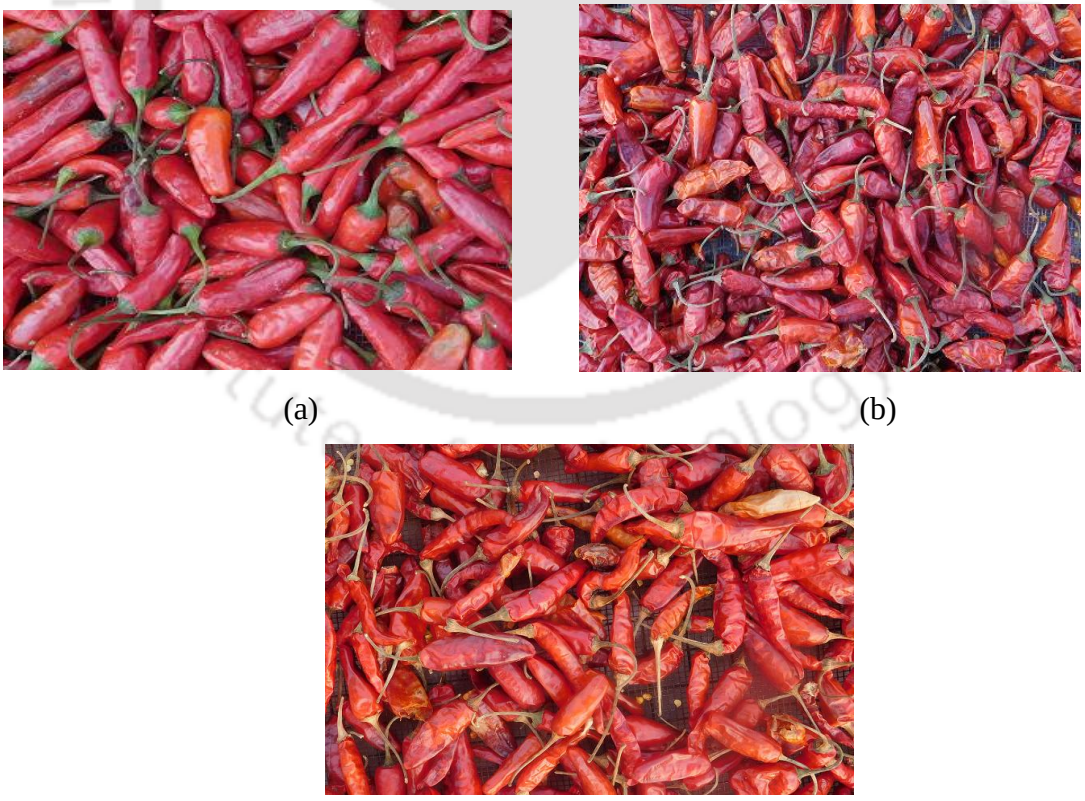

Fig. 7.11(a) Ripe chilli pods before drying (b) Chilli pods after the solar drying (c) Chilli pods after the sun drying.

It has been observed qualitatively that the colour quality of the solar dried chilli pods is better than that of the open sun dried ones. Further, it has been also noticed that the original colour of the chilli is preserved in the solar dried sample. As evident from the photographs that the colour of the solar dryer drying chilli is bright and dark reddish while the open sun dried chilli is pale and red.

The mass of the moisture evaporated from 20 kg of the chilli while reducing the moisture content to 9.6% (w.b.) from the initial value of 73.5% (w.b.), was 14.1 kg. The average intensity of the solar radiation incident on the surface of the solar air heater was found to be 556 W/m^2, and the total area of the solar collector was 4 m^2. The power consumed by the blower was 250 W, and the dryer was operated daily for 10 h. The heat required to evaporate14.1 kg of moisture was found to be 38.5 MJ. The latent heat of evaporation of water was taken at an average drying air temperature of 50 ºC which is 2.4 MJ/kg. It was increased by 15% because of the bound moisture (Ayensu and Asiedu - Bondzie, 1986) content.

The total energy input to the drying system during the entire drying period was 356.3 MJ. Applying Eq. (6.19), the overall energy efficiency of the drying system was found to be 10.8%. The specific energy consumption was found to be 6.8 kW h per kg of moisture which is close to the value (5.26 kW h/kg) reported by Fudholi *et al*., 2014a. The electrical energy consumption per kg of moisture removal was 0.7 kW h which was only 10.3% of the specific energy consumption. Thus, 90% of the total energy used for drying the product in the newly developed dryer was harvested from the free and eco - friendly solar energy.

The integration of the heat storage with the solar dryer incurs an additional capital cost. In this drying system, the second solar air heater is connected in series to the first one to produce air at sufficient temperature so that the wax in the storage melts completely. If there were no heat storage in the dryer, the temperature of the hot air produced by the first solar air heater would have been almost sufficient for the drying application [the average air temperature (47 ºC) at the outlet of the first solar air heater was close to the average air temperature (50 ºC) at the inlet of the drying chamber]. While designing the dryer, the area of the solar air heater panel was estimated considering the amount of energy stored in PCM module and the required temperature of hot air for the drying application. Therefore, the initial capital cost of the dryer increases due to the additional cost of the second solar air heater and the heat storage module.

The integration of heat storage into the solar dryer has some benefits too. The main benefit derived from the heat storage is that it supplies air at nearly constant temperature to the drying chamber during the cloudy period. Further, it also reduces the risk of overheating of the product during the peak sunshine hours. The drying process can be accelerated during the low-

intensity solar radiation period by extracting the heat from the storage and smoothing the drying air temperature. It eliminates the need for the auxiliary heat source for a small duration during the fluctuation in the solar radiation.

When the temperature of the drying chamber drops during the drying period due to cloud cover, the temperature of the product and the wall of the drying chamber also decrease. Some percentage of the sensible heat has to be wasted to bring back the temperature to the normal condition after the cloud cover. However, if a constant temperature is maintained in the drying chamber, this loss can be avoided. Thus, the integration of the thermal storage with the solar dryer maintains a constant temperature inside the drying chamber which helps in enhancing the total drying time and improving the quality and quantity of the product dried.

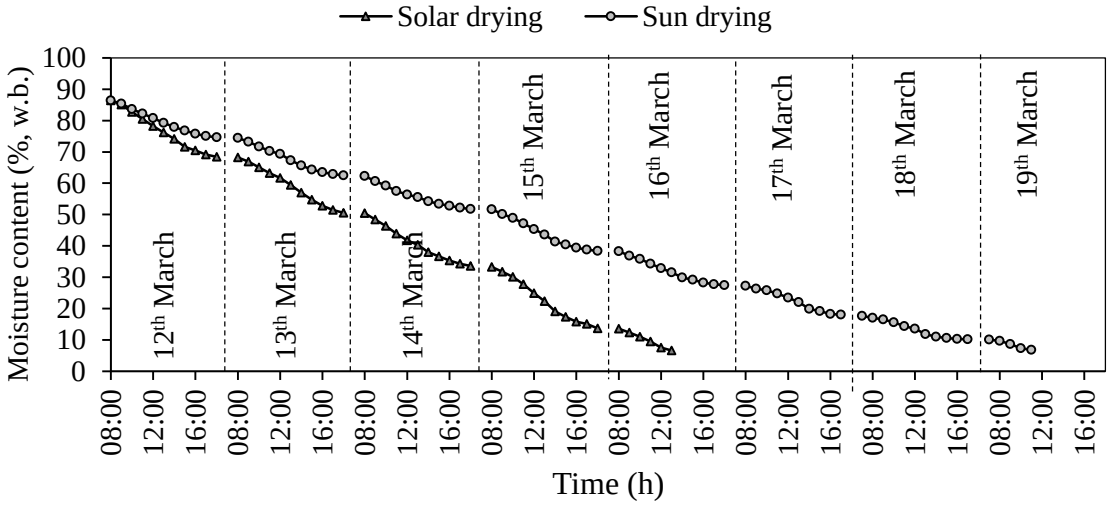

Fig. 7.12 MR vs drying time of the solar dried and sun dried samples of green chilli.

7.6 Drying of Green Chilli

The dryer was also tested by drying 20 kg of green chilli of the local variety during the period of 12th March to 16th March 2016. Two samples of 100 g were dried separately in the solar dryer and the direct sun to measure the moisture loss of the chilli and to compare the drying time. It was found that the solar dried sample dried faster than the open sun dried one. The moisture content of the solar dried sample was reduced from the initial moisture content of 83.4% (w.b.) to the final moisture content of 6.7% (w.b.) in 45 h while the sun dried sample took 80 h as shown in Fig. 7.12. The average drying air temperature in the solar dryer was 42 ^{o}C. However, the whole mass of the chilli dried in the main trays of the dryer took longer drying time (35 h) in comparison to the sample. It was due to the high drying air temperature. The solar dried sample was positioned near the plenum chamber throughout the drying experiment,

as a result it was subjected to the high temperature in comparison to the chilli pods dried in the main trays. The trays located near the plenum chamber were exposed to the high drying air temperature while the one located at the farthest distance from the plenum chamber was exposed to the lowest temperature. Therefore, the drying trays were exchanged from one end to the other end of the dryer every two hours.

Fig. 7.13 (a) Photograph of the freshly harvested green chilli (b) Photograph of the chilli after solar dryer drying (c) Photograph of the chilli after the sun drying.

The photographs of the chilli pods taken before and after drying are shown in Fig.7.13. It was observed that the open sun dried sample turned ripe during the drying period resulting in loss of the original green colour. However, the solar dryer dried chilli pods almost retained the green colour of the chilli. Therefore, it can be concluded that drying of green chilli in the direct open sun is not favourable.

7.7 Economic Analysis

Economic analysis of the dryer is carried out based on the annualised cost method (Sreekumar, 2010; Jain and Tewri, 2015). The cost of drying of 1 kg of dried product in the solar dryer has

been compared with the cost of the product dried in the electric dryer. The cost per kg of dried product is calculated by the following equation.

$$C_{dr} = \frac{C_a}{m_{dpa}} \tag{7.20}$$

where C_a is the annualised cost of the dryer, and m_{dpa} is the quantity of product dried in the dryer per year.

The quantity of the product dried in the dryer per year is calculated as follows

$$m_{dpa} = \frac{m_{dpb} N_y}{N_b} \tag{7.21}$$

where m_{dpb} denotes the mass of dried product per batch, N_y is the number of days of operation of the dryer per year, and N_b is the number of drying days per batch. The mass of dried chilli removed from the solar dryer per batch was 6 kg and the drying was completed in 4 days operating the dryer daily for 10 h. The dryer is expected to be operated for 250 days per year.

The annualised cost of the dryer is calculated by employing the following equation.

$$C_a = C_{ac} + C_m - V_a + C_{rf} + C_{re} \tag{7.22}$$

where C_{ac} is the annual capital cost, V_a is the annual salvage value, C_m is the annual maintenance cost, C_{rf} is the annual running fuel cost, C_{re} is the annual electricity cost for running the blower or fan. The annual capital cost is given by

$$C_{ac} = C_{cd} F_c \tag{7.23}$$

where C_{cd} is the capital cost of the dryer and F_c is the capital recovery factor. The capital recovery factor is given by Eq. (7.24).

$$F_c = \frac{i(1+i)^n}{(1+i)^n - 1} \tag{7.24}$$

The interest rate (i) is assumed to be 10% and the life period (n) is assumed to be 10 years. The annual salvage value is calculated by Eq. (7.25).

$$V_a = VF_s \tag{7.25}$$

The salvage value (V) is taken as the 10% of the capital cost of the dryer. The salvage fund factor (F_s) is evaluated by the following equation.

$$F_s = \frac{i}{(1+i)^n - 1} \tag{7.26}$$

The annual running cost of the solar dryer is the running cost of the blower. However, the annual running cost of the electric dryer is the sum of the annual energy cost for running the dryer and the running cost of the fan of the dryer. The annual running cost of the solar dryer is calculated by the following equation.

$$C_{re} = t_{hr} \times p_{bl} \times C_{ele} \tag{7.27}$$

where t_{hr} is the annual running hour of the dryer, p_{bl} is the power consumed by the blower (250 W), and C_{ele} is the unit cost of electricity (Rs. 6.25 per unit).

Table 7.1

Cost of the components of the dryer.

Components	Cost (Rs.)
Solar air heater	25,000
Thermal energy storage	12,000
Blower	8,000
Drying chamber with trays	20,000
Pipe and fitting	5,000
Total cost	70,000

The annual fuel cost of the electric dryer is given by the following equation.

$$C_{rf} = m_{dpa}\left[\left(\frac{M_{db}}{100}\right)\times\left(\frac{h_{fg}C_{ele}}{\eta_d \times 3600}\right)\right] \tag{7.28}$$

where M_{db} denotes the moisture content in dry basis, h_{fg} is the latent heat of evaporation, and η_d is the efficiency of the electric dryer. The efficiency of the electric dryer is assumed to be

75%. The cost of the electric dryer is assumed to be 50% of the solar dryer. The cost breakup of the components of the solar dryer is given in Table 7.1 and the summary of the cost analysis is given in Table 7.2.

Table 7.2

Summary of the economic analysis.

Particulars	**Solar dryer**	**Electric dryer**
Capital cost of the dryer C_{cc}, (Rs.)	70,000	35,000
Life of dryer, *n* (years)	10	10
Interest rate, *i* (%)	10	10
Number of operation of the dryer per year (days)	250	250
Annual capital cost, C_{ac} (Rs)	11,392	5,696
Maintenance cost, C_m (Rs) 10% of annual capital cost (C_{cc})	1,139	569
Salvage value, *V* (Rs.) (10% of the capital cost)	7,000	3,500
Annual salvage value, V_a (Rs.)	439	220
Running cost of the dryer (Rs.)	3,906	24,583
Annualized cost of the dryer (Rs.)	15,998	30,628
Quantity of product dried (kg) per year	375	375
Cost of drying per kg of dried product (Rs.)	42.7	81.4

It has been found from the economic analysis that the cost of drying per kg of dried product in the solar dryer is Rs. 42.7 while the cost of drying per kg of dried product in the electric dryer is Rs. 81.4. Thus, the drying cost in the solar dryer is Rs. 38.7 lower than that of the electric dryer. The percentage saving on the cost of drying per kg of dried product is 47.5%. However, it is costlier than the product dried in the open sun. The drying cost in the open sun is almost negligible. The only drying cost involved in the open sun drying is the labour cost. The labour cost in the sun drying is 100% more than in the solar drying since the product in the open sun dried in 8 days while it took 4 days in the solar dryer (Fig. 7.9). The colour quality of the product dried in the sun drying is inferior to the product dried in the solar dryer. The product dried in the open sun is not hygienic. It was observed that the open sun dried product was contaminated with dust during the drying period due to the blowing of dusty wind. Though, the solar drying incurs some expenses in comparison with the open sun drying, the solar drying

is preferable particularly for drying high value and photosensitive agricultural products such as Ghost chilli, Ginger, large cardamom, medicinal plants, and black pepper as the solar drying products preserve its colour, texture, and nutritional values.

7.7 Summary

Twenty kg of a local variety of red chilli was successfully dried in the hybrid dryer in four sunny days (35 h) from the moisture content of 73.5% (w.b.) to 9.6%. It was also tested by drying green chilli. The exergy efficiency of the SAH - 1 and the SAH - 2 were 0.9% and 0.8%, respectively. The exergy efficiency of the solar air heater increased with increase in the solar radiation intensity. The average energy and exergy efficiencies of the thermal storage varied between 36.4% and 42.2% and 13.7% and 17%, respectively. The energy storage of the dryer helped in maintaining higher drying air temperature than the solar heater outlet temperature after 14:30 h and continuing of the drying operation till 18:00. The temperature of the drying chamber was maintained within a closer range by the heat storage. The integration of the energy storage reduced the drying days by increasing the drying hours per day. The specific energy consumption and the overall efficiency of the drying system were 6.8 kW h per kg moisture and 10.8%, respectively. The electrical energy consumption was 0.7 kW h per kg of moisture. The exergy efficiency of the drying chamber varied was in the range of 24.3–98% with an average of 52.2%.

Economic analysis of the drying system was carried out by annualised cost method. The cost of drying per kg of dried product dried in the solar dryer was found to be Rs. 42.7 while it was Rs. 81.4 in the electric dryer. However, it is costlier than the open sun drying.

Chapter - 8

Conclusions and Scope for the Future Work

8.1 Conclusions

This study concerns with the development and performance investigation of a forced convection hybrid solar dryer consisting of two double-pass solar air heaters, a paraffin wax-based shell and tube latent heat storage module, a parallel flow drying chamber, and a blower. The components of the drying system have been sized based on the mass of air and the energy requirements and fabricated with the locally available materials. It has been tested by drying Ghost chilli, sliced ginger, a local variety of red and green chilli. The Ghost chilli and sliced ginger were dried in the dryer without filling the storage with paraffin wax. The kinetics of the drying process of the Ghost chilli was studied. Energy and exergy analyses of the drying process of Ghost chilli and the ginger were performed. The dryer was then filled with the paraffin wax, red chilli, and green chilli of a local variety were dried in the dryer. The performance of each component of the drying system was evaluated by the energy and exergy analyses. Eventually, economic analysis of the dryer is carried out by annualised cost method. The summary of the drying kinetics analysis of the Ghost chilli, the energy and exergy analyses of the drying process of the Ghost chilli and the ginger, and the performance investigation of the dryer with the latent heat storage are given in the following sections.

8.1.1 Thin layer drying kinetics analysis of Ghost chilli

Two samples of Ghost chilli were dried simultaneously in the solar dryer and in the open sun to study its kinetics of drying. In the solar dryer, the air temperature varied between 44 ^{o}C and 66 ^{o}C, and the sun dried samples were dried in the ambient temperature ranging from 29 ^{o}C to 37 ^{o}C. The moisture content of the chilli samples dried in the solar dryer and the open sun was reduced from 85.5% (w.b.) to 10.5% (w.b.) in 123 h and 193 h, respectively. Eleven thin layer drying models were fitted to the moisture ratio data and regression analysis was performed to select the best model representing the drying process of the chilli. The best model was selected based on the criteria of the highest value of the coefficient of determination (R^2), the lowest

values of the reduced square (x^2) and root mean square error *(RMSE)*. The important conclusions of this study are as follows.

- The drying process of the Ghost chilli occurs in the falling rate period.
- The drying rate of the solar dried sample is faster than that of the sun drying one.
- The Midilli and Kucuk model is the most suitable thin layer drying model to describe the drying process of the Ghost chilli dried in the dryer.
- The Page and the Modified Page models are the two most suitable models for the open sun drying process of the Ghost chilli.
- The colour of the solar drying sample is better than that of the open sun drying one. The original colour is preserved in the solar dried sample.

8.1.2 Energy and exergy analyses of the drying processes of the Ghost chilli and ginger

Nine kg of freshly harvested ripe Ghost chilli and 13 kg of sliced ginger of the thickness varied between 8 mm and 10 mm were dried in the dryer. The Ghost chilli and sliced ginger were successfully dried in the dryer in 42 h and 33 h in the drying air temperature varying between 42 °C and 61 °C and 37 °C and 57 °C, respectively. Energy and exergy analyses of the drying processes of the two products were performed applying the first and the second laws of thermodynamics. The following conclusions are drawn from this study.

- The thermal efficiency of the solar air heater is affected by the inlet air temperature. It deceases with increase in the inlet air temperature. The thermal efficiency of the first solar air heater (SAH - 1) was found to be higher than that of the second solar air heater (SAH - 2).
- The thermal efficiency of the SAH - 1 was in the range of 22.1–40.2% with an average of 32% while the thermal efficiency of the SAH - 2 varied between the 8.5% and 19.5% with an average of 14%. The average overall efficiency of the air heater panel was in the range of 22.9–23.3%.
- The energy and exergetic efficiencies of the drying process may change during successive drying and also from product to product. The exergetic efficiency of the drying processes of both the products was found to be high in the latter stages of the drying periods
- The exergy efficiency was in the range of 21–98% with an average of 63% for the Ghost chilli and 4–96% with an average of 47% for the sliced ginger. The sliced ginger drying

process exhibited higher thermal efficiency and lower exergetic efficiency during the initial stage of drying. The exergetic efficiency increased with progressing in drying time. The overall exergetic efficiency of the drying process of the Ghost chilli was higher than the sliced ginger.

- The specific energy consumption depends on the type of product dried, drying time and the loading of the dryer. The specific energy consumption of the Ghost chilli (18.7 kWh/kg) was higher than that of the sliced ginger (8.8 kW h/kg).
- The higher exergy and lower thermal efficiencies of the drying chamber manifest considerable energy loss in the exhaust of the drying chamber.

8.1.3 Performance tests on the solar dryer with the latent heat storage

Twenty kg of red chilli of the local variety was successfully dried in the hybrid dryer in four consecutive sunny days in the air temperature ranging from 34 ºC to 60 ºC with an average of 50 ºC. The performance of each component the drying system was evaluated by energy and exergy analyses. The following conclusions are drawn from this study.

- The integration of the energy storage reduces fluctuation in the drying air temperature and also extends the drying time beyond the sunshine hours.
- The exergy efficiency of the solar air heater increases with increase in the solar radiation intensity. The exergy efficiency of the SAH - 1 and the SAH - 2 were 0.9% and 0.8%, respectively.
- The average energy and exergy efficiencies of the energy storage were in the range of 36.4–42.2% and 13.7–17%, respectively.
- The exergy efficiency of the drying chamber increases with increase in the drying time. The exergy efficiency of the drying chamber was in the range of 24.2–98% with an average of 52.2%.
- The specific energy consumption of chilli and the overall efficiency of the drying system were 6.8 kW h per kg moisture and 10.8%, respectively.
- The electrical energy consumption is very less compared to the total energy required for drying the product. The electrical energy consumption was 0.7 kW h per kg of moisture which was only 10.3% of the specific energy consumption of the product.
- The cost of drying per kg of dried product in the solar dryer is found to be Rs. 42.7 that of the product dried in the electric dryer is Rs.81.4.

It is always desirable to have high energy and high exergy efficiencies of the drying chamber. The low energy efficiency is the indication of more energy losses from the drying chamber. The high exergy efficiency means low exergy losses while drying the product and high exergy outflow of the drying chamber. The high exergy outflow of the drying chamber indicates that the work potential of the drying air is still available which can be used further. The exergy outflow of the drying chamber goes to the environment and is wasted. If the outflow air can be used some way, the energy efficiency of the drying system can be improved. However, only the outflow air with high exergy can be used further. Therefore, the exergy analysis plays an important role in the thermodynamics analysis of the drying system.

In this study, it was observed from the exergy analysis of different products that the exergy efficiency of the drying chamber increased gradually and became the maximum towards the end of the drying period. The exergy efficiency was minimum at the beginning of the drying process. Initially, the product contains more moisture on the surface and therefore, the moisture evaporation rate is high. The moisture content of the product decreases gradually and the drying air leaves the drying chamber with very low relative humidity at a high temperature. The exergy outflow of the drying chamber also increases gradually and becomes the maximum towards the end of the drying period. Therefore, based on the value of the exergy analysis, one can plan to utilize the exhaust of the drying chamber by recirculating in the same drying chamber or utilizing it for drying fresh product in another drying chamber. This may improve the energy efficiency of the overall drying system.

8.2 Scope for Improvement of the Drying System and Future Study

The main objective of this study was to develop a solar dryer integrated with a latent heat storage module and to dry some of the important agricultural products available in the NER of India. The dryer has been developed and tested by drying different agricultural products. All the products have been dried successfully in the dryer. Nevertheless, there is scope for improvements of the drying system.

8.2.1 Recirculation of the exhaust air

When the dryer was tested, it was observed that the air exhausted from the drying chamber at high temperature during the peak sunshine hour of the day and also towards the end of the drying period of all the products. The exergy efficiency was also found to be high towards the end of the drying periods of all the products. It was due to the low moisture content in the

product at the end stage of the drying periods. As a result, the heat available in the drying air was not utilised efficiently for removing the moisture from the products. It indicates that the exhaust air has the potential for re-utilisation in the drying chamber by heating it further in the solar air heater. Therefore, an exhaust air recirculation system can be integrated into the dryer for recirculating the exhaust air towards the last stage of drying.

8.2.2 Improvement in the efficiency of the solar air heater

The efficiency of the first solar heater was found to be satisfactory. However, the efficiency of the solar air heater (second heater) connected in series with the first was found to be low. The average efficiency of the second solar air heater was found to be 14.5% while the efficiency of the first one was 32.5%. It was due to the high inlet temperature of the second solar air heater. The high inlet temperature caused high absorber plate temperature of the heater resulting in high convection and re - radiation losses. Another cover plate can be fitted over the existing one to reduce the re - radiation and the convection losses and to improve the efficiency of the second heater.

8.2.3 Improvement in the drying chamber

The dryer chamber also needs to be improved further. In order to distribute the hot air more uniformly inside the drying chamber, an air distributor is required to be placed inside the plenum chamber. In addition, some percentage of air leaves the dryer without coming in contact with the surface of the product as air flows parallel to the surface of the product. To effectively use the air for uniform drying, the movement of the air can be changed from top to bottom and bottom to top in each stage.

8.2.4 Quality analysis of the dried products

Qualitatively the colour of the products dried in the dryer was found to be better than that of the same product dried in the open sun. However, quantitative assessment of the quality of the dried product needs to be carried out.

8.3.5 Conversion of the dryer into mixed - mode - type

The dryer can be modified to operate in the mixed - mode - type by simply replacing the top cover of the drying chamber with a transparent wall.

Aghbashlo M, Kianmehr MH and **Arabhosseini A** (2009), Modelling of thin - layer drying of potato slices in length of continuous band dryer, *Energy Conversion and Management,* Vol. 50, pp. 1348–1355.

Aghbashlo M, Mobli H, Rafiee S and **Madadlou A** (2013), A review on exergy analysis of drying processes and systems, *Renewable and Sustainable Energy Reviews,* Vol. 22, pp. 1–22.

Agrawal A and **Sarviya RM** (2016), An experimental investigation of shell and tube latent heat storage for solar dryer using paraffin wax as heat storage material, *Engineering Science and Technology, an International Journal,* Vol. 19, pp. 619–631.

Aguilar-Castro KM, Flores-Prieto JJ, Baltazar-Lopez ME and **Macias-Melo EV** (2012), Design and experimental evaluation of a mixed-mode continuous solar dryer for plaster molds, *Journal of Mechanical Science and Technology*, Vol. 26, pp. 2969–2976.

Akbulut A and **Durmus A** (2010), Energy and exergy analyses of thin layer drying of mulberry in a forced solar dryer, *Energy*, Vol. 35, pp. 1754–1763.

Akintunde TYT (2011), Mathematical modelling of sun and solar drying of chilli pepper, *Renewable Energy*, Vol. 36, pp. 2139–2145.

Akpinar E, Midilli A and **Bicer Y** (2003), Single layer drying behaviour of potato slices in a convective cyclone dryer and mathematical modelling, *Energy Conversion and Management,* Vol. 44, pp. 1689–1705.

Akpinar EK (2006), Mathematical modelling of thin layer drying process under open sun of some aromatic plants, *Journal of Food Engineering,* Vol. 77, 864–870.

Akpinar EK (2008), Mathematical modelling and experimental investigation on sun and solar drying of white mulberry, *Journal of Mechanical Science and Technology,* Vol. 22, pp. 1544–1553.

Akpinar EK (2010), Drying of mint leaves in a solar dryer and under open sun: Modelling, performance analyses, *Energy Conversion and Management*, Vol. 51, pp. 2407–2418.

Akpinar EK and **Bicer Y** (2008), Mathematical modelling of thin layer drying process of long green pepper in solar dryer and under open sun, *Energy Conversion and Management,* Vol. 49, pp. 1367–1375.

Akpinar EK and **Koçyigit F** (2010), Energy and exergy analysis of a new flat-plat solar air heater having different obstacles on absorber plates, *Applied Energy,* Vol. 87, 438–3450.

Alta D, Bilgili E, Ertekin C and **Yaldiz O (**2010), Experimental investigation of three different solar air heaters; Energy and exergy analyses, *Applied Energy,* Vol. 87, pp. 2953 – 2973.

Amer BMA, Hossain MA and **Gottschalk K** (2010), Design and performance evaluation of a new hybrid solar dryer for banana, *Energy Conversion and Management,* Vol. 51, pp. 813–820.

Amjad W, Hensel O, Munir A, Esper A and **Sturm B** (2016), Thermodynamic analysis of drying process in a diagonal - batch dryer developed for batch uniformity using potato slices, *Journal of Food Engineering*, Vol. 69, pp. 238–249.

Aviara NA, Onuoha LN, Falola OE and **Igbeka JC** (2014), Energy and exergy analyses of native cassava starch drying in a tray dryer, *Energy*, Vol. 73, pp. 809–817.

Ayensu A and **Asiedu - Bondzie V** (1986), Solar drying with convective self - flow and energy storage, *Solar & Wind Technology*, vol. 3, pp. 273–279.

Ayyappan A, Mayilsamy K and **Sreenarayanan VV** (2016)**,** Performance improvement studies in a solar greenhouse dryer using sensible heat storage materials, *Heat Mass Transfer*, Vol. 52, pp. 459–467.

Babalis SJ, Papanicolaou E, Kyriakis N and **Belessiotis VG** (2006), Evaluation of thin - layer drying models for describing drying kinetics of figs (Ficus carica), *Journal of Food Engineering*, Vol. 75, 205–214.

Bahnasawy AH and **Shenana ME** (2004), A mathematical model of direct sun and solar drying of some fermented dairy products (Kishk), *Journal of Food Engineering*, Vol. 61, pp. 309–319.

Bahrehmand D and **Ameri M** (2015), Energy and exergy analysis of different solar air collector systems with natural convection, *Renewable Energy*, Vol. 74, pp. 357–368.

Banout J, Ehl P, Havlik J, Lojka B, Polesny Z and **Verner V** (2011), Design and performance evaluation of a double-pass solar drier for drying of red chilli (Capsicum annum L.), *Solar Energy*, Vol. 85, pp. 506–515.

Baruah P (2006), *The tea industry of Assam origin and development*, First Ed. EBH publishers, Guwahati, India.

Bayrak F, Oztop HF and **Hepbasli A** (2013), Energy and exergy analyses of porous baffles inserted solar air heaters for building applications, *Energy and Buildings*, Vol. 57, pp. 338–345.

Belessioties V and **Delyannis E** (2011), Solar drying, *Solar Energy*, Vol. 85, pp. 1665–1691.

Bena B and **Fuller RJ** (2002), Natural convection solar dryer with biomass back-up heater, *Solar Energy*, Vol. 72, pp. 75–83.

Benil H (2013), Experimentally derived efficiency and exergy analysis of a new solar air heater having different surface shapes, *Renewable Energy*, Vol. 50, pp. 58–67.

Berk Z (2009), *Food process engineering and technology*, First Ed. Elsevier, Academic Press.

Bhut Jolokia, From Wikipedia, the free Encyclopaedia, https://en.wikipedia.org./wiki/Bhut_ jolokia#cite_note-20 (Access on 15th January, 2016).

Borah A, Hazarika K and **Khayer SM** (2015), Drying kinetics of whole and sliced turmeric rhizomes Curcuma longa L.) in a solar conduction dryer, *Information Processing in Agriculture,* Vol. 2, pp. 85–92.

Boughali S, Benmoussa H, Bouchekima B, Mennouche D, Bouguettaia H, and **Bechki D** (2009), Crop drying by indirect active hybrid solar - electrical dryer in the eastern Algerian Septentrional Sahara, *Solar Energy,* Vol. 83, pp. 2223–2232.

Boukadoum AB, and **Benzaoui A** (2011), Energy and exergy analysis of solar drying process of Mint, *Energy Procedia,* Vol. 6, pp. 583–591.

Boulemtafes - Boukadoum A and **Benzaoui A** (2011), Energy and exergy analysis of solar drying process of Mint, *Energy Procedia*, Vol. 6, pp. 583–591.

Cakmak G and **Yildiz C** (2011), The drying kinetics of seeded grape in solar dryer with PCM - based solar integrated collector, *Food and bioproducts processing,* Vol. 89, pp. 103–108.

Celma AR and **Cuadros F** (2009), Energy and exergy analyses of OMW solar drying process, *Renewable Energy,* Vol. 34, pp. 660–666.

Cengel YA and **Boles MA** (2010), Thermodynamics, An engineering Approach, Sixth Ed. McGraw - Hill Companies, New Delhi.

Chandra PK and **Singh RP** (1995), Applied Numerical Methods for Food and Agricultural Engineers, *CRC Press, Boca Raton, FL*, pp. 163–167.

Chauhan PM, Choudhury C and **Garg HP** (1996), Comparative performance of coriander dryer coupled to solar air heater and solar air - heater - cum - rock bed storage, *Applied Thermal Engineering,* Vol. 16, pp. 475–4486.

Chavan BR, Yakupitiyage A and **Kumar S** (2008), Mathematical Modelling of Drying characteristics of Indian Mackerel (Rastrilliger kangurta) in Solar - Biomass Hybrid Cabinet Dryer, *Drying Technology,* Vol. 26, pp. 1552–1562.

Chen H, Hernandez CE and **Huang TC** (2005), A study of the drying effect on lemon slices using a closed - type solar dryer, *Solar Energy,* Vol. 78, pp. 97–103.

Choudhury C, Chauhan PM and **Garg HP** (1995), Performance and cost analysis of two - pass solar air heaters, *Heat Recovery Systems & CHP*, Vol. 15, pp. 755–773.

Chowdhury MMI, Bala BK and **Haque MA** (2011), Energy and exergy analysis of the solar drying of jackfruit leather, *Biosystem Engineering*, Vol. 110, pp. 222–229.

Cipliene A, Novosinskas H, Raila A and **Zvicevicius E** (2015), Usage of hybrid solar collector system in drying technologies of medical plants, *Energy Conversion and Management,* Vol. 93, pp. 399–405.

Condori M, Echazu R and **Saravia L** (2001), Solar drying of sweet pepper and garlic using the tunnel greenhouse drier, *Renewable Energy,* Vol. 22, pp. 447–460.

Corzo O, Bracho N, Vasquez A and **Pereira A** (2008), Energy and exergy analysis of thin layer drying of coroba slices, *Journal of Food Engineering,* Vol. 86, pp. 151–161.

Daghigh R, Ruslan MH, Sulaiman MY and **Sopian K** (2010), Review of solar assisted heat pump drying systems for agricultural and marine products, *Renewable and Sustainable Energy Reviews,* vol. 14, pp. 2564–2579.

Darvishi H, Asl AR, Asghari A, Azadbakht M, Najafi G and **Khodaei J** (2014), Study of the drying kinetics of pepper, *Journal of the Saudi Society of Agricultural Sciences,* Vol. 13, pp. 130–13.

Demir V, Gunhan T and **Yagcioglu AK** (2007), Mathematical modelling of convective drying of green table olives, *Biosystems Engineering,* Vol. 98, pp. 47–53.

Devahastin S and **Pitaksuriyarat S** (2005), Use of latent heat storage to conserve energy during drying and its effect on drying kinetics of a food product, *Applied Thermal Engineering,* Vol. 26, pp. 1705–1713.

Diamante LM and **Munro PA** (1993), Mathematical modelling of the thin layer solar drying of sweet potato slices, *Solar energy,* Vol. 51, pp. 271 - 276.

Dincer I and **Rosen MA (2007),** *Exergy, energy, environment and sustainable development,* First Ed. Elsevier, UK.

Dincer I and **Rosen MA** (2011), *Thermal energy storage systems and applications,* Second Ed. John Wiley and Sons, UK.

Dissa AO, Bathiebo DJ, Desmorieux H, Coulibaly O and **Koulidiati J** (2011), Experimental characterisation and modelling of thin layer direct solar drying of Amelie and Brooks mangoes, *Energy,* Vol. 36, pp. 2517–2527.

Doymaz I (2005), Sun drying of figs: an experimental study, *Journal of Food Engineering,* Vol. 7, pp. 403–407.

Doymaz I and **Pala M** (2002), Hot - air drying characteristics of red pepper, *Journal of Food Engineering,* Vol. 55, pp. 331–335.

Dubey RK, Singh V, Upadhyay G, Pandey AK and **Prakash D** (2015), Assessment of phytochemical composition and antioxidant potential in some indigenous chilli genotypes from North East India, *Food Chemistry,* Vol. 2188, pp. 119–125.

Duffie JA and **Beckman WA** (2006), Solar engineering of thermal process, Third Ed. John Wiley and Sons, Inc., New York.

Ekechukwu OV (1999), Review of solar-energy drying systems I: an overview of drying principles and theory, *Energy Conversion & Management,* Vol. 40, pp. 593–613.

El - Beltagy A, Gamea GR and **Essa AHA** (2007), Solar drying characteristics of strawberry, *Journal of Food Engineering,* Vol. 78, pp. 456–464.

El - Sebaii AA, Aboul - Enein S, Ramadan MRI and **El - Gohary HG** (2002), Experimental investigation of an indirect type natural convection solar dryer, *Energy Conversion and Management*, Vol. 43, pp. 2251 - 2266.

El - Sebaii AA and **Shalaby SM** (2013), Experimental investigation of an indirect-mode forced convection solar dryer for drying thymus and mint, *Energy Conversion and Management*, Vol. 74, pp. 109–116.

Erbay Z and **Icier F** (2009), A review of thin layer drying of foods: theory, modeling, and experimental results, *Critical Reviews in Food Science and Nutrition*, Vol. 50, pp. 441–464.

Esakkimuthu S, Hassabou AH, Palaniappan C, Spinnler M, Blumenberg J and **Velraj R** (2013), Experimental investigation on phase change material based thermal storage system for solar air heating applications, *Solar Energy*, Vol. 88, pp. 144–153.

Esen H (2008), Experimental energy and exergy analysis of a double - flow solar air heater having different obstacles on absorber plates, *Building and Environment*, Vol. 43, pp. 1046–1054.

Fargali HM, Nafeh AEA, Fahmy FH and **Hassan MA** (2008), Medicinal herb drying using a photovoltaic array and a solar thermal system, *Solar Energy*, Vol. 82, pp. 1154–1160.

Fatouh M, Metwally MN, Helali AB and **Shedid MH** (2006), Herbs drying using a heat pump dryer, *Energy Conversion and Management*, Vol. 47, pp. 2629–2643.

Faustino JMF, Barroca MJ and **Guine RPF** (2007), Study of the drying kinetics of green bell pepper and chemical characterization, *Food and Bio - products Processing*, Vol. 85, pp. 163–170.

Forson FK, Nazhab MAA, Akuffoa FO and **Rajakaruna H** (2007), Design of mixed -mode natural convection solar crop dryers: Application of principles and rules of thumb, *Renewable Energy*, Vol. 32, pp. 2306–2319
.

Fudholi A, Bakhtyar B, Saleh H, Ruslan MH, Othman MY and **Sopian K** (2016), Drying of salted silver jewfish in a hybrid solar drying system and under open sun: Modelling and performance analyses, *International Journal of Green energy*, Vol. 13, pp. 1135–1144.

Fudholi A, Sopian K, Yazdi MH, Ruslan MH, Gabbasa M and **Kazem HA** (2014a), Performance analysis of solar drying system for red chilli, *Solar Energy*, Vol. 99, pp. 47–54.

Fudholi A, Sopian K, Alghoul MA, Ruslan MH and **Othman OY** (2015), Performances and improvement potential of solar drying system for palm oil fronds, *Renewable Energy*, Vol. 78, pp. 561–565.

Fudholi A, Sopian K, Othman MY and **Ruslan MH** (2014b), Energy and exergy analyses of solar drying system of red seaweed, *Energy and Buildings*, Vol. 68, pp. 121–129.

Garg HP and **Prakash J** (2006), *Solar energy fundamentals and application*, First Revised Ed. Tata McGraw Hill Education Private Ltd, New Delhi, India.

Garg HP, Sharma VK, Mahaja RB and **Bhargave AK** (1985), Experimental study of an inexpensive solar collector cum storage system for agricultural uses, *Solar Energy*, Vol. 35, pp. 321–331.

Ghazanfari A, Emami S, Tabil LG and **Panigrahi S** (2006), Thin - layer drying of flax fiber: II. Modeling drying process using semi - theoretical and empirical models, *Drying Technology*, Vol. 24, pp. 1637–1642.

Goyal RK, Kingsly ARP, Manikantan MR and **Ilyas SM** (2007), Mathematical modelling of thin layer drying kinetics of plum in a tunnel dryer, *Journal of Food Engineering*, Vol. 79, pp. 176–180.

Gulcimen F, Karakaya H and **Durmus A** (2016), Drying of sweet basil with solar air collectors, *Renewable Energy*, Vol. 93, pp. 77–86.

Henderson SM, (1974), Progress in developing the thin layer drying equation, *Trans Am Soc Agr Eng*, Vol. 17, pp. 1167–1178.

Henderson SM and **Pabis S** (1961), Grain drying theory I: Temperature effect on drying coefficient, *Journal of Agricultural Engineering Research*, Vol. 6, pp. 169–174.

Holman JP (1994), Experimental methods for engineers. Sixth ed. McGraw - Hill Book Co., Singapore.

Hossain MA and **Bala BK** (2002), Thin-layer drying characteristics for green chilli, *Drying Technology*, Vol. 20, pp. 489–505.

Hossain MA, Amer BMA and **Gottschalk K** (2008), Hybrid solar dryer for quality dried tomato, *Drying Technology*, Vol. 26, pp. 1591 - 1601.

Hossain MA and **Bala BK** (1999), Geometric dimensions, density and specific heat of chilli as function of moisture content, *International Journal of food properties*, Vol. 2, pp. 175–183.

Hossain MA and **Bala BK** (2002), Thin - layer drying characteristics for green chilli, *Drying Technology*, Vol. 20, pp. 489–505.

Hossain MA and **Bala BK** (2007), Drying of hot chilli using solar tunnel drier, *Solar Energy*, Vol. 81, pp. 85–92.

Jafarkazemi F and **Ahmadifard E** (2013), Energetic and exergetic evaluation of flat plate solar collectors, *Renewable Energy*, Vol. 56, pp. 55–63.

Jain D (2005a), Modelling the system performance of multi - tray crop drying using an inclined multi-pass solar air heater with in-built thermal storage. *Journal of Food Engineering*, Vol. 71, pp. 44–54.

Jain D (2005b), Modelling the performance of greenhouse with packed bed thermal storage on crop drying application, *Journal of Food Engineering*, Vol. 71, pp. 170–178.

Jain D and **Jain RK** (2004), Performance evaluation of an inclined multi - pass solar air heater with in - built thermal storage on deep - bed drying application, *Journal of Food Engineering*, Vol. 65, pp. 497–509.

Jain D and **Pathare PB** (2007), Study the drying kinetics of open sun drying of fish, *Journal of Food Engineering*, Vol. 78, pp. 1315–1319.

Jain D and **Tewari P** (2015), Performance of indirect through pass natural convective solar crop dryer with phase change thermal energy storage, *Renewable Energy*, Vol. 80, pp. 244–250.

Janjai S, Intawee P, Kaewkiew J, Sritus C and **Khamvongsa V** (2011), A large - scale solar greenhouse dryer using polycarbonate cover: Modeling and testing in a tropical environment of Lao People's Democratic Republic, *Renewable Energy*, Vol. 36, pp. 1053– 1062.

Janjai S, Srisittipokakuna N and **Bala BK** (2008), Experimental and modelling performances of a roof - integrated solar drying system for drying herbs and spices, *Energy*, vol. 33, pp. 91–103.

Jayas DS, Cenkowski S, Pabis S and **Muir WE** (1991), Review of thin - layer drying and wetting equations, *Drying Technology*, Vol. 9, pp. 551–588.

Kaewkiew J, Nabnean S and **Janjai S** (2012), Experimental investigation of the performance of a large - scale greenhouse type solar dryer for drying chilli in Thailand, *Procedia Engineering* Vol. 32, pp. 433–439.

Kaleemullah S (2002), Studies on engineering properties and drying kinetics of chillies, Ph.D. thesis, Department of Agricultural Processing, Tamil Nadu Agricultural University: Coimbatore, India.

Kaleemullah S and **Kailappan R** (2004), Moisture Sorption Isotherms of Red Chillies, *Biosystems Engineering*, Vol. 88, pp. 95–104.

Kane CSE, Jamali A, Kouhila M, Mimet A and **Ahachad M** (2008), Single - layer drying behaviour of Mexican tea leaves (Chenopodium Ambrosioides) in a convective solar dryer and mathematical modelling, *Chemical Engineering Communication*, Vol. 195, pp. 787–802.

Karathanos VT (1999), Determination of water content of dried fruits by drying kinetics, *Journal of Food Engineering*, Vol. 39, pp. 337–344.

Karim MA, Perez E and **Amin ZM** (2014), Mathematical modelling of counter flow v -grove solar air collector, *Renewable Energy*, vol. 67, pp. 192–201.

Keey RB (1992), *Drying of loose and particulate materials*, First Ed. Hemispher Publishing Corporation, New York.

Koca A, Oztop HF, Koyun T and **Varol Y** (2008), Energy and exergy analysis of a latent heat storage system with phase change material for a solar collector, *Renewable Energy*, Vol. 33, pp. 567–574.

Koua KB, Fassinou WF, Gbaha P and **Toure S** (2009), Mathematical modelling of the thin layer solar drying of banana, mango and cassava, *Energy*, Vol. 34, pp. 1594–1602.

Koukouch A, Idlimam A. Asbik M, Sarh B, Izrar B, Bah A and **Ansari O** (2015), Thermophysical characterization and mathematical modelling of convective solar drying of raw olive pomace, *Energy Conversion and Management*, Vol. 99, pp. 221–230.

Kucuk H, Midilli A, Kilic A and **Dincer I** (2014), A review on thin - layer drying - curve equations, *Drying Technology*, Vol. 32, pp. 757–773.

Kudra T (2004) Energy Aspects in Drying, *Drying Technology*, Vol. 22, pp. 917–932.

Lahsasni S, Kouhila M, Mahrouz M, Idlimam A and **Jamali A** (2004), Thin layer convective solar drying and mathematical modeling of prickly pear peel (Opuntia ficus indica), *Energy*, Vol. 29, pp. 211–224.

Lamnatou C, Papanicolaou E, Belessiotis V and **Kyriakis N** (2012), Experimental investigation and thermodynamic performance analysis of a solar dryer using an evacuated-tube air collector, *Applied Energy*, Vol. 94, pp. 232–243.

Lane GA (1983), Solar Heat Storage. Latent Heat Material - Volume I: Background and Scientific Principles, Florida: CRC Press.

Leon MA and **Kumar S** (2008), Design and performance evaluation of a solar-Assisted biomass drying system with thermal storage, *Drying Technology*, Vol. 26, pp. 936–947.

Lewis WK (1921), The rate of drying of solid materials, *The Journal of Industrial Engineering and Engineering Chemistry* 3:42.

Lokeswaran S and **Eswaramoorthy M** (2013), Experimental studies on a solar drier system with a biomass back - up heater, *Energy Sources*, Vol. 35, pp. 467–475.

Lopez R, Vaca M, Terres H, Lizardi A, Morales J, Flores J, Lara A and **Chavez S** (2014), Kinetics modelling of the drying of chickpea (Cicer arietinum) with solar energy, *Energy Procedia*, Vol. 57, pp. 1447–1454.

Lopez - Vidana EC, Mendez-Lagunas LL and **Rodriguez - Ramirez J** (2013), Efficiency of a hybrid solar - gas dryer, *Solar Energy*, Vol. 93, pp. 23–31.

Madhlopa A and **Ngwalo G** (2007), Solar dryer with thermal storage and biomass - backup heater, *Solar Energy*, Vol. 8, pp. 449–462.

Mande S, Kumar A and **Kishore VVN** (1999), A study of large-cardamom curing chambers in Sikkim, *Biomass and Bioenergy*, Vol. 16, pp. 463–473.

Mathur R, Dangi RS, Dass SC and **Malhotra RC** (2000), The hottest chilli variety in India, *Current Science*, Vol. 79, pp. 287–288.

McAdams WA (1954*), Heat Transmission*, Third Ed. McGraw - Hill Book Co., New York.

Midilli A and **Kucuk H** (2003a), Mathematical modelling of thin layer drying of pistachio by using solar energy, *Energy Conversion and Management*, Vol. 44, pp. 1111–1122.

Midilli A and **Kucuk H** (2003b), Energy and exergy analyses of solar drying process of pistachio, *Energy*, Vol. 28, pp. 539–556.

Midilli A, Kucuk H and **Yapar Z** (2002), A new model for single-layer drying, *Drying Technology*, Vol. 20, pp. 1503–1513.

Mohajer A, Nematollahi O, Joybari MM, Hashemi SA and **Assari MR** (2013), Experimental investigation of a hybrid solar drier and water heater system, *Energy Conversion and Management*, Vol. 76, pp. 935–944.

Mohamed LA, Kane CSE, Kouhila M, Jamali A, Mahrouz M and **Kechaou N** (2008), Thin layer modelling of Gelidium sesquipedale solar drying process, *Energy Conversion and management*, Vol. 49, pp. 940–946.

Mohamed LA, Kouhila M, Jamali A, Lahsasni S, Kechaou N and **Mahrouz M** (2005), Single layer solar drying behaviour of Citrus aurantium leaves under forced convection, *Energy Conversion and Management*, Vol. 46, pp. 1473–1483.

Mohanraj M (2014), Performance of a solar-ambient hybrid source heat pump drier for copra drying under hot - humid weather condition, *Energy for Sustainable Development*, Vol. 23, pp. 165–169.

Mokhtarian M, Tavakolipour H and **Kalbasi - Ashtari A** (2016), Energy and exergy analysis in solar drying of pistachio with air recycling system, *Drying Technology*, Vol. 34, pp. 1532 - 2300.

Mortezapour H, Ghobadian B, Minaei S and **Khoshtaghaza MH** (2012), Saffron drying with a heat pump - assisted hybrid photovoltaic - thermal solar dryer, *Drying Technology*, Vol. 30, pp. 560–566.

Mujumdar AS and **Devahastin S**, *Fundamental principles of drying*, https://pdfs.semanticscholar.org/1a31/974e36dce10e9e20a0abdb4aa4a81a505782.pdf, (access on 23rd January 2016).

Murthy MVR, (2009), A review of new technologies, models and experimental investigations of solar driers, *Renewable and Sustainable Energy Reviews*, Vol. 13, pp. 835–844.

Nabnean S, Janjai S, Thepa S, Sudaprasert K, Songprakorp R and **Bala BK** (2016), Experimental performance of a new design of solar dryer for drying osmotically dehydrated cherry tomatoes, *Renewable Energy*, Vol. 94, pp. 147–156.

Nag PK (2001), *Power Plant Engineering*, Second Ed. Tata McGraw - Hill, New Delhi, India

Nag PK (2010)**,** *Basic and applied thermodynamics*, Second Ed. Tata McGraw - Hill, New Delhi.

Nourhene B, Mohammed K and **Nabil K** (2008), Experimental and mathematical investigations of convective solar drying of four varieties of olive leaves, *Food and Bioproducts processing*, Vol. 86, pp. 176–184.

.

Omojar AP and **Aldabbagh LBY** (2010), Experimental performance of single and double pass solar air heater with fins and steel wire mesh as absorber, *Applied Energy*, Vol. 87, pp. 3759–3765.

Ong KS (1995), Thermal performance of solar air heaters: Mathematical model and solution procedure, *Solar energy*, Vol. 55, pp. 93–109.

Overhults DG, White GM, Hamilton HE and **Ross IJ** (1973), Drying soybeans with heated air, *Trans. ASAE*, Vol. 16, pp. 112–113.

Ozgener L and O**zgener O** (2009), Exergy Analysis of Drying Process: An Experimental Study in Solar Greenhouse, *Drying Technology*, Vol. 27, pp. 580–586.

Oztop HF, Bayrak F and **Hepbasli A** (2013), Energetic and exergetic aspects of solar air heating (solar collector) systems, *Renewable and Sustainable Energy Reviews*, Vol. 21, pp. 59–83.

Pangavhane DR, Sawhney RL and **Sarsavadia PN** (2002), Design, development and performance testing of a new natural convection solar dryer, *Energy*, Vol. 27, pp. 579–590.

Park SR, Pandey AK, Tyagi VV and **Tyagi SK** (2014), Energy and exergy analysis of typical renewable energy systems, *Renewable and Sustainable Energy Reviews*, Vol. 30, pp. 105–123.

Patel KK and **Kar A** (2012), Heat pump assisted drying of agricultural produce - an overview, *Journal of Food Science Technology*, Vol. 49, pp. 142–160.

Patil R and **Gawande R** (2016), A review on solar tunnel greenhouse drying system, *Renewable and Sustainable Energy Reviews*, Vol. 56, pp. 196–214.

Prasad J, Vijay VK, Tiwari GN and **Sorayan VPS** (2006), Study on performance evaluation of hybrid drier for turmeric (Curcuma longa L.) drying at village scale, *Journal of Food Engineering*, Vol. 75, pp. 497–502.

Rajkumar P, Kulanthaisami S, Raghavan GSV, Gariepy Y and **Orsat V** (2007), Drying Kinetics of Tomato Slices in Vacuum Assisted Solar and Open Sun Drying Methods, *Drying Technology*, Vol. 25, pp. 1349–1357.

Reyes A, Mahn A, Cubillos F and **Huenulaf P** (2013), Mushroom dehydration in a hybrid - solar dryer, *Energy Conversion and Management*, Vol. 70, pp. 31–39.

Reyes A, Mahn A and **Vasquez F** (2014), Mushrooms dehydration in a hybrid - solar dryer, using a phase change material, *Energy Conversion and Management*, Vol. 83, pp. 241–248.

Rhaman H, Karrauppaiyan R, Kishore K and **Denzongpa R** (2009), Traditional practices of ginger cultivation of in Northeast India, *Indian Journal of Traditional Knowledge*, Vol. 8, pp. 23–28.

Rosen MA and **Dincer I** (2003) Exergy - cost - energy - mass analysis of thermal systems and processes, *Energy Conversion and Management*, Vol. 44, pp.1633–1651.

Sacilik K, Keskin R and **Elicin AK** (2006), Mathematical modelling of solar tunnel drying of thin layer organic tomato, *Journal of Food Engineering*, Vol. 73, pp. 231–238.

Saidur R, Boroumandjazi G, Mekhlif S and **Jameel M** (2012), Exergy analysis of solar energy applications, *Renewable and Sustainable Energy Reviews*, Vol.16, pp.350–356.

Sallam YI, Aly MH, Nassar AF and **Mohamed EA** (2015), Solar drying of whole mint plant under natural and forced convection, *Journal of Advanced Research*, Vol. 6, pp. 171–178.

Sami S, Etesami N and **Rahimi A** (2011), Energy and exergy analysis of an indirect solar cabinet dryer based on mathematical modelling results, *Energy*, Vol. 36, pp. 2847–2855.

Sangpradit K (2014), Study of the solar transmissivity of plastic cladding materials and influence of dust and dirt on greenhouse cultivations, *Energy Procedia*, Vol. 56, pp. 566–573.

Saravacos GD and **Maroulis ZB** (2011), Food processing engineering operations, First Ed. CRC press, Taylors and Francis Group, New work.

Sarsavadia PN (2007), Development of a solar-assisted dryer and evaluation of energy requirement for the drying of onion, *Renewable Energy*, Vol. 32, pp. 2529–2547.

Saxena A, Varun and **El-Sebaii AA** (2015), A thermodynamic review of solar air heaters, *Renewable and Sustainable Energy Reviews*, Vol. 43, pp. 863–890.

Sekyere CKK, Forson FK and **Adam FW** (2016), Experimental investigation of the drying characteristics of a mixed mode natural convection solar crop dryer with back up heater, *Renewable Energy*, Vol. 92, pp. 532–542.

Sevik S (2013a), Design, experimental investigation and analysis of a solar drying system, *Energy Conversion and Management*, Vol. 68, pp. 227–234.

Sevik S, Aktas M, Dog H and **Kocak S** (2013b), Mushroom drying with solar assisted heat pump system, *Energy Conversion and Management*, Vol. 72, pp. 171–178.

Shalaby SM and **Bek MA** (2014), Experimental investigation of a novel indirect solar dryer implementing PCM as energy storage medium, *Energy Conversion and Management*, Vol. 83, pp. 1–8.

Sharaf-Eldeen YI, Blaisdell JL and **Hamdy MY** (1980), A model for ear corn drying, *Transaction of the ASAE*, Vol. 23, pp. 1261–1271.

Sharma GP, Verma RC and **Pathare P** (2005), Mathematical modelling of infrared radiation thin layer drying of onion slices, *Journal of Food Engineering*, Vol. 71, pp. 282 - 286.

SharmaVK, Sharma S, Ray RA and **Garg HP** (1986), Design and performance studies of a solar dryer suitable for rural applications, *Energy Conversion Management*, Vol. 26, pp. 111–119.

Shi Q, Zheng Y and **Zhao Y** (2013), Mathematical modeling on thin-layer heat pump drying of yacon (Smallanthus sonchifolius) slices, *Energy Conversion and Management*, Vol. 71, pp. 208–216.

Shringi V, Kothari S and **Panwar NL** (2014), Experimental investigation of drying of garlic clove in solar dryer using phase change material as energy storage, *J Therm Anal Calorim*, Vol. 118, pp. 533–539.

Shymasundar N, Stein E, Rooz E, Bascarn E and **Lee TC** (1992), Design and Simulation of latent heat storage units, final report, Texas: National Energy laboratory, University of Houston.

Singh H, Saini RP and **Saini JS** (2010), A review on packed bed solar energy storage systems. *Renewable and Sustainable Energy Reviews*, Vol. 14, pp. 1059–1069.

Smitabhindu R, Janjai S and **Chankong V** (2008), Optimization of a solar-assisted drying system for drying bananas, *Renewable Energy*, Vol. 33, pp. 1523–1531.

Sreekumar A (2010), Techno-economic analysis of a roof - integrated solar air heating system for drying fruit and vegetables, *Energy Conversion and Management*, Vol. 51, pp. 2230–2238.

Sukhatme SP and **Nayak JK** (2010), *Solar energy principles of thermal collection and storage*, Second Ed. Tata McGraw - Hill, New Delhi.

Tasirin SM, Kamarudin SK, Jaafar K and **Lee KF** (2007), The drying kinetics of bird's chillies in a fluidized bed dryer, *Journal of Food Engineering*, Vol. 79, pp. 695–705.

Thompson TL, Peart PM and **Foster GH** (1968), Mathematical simulation of corn drying: A new model, *Trans. ASAE*, Vol. 11, pp. 582–586.

Tiwari GN, Bhatia PS, Singh AK and **Sutar RF** (1994), Design parameters of a shallow bed solar crop dryer with reflector, *Energy Conversion and Management*, Vol. 35, pp. 535 –542.

Togrul IT and **Pehlivan D** (2002), Mathematical modelling of solar drying of apricots in thin layers, *Journal of Food Engineering*, Vol. 55, pp. 209–216.

Togrul IT and **Pehlivan D** (2004), Modelling of thin layer drying kinetics of some fruits under open-air sun drying process, *Journal of Food Engineering*, Vol. 65, pp. 413–425.

Tunde - Akintunde TY (2011), Mathematical modelling of sun and solar drying of chilli pepper, *Renewable Energy*, Vol. 36, pp. 2139–2145.

Usub T, Lertsatitthankorn C, Poomsaad N, Wiset L, Siriamornpun S and **Soponronnarit S** (2010), Thin layer solar drying characteristics of silkworm pupae, *Food and bio-products processing*, Vol. 88, pp. 149–160.

Varun S and **Sharma N** (2014), Experimental investigation of the performance of an indirect mode natural convection solar dryer for drying fenugreek leaves, *Journal of Thermal Analysis and Calorimetry*, Vol. 118, pp. 523–531.

Vega A, Fito P, Andres A and **Lemus R** (2007), Mathematical modelling of hot - air drying kinetics of red bell pepper (Var. Lamuyo), *Journal of Food Engineering*, Vol. 79, pp. 1460–1466.

Vengaiah PC and **Pandey JP** (2007), Dehydration kinetics of sweet pepper (Capsicum annum L.), *Journal of Food Engineering*, Vol. 81, pp. 282–286.

Verma LR, Bucklin RA, Ednan JB and **Wratten FT** (1985), Effects of drying air parameters on rice drying models, *Transaction of the ASAE*, Vol. 28, pp. 296–301.

Wang CY and **Singh RP** (1978), A single layer drying equation for rough rice, *ASAE*, 3001.

Weiss W and **Buchinger J**, Solar drying, Institute of sustainable technology, http://www.aee-intec.at/0uploads/dateien553.pdf (accessed on 17th February, 2015)

White GM, Ross IJ and **Ponelert R** (1981), Fully exposed drying of popcorn, *Trans Am Soc Agr Eng*, Vol. 24, pp. 466–478.

Yadav S, Kaushal M, Varun and **Siddhartha** (2014), Exergetic performance evaluation of solar air heater having arc shape oriented protrusions as roughness element, *Solar Energy*, Vol. 105, pp. 181–189.

Yaldiz O, Ertekin C and **Uzun HI** (2001), Mathematical modelling of thin layer solar drying of sultana grapes, *Energy*, Vol. 26, pp. 457–465.

Yaldyz O and **Ertekyn C** (2001), Thin layer solar drying of some vegetables, *Drying technology*, Vol. 19, pp. 583–597.

Appendix - 1

Sizing of Energy Storage

A.1 Sizing of Energy Storage

A shell and tube type latent heat storage is chosen as the energy storage for the developed dryer to reduce the fluctuation in the drying air temperature as well as continuing the drying process for a few hours after the sunset. The desired average drying air temperature for the drying system is 50 ^{o}C. The minimum melting temperature of the PCM should be 5 to 10 ^{o}C higher than the desired temperature of the fluid (Lane *et al*., 1983). Assuming that a temperature difference of 10 ^{o}C is desired between the air and the melting temperature of the PCM, then the melting temperature of the PCM should be around 60 ^{o}C, and the charging temperature of the fluid should be around 70 ^{o}C. Therefore, paraffin wax of the melting temperature of the range 58 ^{o}C to 60 ^{o}C is selected as the energy storage material. The storage unit is basically a shell and tube heat exchanger. The paraffin wax is stored in the shell side, and air flows inside the tubes. During the charging process of the energy storage, the heat energy is transferred from the hot air through the walls of the tubes to the wax. The heat transfer process is reverse during the discharging process. The storage is designed based on method proposed by Shymasundar *et al.,* 1992 which is useful for the preliminary design of the shell and tube energy storage. It is designed for supplying hot air at an average temperature of 50 ^{o}C for 2 off - sunshine hours. The design procedures of Shymasundar *et al.*1992 for the preliminary design of the shell and tube latent heat storage are explained in the following sections.

A.2 Design Method

The principle design parameters of the latent heat storage are the effectiveness and the Number of transfer units (NTU). The definition of NTU is slightly different from the conventional fluid flow heat exchanger. In this case, only fluid side heat transfer coefficient is considered instead of the overall heat transfer coefficient.

(a) Determination of effectiveness

The maximum effectiveness of the storage is estimated by Eq. (A.1).

$$\varepsilon_{\max} = \frac{T_f - T_i}{T_m - T_i} \tag{A.1}$$

where T_i is the initial temperature of the fluid, T_f is the final temperature of the fluid, and T_m is the melting temperature of the PCM.

(b) Determination of NTU.

The NTU of the heat exchanger is determined by the following equation

$$\varepsilon_{\max} = 1 - \exp(-NTU) \tag{A.2}$$

(c) Determination of parameter (β)

$$\beta = Nu\left(\frac{k_f}{k_{pf}}\right)\left(\frac{r_i}{r_o}\right) \tag{A.3}$$

where Nu is the Nusselt number, k_f is the thermal conductivity of the fluid, k_{pf} is the thermal conductivity of the PCM, r_i is the inner radius of the pipe, and r_o is the outer radius of the pipe.

(d). Calculation of F_o which is the area of solid PCM formed at inlet of the tube at the end of the discharge period.

The F_o can be calculated from the explicit equation given below developed by Symasudara *et al.*,1992.

$$NTU = \frac{2\pi r_i h_{con} x}{\dot{m}_f C_{pf}} = \ln\left(\frac{F_o}{F}\right) + \frac{\beta}{2}\left[G_o(F) - G_1(F)\right] \tag{A.4}$$

where $$G_o(F) = (1+F)\ln(1+F) - F \tag{A.5}$$

which is solved by numerical method.

Where h_{con} is the convective heat transfer coefficient of the heat transfer fluid (HTF), x is the distance along the tube heat exchanger, $\dot{m}_f$ is the mass flow rate of the HTF and C_{pf} is the specific heat of the HTF.

And $$G_1(F) = \frac{p\left(1+\frac{17p^2}{450}\right)}{\left(1+\frac{p^2}{100}\right)} + \frac{p^2}{4} \quad \text{(A.6)}$$

where $$p = \ln(1+F) \quad \text{(A.7)}$$

where F is known as the frozen fraction and it is defined as the ratio of frozen region in a radial plane to the cross section area of the tube.

$$F = \left[\frac{r_m^2}{r_o^2} - 1\right] \quad \text{(A.8)}$$

Where r_m is the radius of the frozen layer of the PCM and r_o is the outer radius of the heat exchanger tube.

(d). Calculation of the non-dimension time variable (τ_o)

It can be obtained by the following equation

$$\tau_o = \frac{F_o}{2\beta} + \frac{1}{4}\left[(1+F_o)\ln(1+F_o) - F_o\right] \quad \text{(A.9)}$$

(e). Calculation of the outside radius of the tube (r_o)

It is calculated from the definition of the non-dimensional time variable

$$R_o = \left(\frac{k_{pf}(T_m - T_i)t}{\tau_o \rho_{pf} L_{sm}}\right)^{0.5} \quad \text{(A.10)}$$

(f). Pitch circle diameter (D_{tp})

It is the shortest distance between two adjacent tubes. It can be obtained by employing the following equation.

$$D_{tp} = 2r_o(1+F_o)^{0.5} \quad \text{(A.11)}$$

(g). Estimation of the number of tubes (n_{tb}) and the length of the tube (l_{tb})

The number of tubes can be estimated for a given length of the pipe by the following equation.

$$l_{tb} n_{tb} = \frac{NTU \dot{m}_f C_{pf}}{2\pi h_{con} r_i} \quad \text{(A.12)}$$

(h). Computation of the tank diameter (D_t) or the shell diameter.

The tank diameter is given by

$$D_t = D_{tp} \left(2 n_{tb} \sqrt{3/\pi}\right)^{\frac{1}{2}} \quad \text{(A.13)}$$

(i). Determination of the tank volume (V_t)

The tank volume is obtained from the tank diameter by Eq. (A.13)

$$V_t = \pi \frac{D_t^2}{4} l_{tb} \quad \text{(A.14)}$$

(j). Total volume of the tubes (V_{tb})

$$V_{tb} = \frac{\pi d_{tb}^{\ 2}}{4} n_{tb} l_{tb} \quad \text{(A.15)}$$

(i). Volume of the paraffin wax (V_{pf})

$$V_{pf} = V_t - V_{tb} \quad \text{(A.16)}$$

(j). Mass of the PCM (m_{pf})

The mass of PCM required to supply the hot air at the given temperature can be evaluated by Eq. (A.17).

$$m_{pf} = \rho_{pf} V_{pf} \quad \text{(A.17)}$$

(k). Reynolds number

$$\mathrm{R}_e = \frac{2\dot{m}_f}{\pi r_i n_{tb} \mu} \quad \text{(A.18)}$$

A.3 Determination of the LHS Shell and Tube Parameters

The parameters of the LHS unit are calculated by using the properties of materials mentioned in Table A.1. The maximum desired outlet temperature of fluid (air) is 50 ^{o}C and the minimum

is 45 °C. The melting temperature of the PCM is 58 °C. Therefore, applying Eq. (A.1), the maximum and minimum effectiveness of the heat exchanger are found to be 0.75 and 0.60. The number of transfer unit for $\varepsilon_{max} = 0.75$ obtained by employing Eq. (A.2) is 1.417. The Nusselt number for fully developed laminar flow in pipe is taken as 3.66, and then β is calculated which is equal to 0.74.

Table A.1

Input parameters for heat exchanger design calculations.

Particulars	Parameters	Value
PCM	Desired air temperature	50 °C
	Ambient air temperature	25 °C
	Energy storage material	Paraffin wax
	Melting point temperature	58–60 °C
	Solid density	918 kg/m^3
	Specific heat of solid	2.384 kJ/kg - K
	Latent heat of fusion	189 kJ/kg
	Thermal conductivity	0.22 W/m - K
Tube	Tube material	Stainless steel
	Diameter of the tube	0.0254 m
	Length of the tube	2 m
	Thermal conductivity	15 W/m - K
Air	Mass flow rate	0.012 kg/s
	Density of air at 50 °C	0.6158 kg/m^3
	Specific heat	1.044 kJ/kg - K
	Thermal conductivity	0.0442 W/m - K
	Dynamic viscosity	2.934×10^{-5} N - s/m^2
Storage time		2 h

The frozen fraction F_o which is the amount of the paraffin wax solidified at $x = 0$ at the end of the discharge period is determined by the Newton Raphson numerical method by solving Eq. (A.4). The value of F_o is 4.94. The value of the non-dimensional time variable which is equal to 4.52 is determined by employing Eq. (A.9). The outer radius of the tube, and numbers of tubes are calculated for $l_{tb} = 2$ m by employing Eqs (A.10) and (A.12). The outer

radius and the number of tubes are 9 mm and 9.49, respectively. Then the diameter and volume of the shell are calculated by Eqs. (A.13) and (A.14), respectively. The diameter and the volume of the shell are 0.18 m and 0.05 m^3, respectively. The mass of the PCM is calculated by employing Eq. A.17 which is equal to 38 kg. A MATLAB programme is prepared to get the desired parameters of the design calculations of the energy storage with the input parameters given in Table A.1.

Table A.2

Specifications of the energy storage

Particulars	**Value**
Shell material	Mild steel of thickness 2.2 mm
Shell diameter (m)	0.18
Shell volume (m^3)	0.05
Shell length (m)	2
Tube materials	Stainless steel
Tube diameter (m)	0.025
Tube length (m)	2
Number of tubes	9
Mass of PCM (kg)	38

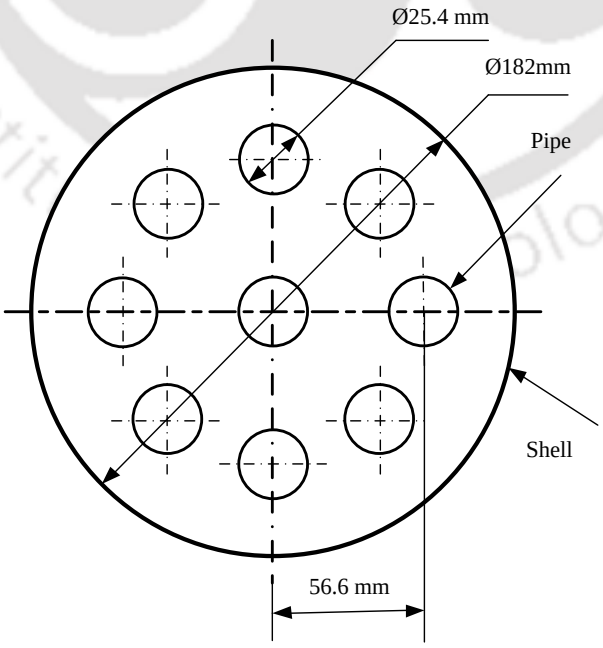

Fig A.1 Pipe arrangement in the storage

It is to be noted that the method proposed by the Shymasundar et al. 1992 is used for only approximate estimation of the parameters. The calculated diameter of the pipe is 18 mm. However, the actual diameter of the pipe used in the storage is 25.4 mm and 9 nos. tubes are arranged in the shell as shown in Fig. A.1. One tube is placed along the axis of the shell and the remaining 8 tubes are placed around the centre tube at an equal distance.

A. 4 MATLAB Programme

MATLAB code of the design calculation of the heat storage

```
% Design parameters
Ti = 25;                    % Inlet temperature of air, ºC
To = 50;                    % Maximum desired temperature of air, ºC
Tomin = 45;                 % Minimum desired temperature of air, ºC
 % Properties of Paraffin Wax
Tm = 58;                % Freezing temperature of paraffin wax, ºC
dm = 918;               % Solid density of  paraffin wax , kg/m3
cm = 2384;              % Specific heat of paraffin wax, J/kg-K
H = 189;                % Latent heat of fusion of paraffin wax, kJ/kg
km = 0.22;              % Thermal conductivity of paraffin wax, W/m-K
% Properties of air at mean fluid temperature
da = 0.6158;                % Density of air , kg/m3
ca = 1044 ;                 % Specific heat of air, J/kg-K
ka = 0.04418;               % Thermal conductivity of air, W/m-K
mu = 2.934*10^-5;           % Dynamic viscosity of air, kg/m-s
% Properties of the tube material
kw = 16;                    % Thermal conductivity of the tube material (SS), W/m-K
emax = (To-Ti)/(Tm-Ti)      % Maximum effectiveness
emin = (Tomin-Ti)/(Tm-Ti)   % Minimum effectiveness
NTU = -log(1-emax)          % Number of transfer unit
Nu = 3.66                   % Nusselt number for the laminar flow in a smooth pipe
Bi = Nu*(ka/km)             % Bita, a non-dimensional number
% Calculation of the melt fraction (Fo) of paraffin wax (% Melt fraction of paraffin wax, calculated by bi-section method)
% Fo = x is melt fraction
% The equation used to find out the melt fraction is
```

```
% NTU = log(Fo/F)+(bi/2)(G1(Fo)-G1(F))
% Where G(F)=(log(1+F)(1+17*(1+F)^2/450)/(1+log(1+F)^2/100))+log(1+F)^2
% bi=0.7350
% NTU=1.4171
% F = Fo*(1-emin)
y = (NTU-log(1/(1-emin)))*(2/bi)
Fo=fzero('((log(1+x)*(1+(17*log(1+x)^2)/450))/(1+log(1+x)^2/100))+log(1+x)^2/4-
(((log(1+0.3939*x)*(1+(17*log(1+0.3939*x)^2)/450))/(1+log(1+0.3939*x)^2/100))+log(1+0
.3939*x)^2/4)-1.3211',6)
F=(1-emin)*Fo                    % Melt fraction at time t and distance, x
GoFo = (1+Fo)*log(1+Fo)-(1+Fo)
tao = Fo/(2*bi)+0.25*GoFo        % Tao a non-dimensional time variable
t = 2  ;                         % storage time, h
Ro = ((km*(Tm-Ti)*t*3600)/(tao*dm*H))^0.5   % Outer radius of the tube, m
Dtp = 2*Ro*(1+Fo)^0.5            % Tube pitch diameter, shortest distance between two tubes, m
L=2                              % Length of the tube, m
ma = 0.012  ;                    % Mass flow rate of air, kg/s
h = (km*bi)/Ro                   % Convective heat transfer rate between the air and wall of the
tube, W/m^2 K
n = (NTU*ma*ca)/(2*pi*h*Ro*L)    % Number of tubes in the heat exchanger
Dt = Dtp*((2*n*(3/pi^0.5)/pi))^0.5   % Tank diameter, m
Vta = (pi*Dt^2*L)/4              % Tank volume, m
Vtu = pi*Ro^2*n*L                % Volume of tubes, m^3
Vpcm = Vta-Vtu                   % Volume of wax, m^3
mpcm = dm*Vpcm                   % Total mass of wax , kg
Re = (2*ma)/(pi*Ro*n*mu)         % Estimation of the Reynolds number to verify
whether the flow is laminar or not)
```

Appendix – B

Uncertainty Analysis

B.1 Uncertainty analysis

The uncertainties in the measurement of various parameters occurs due to many reasons such as calibration, observation, wear and tear, and sensitivity drift. The independent parameters measured with different measuring equipment during the experiment were temperature of air, mass flow rate of air, solar radiation intensity, power input, and the mass loss of the product. The uncertainties in the independent variables are given in Table B.1. The uncertainties in the dependent parameters are calculated using Eq. (B.1). If an experimental result N is a given function of different independent variables $X_1, X_2, X_3, \ldots\ldots\ldots X_n$, and if ΔN is the uncertainty in the results and $\Delta N_1, \Delta N_2, \Delta N_3 \ldots\ldots\ldots\ldots \Delta N_n$ are the uncertainty in the independent variable then the uncertainty in the results is given by (Holman, 1994).

$$\Delta N = \left[\left(\frac{\partial N}{\partial X_1} \Delta N_1 \right)^2 + \left(\frac{\partial N}{\partial X_2} \Delta N_2 \right)^2 + \left(\frac{\partial N}{\partial X_3} \Delta N_3 \right)^2 + \cdots\cdots + \left(\frac{\partial N}{\partial X_n} \Delta N_n \right)^n \right]^{1/2} \quad \text{(B.1)}$$

For example, the thermal efficiency of the solar air heater is estimated by the following equation.

$$\eta = \frac{\dot{m}_a C_{pa} (T_{oSAH-1} - T_{iSAH-1})}{\alpha \tau I A_{SAH-1}} \quad \text{(B.2)}$$

Then the uncertainty in the thermal efficiency for fixed value of C_p, α and τ is given by the following equation.

$$\Delta\eta = \pm \sqrt{\left(\frac{\partial \eta}{\partial \dot{m}_a} \Delta \dot{m}_a \right)^2 + \left(\frac{\partial \eta}{\partial T_{oSAH-1}} \Delta T_{oSAH-1} \right)^2 + \left(\frac{\partial \eta}{\partial T_{iSAH-1}} \Delta T_{iSAH-1} \right)^2 + \left(\frac{\partial \eta}{\partial I} \Delta I \right)^2 + \left(\frac{\partial \eta}{\partial A_{SAH-1}} \Delta A_{SAH-1} \right)^2}$$

(B.3)

$$\frac{\partial \eta}{\partial \dot{m}_a} = \frac{C_{pa}(T_{oSAH-1} - T_{iSAH-1})}{\alpha \tau I A_{SAH-1}} \tag{B.4}$$

$$\frac{\partial \eta}{\partial \dot{m}_a} = \frac{1.005 \times 1000 \times (45-28)}{0.85 \times 0.95 \times 546 \times 4} = 9.68$$

$$\frac{\partial \eta}{\partial T_{oSAH}} = \frac{\dot{m}_a C_{pa}}{\alpha \tau I A_{SAH-1}} \tag{B.5}$$

$$\frac{\partial \eta}{\partial T_{oSAH}} = \frac{0.019 \times 1.005 \times 1000}{0.85 \times 0.95 \times 546 \times 4} = 0.01$$

$$\frac{\partial \eta}{\partial T_{iSAH}} = \frac{\dot{m}_a C_{pa}}{\alpha \tau I A_{SAH-1}} = 0.01 \tag{B.6}$$

$$\frac{\partial \eta}{\partial T_{iSAH}} = \frac{0.019 \times 1.005 \times 1000}{0.85 \times 0.95 \times 546 \times 4} = 0.01$$

$$\frac{\partial \eta}{\partial I} = -\frac{\dot{m}_a \times C_{pa}(T_{oSAH-1} - T_{iSAH-1})}{\alpha \tau I^2 A_{SAH-1}} \tag{B.7}$$

$$\frac{\partial \eta}{\partial I} = -\frac{0.019 \times 1.005 \times 1000 \times (45-28)}{0.85 \times 0.95 \times 546^2 \times 4} == -3.23 \times 10^{-4}$$

$$\frac{\partial \eta}{\partial A_{SAH}} = -\frac{\dot{m}_a \times c_{pa}(T_{oSAH-1} - T_{iSAH-1})}{\alpha \tau I A^2_{SAH-1}} \tag{B.8}$$

$$\frac{\partial \eta}{\partial A_{SAH}} = \frac{0.019 \times 1.005 \times 1000 \times (45-28)}{0.85 \times 0.95 \times 546 \times 4^2} = 0.184$$

$$\Delta\eta = \pm\sqrt{(9.68 \times 0.001)^2 + (0.01 \times 0.2)^2 + (0.01 \times 0.2)^2 + (-3.23 \times 10^{-4} \times 3)^2 + (0.184 \times 0.01)^2}$$

$$\Delta\eta = \pm 3.8\%$$

Similarly, the uncertainty in the other parameters are calculated by following the same procedure and the uncertainty in other parameters are given in Table B.1

Table B.1

Uncertainty in the independent variables and some of the dependent variables.

Parameters	**Uncertainty**
Uncertainty in the temperature measurement (°C)	±0.2
Uncertainly in the solar radiation measurement (W/m^2)	± 3
Uncertainty in the measurement of mass (g)	±0.01
Uncertainty in the measurement of mass flow rate of air (kg/s)	±0.001
Uncertainty in the power measurement (W)	±1
Uncertainty in the moisture content (%)	±2.3
Uncertainty in the thermal efficiency of the solar air heater (%)	±3.8
Uncertainty in the energy efficiency of the thermal storage (%)	±5.7
Uncertainty in the exergy efficiency of the thermal storage (%)	±5.9
Uncertainty in the thermal efficiency of the drying chamber (%)	±2.7
Uncertainty in the exergy efficiency of the drying chamber (%)	±5.9

Appendix - C

MATLAB Code for solving Air Heater Mathematical Model

```
% MATLAB programme for solution of the air heat mathematical model
function fcns =db_air(z)
Tc = z(1)      % Average temperature of the cover temperature, K
Tf1 = z(2)     % 1st fluid pass average temperature
Ta = z(3)      % Average temperature of the absorber plate, K
Tf2 = z(4)     % 2nd fluid pass average temperature, K
Tb = z(5)      % Average temperature of the bottom plate, K
%Atmospheric conditions
Tamb = 298;              % Ambient air temperature, K
p=1.0123*10^5;           % Atmospheric pressure, N/m2
R=287;                   % Gas constant of air, J/kg-K
I=626;                   % Solar radiation intensity, W/m2
Ti=298;                  % Inlet temperature of air, K
Va=1.5;                  % Ambient air velocity, m/s
%Size of air heater
L=2;             % Length of solar air heater, m
W=1;             % Width of the solar air heater, m
D1=0.075;        % Space between the absorber plate and the glaze, m
D2=0.04;         % Space between the absorber plate and the bottom plate, m
th_in=0.02;      % Thickness of the bottom insulation, m
Dh1= (4*D1*W)/(2*(D1+W)); % Hydraulic diameter of the space between the absorber and glaze, m
Dh2=(4*D2*W)/(2*(D2+W)); % Hydraulic diameter of the space between the bottom plate and the absorber, m
A=L*W;                   % Area of the absorber plate, m2
Acr1=W*D1;               % Cross section area of air duct, m2
```

```
Acr2=W*D2            % Cross section area of air duct, m^2
ma=0.012;            % Mass flow rate of air, kg/s
% Properties of air heater construction materials
Aa=0.95;             % Absorptivity of the absorber plate
Ac=0.06;             % Absorptivity of the cover plate
Ea=0.92;             %Emissivity of the absorber plate
Ec=0.90;             %Emissivity of the glass plate
Eb=0.25;             %Emissivity of the bottom plate
Trg=0.85;            %Transmissivity of the glass plate
k_in=0.026;          %Thermal conductivity of the insulation, W/m-K
sig=5.6678*10^-8;    % Stefan Boltzman constant, W/m^2-K^4
g=9.81;              % Acceleration due to gravity, m^2/s
Ts=Tamb-6;           % Sky temperature, K
hw=5.7+3.8*Va;       % Convective heat transfer co-efficient over the glass plate, W/m^2-K
hr_t=Ec*sig*(Tc^2+Ts^2)*(Tc^2-Ts^2)/(Tc-Tamb);     % Radiative heat transfer coefficient, W/m^2.K
Ds_f2=3.9147-0.016082*Tf2+2.9013*10^-5*Tf2^2-1.9407*10^-8*Tf2^3; % Density of air atmospheric air, kg/m^3
Ds_f1=3.9147-0.016082*Tf1+2.9013*10^-5*Tf1^2-1.9407*10^-8*Tf1^3; % Density of air at temperature Tf1, kg/m^3
Ds=3.9147-0.016082*Tamb+2.9013*10^-5*Tamb^2-1.9407*10^-8*Tamb^3;   % Density of ambient air at temperature, kg/m^3
mu_air=(1.6157+0.06523*Tamb-3.0297*10^-5*Tamb^2)*10^-6;          % Dynamic viscosity of atmospheric air, kg/m s
Cp_air=(1.0057+0.000066*(Tamb-27))*10^3;  % specific heat of air, kJ/kg-K
K_air=0.02624+0.0000758*(Tamb-27); % Thermal conductivity of air, W/m-K
% Fluid properties (Air)
mu_f1=(1.6157+0.06523*Tf1-3.0297*10^-5*Tf1^2)*10^-6; % Dynamics viscosity of air at temperature Tf1, kg/m-s
mu_f2= (1.6157+0.06523*Tf2-3.0297*10^-5*Tf2^2)*10^-6; % Dynamic viscosity of air at temperature Tf2, kg/m-s
Cp_f1=(1.0057+0.000066*(Tf1-27))*10^3;   % Specific heat of air at Tf1, kJ/kg-K
Cp_f2=(1.0057+0.000066*(Tf2-27))*10^3; % Specific heat of air at Tf2, kJ/kg-K
Cp=(Cp_f1+Cp_f2)/2; % Average specific heat of fluid, kJ/kg K
```

```
K_f1=0.02624+0.0000758*(Tf1-27); % Thermal conductivity of air at Tf1, W/m-K
K_f2=0.02624+0.0000758*(Tf2-27); % Thermal conductivity of air Tf2
nu_f1=(mu_f1/Ds_f1);          % Kinematic viscosity of air of the 1st fluid pass
nu_f2=(mu_f2/Ds_f2);          % Kinematic viscosity of air of the 2nd  fluid pass
Df_f1=K_f1/(Ds_f1*Cp_f1); % Thermal diffusivity of air the 1st fluid pass , m2/s
Df_f2=K_f2/(Ds_f2*Cp_f2); % Thermal diffusivity of air the 2nd fluid pass, m2/s
Pr_f1=(nu_f1/Df_f1);          % Prandtle number of air of the 1st fluid pass
Pr_f2=nu_f2/Df_f2;            % Prandtle number of air of the 2nd  fluid pass
V_f1=ma/(Ds_f1*Acr1);         % Velocity of air in the 1st fluid pass, m/s
V_f2=ma/(Ds_f2*Acr2;          % Velocity of air in the 2nd fluid pass, m/s
Re_f1=(Ds_f1*Dh1*V_f1)/mu_f1;  % Reynolds number of fluid in the 1st fluid pass
Re_f2=(Ds_f2*Dh2*V_f2)/mu_f2; % Reynolds number of fluid in the 2nd  fluid pass
% Nusselt number for forced circulation
Nu_f1=0.0158*Re_f1^0.8;
Nu_f2=0.0158*Re_f2^0.8;
hc_f1=(Nu_f1*K_f1)/Dh1; % convective heat transfer co - efficient in the 1st fluid pass, W/m-K
hc_f2=(Nu_f2*K_f2)/Dh2; % convective heat transfer co-efficient in the 2nd fluid pass, W/m-K
% Estimation of Overall top and bottom loss co-eff
U_t=hw+hr_t ;     % Overall top loss coefficient , W/m2-K
U_b= k_in/th_in;  % Overall bottom loss coefficient, W/m2 -K
hr_ac=(sig*(Ta^2+Tc^2)*(Ta+Tc))/((1/Ea)+(1/Ec)-1);   % Radiative heat transfer coefficient between the absorber plate and the cover plate, W/m2-K
hr_ab=(sig*(Ta^2+Tb^2)*(Ta+Tb))/((1/Ea)+(1/Eb)-1);    % );   % Radiative heat transfer coefficient between the absorber plate and the bottom plate, W/m2-K
M1=(2*ma*Cp_f1)/A;
M2=(2*ma*Cp_f2)/A;
Q1=M1*(Tf1-Ti);      %Heat gain by the fluid in the 1st pass
Q2=M2*(Tf2-2*Tf1+Ti); % Heat gain by the fluid in the 2nd fluid pass
To=(Ti+(((Q1+Q2)*A)/(ma*Cp_f2)))-273  % Outlet air temperature of the heater, K
Toi=(Ti+(Q1)/(ma*Cp_f1));  % Outlet air temperature in the first fluid pass, K
eff=(ma*Cp*(To+273-Ti)*100)/(I*A) % efficiency
%Mathematical model of the air heater
```

```
fcns(1)=(hc_f1+hr_ac+U_t)*Tc-hc_f1*Tf1-hr_ac*Ta-Ac*I-U_t*Tamb
fcns(2)=hc_f1*Tc-(hc_f1+hc_f1+M1)*Tf1+hc_f1*Ta+M1*Ti
fcns(3)=hr_ac*Tc+hc_f1*Tf1-
(hc_f1+hr_ac+hr_ab+hc_f2)*Ta+hc_f2*Tf2+hr_ab*Tb+Aa*Trg*I
fcns(4)=2*M2*Tf1+hc_f2*Ta-(hc_f2+hc_f2+M2)*Tf2+hc_f2*Tb-M2*Ti
fcns(5)=hr_ab*Ta+ hc_f2*Tf2-(hc_f2+hr_ab+U_b)*Tb+U_b*Tamb
end
% Initial guess T= [300 312 360 314 312]
% result=fsolve(@db_air, T)
```

Appendix - D

Experimental plan

All the experiments were performed at the fixed air flow rate. The other input parameters such as solar radiation intensity, air temperature and relative humidity of the drying air are nature dependent.

Exp. No.	Experiment	Independent variable	Constants	Dependent variable
1	Drying kinetics analysis of Ghost chilli	-Solar radiation	-Mass flow rate of air -Electrical energy input -Product type	-Air temperature -Relative humidity -Drying rate -Drying time
2	Energy and exergy analyses of Ghost chilli and sliced ginger	-Product type -Quantity of product dried -Solar radiation intensity	Mass flow rate of air -Electrical energy input	-Air temperature -Relative humidity -Drying time -Thermal efficiency of solar air heater and drying chamber -Exergy efficiency of the drying chamber -Specific energy consumption of product
3	Performance test on the solar dryer with the latent heat storage	-Product type -Quantity of product dried -Solar radiation intensity	-Mass flow rate of air -Electrical energy input -Mass of energy storage material	-Air temperature -Relative humidity -Solar radiation intensity -Thermal efficiency of solar air heater, energy storage, and drying chamber -Exergy efficiency of the solar air heater, energy storage, and drying chamber -Specific energy consumption

International Journal Papers

1. D.K. Rabha, P. Muthukumar, C. Somayaji (2017). Experimental Investigation of Thin Layer Drying Kinetics of Ghost Chill Pepper (Capsicum Chinense Jacq.) Dried in a Forced Convection Solar Tunnel Dryer. **Renewable Energy** 105: 583–589.
2. D.K. Rabha, P. Muthukumar, C. Somayaji (2017). Energy and exergy analyses of the solar drying processes of Ghost Chilli Pepper and ginger. **Renewable Energy** 105: 764–773.
3. D.K. Rabha, P. Muthukumar (2017). Performance Studies on a Forced Convection Solar Dryer Integrated With a Paraffin Wax - Based Latent Heat Storage System. **Solar Energy** 149:214–226.

International Conference

1. D.K. Rabha, P. Muthukumar, C. Somayaji. Design and analytical study of a solar dryer integrated with shell and tube paraffin based latent heat storage for drying chilli. Proceedings of the 23rd National Heat and Mass Transfer Conference and 1st International **ISHMT - ASTFE** Heat and Mass Transfer Conference IHMTC2015 17–20 December, 2015, Liquid Propulsion Systems Centre, Indian Space Research Organization, Thiruvananthapuram, India.